



JAEA-Research

2020-007

DOI:10.11484/jaea-research-2020-007

**Status of Study of Long-term Assessment
of Transport of Radioactive Contaminants
in the Environment of Fukushima (FY2018)
(Translated Document)**

Fumiya NAGAO, Tadafumi NIIZATO, Yoshito SASAKI, Satomi ITO
Takayoshi WATANABE, Terumi DOHI, Takahiro NAKANISHI, Kazuyuki SAKUMA
Hiroki HAGIWARA, Hironori FUNAKI, Tadahiko TSURUTA, Toshiharu MISONOU
Kazuya YOSHIMURA, Shigeo NAKAMA, Hiroshi KURIKAMI, Masahiko MACHIDA
Susumu YAMADA, Mitsuhiro ITAKURA, Alex MALINS, Masahiko OKUMURA
Minsik KIM, Xudong LIU, Masaaki YAMAGUCHI, Yasuo ISHII
Kotomi MUTO, Hisaya TAGOMORI, Hiroshi SAITO, Hiroshi TAKEMIYA
Akiyuki SEKI, Akihiro KITAMURA and Kazuki IIJIMA

Collaborative Laboratories for Advanced Decommissioning Science
Fukushima Research Institute
Sector of Fukushima Research and Development

October 2020

Japan Atomic Energy Agency

日本原子力研究開発機構

JAEA-Research

本レポートは国立研究開発法人日本原子力研究開発機構が不定期に発行する成果報告書です。
本レポートの入手並びに著作権利用に関するお問い合わせは、下記あてにお問い合わせ下さい。
なお、本レポートの全文は日本原子力研究開発機構ホームページ (<https://www.jaea.go.jp>)
より発信されています。

国立研究開発法人日本原子力研究開発機構 研究連携成果展開部 研究成果管理課
〒319-1195 茨城県那珂郡東海村大字白方2番地4
電話 029-282-6387, Fax 029-282-5920, E-mail:ird-support@jaea.go.jp

This report is issued irregularly by Japan Atomic Energy Agency.
Inquiries about availability and/or copyright of this report should be addressed to
Institutional Repository Section,
Intellectual Resources Management and R&D Collaboration Department,
Japan Atomic Energy Agency.
2-4 Shirakata, Tokai-mura, Naka-gun, Ibaraki-ken 319-1195 Japan
Tel +81-29-282-6387, Fax +81-29-282-5920, E-mail:ird-support@jaea.go.jp

© Japan Atomic Energy Agency, 2020

**Status of Study of Long-term Assessment of Transport of Radioactive Contaminants
in the Environment of Fukushima (FY2018) (Translated Document)**

Fumiya NAGAO, Tadafumi NIIZATO, Yoshito SASAKI, Satomi ITO,
Takayoshi WATANABE, Terumi DOHI, Takahiro NAKANISHI, Kazuyuki SAKUMA,
Hiroki HAGIWARA, Hironori FUNAKI, Tadahiko TSURUTA, Toshiharu MISONOU,
Kazuya YOSHIMURA, Shigeo NAKAMA, Hiroshi KURIKAMI, Masahiko MACHIDA⁺¹,
Susumu YAMADA⁺¹, Mitsuhiro ITAKURA⁺¹, Alex MALINS⁺¹, Masahiko OKUMURA⁺¹,
Minsik KIM⁺¹, Xudong LIU^{*1}, Masaaki YAMAGUCHI⁺², Yasuo ISHII^{*2},
Kotomi MUTO^{*3}, Hisaya TAGOMORI^{*4}, Hiroshi SAITO^{*5}, Hiroshi TAKEMIYA⁺¹,
Akiyuki SEKI⁺¹, Akihiro KITAMURA⁺³ and Kazuki IJIMA

Collaborative Laboratories for Advanced Decommissioning Science
Fukushima Research Institute, Sector of Fukushima Research and Development
Japan Atomic Energy Agency
Miharu-machi, Tamura-gun, Fukushima-ken

(Received May 22, 2020)

The accident of the Fukushima Daiichi Nuclear Power Station, Tokyo Electric Power Company Holdings, Inc. occurred due to the Great East Japan Earthquake, Sanriku offshore earthquake, of 9.0 magnitude and the accompanying tsunami. As a result, large amount of radioactive materials was released into the environment.

Under these circumstances, Japan Atomic Energy Agency (JAEA) has been conducting “Long-term Assessment of Transport of Radioactive Contaminants in the Environment of Fukushima” concerning radioactive materials released in environment, especially migration behavior of radioactive cesium since November 2012.

This report is a summary of the research results that have been obtained in environmental dynamics research conducted by JAEA in Fukushima Prefecture.

Keywords: TEPCO’s Fukushima Daiichi Nuclear Power Station Accident, Radiocesium, Forest, Water System, City Area, Forest Fire

This document is the English translation of “Status of Study of Long-term Assessment of Transport of Radioactive Contaminants in the Environment of Fukushima (FY2018)” (JAEA-Research 2019-002) except Chapter 5.

+1 Center for Computational Science and e-Systems

+2 Sector of Nuclear Fuel, Decommissioning and Waste Management Technology Development

+3 Naraha Center for Remote Control Technology Development

*1 Post - Doctoral Fellow until March 31 2019.

*2 Senior Post-Doctoral Fellow until March 31 2018.

*3 Fukushima Environmental Safety Center until March 31, 2019.

*4 Kyusyu Environmental Evaluation Association

*5 On loan to IAEA

福島における放射性セシウムの環境動態研究の現状（平成 30 年度版）（翻訳資料）

日本原子力研究開発機構 福島研究開発部門 福島研究開発拠点
福島環境安全センター

長尾 郁弥、新里 忠史、佐々木 祥人、伊藤 聡美、渡辺 貴善、土肥 輝美、中西 貴宏、
佐久間 一幸、萩原 大樹、舟木 泰智、鶴田 忠彦、御園生 敏治、吉村 和也、
中間 茂雄、操上 広志、町田 昌彦⁺¹、山田 進⁺¹、板倉 充洋⁺¹、Alex Malins⁺¹、
奥村 雅彦⁺¹、金 敏植⁺¹、Xudong Liu^{*1}、山口 正秋⁺²、石井 康雄^{*2}、武藤 琴美^{*3}、
田籠 久也^{*4}、齊藤 宏^{*5}、武宮 博⁺¹、関 暁之⁺¹、北村 哲浩⁺³、飯島 和毅

（2020 年 5 月 22 日 受理）

2011 年 3 月 11 日に発生した太平洋三陸沖を震源とするマグニチュード 9.0 の東北地方太平洋沖地震とそれに伴って発生した津波により、東京電力株式会社（現東京電力ホールディングス株式会社）福島第一原子力発電所の事故が発生し、その結果、環境中へ大量の放射性物質が放出された。この事故により放出された放射性核種は、その大部分が森林に沈着している。これに対し、面積が広大であり大量の除去土壌などが生じる、多面的な森林の機能が損なわれる可能性があるなどの問題があり、生活圏近傍を除き、汚染された森林の具体的な除染計画はない。そのため、未除染の森林から放射性セシウムが流出し、既に除染された生活圏に流入することで空間線量率が上がってしまうのではないかと（外部被ばくに関する懸念）、森林から河川に流出した放射性セシウムが農林水産物に取り込まれることで被ばくするのではないかと、規制基準値を超えて出荷できないのではないかと（内部被ばくに関する懸念）などの懸念があり、避難住民の帰還や産業再開の妨げとなる可能性があった。

日本原子力研究開発機構では、環境中に放出された放射性物質、特に放射性セシウムの移動挙動に関する「長期環境動態研究」を 2012 年 11 月より実施している。この目的は、自治体の施策立案を科学的側面から補助する、住民の環境安全に関する不安を低減し、帰還や産業再開を促進するといった点にある。本報告書は、原子力機構が福島県で実施した環境動態研究におけるこれまでの研究成果について取りまとめたものである。

本報告書は JAEA-Research 2019-002 を英訳したものである（5 章を除く）。
福島県環境創造センター（駐在）：〒963-7700 福島県田村郡三春町深作 10-2

+1 システム計算科学センター

+2 核燃料・バックエンド研究開発部門

+3 櫛葉遠隔技術開発センター

*1 2019 年 3 月まで任期付研究員

*2 2018 年 3 月まで任期付研究員

*3 2019 年 3 月にて退職

*4 九州環境管理協会

*5 国際原子力機関へ出向中

Contents

1. Overview of the Fukushima environmental dynamics research	1
1.1 Introduction	1
1.2 Characteristic of the research and difference from existing technology	2
1.3 Important knowledge from our studies	7
1.4 Social effects and operational effects by the results	7
1.5 Outline of this report	14
2. Forest dynamics	15
2.1 Outline	15
2.2 Dynamics of dissolved radioactive cesium in forests	17
2.3 Distribution and outflow of radioactive cesium in forest area	26
2.4 Initial deposition behavior	41
3. Dynamics in river system	55
3.1 Outline	55
3.2 Headwaters region	57
3.3 Concentration of dissolved radioactive cesium and its evolution mechanism in rivers	65
3.4 Changes in concentration of particulate radioactive cesium in rivers and its migration and sedimentation behavior	73
3.5 Riverbed soil	81
3.6 Reservoir	87
3.7 Estuary and costal area	98
4. Urban area	111
4.1 Outline	111
4.2 Investigation of monitoring methods	112
4.3 Decreasing tendency of the air dose rate	117
4.4 Distribution and migration of ¹³⁷ Cs	123
5. Modeling research on environmental dynamics	130
5.1 Outline	130
5.2 Terrestrial dynamics model at river-basin scale (evaluation of year-average dynamics)	136
5.3 Terrestrial dynamics model at river-basin scale (dynamics model for water circulation, sediment and ¹³⁷ Cs)	142
5.4 River system dynamics model	154
5.5 Depth migration model	168
5.6 Dose rate evaluation model	173

5.7	Compartment model for river system dynamics considering the migration to agricultural, forest and fishery products	179
5.8	Example of model integration	183
5.9	Verification of the models	187
5.10	Future subjects	188
6.	Mountain forest fire	190
6.1	Outline	190
6.2	Dispersion	192
6.3	Air dose rate at mountainous area	203
6.4	Dynamics of forest floor	205
6.5	Evaluation of effluent effect on the downstream region by the mountain forest fire	216
7.	Comprehensive evaluation system	224
7.1	Outline	224
7.2	Environmental monitoring database	225
7.3	Integrated analysis supporting environment	226
7.4	Environmental restoration knowledge base	230
7.5	Future subjects	231
8.	Future subjects	232
	Acknowledgement	233
	References	234

目 次

1.	福島環境動態研究の全体概要	1
1.1	はじめに	1
1.2	研究の特徴および従来技術との相違	2
1.3	研究により得られた主な知見	7
1.4	成果による社会的効果・実施効果	7
1.5	本書の構成	14
2.	森林動態	15
2.1	概要	15
2.2	森林中の溶存態放射性セシウム動態	17
2.3	森林域における放射性セシウムの分布と流出	26
2.4	初期沈着挙動研究	41
3.	水系動態	55
3.1	概要	55
3.2	源頭域	57
3.3	河川における溶存態放射性セシウム濃度と生成メカニズム	65
3.4	河川における懸濁態放射性セシウムの濃度変化と移行・堆積挙動	73
3.5	河床土	81
3.6	貯水池	87
3.7	河口・沿岸域	98
4.	市街地	111
4.1	概要	111
4.2	モニタリング手法の検討	112
4.3	空間線量率の減少傾向	117
4.4	¹³⁷ Cs 動態	123
5.	環境動態に関する解析的研究	130
5.1	概要	130
5.2	流域スケール陸域動態モデル（年平均の動態評価）	136
5.3	流域スケール陸域動態モデル（水循環-土砂- ¹³⁷ Cs の動的モデル）	142
5.4	水域動態モデル	154
5.5	深度移行モデル	168
5.6	線量率評価モデル	173
5.7	農林水産物への移行を考慮した流域動態コンパートメントモデル	179
5.8	放射性セシウムの移行に伴う線量率変化	183
5.9	モデル検証	187
5.10	今後の課題	188

6.	林野火災	190
6.1	概要	190
6.2	飛散	192
6.3	山域空間線量率	203
6.4	林床動態	205
6.5	山林火災による下流域への流出影響評価	216
7.	包括的評価システム	224
7.1	概要	224
7.2	環境モニタリングデータベース	225
7.3	統合解析支援環境（解析事例サイト）	226
7.4	環境回復知識ベース	230
7.5	今後の課題	231
8.	課題	232
	謝辞	233
	参考文献	234

List of Tables

Table 1-1	Main results of Fukushima Environmental Dynamics Research	8
Table 2.2-1	Concentration of radioactive cesium in sap of <i>Acer rufinerve</i>	21
Table 2.2-2	Concentration of radioactive cesium and its transfer coefficient for mushroom taken in Irikubo, Yamakiya District, Kawamata Town	24
Table 2.2-3	Concentration and its ratio for radioactive cesium in litter and effluent at wood woollyfoot growing place	24
Table 2.3-1	Amount of ¹³⁷ Cs outflow accompanied by soil loss	32
Table 2.3-2	Increase in the amount of sediment and the amount of ¹³⁷ Cs outflow at the erosion control dam	35
Table 2.3-3	¹³⁷ Cs outflow rate at the erosion control dam	35
Table 2.4-1	The soil-to-lichen aggregated transfer factor (T_{ag}) for the Fukushima derived ¹³⁷ Cs ($m^2 kg^{-1}$)	47
Table 3.5-1	Results of separation and quantitative analysis of 250-106 μm fractions at the sites A and D	86
Table 3.6-1	Effective half-life and decay component of dissolved and suspended ¹³⁷ Cs concentration in each reservoir in four years (from 3 years to 7 years after the accident), and the initial ¹³⁷ Cs concentration just after the accident	92
Table 3.6-2	Deposition amount and deposition rate of ¹³⁷ Cs at each sampling point in Ogaki dam	94
Table 3.7-1	Significant investigation items that has been conducted so far at the estuaries and coastal areas	99
Table 4.4-1	Investigated objects and the number of data	125
Table 4.4-2	Relative ¹³⁷ Cs deposition amount on components in 2015	127
Table 4.4-3	List of the measurement results	128
Table 5.1-1	List of analytical model	135
Table 5.2-1	Total amount of soil and ¹³⁷ Cs flowing out from river basin into the sea in a year after the fallout	139
Table 5.2-2	Amount of soil outflow and dynamics of ¹³⁷ Cs for each land use	139
Table 5.2-3	Cases in the sensitivity analysis	140
Table 5.3-1	Features of each river basin	147
Table 5.3-2	Set values of distribution coefficient K_d	152
Table 5.4-1	Outflow rate of suspended sediment and ¹³⁷ Cs to the downstream for different water levels in the dam lake	157
Table 6.2-1	Concentration of ¹³⁷ Cs for three places at normal time and at the time of the fire (Fukushima Prefecture, JAEA and NIES, 2017)	199

Table 6.4-1	Date of sampling-----	209
Table 6.4-2	Outflow amount and outflow rate of ^{137}Cs in the monitoring period (from June to December, 2017) -----	215
Table 6.5-1	Concentration of particulate ^{137}Cs (Bq kg^{-1}) in the Takase River and the Maeda River at the time of the water discharge (Bq kg^{-1})-----	219

List of figures

Fig. 1-1	Overview of Fukushima Environmental Dynamics Research	5
Fig. 2.1-1	Air dose rate and land use	16
Fig. 2.2-1	Migration of radioactive cesium in forest ecosystem	18
Fig. 2.2-2	Taking sap sample from <i>Acer rufinerve</i>	19
Fig. 2.2-3	<i>Gymnopus peronatus</i> (Forest floor of sampling place)	19
Fig. 2.2-4	Mycelium grown in fallen leaves	19
Fig. 2.2-5	Collecting effluent from fallen leaves	19
Fig. 2.2-6	Effluent taken from fallen leaves	19
Fig. 2.2-7	Autoradiograph of bark and branches/leaves of <i>Acer rufinerve</i>	21
Fig. 2.2-8	Anatomy of a tree trunk	21
Fig. 2.2-9	Concentration of radioactive cesium in bark and branches/leaves of <i>Acer rufinerve</i>	22
Fig. 2.2-10	Percentage of plant dry weight (A) and radioactive cesium content (B) for each part of <i>Eleutherococcus sciadophylloides</i>	22
Fig. 2.3-1	Main processes of material transfer in forested environment	26
Fig. 2.3-2	Study area	28
Fig. 2.3-3	Outline of experimental plot set in a forest	28
Fig. 2.3-4	Situation of the upstream of erosion control dam (left photograph: Kawafusa District, Namie Town) and surface model produced by the surveying data using 3D laser scanner (right figure) ..	29
Fig. 2.3-5	Sampling of the tree by cutting down	31
Fig. 2.3-6	Method for sampling of soil and the tree	31
Fig. 2.3-7	Amount of ¹³⁷ Cs outflow in decontaminated area (a) and burnt site by forest fire (b)	33
Fig. 2.3-8	Outflow and inflow of ¹³⁷ Cs based on forest floor	34
Fig. 2.3-9	Deposit amount of ¹³⁷ Cs in the aboveground and belowground of plantation cedar forests (Ogi District, Kawauchi Village)	36
Fig. 2.3-10	Concentration and deposition amount of ¹³⁷ Cs in each part of a cedar tree (Ogi District, Kawauchi Village)	38
Fig. 2.3-11	Changes of ¹³⁷ Cs concentration in each tree part over the years	38
Fig. 2.3-12	Depth distribution of ¹³⁷ Cs deposition in the belowground (Yamakiya District, Kawamata Town)	39
Fig. 2.4-1	One kind of Parmelioid lichen species	42
Fig. 2.4-2	Study points for air dose measurement in mountain area	43
Fig. 2.4-3	Measurement situation using a hot spot finder (right) and the detector (left)	44

Fig. 2.4-4	Measurement situation using a gamma plotter (GP) (right) and the detector (left)	44
Fig. 2.4-5	The Relationship between the ¹³⁷ Cs activity concentration in all 44 lichens and the ¹³⁷ Cs deposition density on soil at each of the lichen sampling points	46
Fig. 2.4-6	Distribution of air dose rate at Mt. Juman (measurement height: 20 cm) (measured on November 5, 2015).....	48
Fig. 2.4-7	Distribution of airdose rate at Mt. Koutaishi. The dose rate at 20 cm height was measured by a hot spot finder (HSF), and that at 5 cm height was measured by a gamma plotter (GP)	48
Fig. 2.4-8	Comparison of dose rate distribution obtained by airborne monitoring and walking survey (HSF) at Mt. Higakure (measurement height: 20 cm)	49
Fig. 2.4-9	Scatter-plot of ¹³⁷ Cs content vs particle volume.....	50
Fig. 2.4-10	Radioactivity change of CsMPs by heating.....	51
Fig. 2.4-11	Electron microscopy images of CsMP before and after heating (upper photographs) and results of element analysis by SEM-EDS (lower figure)	51
Fig. 2.4-12	Sampling points of lichens near 1F (upper right figure) and electron microscope images of CsMP in lichens (lower photographs)	53
Fig. 3.1-1	Investigation spots	55
Fig. 3.2-1	Investigated regions	57
Fig. 3.2-2	Litter bags set on forest floor (litter of conifer)	58
Fig. 3.2-3	Spatial distribution of dissolved ¹³⁷ Cs concentration (Bq L ⁻¹) at the spots in the headwaters observation	60
Fig. 3.2-4	Dissolution test of litter and soil.....	61
Fig. 3.2-5	Temporal changes in the spatial distribution of dissolved ¹³⁷ Cs concentration (Bq L ⁻¹) in the longitudinal investigation along the river.....	62
Fig. 3.2-6	Relation between deposition amount of ¹³⁷ Cs in river basin and concentration of dissolved ¹³⁷ Cs in river water.....	63
Fig. 3.2-7	Relation between normalized concentration of dissolved ¹³⁷ Cs and concentration of dissolved organic carbon (DOC).....	63
Fig. 3.3-1	Location of rivers investigated	66
Fig. 3.3-2	Relation between distribution of dissolved ¹³⁷ Cs concentration (left) and mean ¹³⁷ Cs deposition amount in the river basin (right) in 2016---	67
Fig. 3.3-3	Relation between normalized dissolved ¹³⁷ Cs concentration and concentration of coexisting inorganic ions or DOC in 2016.....	68

Fig. 3.3-4	Relation between forest coverage and normalized dissolved ^{137}Cs concentration and coexisting inorganic ions	69
Fig. 3.3-5	Relation between deposition amount of ^{137}Cs in forests and normalized dissolved ^{137}Cs concentration	69
Fig. 3.3-6	Relation between average rainfall amount in ten days and concentration of dissolved ^{137}Cs for the Ukedo River, the Takase River, the Kuma River and the Tomioka River	70
Fig. 3.3-7	Temporal change in concentration of dissolved ^{137}Cs in the Ohta River, the Odaka River, the Ukedo River and the Takase River	71
Fig. 3.3-8	Relation between temperature and concentration of dissolved ^{137}Cs in the Ohta River, the Odaka River, the Ukedo River and the Takase River	71
Fig. 3.3-9	Temporal changes in concentration of dissolved ^{137}Cs in the Ohta River, the Odaka River, the Ukedo River and the Takase River (two components)	72
Fig. 3.4-1	Location map of the investigated rivers	74
Fig. 3.4-2	Temporal changes in concentration of particulate and dissolved ^{137}Cs in the Ohta River, the Odaka River, the Ukedo River and the Takase River	76
Fig. 3.4-3	Outflow rate of ^{137}Cs per year for the Ohta River, the Odaka River, the Ukedo River, the Takase River, the Maeda River, the Kuma River and the Tomioka River	77
Fig. 3.4-4	Temporal changes in air dose rates for the Ukedo River, the Takase River and the Kuma River	78
Fig. 3.4-5	Amount of sediment transfer in September 2015 at the time of water discharge caused by the heavy rain in Kanto-Tohoku district	78
Fig. 3.4-6	Temporal changes in air dose rate distribution at the cross section of flood plain and depth distribution of radioactive cesium	80
Fig. 3.5-1	Sampling position in the Tomioka River	82
Fig. 3.5-2	Relation between ^{137}Cs concentration and particle size fraction	82
Fig. 3.5-3	Proportion of ^{137}Cs per particle size fraction	83
Fig. 3.5-4	Proportion of mineral composition per particle size fraction	84
Fig. 3.5-5	Separation results of minerals from 250-106 μm fraction at the sites A and D	85
Fig. 3.5-6	Concentration of radioactivity in respective minerals at the sites A and D	86
Fig. 3.6-1	Location of the investigated spots	88
Fig. 3.6-2	Temporal change in concentration of dissolved ^{137}Cs	90

Fig. 3.6-3	Temporal change in concentration of suspended ^{137}Cs	90
Fig. 3.6-4	Apparent distribution coefficient in each reservoir	93
Fig. 3.6-5	Sampling spots of bottom sediment in Ogaki dam	93
Fig. 3.6-6	Vertical distribution of ^{137}Cs concentration and particle size of bottom sediment in Ogaki dam	95
Fig. 3.7-1	Predicted seabed sediments map (left) and Bathymetric map (right)	100
Fig. 3.7-2	Bathymetric map and distribution of silt particles near the mouth of the Ukedo River	101
Fig. 3.7-3	^{137}Cs concentration as a function of the distance from the coast (from FY2013 to FY2016)	102
Fig. 3.7-4	^{137}Cs inventory as a function of the distance from the coast (from FY2013 to FY2016)	102
Fig. 3.7-5	Vertical distribution of ^{137}Cs in seabed sediment (near the mouth of the Ukedo River)	103
Fig. 3.7-6	Mean shear stresses at the bottom layer	104
Fig. 3.7-7	Temporal changes of ^{137}Cs in seabed sediment	105
Fig. 3.7-8	Concentration of dissolved ^{137}Cs (FY2014-FY2017)	106
Fig. 3.7-9	Concentration of particulate ^{137}Cs (FY2014-FY2017)	106
Fig. 3.7-10	Investigation position and measurement layout for moored survey	108
Fig. 3.7-11	Deposition amount of sediment (left) and deposition amount of ^{137}Cs (right)	108
Fig. 3.7-12	Results of sediment flux based on the towing survey	110
Fig. 4.2-1	Study sites	112
Fig. 4.2-2	Evaluation of the height conversion factor (decreasing of count rate with height)	113
Fig. 4.2-3	Distribution map of air dose rate	114
Fig. 4.2-4	Comparison of the air dose rate obtained by ground-based survey and AUH survey	115
Fig. 4.2-5	Spatial distribution of conversion factor (for Okuma Town)	116
Fig. 4.2-6	Mesh size and uncertainty of the results of AUH survey	116
Fig. 4.3-1	Investigation points	118
Fig. 4.3-2	Histogram of λ at the 170 measurement points that had been analyzed and evaluated	119
Fig. 4.3-3	Decreasing rate of air dose rate	120
Fig. 4.3-4	Decreasing rate of surface dose rate	120
Fig. 4.3-5	Frequency distribution of λ/λ_s	120
Fig. 4.3-6	Comparison of the distribution of λ and λ_s	121
Fig. 4.3-7	Photographs around the measurement points	122

Fig. 4.3-8	Comparison of the distribution of λ in forest, near tree, and in open land	123
Fig. 4.4-1	Relation between surface count rate and ^{137}Cs deposition amount	124
Fig. 4.4-2	Catchment to be investigated	126
Fig. 4.4-3	Temporal changes in relative ^{137}Cs deposition amount at permeable surfaces, paved surfaces and roofs	127
Fig. 5.1-1	Analytical models and their scopes of application	133
Fig. 5.1-2	Main subjects and examples of the model application	133
Fig. 5.1-3	Scale of time and space studied by the terrestrial/river-system dynamics models	134
Fig. 5.2-1	Analytical process in SACT	137
Fig. 5.2-2	Amount of ^{137}Cs outflow into the sea in a year, calculated by the sensitivity analysis for each case	141
Fig. 5.2-3	Prediction map of ^{137}Cs deposition until 100 years after the fallout for the basic case	142
Fig. 5.3-1	Outline of GETFLOWS	143
Fig. 5.3-2	Distribution of ^{137}Cs deposition in five river basins close to the 1F (the Odaka River, the Ukedo River, the Maeda River, the Kuma River, and the Tomioka River), the upper river basin of the Ohta River, and Oginosawa River basin in Tomioka River basin area (data taken by the fourth airborne radiation monitoring in November 2011)	145
Fig. 5.3-3	Three-dimensional geological structure model (River basin areas of the Odaka River, the Ukedo River, the Maeda River, the Kuma River and the Tomioka River)	146
Fig. 5.3-4	Three-dimensional geological structure model (Oginosawa River basin)	146
Fig. 5.3-5	Three-dimensional geological structure model (upper river basin of the Ohta River)	147
Fig. 5.3-6	(a) Outflow amount and (b) outflow ratio of ^{137}Cs from five river basins at heavy rainfall such as typhoon	148
Fig. 5.3-7	Rainfall patterns applied in the analysis	149
Fig. 5.3-8	Example of analytical results	150
Fig. 5.3-9	(a) Amount of erosion and sedimentation, and (b) ratio of remaining ^{137}Cs , in the period from May, 2011 to December, 2015	151
Fig. 5.3-10	Comparison between measured data and calculated value for suspended and dissolved cesium	152
Fig. 5.4-1	Conceptual image of river system dynamics model	156

Fig. 5.4-2	Measured values of the concentration of suspended sediment at the observation spots in the upstream of dam lake, and input values in the analysis by FLESCOT	158
Fig. 5.4-3	Measured values of ¹³⁷ Cs concentration at the observation spots in the upstream of dam lake, and input values in the analysis by FLESCOT	158
Fig. 5.4-4	Comparison between measured values of the concentration of suspended sediment at the observation spots in the downstream of dam lake and results of analysis by FLESCOT.....	159
Fig. 5.4-5	Comparison between measured values of ¹³⁷ Cs concentration at the observation spots in the downstream of dam lake and results of analysis by FLESCOT.....	159
Fig. 5.4-6	Effect of strength/duration of rainfall and capacity of dam on the outflow rate of ¹³⁷ Cs to the downstream	160
Fig. 5.4-7	Contribution ratio of rainfall scale and each particle size to the outflow of ¹³⁷ Cs (long-time rain).....	160
Fig. 5.4-8	Schematic image for the behavior of sediment and radioactive cesium flowing into dam lake at the time of heavy rain	161
Fig. 5.4-9	Aerial photograph near the estuary of the Ukedo River investigated by the simulation	162
Fig. 5.4-10	Deposition amount of sediment at the cross section of red ellipse shown in Fig. 5.4-9.....	163
Fig. 5.4-11	The deposition amount of ¹³⁷ Cs at the time of typhoon in September 2015, which was evaluated by the simulation	164
Fig. 5.4-12	Air dose rate measured in 2013 by unmanned helicopter	164
Fig. 5.4-13	Schematic diagram of five-level nest structure	165
Fig. 5.4-14	Nest structure of the simulation region including the Ukedo River and the 1F	166
Fig. 5.4-15	Water flow around the estuary at the time of flood.....	166
Fig. 5.4-16	Diffusion status of dissolved cesium originating from the river at the time of flood by typhoon	167
Fig. 5.4-17	Distribution of deposited sediment originating from the river at 30 hours after the end of flood by typhoon	167
Fig. 5.5-1	Conceptual image of the developed model	170
Fig. 5.5-2	Comparison of the results calculated by the present model with the measured values	172
Fig. 5.5-3	Influence of the difference in sorption/desorption parameters on the depth profile of radioactive cesium	172

Fig. 5.5-4	Results of the trial analysis reproducing the depth distribution of radioactive cesium with a maximum near the surface region	173
Fig. 5.5-5	Conceptual diagram of the relation between the mechanism of radioactive-cesium migration in the depth direction estimated by the analysis and its depth profile	173
Fig. 5.6-1	Schematic image of the dose evaluation model, ADRET	175
Fig. 5.6-2	Analytical result of radiation dose rate in simple mountain and valley topography	175
Fig. 5.6-3	Conceptual drawing of geometry-making tool for the PHITS calculation, 3D-ADRES, to evaluate radiation dose rate considering topography and structures on land	176
Fig. 5.6-4	Examples of the analysis for the forest in Ogi District, Kawauchi Village and city areas of Okuma Town and Tomioka Town	176
Fig. 5.6-5	Region affected by radiation on flat land	177
Fig. 5.6-6	Comparison of the analytical results with the measured values	178
Fig. 5.6-7	Analysis of decontamination effects	178
Fig. 5.7-1	Migration route considered in the CMFW (among the dynamic compartments)	180
Fig. 5.7-2	Connection among the compartments for the Ukedo River basin	180
Fig. 5.7-3	Fitting situation of compartments in forest	182
Fig. 5.7-4	Stock-flow of radioactive cesium five years after the fallout for the Ukedo River basin	182
Fig. 5.7-5	Effect of each migration route from forests to rivers on the concentration of radioactive cesium in freshwater fish	183
Fig. 5.8-1	Image of application of analytical results obtained by the SACT to the boundary condition of the side inflow in the TODAM	184
Fig. 5.8-2	Distribution of sediment deposition in dam lake, river beds, and flood plain for the Ukedo River estimated by the SACT-TODAM model	184
Fig. 5.8-3	Relation between decrease in dose rate caused by the migration of radioactive cesium into deep region and the sorption rate of radioactive cesium on irreversible sites	186
Fig. 5.8-4	Distribution of changes in dose rate before and after the typhoon attack in September 2011	186
Fig. 5.8-5	Distribution of changes in dose rate around the confluence point of the Ukedo and the Takase Rivers before and after the typhoon attack in September 2011	187

Fig. 6.1-1	Forest fires occurred after the 1F accident	191
Fig. 6.2-1	Monitoring points of atmospheric dust	193
Fig. 6.2-2	Image of particle isolation in filter	194
Fig. 6.2-3	Analytical results of levoglucosan	196
Fig. 6.2-4	Relation between number of trapped particles per field of view of microscope (1740 μm \times 1200 μm) and concentration of ^{137}Cs	196
Fig. 6.2-5	Photographs of filters after sampling the atmospheric suspended dust	197
Fig. 6.2-6	Relation between number of trapped particles in a field of view (1740 μm \times 1200 μm) of microscope and wind speed	198
Fig. 6.2-7	Relation between ^{137}Cs concentration and wind speed at normal time	199
Fig. 6.2-8	Microscope images of particles isolated from the filters at three places	201
Fig. 6.3.1	Comparison of air dose rate distribution among the time before/after the fire and ten months after the fire (red line: burnt region)	204
Fig. 6.3.2	Changes in air dose rate	205
Fig. 6.4-1	Air dose rate around the investigated area (as of November 18, 2016)	207
Fig. 6.4-2	Map of investigation sites	207
Fig. 6.4-3	Experimental plot set at the cedar forest along the Nanoka-sawa	208
Fig. 6.4-4	Concentration of ^{137}Cs in bark and aggregated transfer factor (T_{agg})	210
Fig. 6.4-5	Concentration (left) and amount (right) of ^{137}Cs in litter and duff layers	211
Fig. 6.4-6	Relation between distance from the spreading fire site of cedar forest and ^{137}Cs deposition amount in litter layer	212
Fig. 6.4-7	Concentration (left) and deposition amount (right) of ^{137}Cs in soil layer	212
Fig. 6.4-8	Situation of forest slope at Japanese cedar forest	213
Fig. 6.4-9	Outflow amount of ^{137}Cs from forest slope at cedar forest	214
Fig. 6.5-1	Investigation spots and the location of Mt. Juman	217
Fig. 6.5-2	Concentration of ^{137}Cs in water of the Takase River at the time of normal water level (upper: particulate state, lower: dissolved state)	218
Fig. 6.5-3	Concentration of ^{137}Cs in water of the Maeda River at the time of normal water level (upper: particulate state, lower: dissolved state)	219
Fig. 6.5-4	Air dose rate at the flood plain of the Takase River	220
Fig. 6.5-5	Air dose rate at the flood plain of the Maeda River	220
Fig. 6.5-6	Depth distribution of ^{137}Cs concentration at the flood plain of the Takase River	221
Fig. 6.5-7	Depth distribution of ^{137}Cs concentration at the flood plain of the Maeda River	221

Fig. 6.5-8 Depth distribution of ^{137}Cs concentration at the bottom sediment of
Ishikuma sand - trap dam(left: inflow part, right: center of the lake)--222

Fig. 6.5-9 Depth distribution of ^{137}Cs concentration at the bottom sediment of Shirasago
reservoir (left: inflow part, right: center of the lake)-----222

Fig. 7.1-1 Conceptual diagram of comprehensive evaluation system-----225

Fig. 7.2-1 Displayed example of environmental radiation monitoring database
(measurement results of air dose rates by aerial monitoring)-----226

Fig. 7.3-1 Example of the analytical results (concentration of radioactive cesium) by
SACT displayed on a web browser -----228

Fig. 7.3-2 Example of the displayed analytical results
(amount of radioactivity in forest) by CMFW on a web browser-----229

Fig. 7.4-1 Structure of environmental restoration knowledge base -----231

List of authors

Chapter	Author(s)	Affiliation*
Summary Editor	Fumiya NAGAO, Akihiro KITAMURA, Kazuki IJIMA	*1
2.1	Tadafumi NIIZATO	*1
2.2	Yoshito SASAKI, Satomi ITO	*1
2.3	Tadafumi NIIZATO, Takayoshi WATANABE	*1
2.4	Terumi DOHI	*1
3.1	Takahiro NAKANISHI	*1
3.2	Kazuyuki SAKUMA	*1
3.3	Takahiro NAKANISHI	*1
3.4		
3.5	Hiroki HAGIWARA	*1
3.6	Hironori FUNAKI	*1
3.7	Tadahiko TSURUTA, Toshiharu MISONOU	*1
4.1	Kazuya YOSHIMURA	*1
4.2		
4.3	Shigeo NAKAMA	*1
4.4	Kazuya YOSHIMURA	*1
5	Hiroshi KURIKAMI, Kazuyuki SAKUMA, Akihiro KITAMURA	*1
	Masahiko MACHIDA, Susumu YAMADA, Mitsuhiro ITAKURA, Alex MALINS, Masahiko OKUMURA, Minsik KIM, Xudong LIU	*2
	Masaaki YAMAGUCHI	*3
6.1	Tadafumi NIIZATO	*1
6.2	Terumi DOHI, Yasuo ISHII, Hiroki HAGIWARA, Kotomi MUTO, Hisaya TAGOMORI, Tadahiko TSURUTA, Kazuki IJIMA	*1
6.3		
6.4	Tadafumi NIIZATO	*1
6.5	Takahiro NAKANISHI	*1
7	Fumiya NAGAO, Hiroshi SAITO, Akihiro KITAMURA*4	*1
	Hiroshi TAKEMIYA, Akiyuki SEKI	*2

* Affiliation of that time of publication of JAEA-Research 2019-002 (Japanese document).

*1 Collaborative Laboratories for Advanced Decommissioning, Fukushima Research Institute

*2 Center for Computational Science and e-Systems

*3 Sector of Nuclear Fuel, Decommissioning and Waste Management Technology Development

1 Overview of the Fukushima environmental dynamics research

1.1 Introduction

The accident of the Fukushima Daiichi Nuclear Power Station (hereinafter the accident is simply referred to “the accident”, power station is referred to “1F”), Tokyo Electric Power Company Holdings, Inc. occurred due to the Great East Japan Earthquake, Sanriku offshore earthquake, of 9.0 magnitude and the accompanying tsunami. As a result, large amount of radioactive materials was released into the environment. Most of the radioactive materials discharged by the accident is being deposited in forests (Kitamura et al., 2014)¹⁾. For the contaminated forests, specific decontamination plan has not yet been formulated except for those near to the living sphere due to the problems such as; the area of forests is so large that huge amount of decontaminated soil will be produced, and the various beneficial functions of forests will be possibly impaired. For this reason, there have been the anxiety such as; air dose rates may increase due to the cesium flow from the non-decontaminated forests to already decontaminated living sphere (anxiety for external exposure), we may be exposed to radiation due to the incorporation of radioactive cesium flowing out from forests to rivers into agricultural, forestry and fishery products, and the products cannot be shipped due to the high radioactivity beyond the regulatory limits (anxiety for internal exposure). Therefore, there has been a possibility that the above anxiety could hamper the evacuees’ return and the restart of industry.

Under these circumstances, Japan Atomic Energy Agency (JAEA) has been conducting “Long-term Environmental Dynamics Research” concerning radioactive materials released in environment, especially migration behavior of radioactive cesium since November 2012. This research aims at the following three subjects.

- To clarify the behavior of radioactive cesium in living sphere and develop the future prediction models.
- To propose countermeasures for migration reduction considering the evaluation results of radiation dose and migration behavior.
- To construct comprehensive evaluation system for long-term investigation data, migration prediction, radiation dose evaluation, and countermeasures for radiation reduction.

Through these studies, we evaluate the migration of radioactive cesium in the future, and understand the degree of the effect based on the evaluation. Also, we will lead to the proposal of reasonable countermeasures by estimating their effects. Furthermore, we disclose the information that is helpful for diversified and comprehensive judgment by interrelating the obtained knowledge.

With these activities, it is expected that the planning of policy by local governments can be supported from the scientific side, the residents’ anxiety about the environmental safety will be reduced, and residents’ return and industrial restart are promoted.

1.2 Characteristic of the research and difference from existing technology

For these purposes, JAEA has promoted the research based on the following approaches.

- We clarify the individual migration behavior of radioactive cesium from forests to estuaries. By combining these results, we analyze the migration of cesium as a series of process. Herewith, we quantitatively overlook the migration and deposition behavior of radioactive cesium in the whole river system. Also, we construct mathematical models by extracting the main phenomena dominating the migration of radioactive cesium.
- We conduct case study for migration and deposition behavior of radioactive cesium supposing the changes in various natural phenomena and environmental condition.
- We deductively confirm the phenomena estimated by the investigation. Also, we predict the future distribution of radioactive cesium in environment and air dose rate, and provide the results timely as information for local governments to plan their policy.

More specifically, as the first objective among those described in Section 1.1, investigation was carried out for eight river systems (the Ohta River, the Odaka River, the Ukedo River, the Maeda River, the Kuma River, the Tomioka River, the Ide River and the Kido River). We systematically investigated the river systems from the forests that are the source of water to the estuaries. We clarified the factors dominating the migration of radioactive cesium by quantitatively comparing and evaluating the migration and deposition behavior of radioactive cesium in the whole river systems. As to the second objective, the effect of the migration reduction method was investigated based on the specific experiments. Also, we prepared analytical tools that enable the prediction of behavior under various conditions based on the knowledge obtained by the investigation.

In these studies, in order to temporally and spatially predict the migration of radioactive cesium, it is necessary to make models based on the data obtained by the investigation and the other existing data. As a method for the prediction, there are two approaches. One is a statistical approach where data obtained in the past are statistically analyzed and the temporal changes are extrapolated to the future. The other is a phenomenological approach where each physicochemical phenomenon is modeled and the future movements are calculated as a whole. In the statistical approach that has been conventionally conducted, approximate future prediction is possible without being deeply involved if there are enough data. Also, it has an advantage that the calculation amount is relatively small. However, the statistical approach has a disadvantage that it is not possible to investigate the situation where various conditions have been changed, because the past tendency of the temporal changes is directly extrapolated to the future. For this reason, there has been difficulty in investigating what kind of phenomena is the main factor dominating the redistribution of radioactive cesium and what kind of changes happen if the countermeasures such as decontamination is conducted.

Under these circumstances, in environmental dynamics research, we constructed the process for

whole river systems by combining the individual phenomenon base on the physicochemical phenomenological models that are the dominating factors, which was clarified by the investigation research. With this process, we can analyze under various supposed conditions. Herewith, it became possible to predict behavior under various natural phenomena and conditions, and realize the environment for case studies that are necessary for the planning of the countermeasures.

As to the third objective, we have prepared three comprehensive evaluation systems. These are, 1) the environmental monitoring database in which the air dose rates and concentration of radioactivity in soil that had been obtained by various organizations are integrated, 2) the analysis example base that presents the results of analytical research, and 3) the base information Q&A in which the knowledge based on the obtained results are presented with easy-to-understand words. These three evaluation systems have been released sequentially.

More specifically, the investigation research was conducted by setting the subjects that correspond to various anxiety of residents, presented in Fig. 1-1. Also, as an incidental accident, we investigated the forest fire in Mountain Juman (Mt. Juman), which may possibly influence the outflow amount of radioactive cesium.

This is a blank page.

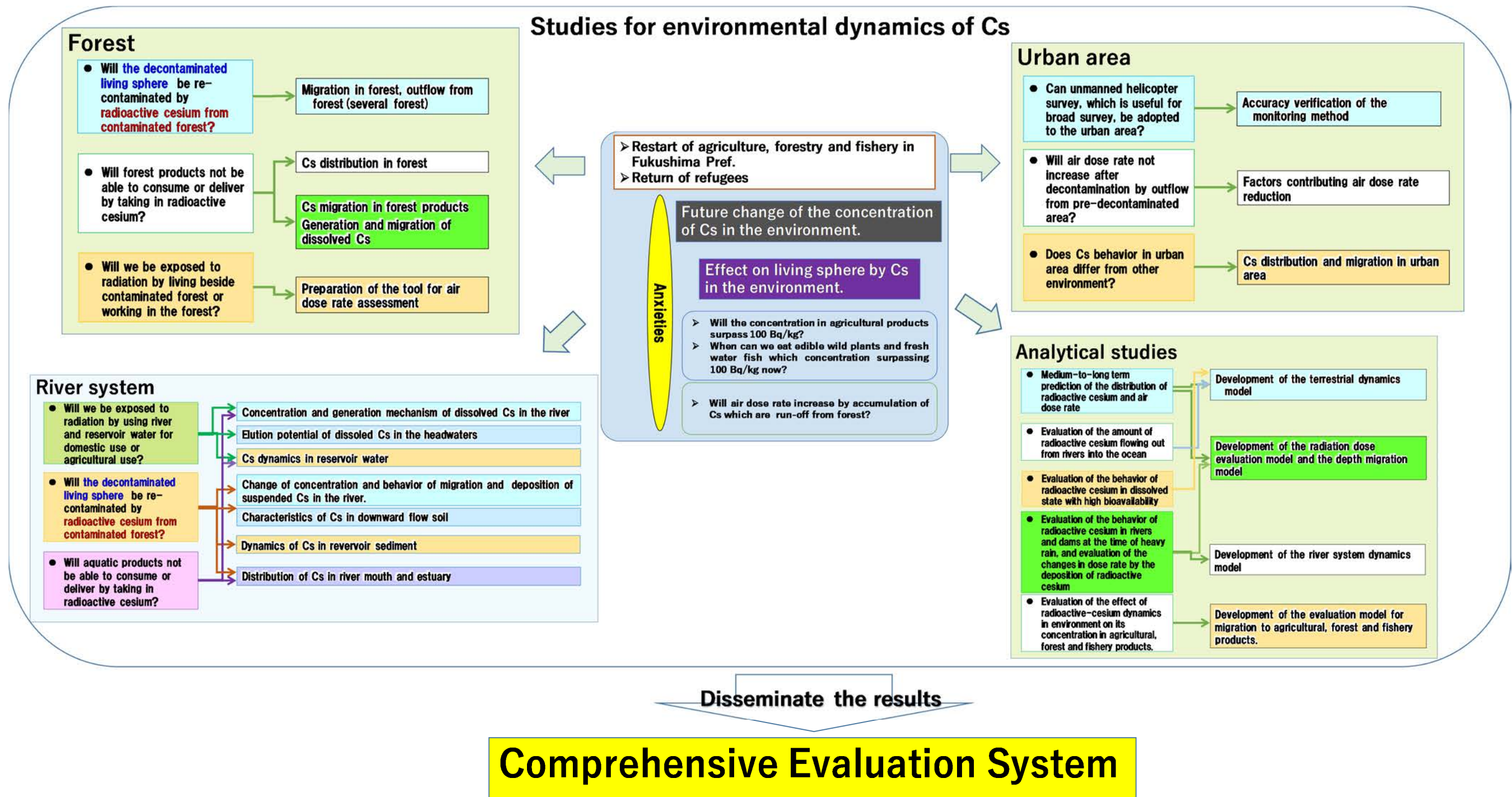


Fig. 1-1 Overview of Fukushima Environmental Dynamics Research.

1.3 Important knowledge from our studies

The outline of the results presented in this report is shown in Table 1-1. The main results are as follows.

- The rate of cesium outflow from forests was low (<1%), and it depended on the coverage of forest floor. The cesium outflow rate sometimes temporarily increased due to the decrease in the coverage of forest floor by fire etc. However, the outflow rate again decreased with the recovery of the coverage.
- For river system, the concentration of dissolved radioactive cesium was lower than 1 Bq L⁻¹. The concentration tends to be decreasing with time as a whole although there was seasonal variations. Also, both the concentration of particulate/deposited cesium (rivers and estuaries) and air dose rates tend to be decreasing.
- For city area, it became possible to measure air dose rates by unmanned helicopter survey. It was found that the air dose rate is decreasing faster than that estimated by the physical decay of radioactive cesium.
- The above phenomena were described by the mathematical models. We searched the main factors dominating the cesium migration by conducting various case studies. Also, we are constructing models towards the future prediction.

1.4 Social effects and operational effects by the results

The information based on scientific evidence has been presented timely and appropriately to local governments etc. Based on such knowledge, we have contributed to the planning of local governments such as the planning of reasonable safety countermeasures and the cancellation of the evacuation order. Furthermore, the prediction results are being used as basic information concerning the planning for the recovery of agriculture, forestry and fisheries. The individual research has been timely reported in newspaper and television (e.g. Fukushima-Minpo on 27 September 2013, 28 March 2017, Fukushima edition, Asahi Shimbun on 8 March 2015, Denki Shimbun on 14 May 2018, etc.). We will continue to provide new results and knowledge obtained by the research.

Table 1-1 Main results of Fukushima Environmental Dynamics Research. (1/6)

Category	Main results	chapter in this report
Forest	<ul style="list-style-type: none"> ● Radioactive cesium is mostly distributed in branches and leaves in trees, and it migrates in trees. The concentration of radioactive cesium in timber stem is relatively low. 	2.2
	<ul style="list-style-type: none"> ● Radioactive cesium released from litter layer in forest bed. Decomposed litter tend to release more radioactive cesium. 	2.2
	<ul style="list-style-type: none"> ● The coverage of the ground in forests considerably affects the migration of radioactive cesium. The outflow rate of radioactive cesium is 0.1% for non-decontaminated forests, and 2-3% for decontaminated places and fire sites. In the latter areas, the outflow rate became lower than 1% with the recovery of the coverage. 	2.3, 7.4
	<ul style="list-style-type: none"> ● About 90% of radioactive cesium is distributed in the underground litter and soil, and about 10% exists in trees on the ground. The amount of radioactive cesium in litter layer is about 6-20%, and most of it exists in soil layer shallower than 3 cm. 	2.3
	<ul style="list-style-type: none"> ● The concentration of radioactive cesium in lichens 2 years after the accident had good correlation with the deposition flux in soils immediately after the accident. 	2.4
	<ul style="list-style-type: none"> ● The distribution of radioactive cesium along the mountain trails and constant altitude tends to depend on the orientation. 	2.4
	<ul style="list-style-type: none"> ● The cesium-rich microparticles (CsMP) were extracted from soil and dust samples, and we divided them into two categories by difference of the spatial distribution and the specific activity. 	2.4
	<ul style="list-style-type: none"> ● We have modeled the trees and soil layer, and developed tools to analyze air dose rate in forests and the adjacent areas by placing radioactive source. 	5.6
	<ul style="list-style-type: none"> ● The increase in radioactive cesium by the migration from tree crown to litter layer and the decrease by that from litter layer to soil layer were cancelled, so that it was presumed that the decay of air dose rate became almost same as that estimated by the physical decay. 	5.6

Table 1-1 Main results of Fukushima Environmental Dynamics Research. (2/6)

Category	Main results	chapter in this report
River system	<ul style="list-style-type: none"> ● The concentration of particulate cesium and deposited cesium, and air dose rate are decreasing with time. The outflow of radioactive cesium to the downstream is reduced by the deposition of particulate cesium on the bottom of reservoirs. 	3.2
	<ul style="list-style-type: none"> ● Spring water scarcely contains dissolved ¹³⁷Cs. It is suggested that dissolved ¹³⁷Cs eluted from soils and litter flowing as ground water. 	3.3, 3.6
	<ul style="list-style-type: none"> ● The concentration of dissolved cesium in rivers and dams is less than 1 Bq/L. Although seasonal fluctuations are seen, it is decreasing with time. 	3.4
	<ul style="list-style-type: none"> ● Due to the difference in mineral composition, radioactive cesium distribution not dependent on particle size is observed. 	3.5
	<ul style="list-style-type: none"> ● The decreasing rate of the radioactive cesium concentration in rivers and reservoirs is becoming more moderate. 	3.3, 3.6
	<ul style="list-style-type: none"> ● The concentration of radioactive cesium in marine soil is less than 100 Bq/kg at 99.8% of coastal waters, and it is decreasing with time. 	3.7

Table 1-1 Main results of Fukushima Environmental Dynamics Research. (3/6)

Category	Main results	chapter in this report
City area	<ul style="list-style-type: none"> ● The influence of land use on the measurement accuracy of the unmanned helicopter survey is small, and it is possible to evaluate the air dose rate distribution with precision comparable to that of the flat land. 	4.2
	<ul style="list-style-type: none"> ● The measurement accuracy of the unmanned helicopter survey is affected by the local distribution of air dose rate and the spatial resolution. 	4.2
	<ul style="list-style-type: none"> ● Even in the area after decontamination, the air dose rate decreases more rapidly than that estimated by the physical decay. 	4.3
	<ul style="list-style-type: none"> ● The air dose rate decreases rapidly on pavement surface, while the decreasing rate tends to be relatively slow in unpaved surface or near the forest. 	4.3
	<ul style="list-style-type: none"> ● The localized outflow and deposition of sediment does not influence the decreasing speed of air dose rate. 	4.3
	<ul style="list-style-type: none"> ● Radioactive cesium abundance in the region specific to city areas (pavement surfaces and buildings) is remarkably lower than that in soil, and the contamination in city areas is limited. 	4.4
	<ul style="list-style-type: none"> ● It is estimated that the majority of radioactive cesium deposited on the region specific to the city areas had outflowed due to the initial wash off and weathering effect just after the accident. 	4.4
	<ul style="list-style-type: none"> ● Radioactive cesium in city areas outflows mainly in the dissolved state. 	4.4

Table 1-1 Main results of Fukushima Environmental Dynamics Research. (4/6)

Category	Main results	chapter in this report
Analytical research	<ul style="list-style-type: none"> ● The analysis was conducted for 14 river systems in Hamadori District and Nakadori District. A prediction map for the deposition amount until 100 years later was prepared. 	5.2
	<ul style="list-style-type: none"> ● Detailed analysis taking rainfall etc. into consideration was conducted and the following results were obtained. <ul style="list-style-type: none"> ➤ The outflow rate of cesium from rivers to the sea was low in a river basin with dams. It tends to be higher in case that there are many paddy fields etc. in the river basin. ➤ Most of radioactive cesium flowing out into rivers were accompanied by soil erosion near rivers and along the swamp of forests. ➤ Concentration of radioactive cesium in river water tends to be high when concentration of floating sediment (turbidity) is high. In addition, the concentration of cesium in river water sometimes higher in several hours to several days after heavy rain. 	5.3
	<ul style="list-style-type: none"> ● By analyzing the dam lakes, it was clarified that most of radioactive cesium flowing into the dam lake together with sediment during rainfall was accumulated in the lake bottom. Also, the proportion of such deposited cesium decreases as the strength and duration of rainfall increases, and it depends on the particle size and the distribution coefficient of sediment. 	5.4
	<ul style="list-style-type: none"> ● Based on the analysis combining multiple models, we evaluated the behavior that cesium-sorbed sediment is deposited on flood plain, and surrounding air dose rate changes with the deposition of cesium. 	5.4

Table 1-1 Main results of Fukushima Environmental Dynamics Research. (5/6)

Category	Main results	chapter in this report
Analytical research	<ul style="list-style-type: none"> ● We conducted the radiation transport analysis and the depth migration analysis of radioactive cesium, and clarified the influence of depth, distance and topography on cesium migration. 	5.5, 5.6
	<ul style="list-style-type: none"> ● It was estimated that approximately 8.4 TBq of radioactive cesium has flowed from the Abukuma River and the rivers at Hamadori District, Fukushima Prefecture into the sea in the first year after the accident. It was also estimated that the contribution from the fields accounted for 47% and the contribution from the forests accounted for 41% for the outflow. 	5.7
	<ul style="list-style-type: none"> ● The case study on radioactive cesium incorporated in freshwater fish was conducted. It was suggested that the observed decreasing tendency of the cesium concentration in freshwater fish is possibly represented by considering the contribution of the fallen leaves directly flowing into the rivers as well as the contribution from the litter lays in forests. 	5.7

Table 1-1 Main results of Fukushima Environmental Dynamics Research. (6/6)

Category	Main results	chapter in this report
Mountain fire (Case of Mountain Juman, 2017)	<ul style="list-style-type: none"> ● The possibility of dispersion of radioactive materials from burned area is undeniable, but its effect is extremely low. ● Migration of radioactive materials didn't occur enough to change the air dose rate, because the air dose rate had change little before and after mountain fire. ● The amount of cesium runoff in the fire spread site of Mt. Juman, Fukushima Prefecture was about 13 times as much as the non-spread site based on the observation that had been conducted for about half a year from two months after the fire. ● The cesium outflow rate in the fire spread site was calculated to be 2.6%, which is a little higher than that in the normal places. However, it was within the range of the data that had been taken, and no significant increase in runoff rate was observed. ● Main factors related to the distribution of cesium and the outflow situation were burning of litter layers and underlying vegetation covering the forest floor. ● It was confirmed that there was no outflow effect on the downstream area by this forest fire. It is considered that this is because the burnt area was small compared with the river basin area. 	<p>6.2</p> <p>6.3</p> <p>6.4</p> <p>6.4</p> <p>6.4</p> <p>6.5</p>
Comprehensive evaluation system	<ul style="list-style-type: none"> ● We prepared the environmental monitoring database that collects measurement data obtained inside and outside JAEA and open the data to the public. ● We prepared the integrated analysis support environment that releases the analytical tools developed by JAEA and the accompanying research results ● We prepared the environmental recovery knowledge base that presents knowledge inside and outside JAEA in a Q&A format with easy-to-understand words according to the user's knowledge and interest level. 	<p>7.2</p> <p>7.3</p> <p>7.4</p>

1.5 Outline of this report

This report is a summary of the research results that have been obtained in environmental dynamics research conducted by JAEA in Fukushima Prefecture. The outline of each chapter is as follows.

In the Chapter 1, we give an outline of the long-term environmental dynamics research in Fukushima Prefecture.

The Chapter 2 deals with the knowledge obtained for the environmental dynamics of radioactive cesium and air dose rates in forests.

In the Chapter 3, we present the knowledge obtained for the environmental dynamics of radioactive cesium in river systems.

The Chapter 4 describes the results for environmental dynamics of radioactive cesium and air dose rates in city areas.

In the Chapter 5, we present the results obtained for the mountain fire accident occurred in Mt. Juman, Fukushima Prefecture.

The Chapter 6 gives an outline of the comprehensive evaluation system prepared by JAEA to transmit the information on the Fukushima environmental dynamics research.

In the Chapter 7, we summarize the above results, and describe the present subjects in environmental dynamics research and present its future perspective.

In the final Chapter 8, future subjects of studies presented above are summarized.

2 Forest dynamics

2.1 Outline

In the area contaminated with radioactive materials due to the 1F nuclear accident, air dose rates have generally been decreasing compared to those just after the accident. However, in the areas of Hamadori District and Abukuma Mountains, especially in the northwest and southwest directions of the 1F, there remains region where the air dose rates are still high (Nuclear Regulatory Commission, 2018²); Nuclear Regulatory Agency³); Fig. 2.1-1). Since the high air-dose-rate regions are mostly occupied by mountain forests (Ministry of Agriculture, Forestry and Fisheries⁴); The Earth Observation Research Center, Japan Aerospace Exploration Agency, 2012⁵); Fig. 2.1-1), it is important to understand the dynamics of radioactive cesium in mountain forests to make the measures for environmental restoration. Comparing the geographical conditions of Fukushima and the areas affected by the Chernobyl nuclear accident (Belarus Republic and Ukraine), the annual precipitation in Fukushima is about twice as large, and there are lots of mountains and hilly areas in Fukushima (Japan Meteorological Agency⁶); edited by National Astronomical Observatory of Japan, 2016⁷). This means that materials are potentially easy to migrate in Fukushima compared with the region affected by the Chernobyl nuclear accident. Therefore, as to the environmental dynamics of radioactive cesium in forests, it would be important to estimate the migration of radioactive cesium especially amount of cesium outflow from forests considering various forest environments. Furthermore, in order to restart the use of forest resources, it will be important to know the distribution of radioactive cesium in various parts of forests and its migration into the forest products based on the distribution change over the years. In addition, due to the cancellation of the evacuation order and progress of residents' return, the opportunities for activities in forests and its surroundings are expected to further increase. In order to avoid unexpected radiation exposure in forests and make the appropriate measures for reducing the radiation exposure, it is essential to develop the tools for future prediction of air dose rates in forests and its surroundings.

The investigation on the migration of radioactive cesium in trees showed that the movement of sap may contribute to the cesium migration. Also, the investigation of the outflow from forests revealed that the rate of radioactive-cesium outflow from a non-decontaminated forest was less than 1% of the total deposition amount of radioactive cesium in the forest, which means that radioactive cesium tends to remain in forests. From these results, we clarified that it is important to investigate and observe the distribution of radioactive cesium in forests and predict its transfer into forest products. For the area where the decontamination has been conducted, the investigation revealed that the amount of radioactive-cesium outflow was about 3.5 times that for non-decontaminated area, and the rate of the outflow from the forests was less than 1% of the total amount of the deposition. Furthermore, it was also found that the amount of radioactive-cesium outflow decreased to one third because the coverage (area ratio where a forest floor is covered with the litter and the understory vegetation) that had been 30% just after the decontamination recovered to about 60%. From these results, it was elucidated that the increase in the outflow amount due to the decontamination ended in nearly one year, and it recovered to the same level as that for non-decontaminated area in the second year after the decontamination because of the recovery of the vegetation. These results were reported to the local governments and used as basic materials for briefing sessions for residents held by the local governments.

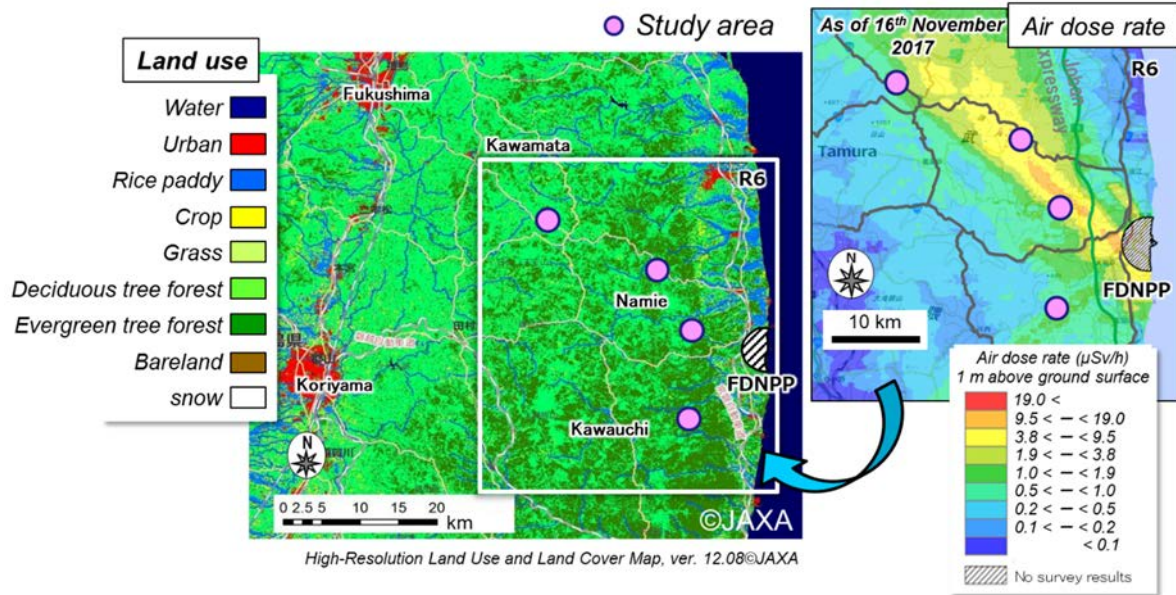


Fig. 2.1-1 Air dose rate and land use.

For air dose rate map, the results of aerial monitoring by the Nuclear Regulatory Agency were used (Extension Site of Distribution Map of Radiation Dose/Map of the Geographical Survey Institute)³⁾. For land use map, the JAXA High Resolution Land-Use and Land-Cover Map in Japan (All over Japan, ver.12.08) by Earth Observation Research Center (EORC)⁵⁾, Japan Aerospace Exploration Agency (JAXA) was used.

FDNPP ; Fukushima Daiichi Nuclear Power Plant, Tokyo Electric Power Company Holdings. Inc.

2.2 Dynamics of dissolved radioactive cesium in forests

2.2.1 Objectives

At the accident caused by the Great East Japan Earthquake in March 2011, radioactive materials have fallen mainly in the east part of Fukushima Prefecture (Chino et al., 2011)⁸⁾. Among the radioactive materials, a large amount of radioactive cesium that has relatively long half-life is still remaining in the environment. For deciduous forests, radioactive materials released by the accident were deposited on the forest floors and branches/bark in trees because it was before shooting buds at the time of the accident. For evergreen coniferous forests, they were deposited on the forest floors and foliage/bark in trees.

Radioactive cesium deposited on a forest floor existed mostly in the litter layer just after the accident. Since radioactive cesium is strongly adsorbed on clay minerals, it is now mostly trapped at the surface of soil layer. It was found that the amount of radioactive cesium outflowing from forests was less than 1% of that deposited on the forest floor (Niizato et al., 2016)⁹⁾. Therefore, it is expected that radioactive cesium will remain in forests for a long time. Fig. 2.2-1 shows the possible migration behavior of radioactive cesium in a forest. It was reported that the radioactive materials attached to trees are incorporated into plants through tree barks (Mahara et al., 2014¹⁰⁾; Wang et al., 2016¹¹⁾). Thus, radioactive cesium was detected not only on barks but also in sapwood and heartwood (Kuroda et al., 2013)¹²⁾. Considering the fact that the radioactive cesium was observed inside of leaves that came out after the accident (Kanasashi et al., 2015)¹³⁾, it was suggested that radioactive cesium migrated in the body of tree. Although it is considered that radioactive cesium migrates in a tree with water, the detailed mechanism has not been clarified. In this chapter, we present the results of the investigation on the distribution of radioactive cesium in broad-leaved trees, the migration of radioactive cesium in dissolved state, and the migration of dissolved radioactive cesium outflowing from litter in forest floor.

2.2.2 Methods

a) Distribution of radioactive cesium in broad-leaved trees and migration of dissolved radioactive cesium

As test tree samples, we used bushy *Acer rufinerve* (a type of maple) taken at Irikubo, Yamakiya District, Kawamata Town, Date County, Fukushima Prefecture. The sap samples were taken from March to April of 2016. The sap was collected by the following procedure. A hole (diameter: 6.5mm, depth: 5.5 cm) was made with a drill on a relatively broad trunk among bushy trees. Then, a plastic tube was inserted in the hole, and the sap was collected in a polypropylene container of 2 L capacity using a silicone tube (Fig. 2.2-2). After being filtrated by a membrane with 0.45 μm pores, the sap was put in a U8 container, then the radioactivity was measured. The tree samples (bark, timber, and branches/leaves) were taken in September 2016. The sample was dried at 105°C until the weight became constant. After pulverizing, the sample was put in a U8 container, then the radioactivity was measured.

At the same area, we collected young tree of *Eleutherococcus sciadophylloides* (Japanese name: Koshiabura) that were about 1-3 year-old trees (Tree height: 15 cm, 25 cm, 107 cm). And we collected the whole tree; above-ground parts (branches, leaves, stem) and under-ground parts (roots). After dried at 105°C

to constant weight, these samples were crushed and were put into U8 container (100 mL volume) and analyzed for radioactivity.

b) Migration of dissolved radioactive cesium from litter in forest floor

As test samples, fruiting body of *Gymnopus peronatus*, a kind of deciduous degradable fungi, and fallen leaves at the generating places of fruiting body were taken at Irikubo, Yamakiya District, Kawamata Town, Date County, Fukushima Prefecture, in September 2017 (Figs. 2.2-3 and 2.2-4). For litter layer, sample water in litter layer was first extracted (Figs. 2.2-5 and 2.2-6). Then, the litter was dried at 105°C until the weight became constant. After pulverizing, the sample was put in a 100 mL U8 container, then the radioactivity was measured. Further, fallen leaves at the generation places of fruiting body were put in a 1 L plastic container, then cultivated at 25°C under aerobic condition for 65 days. Water was extracted from the fallen leaves after the cultivation, and then the fallen leaves were dried at 105°C until the weight became constant. After pulverizing, the sample was put in a U8 container, then the radioactivity was measured. Water extracted from fallen leaves was filtrated by membrane with 0.45 μm pores. Then it was put in a U8 container, and the radioactivity was measured.

The transfer coefficient from fruiting body to litter or soil was calculated by the following equation,

Transfer coefficient (TF) =

$$[\text{^{137}Cs in a plant body (Bq/kg-DW)}] \times [\text{^{137}Cs in soil or litter (Bq/kg-DW)}]^{-1}$$

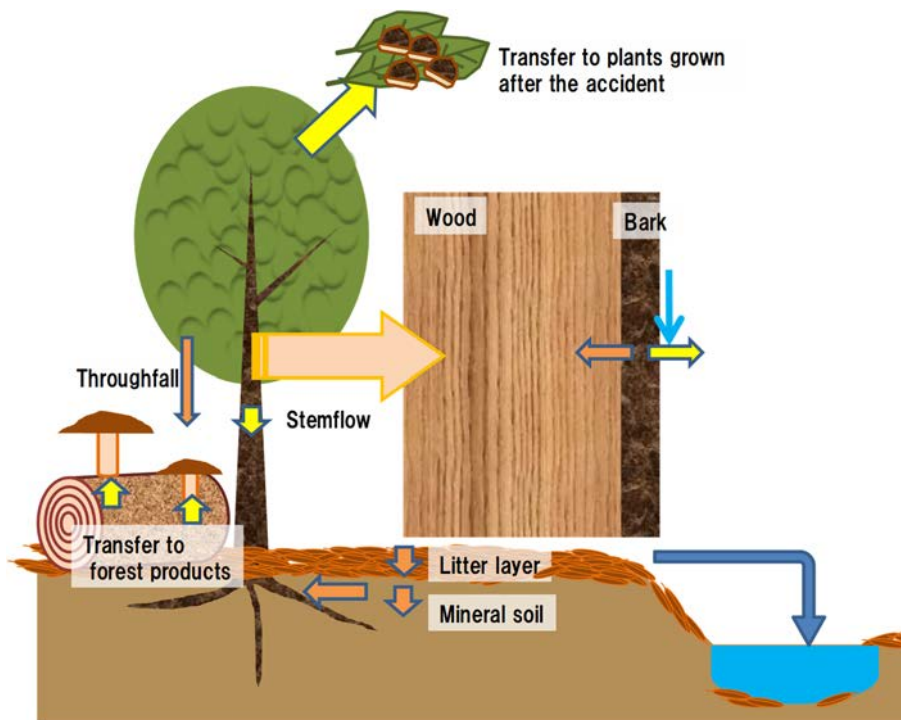


Fig. 2.2-1 Migration of radioactive cesium in forest ecosystem.



Fig. 2.2-2 Taking sap sample from *Acer rufinerve*.



Fig. 2.2-3 *Gymnopus peronatus*
(Forest floor of sampling place).



Fig. 2.2-4 Mycelium grown in fallen leaves.



Fig. 2.2-5 Collecting effluent from fallen
leaves.



Fig. 2.2-6 Effluent taken from fallen leaves.

2.2.3 Results and discussion

a) Distribution of radioactive cesium in broad-leaved trees and migration of dissolved radioactive cesium

Water in soil is absorbed from root hair of a tree with minerals, and transported to the xylem. In the case of conifer, the absorption of water from the root depends on the tensile force by the evaporation. Although the driving force of upward water flow in broad-leaved trees (dicotyledon) has not yet been clarified, it is presumed that roots actively lift water like the upward water transfer in a sponge cucumber (Kuroda, 2008)¹⁴⁾. It was observed that the concentration of dissolved ^{137}Cs ($<0.45 \mu\text{m}$) in sap of *Acer rufinerve* collected in a month of early spring was 30.6 Bq L^{-1} . It was also found that radioactive cesium was contained in sap flowing in trees (Table 2.2-1).

The measurement of the autoradiography for bark revealed that radioactive cesium is inhomogeneously distributed on bark surface in a spot-like pattern. The result suggests that radioactive cesium deposited at the time of the accident was so hard to migrate that it was adsorbed on the bark surface without being dissolved. Such spot-like deposition of radioactive cesium was also reported for the other plants (Sasaki et al., 2016)¹⁵⁾. The measurement of the autoradiography for branches and leaves showed that radioactive cesium exists mainly in veins of leaves. It was found that radioactive cesium in the other parts was homogeneously distributed. Since veins of leaves consist of vascular tissue through which water and nutrients pass, it is considered that radioactive cesium migrates through these tissues. The spot-like signals were seen in twigs of the Stem1. These signals suggest that radioactive cesium was adsorbed on twigs that are slow to grow at the time of the accident (Fig. 2.2-7).

It was found that the concentration of radioactive cesium in a stem was the highest in the bark (inner bark+outer bark), and its concentration in the xylem was about one-tenth of that in the bark. We also found that the concentration of radioactive cesium in the branches and leaves was almost constant, and its concentration was almost the same as that in the bark where the concentration was the highest in the stem (Figs. 2.2-8 and 2.2-9). The results suggest that radioactive cesium is being supplied into newly generating branches and leaves. Since dissolved radioactive cesium was contained in sap, it is considered that radioactive cesium is being supplied with the sap into newly generating branches and leaves.

Some edible forest products that use the newly generated parts after the 1F accident as food are restricted in some areas of Fukushima Prefecture. *Eleutherococcus sciadophylloides* is a wild plants that have edible sprouts and restricted in a wide area. We investigated radioactive cesium depth profile in the soil, the amount of plants and the amount of radioactive cesium in the above-ground parts (leaves and stems) and underground parts (roots) of the young trees. According to the analysis, it was found that 90% or more of the roots were present at a depth of 0-10 cm soil that had a large amount of radioactive cesium (Fig.2.2-10). The roots also contained radioactive cesium at the same concentration as the aboveground parts, suggesting that the radioactive cesium has transferred to the underground parts as well as the aboveground parts of the plant (Ito et al., 2019)¹⁶⁾.

Table 2.2-1 Concentration of radioactive cesium in sap of *Acer rufinerve*.

Concentration of radioactive cesium (Bq L ⁻¹)	
¹³⁴ Cs	5.78
¹³⁷ Cs	3.06×10

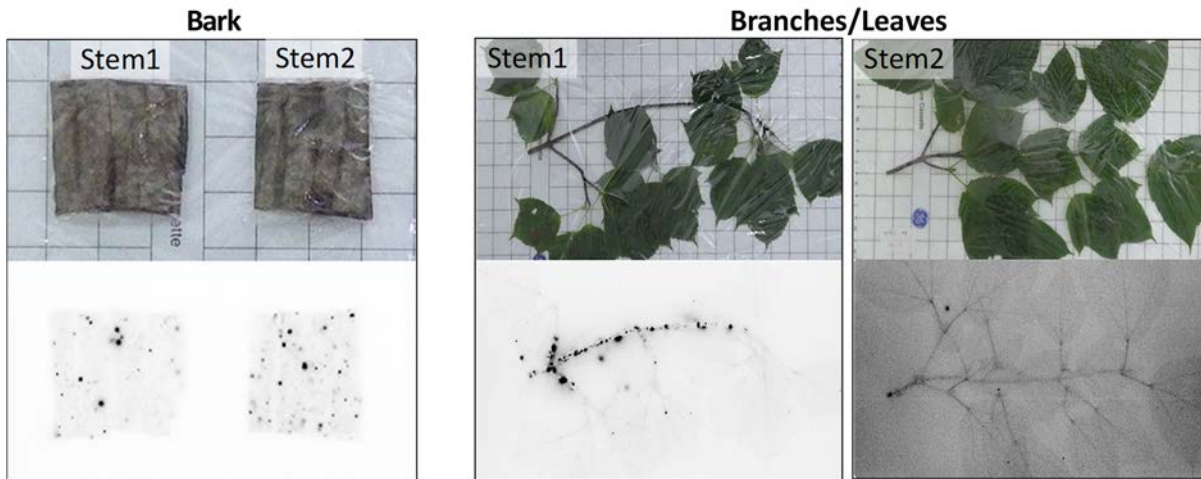


Fig. 2.2-7 Autoradiograph of bark and branches/leaves of *Acer rufinerve*.

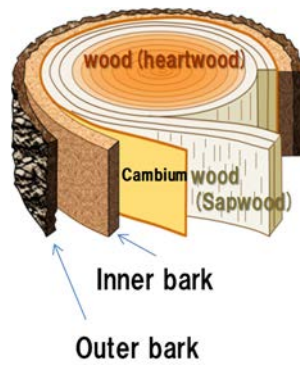


Fig.2.2-8 Anatomy of a tree trunk.

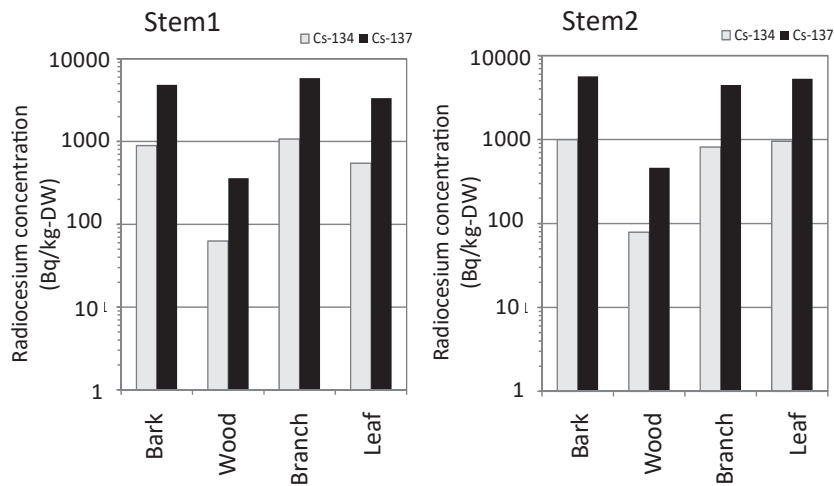


Fig. 2.2-9 Concentration of radioactive cesium in bark and branches/leaves of *Acer rufinerve*.

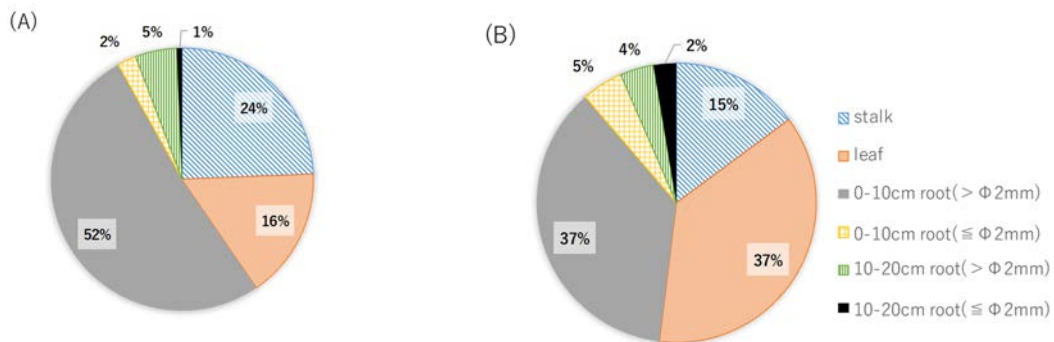


Fig. 2.2-10 Percentage of plant dry weight (A) and radioactive cesium content (B) for each part of *Eleutherococcus sciadophylloides*.

b) Migration of dissolved radioactive cesium from litter in forest floor

We found that hypha was attached to the surface of fallen leaves around the area where *Gymnopus peronatus*, a kind of litter-degrading bacteria, was growing (Figs. 2.2-3 and 2-2-4). As described above, radioactive cesium was contained in the leaves that had generated after the accident, and it was also contained in the fallen leaves. Fallen leaves are gradually decomposed by the action of organisms such as microorganisms and small insects. Although radioactive cesium is considered to migrate during the decomposition process of fallen leaves, its detailed mechanism has not yet been clarified. At least, it is presumed that radioactive cesium migrated from litter to fruiting body (mushroom) of litter-degrading bacteria. Here we report the investigation results for dissolved radioactive cesium outflowing from fallen leaves at litter-degrading bacteria growing points. The transfer coefficient of wood woollyfoot used as test samples was 1.2, and that taken at the other place in the forest was 1.7 (Table 2.2-2). It is known that a transfer coefficient of a fruiting body is widely distributed. Actually, the transfer coefficients of mushroom taken in this district widely ranged in the order from 0.1 to 10 (Table 2.2-2). The concentration of ¹³⁷Cs in forest rain water supplied to the forest floor was in the order of 10⁻¹ Bq L⁻¹, while that in water outflowing from litter

layer was about one-hundred times higher, i.e., 11.2 Bq L^{-1} . We also measured the concentration of dissolved ^{137}Cs in litter layer after cultivating in aerobic condition for 65 days. As a result, it was found that the concentration was 90.5 Bq L^{-1} (Table 2.2-3). We found that dissolved radioactive cesium further outflowed from the decomposed litter. The ratio of the concentration of radioactive cesium in decomposed litter to that in suspended radioactive cesium in outflowing water (decomposed litter/effluent) ranged from 1.1×10^2 to 7.5×10^2 . It was reported that the distribution coefficient (K_d) of radioactive cesium that is the concentration ratio of soil in equilibrium state in paddy field of Japan is $2,286 \text{ L kg}^{-1}$ (geometrical mean value) (Ishikawa et al., 2007)¹⁷⁾. Since the distribution coefficient (K_d) is a value in equilibrium state, we cannot simply compare, but we could at least say that radioactive cesium tends to easily outflow from litter. As described above, since radioactive cesium is strongly trapped in clay minerals, radioactive cesium sorbed in soil is hard to migrate. We found that water outflowing from litter contained more dissolved radioactive cesium than forest rain water. Since potassium and cesium belonging to the same group in the periodic table are essential elements in organisms, they are easily incorporated in organisms. Therefore, it is presumed that dissolved radioactive cesium is easily absorbed again through roots, in contrast to radioactive cesium adsorbed in clay minerals. In forests of konara oak (*Quercus serrata*), it was reported that rain water continuously flows in litter layer, which is called “litter flow” (Wakamatsu et al., 2016)¹⁸⁾. It is considered that rain water does not vertically sorbed in litter, but it migrates horizontally in litter layer carrying the dissolved radioactive cesium accumulated in the litter layer. There is another possibility that dissolved radioactive cesium generated by the litter decomposition migrates from litter layer to rivers.

Table 2.2-2 Concentration of radioactive cesium and its transfer coefficient for mushroom taken in Irikubo, Yamakiya District, Kawamata Town.

Species	Sampling time	Concentration of ^{137}Cs in fruiting body (Bq/kg-dry weight)	Concentration of ^{137}Cs in soil (S) or litter (L) near fruiting body (Bq/kg-dry weight)	Transfer coefficient
<i>Tylophilus eximius</i>	July, 2016	2.1×10^3	2.8×10^4 (S)	0.08
<i>Amanita virosa</i>	August, 2016	1.2×10^4	5.0×10^4 (S)	0.24
<i>Boletus speciosus</i>	August, 2016	5.4×10^3	2.3×10^4 (S)	0.23
<i>Ramaria flava</i>	August, 2016	3.5×10^4	3.0×10^4 (S)	12
<i>Pseudoaustroboletus valens</i>	August, 2016	7.3×10^4	3.0×10^4 (S)	2.4
<i>Amanita caesareoides</i>	August, 2016	3.3×10^4	1.6×10^4 (S)	2.1
<i>Leccinum extremiorientale</i>	August, 2016	9.4×10^4	4.2×10^4 (S)	2.5
<i>Leccinum extremiorientale</i>	August, 2016	8.7×10^4	2.7×10^4 (S)	3.2
<i>Leccinum extremiorientale</i>	August, 2016	6.9×10^4	3.7×10^4 (S)	1.8
<i>Gymnopus peronatus</i>	September, 2016	1.1×10^4	6.8×10^3 (L)	1.7
<i>Gymnopus peronatus</i> *	September, 2016	1.0×10^4	8.4×10^3 (L)	1.2

* Effluent extracted from litter

Table 2.2-3 Concentration and its ratio for radioactive cesium in litter and effluent at wood woollyfoot growing place.

		Concentration of ^{137}Cs	Ratio of ^{137}Cs concentration (litter/effluent)
Just after sampling fruiting body	Litter (Bq kg ⁻¹)	8.43×10^3	7.5×10^2
	Effluent (Bq L ⁻¹)	1.12×10	
65 days after sampling fruiting body	Litter (Bq kg ⁻¹)	9.76×10^3	1.1×10^2
	Effluent (Bq L ⁻¹)	9.05×10	

2.2.4 Future subjects

As described above, the investigation of radioactive-cesium migration in tree bodies revealed that the movement of sap possibly contributed to the migration of radioactive cesium. In order to clarify the future migration behavior of radioactive cesium in forests, it is necessary to investigate the changes in the concentration over the years and the migration of radioactive cesium into underground such as roots. Thereby, we can estimate the flux of radioactive cesium in whole trees. Based on such investigation, we will be able to obtain the basic data that predict how concentration of radioactive cesium in timber will change, towards the regeneration of forestry. Also, it is necessary to clarify the role of sap as a transfer medium in the migration of radioactive cesium in future.

We have elucidated that radioactive cesium in dissolved state is easy to outflow from litter (organic materials) with high bioavailability. From now, it is needed to clarify the dynamics of radioactive cesium in organic materials that are decomposed through various processes. Also, it is necessary to clarify how radioactive cesium migrates to organisms mainly in forest products, such as the migration from litter to litter or that from litter to soil.

2.3 Distribution and outflow of radioactive cesium in forest area

2.3.1 Objectives

When we look at the material transfer process in forest areas, radioactive cesium is considered to move from tree crowns to the forest floor by throughfall, stem flow, and litterfall. For forest floor, radioactive cesium seems to outflow from the forest accompanied by soil erosion and surface water flow (overland flow). Therefore, we consider that we can understand the migration behavior of radioactive cesium in whole forest area by measuring the amount of cesium inflow and outflow based on the forest floor to which all migration processes in the forest are related (Fig. 2.3-1). In order to investigate the distribution of radioactive cesium in forest area, it is needed to divide a forest into two parts, i.e., the above-ground part (trees) and the belowground part (litter and soil layer). Further, we have to continuously measure the distribution in each part of tree and in soil at the depth direction, and their changes over the years. Through these investigations, it is expected that we can obtain the knowledge on the migration behavior of radioactive cesium in forest products and its mechanism. With respect to the migration of radioactive cesium in forest products and the generation of dissolved radioactive cesium, please refer to section 2.2, “Dynamics of dissolved Cs in forests”. Concerning the development of air-dose-rate prediction tools for forest area, please refer to chapter 5, “Modeling Research on Environmental Dynamics”.

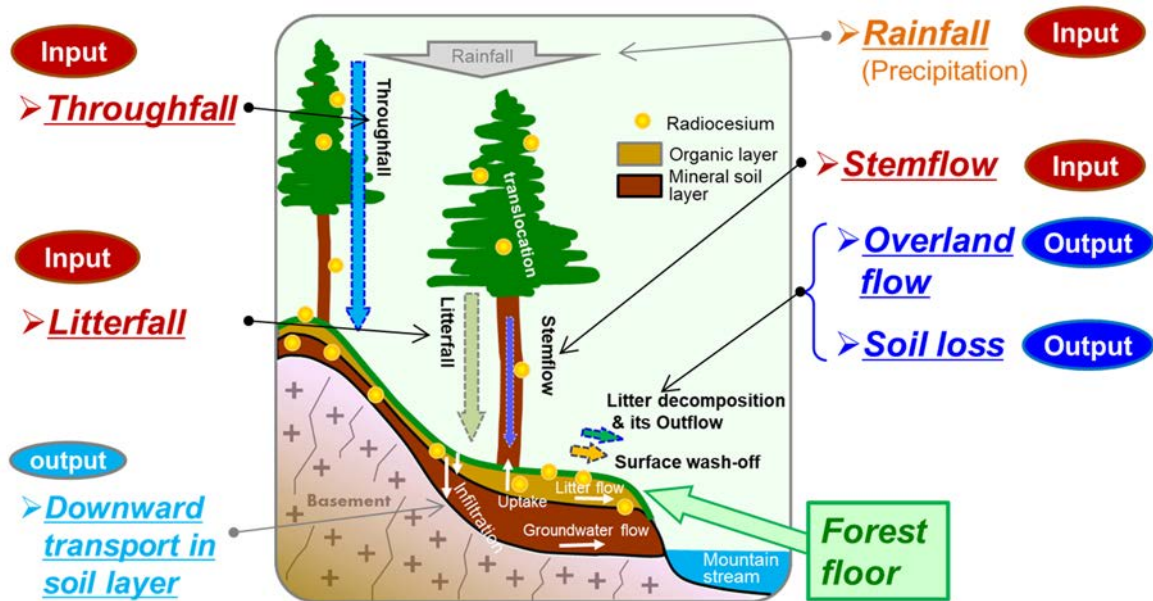


Fig. 2.3-1 Main processes of material transfer in forested environment.

2.3.2 Methods

(1) Investigation and observation on migration situation of radioactive cesium in forest area

Material transfer in a forest area is considered to depend on the kind of trees in the forest, topography, soil, weather and the situation of the forest floor. Therefore, we measured the amount of radioactive-cesium migration at several observation sites with different forest environment (Fig. 2.3-2) (Niizato et al., 2016)⁹⁾. In each site, we set an experimental plot whose four sides were surrounded by stainless steel plates. All of the soil and surface water flowing out from the plot was collected in the catchment box placed at the lower end of the plot. Also, a rain gauge for throughfall and a trap for stemflow/litterfall were set near the plot. By these apparatuses, we measured the migration of radioactive cesium, then collected samples (Fig. 2.3-3). The samples were taken at the interval of several weeks to several months depending on the weather. The pretreatments such as drying were carried out after taking samples. Then, concentration of radioactive cesium (Bq kg^{-1} or Bq L^{-1}) was measured by germanium (Ge) semiconductor detector. The amount of radioactive-cesium migration was obtained from the measured concentration multiplied by the total amount of the sample (kg or L). For the outflow from the experimental plot, the amount of radioactive-cesium migration per 1 m^2 was obtained from the measured result divided by the area of the experimental plot. In the case of stem flow, it was obtained from the measured result divided by the area of the tree branch (crown projection area). For throughfall, the amount of radioactive-cesium migration (Bq m^{-2}) was calculated by multiplying the rainfall amount ($\text{mm}=\text{L m}^{-2}$) by the concentration of radioactive cesium (Bq L^{-1}). Concerning litterfall, the sampling area was set to 1 m^2 square, then the amount of radioactive-cesium migration per 1 m^2 (Bq m^{-2}) was obtained by multiplying the dry weight (kg) of the litterfall sample by the radioactive-cesium concentration. For the forest environment of the observation sites, we conducted the inspection of vegetation, the measurement of topography and the investigation of soil. Also, we measured the temperature and rainfall using weather observation apparatuses placed at the observation sites. In addition, we referenced the data that are open to the public at the neighboring weather observation sites (for example, regional weather stations of the Ministry of Land, Infrastructure and Transport and the Japan Meteorological Agency). The coverage of forest floor (area where a forest floor is covered with the litter layer and the lower vegetation) in the experimental plot was calculated by analyzing the photograph of the forest floor when the coverage was low. In case the coverage was high, it was obtained by the exposed area of soil layer that was measured at the site.

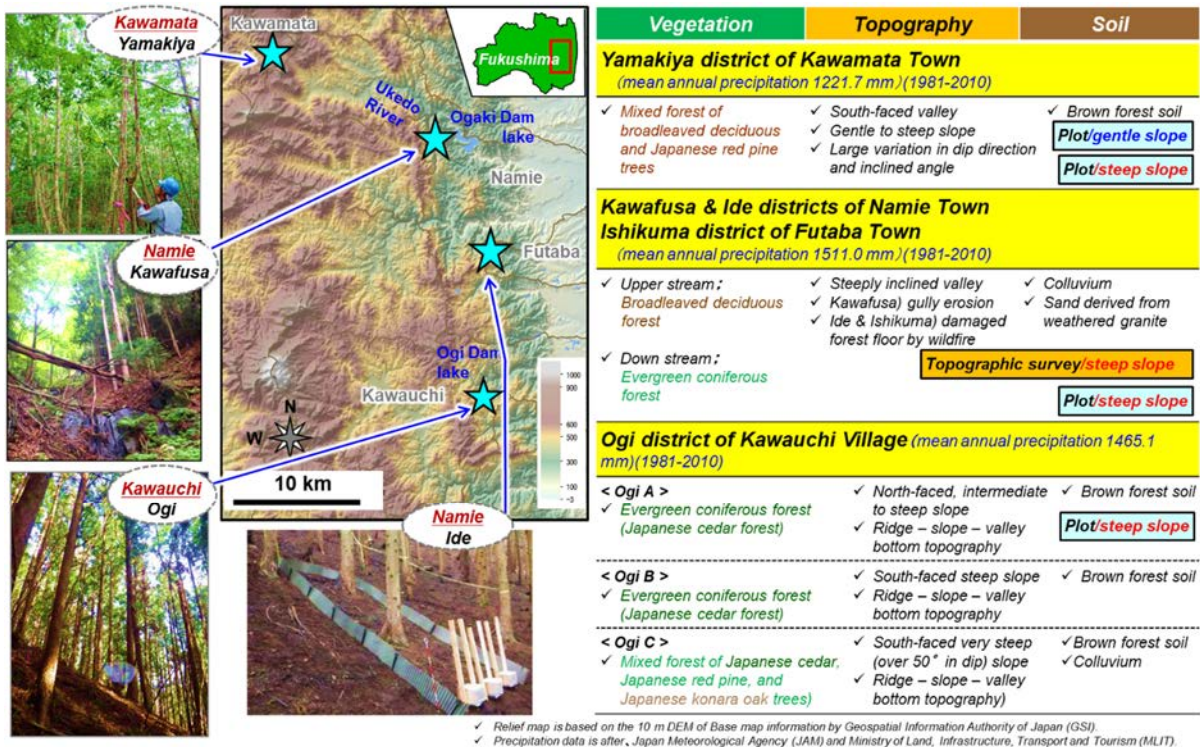


Fig. 2.3-2 Study area.

The shaded-relief map was cited from the results of the aerial laser measurements by the Geospatial Information Authority of Japan. For the precipitation in Ide District, Namie Town and Kawauchi Village, the data from the Meteorological Agency were used. For the rainfall in Kawamata Town, the data from the Water and Disaster Management Bureau, Ministry of Land, Infrastructure and Transport were used.

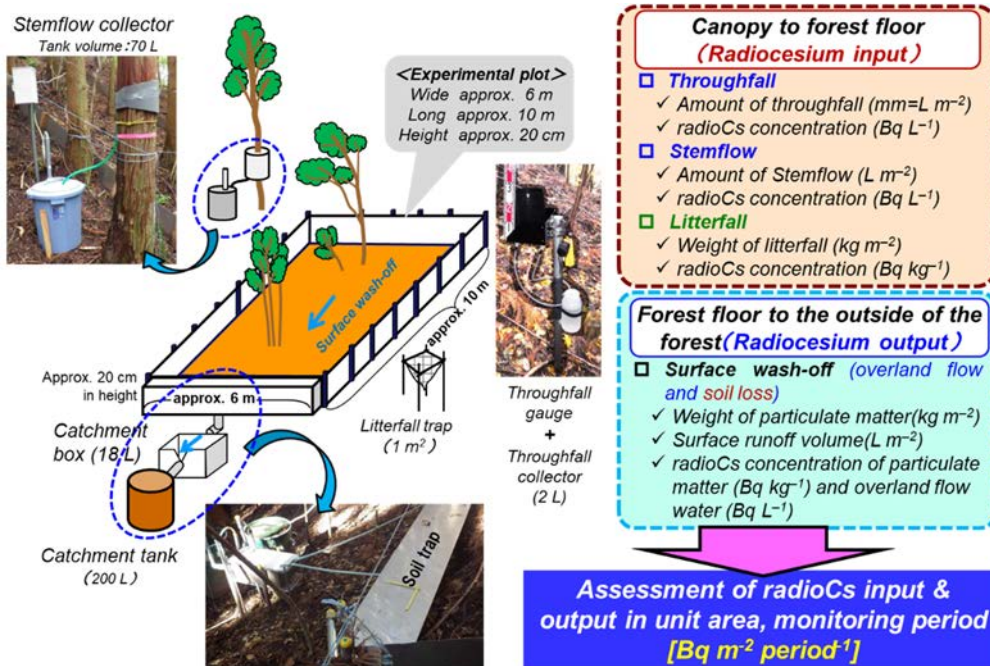


Fig. 2.3-3 Outline of experimental plot set in a forest.

(2) Observation of radioactive cesium outflow in mountain area

The measurement of radioactive-cesium inflow and outflow at the observation site was limited to the area where the observation frame and the instruments can be placed. However, in Abukuma Mountains, there are lots of steep and thin-soil mountain forests (mountain areas) designated as the soil Erosion Control Forest where it was difficult to set the instruments. In these mountain areas, the amount of radioactive-cesium outflow is expected to be large compared with that in village-vicinity mountain, because the amount of sediment outflow is large. Therefore, we used the erosion control dam at the small basin exit in mountain area as an apparatus for sampling sediment. Using this erosion control dam, we measured the amount of radioactive cesium outflowing from the river basin (Fig. 2.3-4 left ; Watanabe et al., 2017¹⁹). The river basin area measured by the erosion control dam was 2.1 ha, and the outflowing sediment was deposited within several meters of the upstream of the dam. For this reason, the survey with the three-dimensional (3D) laser scanner was repeatedly conducted once a year in this region. Based on the changes in the ground surface measured by the survey, we calculated the changes in the amount of sediment deposited on the erosion control dam (Fig. 2.3-4 right). Using the 3D laser scanner, we were able to obtain the coordinate data on material surface in a unit of mm at about 1 cm interval in a short time. Therefore, we could clarify the detailed amount of sediment deposited on the erosion control dam where large amount of sediment outflow is expected. Furthermore, we estimated the amount of radioactive cesium migrating from the mountain forest near the erosion-control-dam area to the dam by the weight of sediment multiplied by the concentration of radioactive cesium in deposited sediment taken in the erosion control dam (Watanabe et al., 2017)¹⁹. The amount of outflow and the outflow rate of radioactive cesium from river basin were calculated by the following equations,

$$C_{S_{out}} = S_i \times D \times C_{S_{conc}}, \quad C_{S_{rate}} = C_{S_{out}} / (C_{S_{depo}} \times A),$$

where $C_{S_{out}}$ is amount of ^{137}Cs outflow from river basin [Bq], S_i is amount of increase in sediment [m^3], D is density [kg m^{-3}], $C_{S_{conc}}$ is concentration of ^{137}Cs radioactivity [Bq kg^{-1}], $C_{S_{rate}}$ is outflow rate of ^{137}Cs from river basin [%], $C_{S_{depo}}$ is amount of ^{137}Cs deposition in river basin [Bq m^{-2}], and A is area of river basin [m^2].

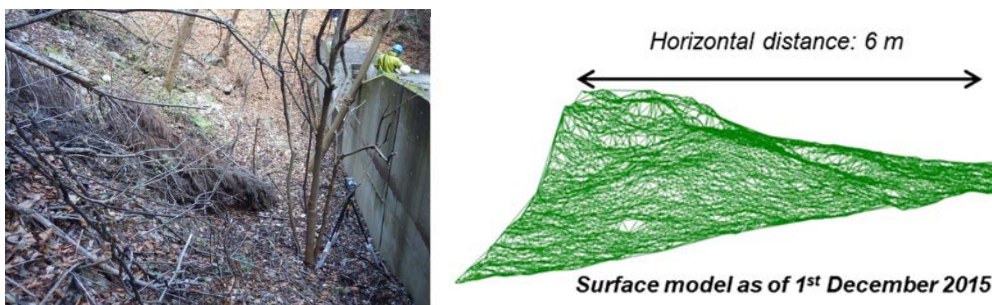


Fig. 2.3-4 Situation of the upstream of erosion control dam (left photograph: Kawafusa District, Namie Town) and surface model produced by the surveying data using 3D laser scanner (right figure).

(3) Investigation of radioactive-cesium distribution in forest area

As to the distribution of radioactive cesium in forest area, we compared the aboveground part (trees) and belowground part (litter and soil layer). Also, we investigated the situation of the radioactive-cesium distribution in each part of tree on the ground and its depth distribution in belowground soil. In addition, we conducted the inspection on the change in the distribution situation of radioactive cesium over the years. For trees on the ground, we measured the amount of radioactive cesium in cedar plantation forests that abound in Fukushima Prefecture. In the measurements, we first measured the diameter of all standing cedar trees (diameter of trunk at 1.3 m height; breast-height diameter), then samples were taken by cutting down five trees with most frequent breast-height diameter (Fig. 2.3-5). Since it is known that the concentration of radioactive cesium in a tree is different among bark, sapwood, and heartwood (Ministry of Agriculture, Forestry and Fisheries, 2016²⁰, etc.), we separated the cut-over tree into bark, sapwood, and heartwood. Then we measured the concentration of radioactive cesium in each part. Further, according to the method reported by Kajimoto et al. (2014)²¹, we measured the breast-height diameter and the height of the cut-over trees on the site. Also, we measured the density (volume density) of each part of the tree in the laboratory. Based on the measurement results, we calculated the standing trees biomass on the ground. From the biomass and concentration of radioactive cesium in each part of the tree, we calculated the amount of radioactive cesium accumulated in trees on the ground.

The sampling by cutting tree took long time for the cutting work and the sample pretreatment. In addition, standing trees were lost by the sampling. For these reasons, it was not possible to continuously investigate the same standing tree. Therefore, we obtained the samples from the same standing tree for several years without cutting down it by taking parts of the tree with a hatchet or increment borer (Fig. 2.3-6). The concentration of ^{137}Cs for each tree part obtained by this sampling method was compared by normalizing the deposition amount of ^{137}Cs at the sampling site.

Concerning the amount of belowground radioactive cesium, the deposited organic layer and soil layer were collected in the same cedar forest where the standing cedar tree was cut out. The deposited organic layer is divided into two kinds. One is the litter layer where fallen leaves and branches without decomposition are deposited. The other is the humus layer under the litter layer where fallen leaves and branches or a part of them are decomposed so much that their original forms are not clear. There was a possibility that the amount of radioactive-cesium accumulation was different depending on the degree of decomposition of fallen leaves and branches. Therefore, we collected the samples separately by distinguishing litter layer from humus layer. The soil layer was collected every 1 cm up to a depth of 20 cm with a scraper plate (Fig. 2.3-6). The amount of radioactive cesium was calculated from the radioactive-cesium concentration in the sample and its weight per 1 m².



Fig. 2.3-5 Sampling of the tree by cutting down.



Fig. 2.3-6 Method for sampling of soil and the tree.

2.3.3 Results and discussion

(1) Investigation and observation of migration situation for radioactive cesium in forest areas

For the observation site where the coverage of the forest floor exceeded 80%, the amount of ^{137}Cs outflow from 2013 to 2016 was less than 1% of the amount of the ^{137}Cs deposition at the observation site irrespective of the rainfall or vegetation in each year (Table 2.3-1). Except for the observation data in 2015 when the amount of outflow increased by the renovation work of the experimental plot, the amount of radioactive-cesium outflow from April to November in each year was in the range of 0.02–0.18%. Although the amount of radioactive-cesium outflow in gentle slopes tended to be lower than that in steep slopes, there was neither increase nor decrease in the outflow over the years. In addition, the amount of the ^{137}Cs outflow was nearly constant within each observation site (Table 2.3-1). As described later, radioactive cesium in forest soil was

remaining at 0–3 cm of the soil surface even in 2017, eight years since the accident (2.3.3(3)). Assuming the dry density of soil to be 1 g cm⁻³, the erosion depth at the experimental plot estimated from the amount of soil outflow was less than 1 mm in a year (Niizato et al., 2016)⁹⁾. With such extremely low erosion rate, it will take more than 30 years to erode forest soil by 3 cm. Therefore, we can consider that the clear change in the amount of radioactive-cesium outflow was not observed over the years, because radioactive cesium continues to be trapped in soil particles and the distribution depth of radioactive cesium is overlapped with the erosion depth of forest soil at present.

Table 2.3-1 Amount of ¹³⁷Cs outflow accompanied by soil loss.

The amount of ¹³⁷Cs deposition was taken from the 6th aerial monitoring data (Nuclear Regulatory Commission, 2018)²⁾.

The observation data from 2013 to 2014 were obtained by Niizato et al., (2016)⁹⁾.

For the amount of ¹³⁷Cs deposition and its outflow, the data were corrected to those on April 1, 2013 considering the radioactive decay.

Experimental plot	Ogi district, Kawauchi Villadge				Yamakiya district, Kawamata Town							
	KA-plot (Evergreen coniferous forest, Japanese cedar forest, steep slope)				KE-plot* (Deciduous broadleaved forest ; gentle slope)			KW-plot (Deciduous broadleaved forest, steep slope)				
Monitoring period	10 June 2013 – 18 Nov.	11 April 2014 – 8 Oct.	25 June 2015 – 28 Oct.	12 April 2016 – 15 Dec.	29 March 2013 – 19 Nov.	7 April 2014 – 20 Oct.	12 April 2016 – 29 Nov.	28 June 2013 – 19 Nov.	7 April 2014 – 20 Oct.	30 June 2015 – 5 Nov.	12 April 2016 – 29 Nov.	
Throughfall [mm]												
Monitoring period [mm]	518	914	748	1023	1101	1251	628	920	1251	484	628	
April – November [mm]	-	-	866	1399	-	-	672	-	-	737	672	
¹³⁷ Cs deposition [kBq m ⁻²]	487				497			497				
<small>*decay corrected on 1st April 2013</small>												
¹³⁷ Cs outflow via soil loss												
Monitoring period [Bq m ⁻²]	514	176	1200 ^{*1}	580	245	304	88	480	600	1900 ^{*1}	869	
April – November [Bq m ⁻²]	776	238	2333 ^{*1} (151) ^{*2}	571	253	377	89	810	744	3607 ^{*1} (180) ^{*2}	876	
Outflow rate[%] <small>(monsoon season, April – Nov.)</small>	0.16	0.05	0.48 ^{*1} (0.03) ^{*2}	0.12	0.05	0.08	0.02	0.16	0.15	0.73 ^{*1} (0.04) ^{*2}	0.18	

*1: Increase in the amount of outflow by the renovation work of the experimental plot.

*2: Values calculated excluding the effect of the renovation work of the experimental plot.

Throughfall in 2013 and 2014 represents the amount of rainfall outside forests (Observation site in Yamakiya District by the Water and Disaster Management Bureau, Ministry of Land, Infrastructure, and Transport²²⁾).

On the other hand, in the case of the observation site where the coverage of the forest floor is less than 30% due to the decontamination work or forest fire, the outflow rates tended to be high compared with the observation site with high coverage located in the same forest (Fig. 2.3-7). The ¹³⁷Cs outflow rate is 0.66% in the decontaminated area (0.18% in non-decontaminated area), and 2.58% in the burnt site (0.15% in unburnt sites). However, these outflow rates were not so high compared with those already measured in Fukushima Prefecture (Nishikiori et al., 2015²³⁾, etc.), and the values were included in the high group within the range of the past observation data. Further, even in mountain areas where the sediment outflow described later was expected to be the highest, the outflow rate of ¹³⁷Cs was estimated to be 0.36% in a year (Watanabe et al., 2017¹⁹⁾; 2.3.3(2)). From the above discussion, it was concluded that the outflow rate of ¹³⁷Cs from forest area was at most about several % in the place where the high outflow rate was expected from the viewpoint of the amount of rainfall, the slope of the land, and the coverage.

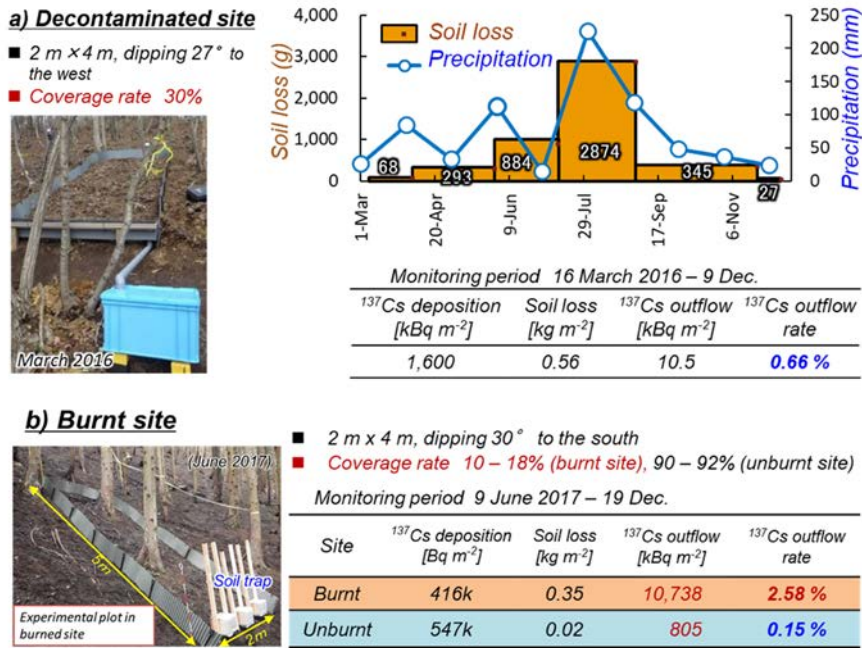


Fig. 2.3-7 Amount of ¹³⁷Cs outflow in decontaminated area (a) and burnt site by forest fire (b).

The results in the decontaminated area were obtained in Yamakiya District, Kawamata Town, and those in the burnt site were obtained in Ishikuma District, Futaba Town.

In forest areas, in addition to the ¹³⁷Cs outflow from the forest floor to outside of the forest, ¹³⁷Cs also migrates from tree crowns to the forest floor. In the present study, on the basis of the results obtained from 2013 to 2016, we compared the ¹³⁷Cs outflow from the forest floor to outside of the forest as well as the ¹³⁷Cs migration amount accompanied by the main transfer process from tree crowns, i.e., litterfall, stem flow and throughfall at each observation site and each year (Fig. 2.3-8). When we compare the ¹³⁷Cs migration amount from tree crowns to the forest floor with the outflow amount from the forest floor to outside of the forest, it was revealed that the migration amount from tree crowns exceeded the outflow amount irrespective of the observation site or observation year, except for the data in 2015 at the time of the renovation of the experimental plot. The ¹³⁷Cs outflow amount was almost within a certain range at each observation site although there was some increase or decrease as described above. On the other hand, the amount of migration from tree crowns to the forest floor tended to decrease from 2013 to 2016, although there was a difference in the absolute amount. In particular, we observed that the amount of the migration clearly decreased by litterfall and stem flow. The litterfall is a process where ¹³⁷Cs is mechanically eliminated from a tree by fallen leaves and branches, while the stem flow is a process in which ¹³⁷Cs is eliminated from a tree surface by washing. In these processes, it is considered that the amount of ¹³⁷Cs in trees was gradually decreasing.

If we assume that the amount of ¹³⁷Cs migration from tree crowns will decrease in future, it is estimated that the amount of ¹³⁷Cs migration will fall below that of the ¹³⁷Cs outflow or settle to the same level. In both cases, the amount of ¹³⁷Cs outflow and the amount of migration from tree crowns is expected to be about several % of the ¹³⁷Cs deposition amount at the observation site. Therefore, forest area tends to fix ¹³⁷Cs in the forest (the forest behaves as a sink of ¹³⁷Cs in environment; Niizato et al., 2016⁹⁾). Based on the observation results obtained from 2013 to 2016, it is considered that such tendency will continue in future.

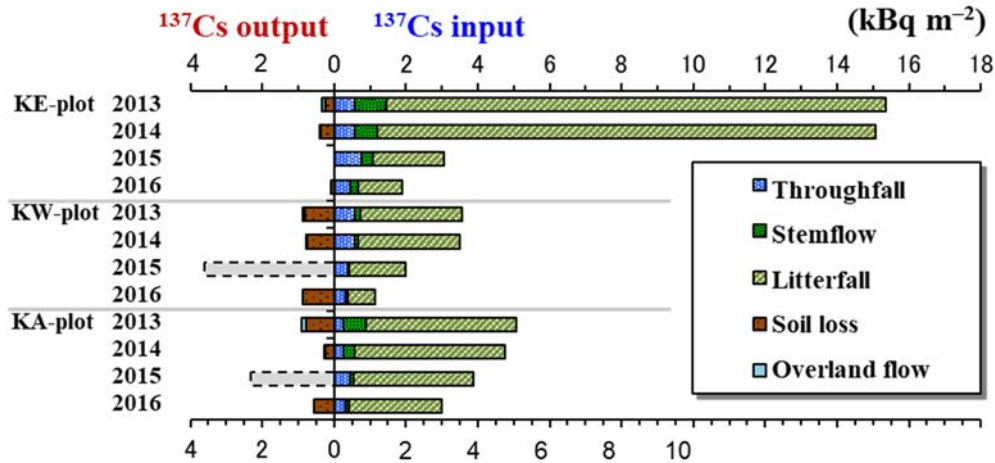


Fig. 2.3-8 Outflow and inflow of ¹³⁷Cs based on forest floor.

KE- and KW-plots ; Yamakiya District, Kawamata Town (KE, gentle slope ; KW, steep slope)

KA-plot ; Ogi District, Kawauchi Village (steep slope)

※: The observation data from 2013 to 2014 were obtained by Niizato et al., 2016⁹⁾.

※: For the amount of ¹³⁷Cs migration, the data were corrected to those on April 1, 2013 considering the radioactive decay.

※: The increase of the outflow in 2015 was due to the renovation work of the experimental plot.

※: For KE plot, the observation was not conducted in 2015 due to the renovation work of the experimental plot.

(2) Observation of radioactive-cesium outflow in mountain area

Table 2.3-2 shows the changes in sediment at the erosion control dam calculated from the land surface model. It was found that the sediment increased by 2.5 m³ in 36 months from 2013 to 2016. In particular, the increase of 1.8 m³ was concentrated in three months from September 2, 2015 to December 1, 2015. Further, it was estimated that the amount of ¹³⁷Cs deposited in the erosion control dam was 685 MBq in 36 months (Watanabe et al., 2017)¹⁹⁾.

As to the amount of precipitation and sediment outflow, the relation as a component of the equation for soil erosion runoff prediction such as USLE (Universal Soil Loss Equation) is well known (Wischmeier and Smith, 1978²⁴⁾; Hillel, 2003²⁵⁾). Therefore, it is considered that the intensive increase in the deposition amount from September 2015 to December 2015 was caused by the increase in the sediment transfer from the river basin to the erosion control dam due to the heavy rain at the time of the Typhoon No. 18 etc. This heavy rain was “Record-breaking heavy rain in the Kanto and Tohoku regions” (Japan Meteorological Agency, 2015)²⁶⁾. At the AMeDAS (Automated Me-teorological Data Acquisition System, Japan Meteorological Agency) station located 10 km northwest of the erosion control dam investigated, the rainfall amounted to 114 mm on September 9, 2015, 171 mm on September 10, 2015, and 90.5 mm on September 11, 2015. The maximum 72-hour rainfall reached 387.5 mm at 7:00 am on 11 September 2015 (Japan Meteorological Agency, 2015)²⁶⁾. The value significantly exceeded 296 mm on August 5–8, 1989 which was the maximum value so far, so the rainfall amount was the maximum as 72-hour precipitation in the observation history at that point. Considering that a heavy rainfall where the 72-hour precipitation amount exceeds 250 mm has occurred at every 10 years (Japan Meteorological Agency, 2018)⁶⁾, we were able to observe the amount of radioactive cesium flowing out with sediment due to the rarely heavy rain occurring once in 10 years or more (Watanabe

et al., 2017)¹⁹).

The amount of ¹³⁷Cs migrating from the river basin to the erosion control dam in 36 months was 1.08% (0.36% per year) of the total amount of the ¹³⁷Cs deposition in the river basin (Table 2.3-3). On the other hand, the results of the ¹³⁷Cs outflow at the experimental plot of the forest slope in Abukuma Mountains showed that the ¹³⁷Cs outflow rates in rainy season (from April to November) from 2013 to 2016 ranged from 0.05% to 0.18% (Niizato et al., 2016⁹); Section 2.3.2 (1)). Since the investigated river basin around the erosion control dam was designated as the erosion control forest to prevent sediment runoff (Fukushima Prefecture, 2017)²⁷), the amount of sediment outflow is considered to be large. However, except for the rarely heavy rain from September 2015 to December 2015, it was found that the outflow rate of ¹³⁷Cs migrating from the river basin to the erosion control dam was almost equal to that migrating from the forest slopes in the period of normal rainfall. From these results, even in the river basin where the amount of sediment transport was large like the mountainous area and the accompanied ¹³⁷Cs outflow rate was expected to be high, the ¹³⁷Cs outflow rates from the basin were as low as those from the other forests in case of normal rainfall (Watanabe et al., 2017)¹⁹).

Table 2.3-2 Increase in the amount of sediment and the amount of ¹³⁷Cs outflow at the erosion control dam (Watanabe et al., 2017)¹⁹.

Monitoring period	Increment of sediment [m ³]	Sediment ¹³⁷ Cs concentration (mean ± SD) [kBq kg ⁻¹]	¹³⁷ Cs outflow [MBq]
① 29 th Aug. 2013 – 3 rd Dec. 2014	0.5	261 ± 58	131 ± 29
② 3 rd Dec. 2014 – 2 nd Sept. 2015	0.1	399 ± 70	40 ± 7
③ 2 nd Sept. 2015 – 1 st Dec. 2015	1.8	271 ± 41	488 ± 74
④ 1 st Dec. 2015 – 1 st Sept. 2016	0.1	–	27 ± 4 *

*Estimation using the ¹³⁷Cs deposition of sediment collected on 1st Dec. 2015 (period ③)

Table 2.3-3 ¹³⁷Cs outflow rate at the erosion control dam (Watanabe et al., 2017)¹⁹.

Monitoring period	¹³⁷ Cs outflow rate converted per year		
① 29 th Aug. 2013 – 3 rd Dec. 2014	15 months	0.21% (0.17%)	0.27% (0.14%)
② 3 rd Dec. 2014 – 2 nd Sept. 2015	9 months	0.06% (0.08%)	
③ 2 nd Sept. 2015 – 1 st Dec. 2015	3 months	0.77% (3.1%)	
④ 1 st Dec. 2015 – 1 st Sept. 2016	9 months	0.04% (0.06%)	

(3) Distribution status of radioactive cesium in forest area

As described above in (1) and (2), the outflow rates of ¹³⁷Cs from forest area were in the order of several %. This means that forests tend to play a role in trapping ¹³⁷Cs in environment. In order to clarify the trapping mechanism of forests, the forest environment was divided into two parts; the aboveground part (mainly trees) and the belowground part (mainly litter and soil layer). Then, we investigated the distribution of radioactive cesium in forests and its changes over the years.

Distribution of aboveground and belowground radioactive cesium

From the investigation results at the plantation cedar forests in FY2015, it was revealed that the amount of ¹³⁷Cs deposited in trees on the ground was about 20 kBq m⁻², and the total amount of ¹³⁷Cs deposited in the belowground organic layer (litter layer and humus layer) and in soil layer was 250 kBq m⁻². The results showed that over 90% of the total ¹³⁷Cs was trapped in the belowground (Fig. 2.3-9). According to the results for deciduous broad-leaved forests (konara oak forests) and coniferous forests (cedar and cypress forests) by the other institutes (Imamura et al., 2017²⁸); Forestry Agency, 2018²⁹), the amount of ¹³⁷Cs in aboveground trees had decreased from 2011 to 2012, and the proportion of ¹³⁷Cs contained in the deposited organic layer and mineral soil in the belowground area had greatly increased. Further, it was reported that the amount of ¹³⁷Cs in trees was less than 7% in 2017 (Forestry Agency, 2018)²⁹). For this reason, the amount of the ¹³⁷Cs deposition in trees on the ground is considered to be about 10% of the total deposition amount in all forest environment in 2017, which suggests that about 90% of ¹³⁷Cs exists in the belowground region.

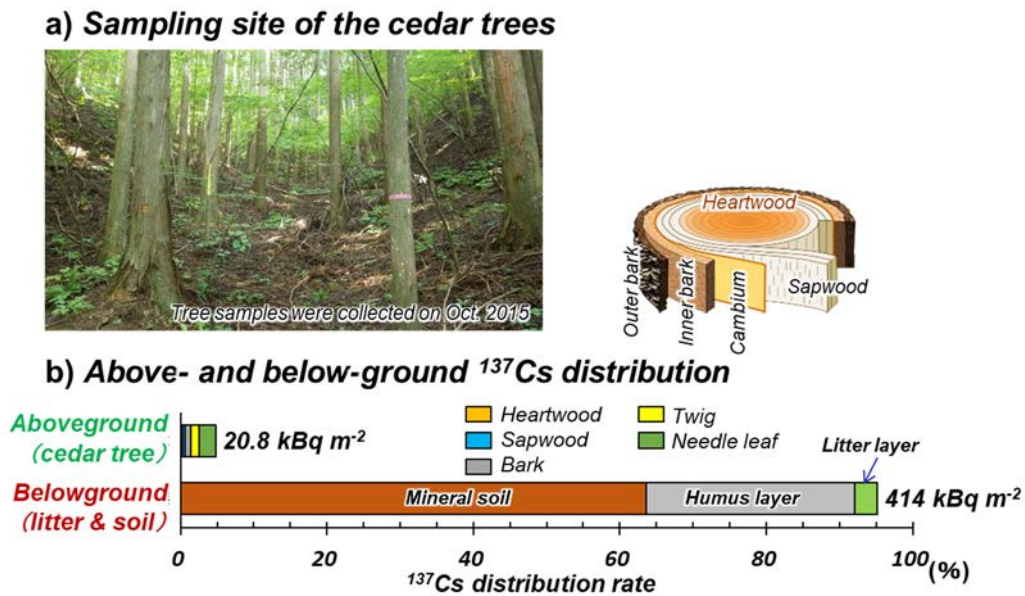


Fig. 2.3-9 Deposit amount of ¹³⁷Cs in the aboveground and belowground of plantation cedar forests (Ogi District, Kawauchi Village).

Distribution of radioactive cesium in trees on the ground

The concentration of ¹³⁷Cs in each part of a cedar tree was the highest in the bark, and then in the order of needle leaves, twigs and xylem (sapwood and heartwood) (Fig. 2.3-10 a)). In terms of breast-height diameter, it was found that the concentration of ¹³⁷Cs was extremely high in the bark of a cedar tree with a breast-height 15–20 cm at the forest edge and in needle leaves of cedar trees with a breast-height 25–30 cm along work roads in forests. However, the concentration of ¹³⁷Cs was generally in the order of bark, needle leaves, twigs, and xylem. On the other hand, the amount of ¹³⁷Cs deposition in each part of a tree was in the order of needle leaves, twigs, and bark, and it was the lowest in xylem (sapwood and heartwood), reflecting the ¹³⁷Cs concentration and biomass in each part of the tree. In contrast, the amount of ¹³⁷Cs deposition was high in large cedar trees, which have large biomass due to its large breast-height diameter (Fig. 2.3-10 b)). The similar

tendency of the ^{137}Cs concentration in each tree part was reported by the other institutes (e.g., Forestry Agency, 2018²⁹).

According to the investigation of pine forests around the Chernobyl nuclear power plant, it was reported that the ^{137}Cs concentration was high in twenty-year-old trees and low in sixty-year-old ones (Shaw et al., 2003)³⁰. The result was interpreted by the fact that young trees actively absorbed nutrients and the effect of dilution was small due to small biomass. The cedar trees investigated in the present study were estimated to be from 38 to 48 years old based on their annual rings. Since the ages of the present cedar trees were not so different among the trees, it is hard to consider the differences in bioactivity due to the age. Also, the biomass of a tree was proportional to the amount of ^{137}Cs deposition, so that there was no dilution effect. Here, it should be noted that the surface area of needle leaves, twigs and bark is considered to be proportional to their biomass. Therefore, if the initial deposition amount of ^{137}Cs was proportional to the surface area of needle leaves, twigs and bark, it can be considered that the difference between the ^{137}Cs concentration and its deposition amount in cedar trees investigated in the present study was due to the difference in the situation of the ^{137}Cs initial deposition related to the location and the biomass of the trees.

In order to analyze the changes in the ^{137}Cs concentration and its deposition amount in each tree part, it is necessary to estimate the amount of ^{137}Cs that was eliminated from the tree. For cedar forests in Kawauchi Village, the amount of the ^{137}Cs deposition in trees on the ground was 20 kBq m^{-2} as of 2015 (Fig. 2.3-9). In addition, the amount of ^{137}Cs migrating from tree crowns to the forest floor by litterfall, stem flow and throughfall, i.e., ^{137}Cs being eliminated from the tree, was calculated to be about $3\text{--}4 \text{ kBq m}^{-2}$ in a year from 2015 to 2016 (Fig. 2.3-8). From these observation data, it was revealed that about 15–20% of ^{137}Cs in trees was eliminated per 1 m^2 in a year. Considering that the main processes of the ^{137}Cs elimination from trees were litterfall, stem flow and throughfall, about $3\text{--}4 \text{ kBq m}^{-2}$ of ^{137}Cs was eliminated from needle leaves, twigs and bark in a year. When the amount of the ^{137}Cs elimination (kBq m^{-2}) was divided by the biomass (kg m^{-2}) of needle leaves, twigs and bark, the changes in the ^{137}Cs concentration can be estimated. As a result, it was obtained that the decrease in the ^{137}Cs concentration was about $700\text{--}900 \text{ Bq kg}^{-1}$ in a year. According to the investigation results of bark and xylem of 43–54-year-old cedar trees in Kawauchi Village (Fig. 2.3-11 b)) from 2015 to 2017, the decrease in the ^{137}Cs concentration was observed in only one sample (leftmost bar chart in Fig. 2.3-11 b)). Although the amount of concentration change exceeded the error range, it did not reach the change of the order. For the ^{137}Cs concentration in the other cedar trees, the values were almost constant or changing within a year, but it did not show clear changes over the years. The reason for obtaining such results are possibly that; 1) the amount of radioactive cesium deposition in each tree part was different because the sampling height (about 10 cm) and direction (about 20–45 degree) were slightly different in each year, or 2) the trees absorbed ^{137}Cs from soil through the roots. However, the investigation period was so short, about 2–3 years, that we have not yet obtained the clear conclusion.

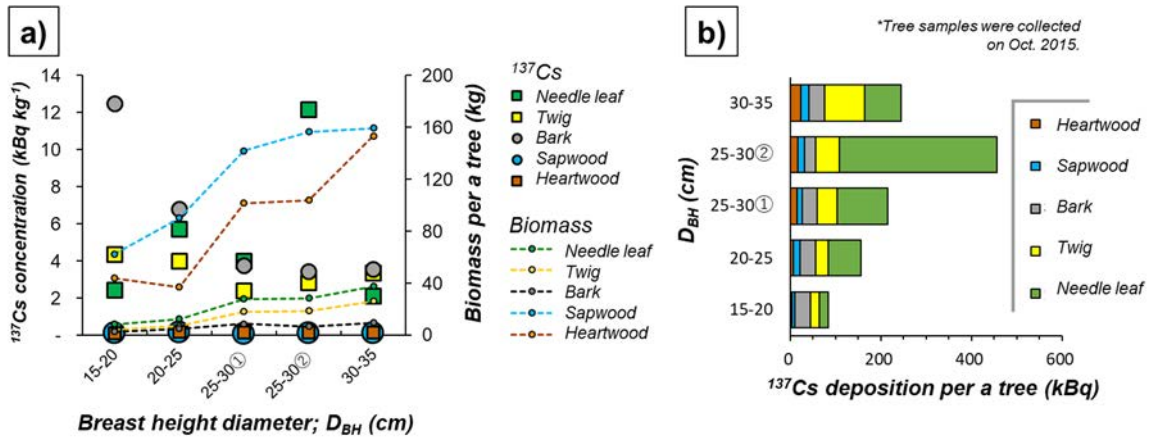


Fig. 2.3-10 Concentration and deposition amount of ^{137}Cs in each part of a cedar tree (Ogi District, Kawauchi Village).

a) ^{137}Cs concentration and biomass in each tree part, and b) amount of ^{137}Cs deposition in each tree part.

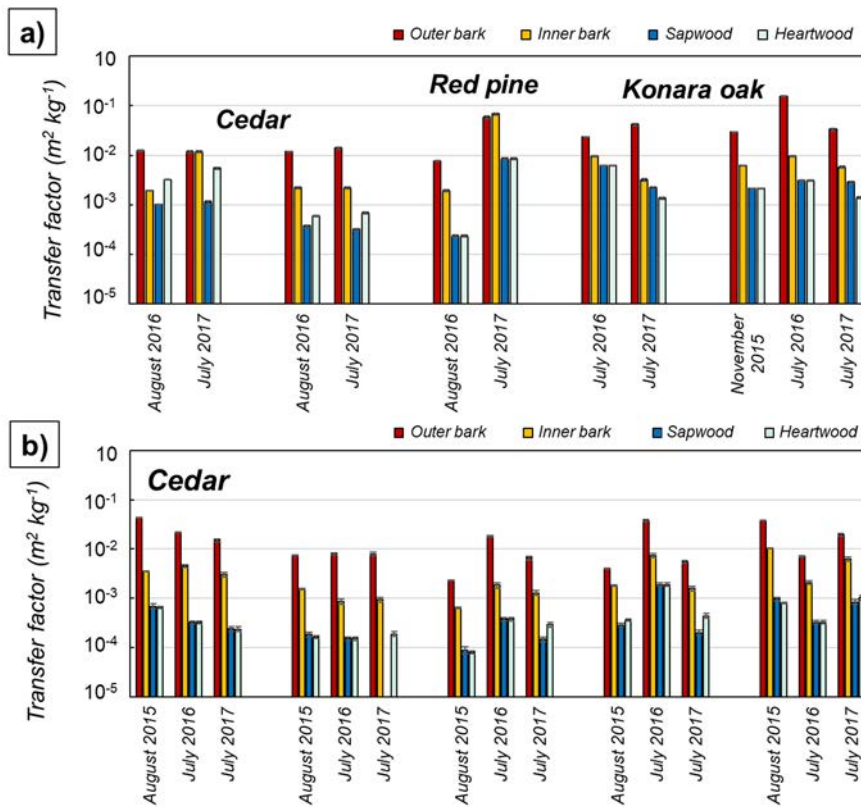


Fig. 2.3-11 Changes of ^{137}Cs concentration in each tree part over the years.

The error bar shows the measurement error.

a) Yamakiya District, Kawamata Town b) Ogi District, Kawauchi Village

The vertical axis represents the ^{137}Cs concentration normalized by the amount of ^{137}Cs deposition in soil at the sampling site.

Distribution of radioactive cesium in belowground litter and soil

In terms of the deposition amount of ^{137}Cs by depth, the depth distribution of ^{137}Cs in belowground litter layer and mineral soil showed a clear changing tendency (Fig. 2.3-12). The deposition amount of ^{137}Cs in litter layer showed the rapid decrease from July 2011 to December 2012. After that, slight fluctuations were sometimes observed, but it never increased although the decreasing rate gradually became low. On the other hand, the deposition amount of ^{137}Cs in soil layer showed a tendency to increase in parallel with the decrease of that in the litter layer. However, the depth distribution of the ^{137}Cs deposition in soil layer showed that most of ^{137}Cs exists in the depth from 0 to 3 cm. We could not observe any significant changes in the distribution since July 2014 (Fig. 2.3-12). From these results, it can be understood that ^{137}Cs had migrated from litter layer to soil layer since 2011, but it hardly migrated from the surface soil layer to the deeper layer. In conclusion, we can say that ^{137}Cs will be trapped in litter layer and surface soil within 3 cm depth for long time.

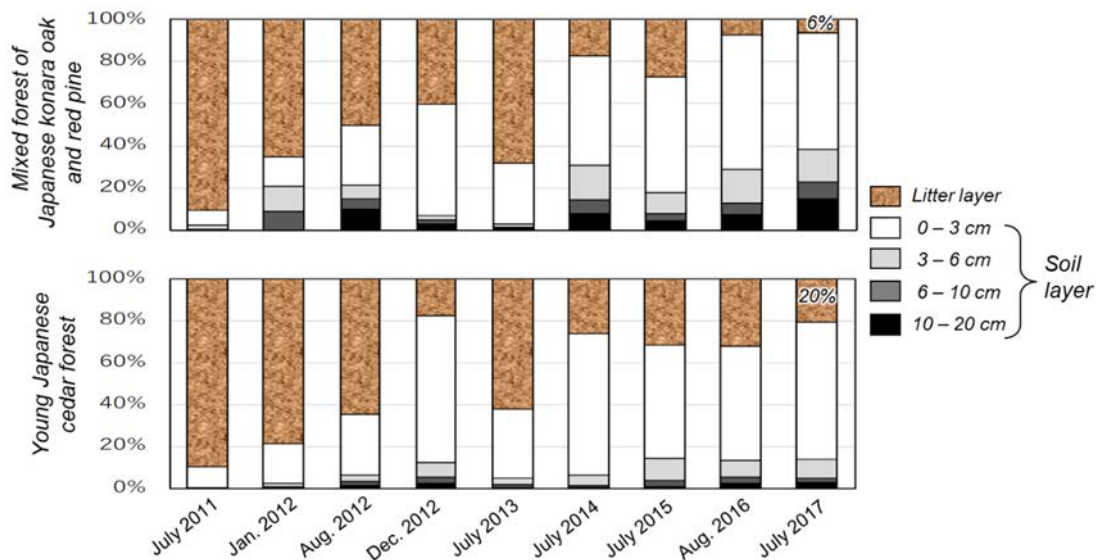


Fig. 2.3-12 Depth distribution of ^{137}Cs deposition in the belowground (Yamakiya District, Kawamata Town).

The vertical axis represents the ratio to the total deposition amount of ^{137}Cs in the belowground region of the sampling spot.

The data before July 2014 were taken by the Nuclear Regulatory Agency (2015)³¹).

2.3.4 Future subjects

To summarize the above discussion, the following conclusions were obtained.

- Migration of ^{137}Cs in forest and its outflow from the forest.
 - ✓ The outflow rate of radioactive cesium from non-decontaminated forest was about 0.1% in a year. The outflow rate tentatively became 2–3% in the decontaminated area and the burnt site. But it is presumed that the outflow rate again became lower than 1% with the recovery of the coverage (It will need about one year for the recovery.).
 - ✓ Even in the forest designated as erosion control forest where the sediment outflow was high, the rate

of the ^{137}Cs outflow in a year was less than 1%.

- ✓ The situation of the coverage (coverage rate) on the ground surface of forests considerably affected the outflow of ^{137}Cs . But the outflow rate of ^{137}Cs was estimated to be up to several %.
- ✓ The amount of ^{137}Cs migration from tree crowns to the forest floor was larger than that from the forest floor to the outside of the forest. Forests tended to behave as sink for radioactive cesium in environment.
- Distribution of radioactive cesium in forests
 - ✓ About 90% of ^{137}Cs was distributed in belowground litter layer and soil layer. On the ground, about 10% of ^{137}Cs was distributed in trees.
 - ✓ The amount of radioactive cesium in litter layer tended to decrease. About 5–20% of radioactive cesium was mostly trapped in soil layer shallower than 3 cm.
 - ✓ The trapped ^{137}Cs hardly migrated from top soil layer to the deep region. The ^{137}Cs will be trapped in litter layer and soil surface shallower than 3 cm for long time.

Regarding the change of the radioactive-cesium concentration in trees constituting the forest over the years, the investigation period was so short, 2–3 years, that we were unable to obtain the data that are enough to be used in the future prediction of the concentration. On the other hand, concerning the outflow of radioactive cesium in forests and out of forests, the satisfactory results described above were obtained based on the data taken in the 5-year investigation. As a future subject, it will become important to know the changes over the years concerning the amount of radioactive cesium in trees and its concentration in each part of a tree. It is needed to investigate and observe the amount of ^{137}Cs elimination from trees and the distribution of ^{137}Cs in each tree part as well as the changes in ^{137}Cs concentration over the years. The continuation of such investigation and observation will enable us to estimate the ^{137}Cs migration from soil to trees over the years. These data on the changes over the years will become the data by which the validity of the prediction results by the compartment model is confirmed. It would be important to continuously conduct such long-term study and let the prediction results be reliable, considering that such study will lead to future prospects for eliminating the anxiety in restarting the utilization of forest resources and conservation of forest environment.

2.4 Initial deposition behavior

2.4.1 Objectives

Radioactive cesium (Cs) was released into the environment by the accident, Tokyo Electric Power Company Holdings Inc. In order to predict how radioactive cesium will be eluted from the deposited materials and how it will migrate to the environment and biological system in future, it is essential to clarify the initial deposition behavior of radioactive cesium as to in which direction and what kind of chemical form it was deposited.

In this section, we describe the results of the investigation that had been conducted to clarify the initial deposition behavior of radioactive cesium. The results presented in this section are, (1) the evaluation of initial deposition amount of radioactive cesium investigated using lichens, (2) the investigation on the distribution of radioactive cesium that had been initially deposited in mountain forests, and (3) the evaluation of physicochemical properties of radioactive cesium particulates that had been initially deposited. For the result (1), we investigated the possibility in evaluating the amount of initial Cs deposition based on the concentration of radioactive cesium in lichens (symbiont of fungi and algae), focusing on lichens that has a property to trap atmospheric pollutants (Seaward, 2002³², NashIII, 2008³³). With respect to (2), we investigated the characteristic of the detailed distribution of remaining radioactive cesium deposited in mountain forests (Kitamura et al., 2014¹, Koarashi et al., 2012³⁴), which could not be clarified by the distribution map of air dose rate obtained by the aerial monitoring. Concerning (3), we focused on radioactive cesium-bearing microparticles (CsMPs) (Adachi et al., 2013³⁵, Abe et al., 2014³⁶, Yamaguchi et al., 2016³⁷, Satou et al., 2016³⁸, Ono et al., 2017³⁹) that they are one of the initial deposition forms of radioactive cesium. We investigated the distribution of CsMPs and their physicochemical properties, and developed an effective method to analyze CsMPs.

2.4.2 Methods

(1) Relationships between Cs activity concentration in lichens and Cs deposition

We have investigated lichens around the 1F (within a radius of about 60 km) from December 2012 to February 2013 at the sixteen points where air dose rates were different (Dohi et al., 2015)⁴⁰. In order to apply this method to a wide range of Japan in the future, we have collected 44 samples of 9 species of parmelioid lichens (Fig. 2.4-1) (Dohi, 2016)⁴¹ among lichens growing in cherry trees widely distributed in public places in Japan. These lichen species were identified as below: *Canoparmelia aptata* (Kremp.) Elix & Hale, *Flavoparmelia caperata* (L.) Hale, *Myelochroa leucotyiza* (Nyl.) Elix & Hale, *Parmotrema austrosinense* (Zahlbr.) Hale, *P. clavuliferum* (Räsänen) Streimann, *P. reticulatum* (Taylor) M.Choisy, *P. tinctorum* (Nyl.) Hale, *Punctelia borreri* (Sm.) Krog, and *P. rudecta* (Ach.) Krog. The concentration of radioactive cesium in lichens was measured by a cesium iodide (CsI) scintillation counter (FD-08Cs40, Techno-X Co, Ltd/). The activities for Cs in all lichen samples were decay corrected to that on the final sampling date (February 5, 2013). In order to evaluate the relationship between the concentration of radioactive ¹³⁷Cs in lichens and the initial ¹³⁷Cs deposition amount at the early stage after the accident, ¹³⁷Cs deposition density in soil at each sampling point was estimated by means of the GIS software (ArcGIS, ESRI) with the inverse distance weighted (IDW). The data for interpolation was based on the measurement results of radioactive cesium deposition in soil, which had been conducted by the Ministry of Education, Culture, Sports, Science and

Technology (MEXT, 2011)⁴²⁾⁴³⁾ between June and July of 2011 within a 100 km radius area from the 1F. The estimated deposition amount of ^{137}Cs in soil was also corrected to that on the final sampling date of lichen samples. Their correlation was evaluated by calculating the Spearman's rank correlation coefficient.

In order to compare and evaluate the storage capacity of ^{137}Cs among the nine lichen species, the aggregated transfer factor (T_{ag}) of ^{137}Cs per unit area (IAEA 2009)⁴⁴⁾ in soil-to-lichen was obtained. The significant differences in the data were evaluated by the non-parametric method (Steel-Dwass test, Mann-Whitney's test). For the details of these investigation methods, please refer to Dohi et al (2015)⁴⁰⁾.



Fig. 2.4-1 One kind of Parmelioid lichen species (Dohi, 2016)⁴¹⁾.

(2) Investigation of radioactive cesium distribution in mountainous area

We investigated radiation dose distribution of seventeen mountainous areas in total within 50 km from the 1F in Fukushima Prefecture, i.e., several mountains per each direction of the plume trajectory were selected (Fig. 2.4-2) (Dohi et al., 2016)⁴⁵⁾. As the back-pack measurement system “Hot Spot Finder (HSF)”, a radiation detector, (detector: CsI(Tl) scintillator) connected with GPS was adopted, and air dose rates at 1 m and 20 cm height were measured (Fig. 2.4-3) (Dohi et al., 2016)⁴⁵⁾. In some mountain areas, a gamma plotter system (GP) (Fig. 2.4-4) (detector: plastic scintillator) was used. The measurements had been performed from September 2015 to March 2017 focusing on the mountain trails. For some mountainous areas, a more detailed radiation dose distribution was investigated on two routes around the mountain trail that maintain constant altitudes and general mountain trails.

In three mountains near the 1F (Mt. Higakure, Mt. Juman, and Mt. Okura), the air dose rates were compared between our walking survey data and wide-range survey data by aerial monitoring (the tenth monitoring from September 12 to November 4, 2015) using the GIS software (ArcGIS, ESRI). For the comparison, the both radiation data were decay-corrected to those on November 4, 2015. The relation between altitude/land-coverage and air dose rate was investigated based on the Base Information in Geographic Information System (GIS), Geospatial Information Authority of Japan⁴⁶⁾, and the Land-Cover Map of the Earth Observation Research Center (EORC)⁴⁷⁾, Japan Aerospace Exploration Agency (JAXA) (Oda et al., 2016)⁴⁸⁾. For the details of the investigation methods and analytical methods, please refer to Dohi et al. (2016)⁴⁵⁾ and Oda et al. (2016)⁴⁸⁾.

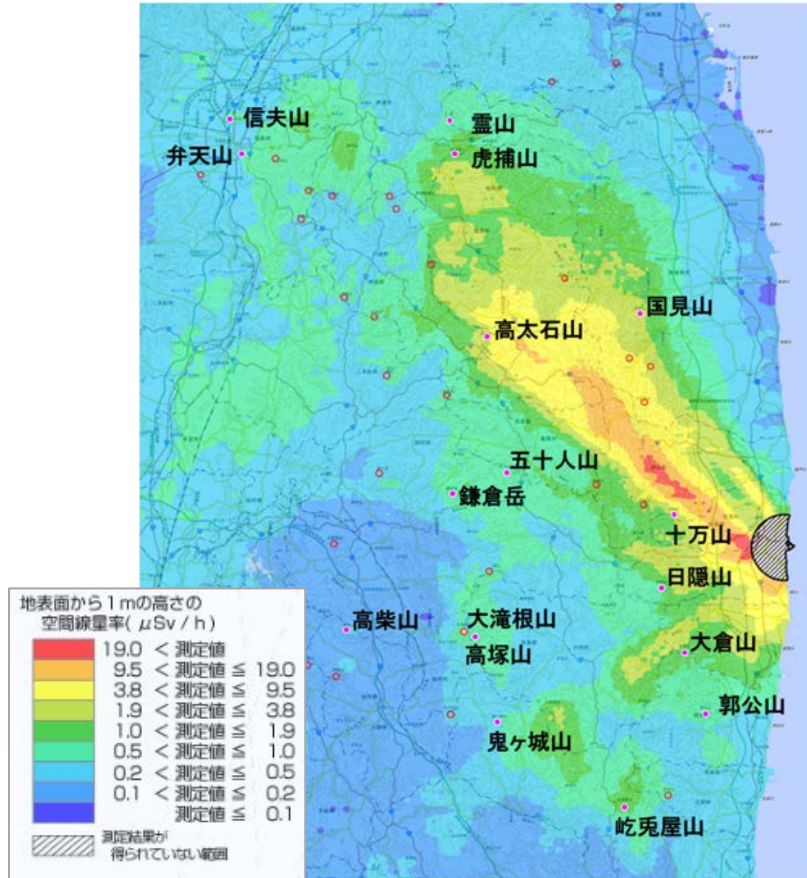


Fig. 2.4-2 Study points for air dose measurement in mountain area.

(Data on air dose rate are cited from the Extension Site of Distribution Map of Radiation Dose as of November 7, 2014, <https://ramap.jmc.or.jp/map/>)

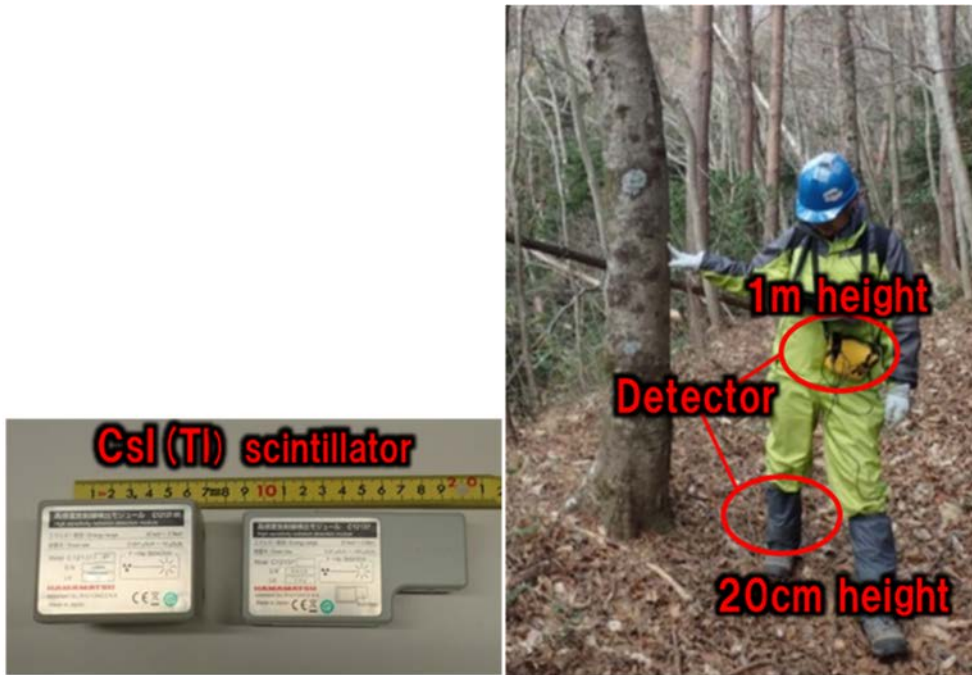


Fig. 2.4-3 Measurement situation using a hot spot finder (right) and the detector (left).



Fig. 2.4-4 Measurement situation using a gamma plotter (GP) (right) and the detector (left).

(3) Evaluation of the physicochemical properties of the radioactive cesium-bearing microparticles (CsMPs) and the development of their analysis

In this section, we report on the spatial distribution, evaluation of the physicochemical properties, and analytical method for the radioactive cesium-bearing microparticles (CsMPs) collected within Fukushima prefecture.

a) Spatial distribution of the CsMPs

The investigation of the CsMPs distribution had been conducted around the 1F, in Okuma Town and Futaba Town (north-northwest and north-west directions from the 1F) from January 2014 to January 2017. The CsMPs were collected in soil and air dust samples. Soil cores were sampled to depth of 5 cm (Satou et al., 2016)³⁸⁾, and also surface soil was collected by a shovel. (Satou et al., 2018)⁴⁹⁾. Dust samples were manually collected using a dust sampler (Satou et al., 2018)⁴⁹⁾. The shape and elemental composition including trace elements were analyzed by a scanning electron microscope (SEM) (Satou et al., 2016³⁸⁾, 2018⁴⁹⁾).

b) Evaluation of physicochemical properties of the CsMPs

Six CsMPs isolated from the non-woven fabrics in Fukushima Prefecture (collected six months after the accident) were provided from the National Agriculture and Food Research Organization. For thermal characterization of the CsMPs, their heating test at elevated temperature was conducted using a thermal analysis equipment. The CsMP sample was put inside a hole made on a platinum plate during the test. The shape and elemental composition of the CsMPs were analyzed by SEM. The inner structure of the CsMPs after heating was observed by a transmission electron microscope (TEM) (Okumura et al., 2018)⁵⁰⁾.

c) Development of analytical method for the CsMPs

In order to develop an efficient methodology for separating the CsMPs in environmental samples, the tests had been conducted using the environmental samples such as lichens and litter collected along the south and west plume trajectories within 3 km area from the 1F from January 2016 to January 2017 (Tagomori et al., 2017⁵¹⁾, Dohi et al., 2018⁵²⁾). In this study, we established a separation method for CsMPs from the samples. These samples were first digested within hydrogen peroxide and then an automatic particle analyzer system based on a field emission electron probe micro analyser (FE-EPMA) was used for detecting CsMPs within lots of mineral-like and metallic particles quickly. (Tagomori et al., 2017⁵¹⁾, Dohi et al., 2018⁵²⁾).

For the above-mentioned items a), b) and c), the measurement of autoradiography was conducted using imaging plates to search the CsMPs. The particle-shaped spots separated by a constant exposure time were used as an indication of the search. For evaluating the property of the respective isolated particles, the morphological observation and the elemental composition analysis were conducted using SEM and FE-EPMA. The quantitative radioactivity analysis of ¹³⁴Cs and ¹³⁷Cs was carried out by γ -ray spectrometry using Ge semiconductor detector. For the details of the investigation and measurement methods, please see the references; Satou et al (2016³⁸⁾, 2018⁴⁹⁾), Okumura et al (2018)⁵⁰⁾, Tagomori et al (2017)⁵¹⁾, and Dohi et al (2018)⁵²⁾.

2.4.3 Results and discussion

(1) Relation between Cs activity concentration in lichens and Cs deposition

The activity concentration of ¹³⁷Cs in lichens ranged from 7.6 to 1740 kBq kg⁻¹, while the ¹³⁷Cs deposition density on soil (calculated value) was estimated to be between 45.8 to 2920 kBq m⁻². Since a significant positive correlation was found between the ¹³⁷Cs activity concentration in lichens and ¹³⁷Cs deposition density on soil (n = 44) based on the calculated the Spearman's rank correlation coefficients as $r = 0.90$ ($P < 0.01$), it was revealed that the ¹³⁷Cs concentration in lichens two years after the accident was well correlated with the initial ¹³⁷Cs deposition amount in soil (Fig. 2.4-5) (Dohi et al., 2015)⁴⁰⁾. These results suggested the

possibility that radioactive cesium remained in lichens even after 2 years, and the cesium concentration in lichens reflected the initial deposition amount at the time of the accident. In particular, the two dominant species, FC: *Flavoparmelia caperata* ($n = 12$) and PC: *Parmotrema clavuliferum* ($n = 11$), showed strong positive correlations, for which the r values were 0.92 ($P < 0.01$) and 0.90 ($P < 0.01$), respectively. Therefore, it is expected that these species of lichens can be used as an indicator of radioactive cesium concentration. On the other hand, The aggregated transfer factor's (T_{ag}) for ^{137}Cs in soil-to-lichen was compared between these two species of lichens, it was found that the ^{137}Cs accumulation level in *P. clavuliferum* is significantly higher than that in *F. caperata*. (Table 2.4-1). In the previous study, it was reported that radionuclide concentrations in lichens were different depends on their species (Hanson, 1971⁵³), Sawidis et al., 1997⁵⁴). Thus, it would be necessary to clarify the difference in accumulating property for radioactive cesium among the species in applying lichens to the indication of radioactive cesium concentration in future.

The study of this section was carried out as collaboration research with the National Museum of Nature and Science, “Basic Research on the Applicability of Lichens to Biological Indicator for Radioactive Cesium in Environment”.

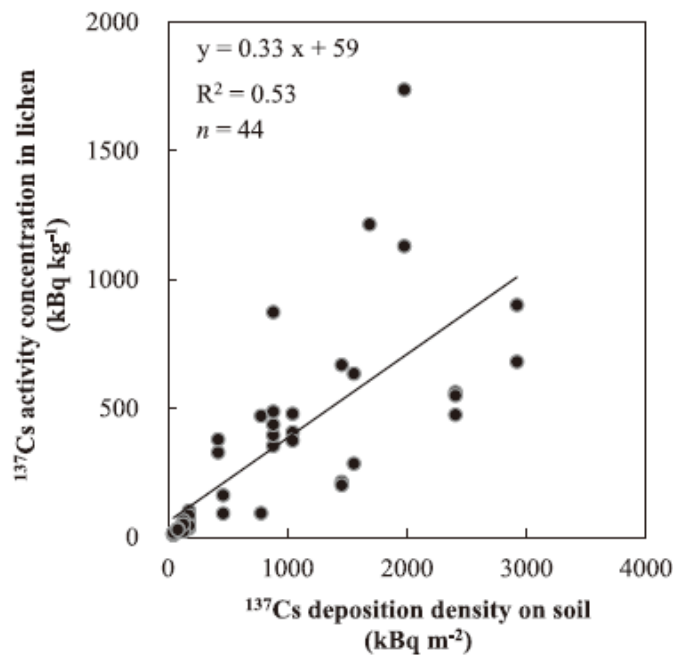


Fig. 2.4-5 The Relationship between the ^{137}Cs activity concentration in all 44 lichens and the ^{137}Cs deposition density on soil at each of the lichen sampling points (Dohi et al., 2015)⁴⁰.

Table 2.4-1 The soil-to-lichen aggregated transfer factor (T_{ag}) for the Fukushima derived ^{137}Cs ($\text{m}^2 \text{kg}^{-1}$) (Dohi et al., 2015)⁴⁰.

Species ^a	n	T_{ag}				
		Range	Median	Mean	Standard deviation	Coefficient of variation (%)
FC	12	0.12–0.99	0.20	0.28	0.24	85
PC	11	0.23–0.88	0.45	0.47	0.18	38
PT	7	0.14–0.90	0.48	0.49	0.23	48
PA	4	0.31–0.72	0.40	0.45	0.18	40
CA	3	0.28–0.78	0.41	0.49	0.26	53
PR	2	0.17–0.23	0.20	0.20	NC ^c	NC ^c
PuB	2	0.35–0.55	0.45	0.45	NC ^c	NC ^c
PuR	2	0.25–0.39	0.32	0.32	NC ^c	NC ^c
ML	1	NA ^b	0.42	0.42	NC ^c	NC ^c
ALL	44	0.12–0.99	0.37	0.40	0.21	53

The ^{137}Cs deposition density on soil and ^{137}Cs activity concentration in lichen were decay corrected to the final sampling date (5 Feb 2013).

^a See Table 1 for abbreviations.

^b NA = not applicable.

^c NC = not calculated.

(2) Investigation of radiation dose distribution in mountainous areas

As a common characteristic in the radiation dose distribution in mountain trails investigated in the present study, the dose distribution in coniferous forests was shown relatively high compared with that in front and behind of the forests (outside of the forests) (Fig. 2.4-6) (Dohi et al., 2016)⁴⁵. In the mountain region where the dose data was obtained in the several directions from mountain top, it was observed that the dose rates faced in the direction of the plume path from 1F tended to be relatively a little higher than those in the other directions. We investigated also altitude dependence of dose distribution in mountain trails. The dose rate tended to be relatively high at high altitude and near the top of the mountain, for example in Mt. Koutaishi (Fig. 2.4-7) (Dohi et al., 2016)⁴⁵. However, there was no noticeable tendency in the other mountain areas. For the mountain areas near the 1F, we tried to investigate the dose rates in two routes around the mountain trail that maintain constant altitude, taking Mt. Hikage as an example. As a result, it was observed that the dose rates around the mountainside (altitude: 350 m) were relatively higher than those at near the top of the mountain (altitude: 500 m). In addition, it was found that there was a tendency of the direction dependence, that is, the dose rates at the western slopes were relatively low, while those at the eastern slopes were high for both altitudes. Since mountain trails generally extend along the ridge of the mountain, it is difficult to evenly obtain the data on the direction and altitude. Therefore, it is hard to evaluate the altitude- and direction-dependences of dose rate. Nevertheless, we obtained a prospect that we will be able to investigate the relation between dose rate and altitude/direction based on the investigation of dose rate by going around at a constant altitude.

Next, we compared the dose rate distribution at 1 m height by walking survey and airborne monitoring for three study areas around 1F (Mt. Higakure, Mt. Juman and Mt. Okura). The results showed the dose rates obtained by walking survey were from half to double of those obtained by airborne monitoring (Fig. 2.4-8) (Oda et al., 2016)⁴⁸. From this result, we obtained a prospect that we will be able to clarify the heterogeneity of the dose distribution, i.e. the cesium deposition, by introducing the walking survey. Also, from the analytical results of dose rate and altitude, it was revealed that the dose rates at mountain trails were high at low altitude regions for Mt. Juman, while these were high at the mountainside for the other two areas (Mt. Higakure and Mt. Okura). As to the relation between land coverage and dose rate, the clear tendencies were not observed.

From now, we will increase the number of the analysis based on the investigation results of dose rate on routes that maintain constant altitude. We will also proceed to investigate the relation between vegetation and dose rate, the comparison with the dose rate data obtained by the airborne monitoring, and the comparison with the simulation results of diffusion status of radioactive cesium just after the accident.

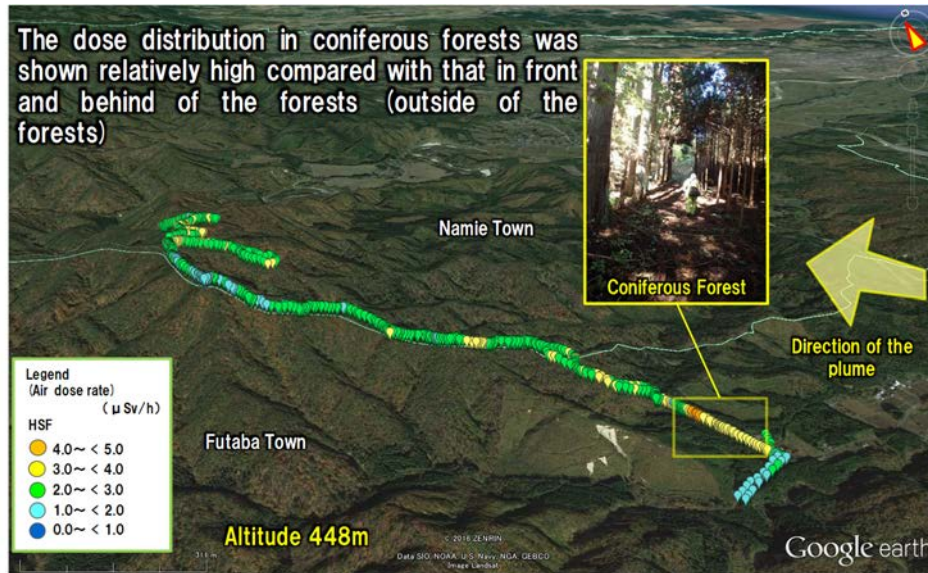


Fig. 2.4-6 Distribution of air dose rate at Mt. Juman (measurement height: 20 cm) (measured on November 5, 2015) (Dohi et al., 2016)⁴⁵.

©2016 ZENRIN, Data SIO, NOAA, U. S. Navy, NGA, GEBCO, Image Landsat.

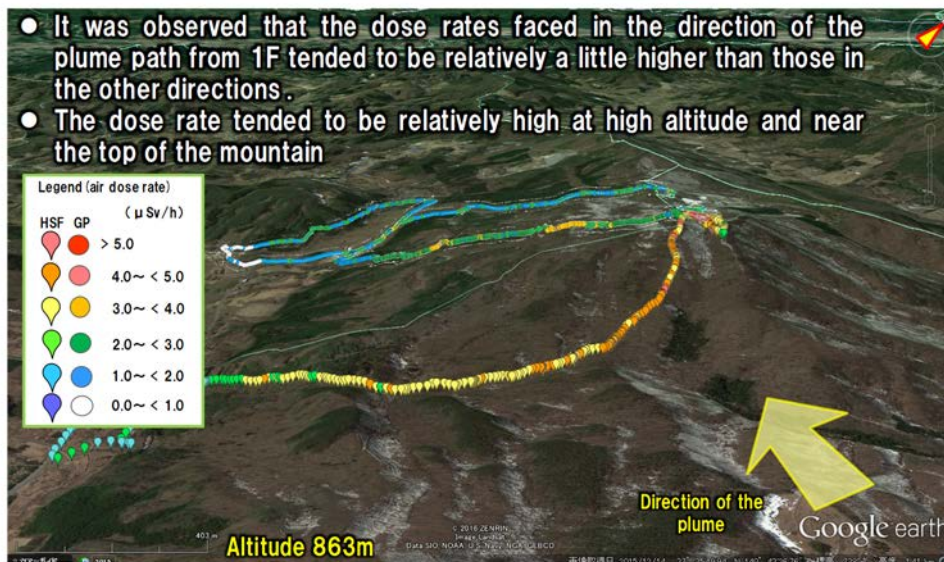


Fig. 2.4-7 Distribution of airdose rate at Mt. Koutaishi. The dose rate at 20 cm height was measured by a hot spot finder (HSF), and that at 5 cm height was measured by a gamma plotter (GP) (Dohi et al., 2016)⁴⁵.

©2016 ZENRIN, Data SIO, NOAA, U. S. Navy, NGA, GEBCO, Image Landsat.

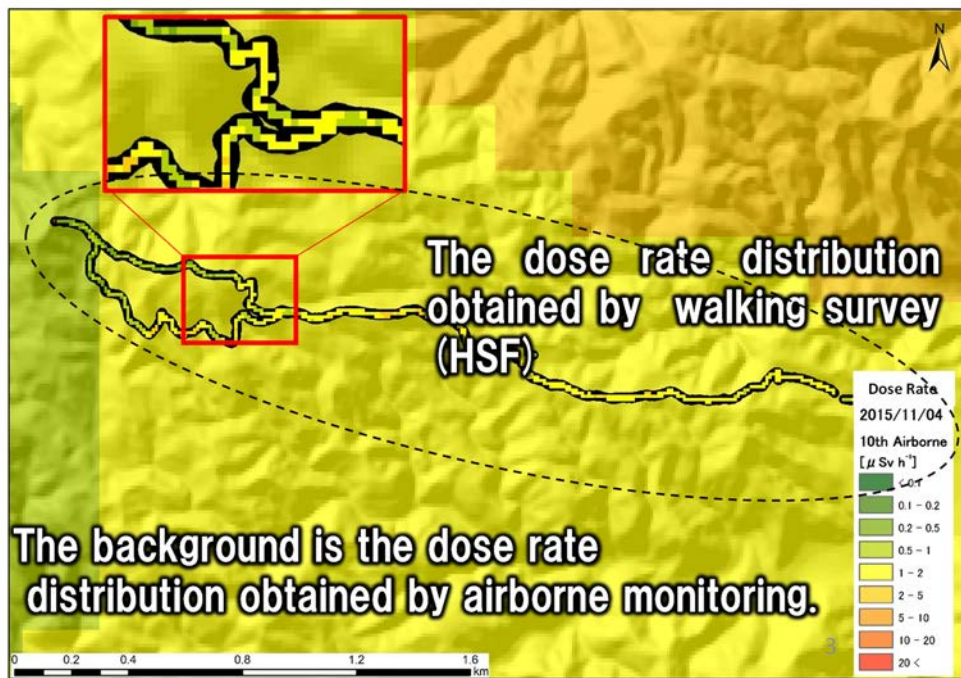


Fig. 2.4-8 Comparison of dose rate distribution obtained by airborne monitoring and walking survey (HSF) at Mt. Higakure (measurement height: 20 cm) (Oda et al., 2016)⁴⁸⁾.

(3) Evaluation of the property of radioactive cesium-rich micro-particles (CsMP) and development of analytical method

a) Spatial distribution of radioactive cesium-bearing microparticles (CsMPs)

Nineteen CsMP samples were extracted from soil and dust collected around the FDNPP. These particles could be roughly identified two types depending on their particle size, common elements contained, the mean values of $^{134}\text{Cs}/^{137}\text{Cs}$ ratio as of March 2011, the tendency of the ^{137}Cs activity per unit volume, and the spatial distribution. One is the “Type A” that is a particle group of about several microns contained Fe, Sn and Cl commonly, and the other is the “Type B” that is a particle group of about several hundred microns contained Na, Mg, Ca and Ba commonly. Based on the $^{134}\text{Cs}/^{137}\text{Cs}$ ratio, it was suggested that the Type A is widely distributed from 1 F to northwest and west side, while the distribution of the Type B is limited to the north-northwest side from 1F (Satou et al., 2018)⁴⁹⁾. Further, we analyzed the relation of ^{137}Cs amount per unit volume between two types (Adachi et al., 2013³⁵⁾; Satou et al., 2016³⁸⁾), which is summarized in Fig. 2.4-9. As a result, it was clarified that the specific radioactivity in the Type A was higher than that in the Type B (Satou et al., 2018)⁴⁹⁾.

As a result of SEM observation, we confirmed that fibrous silicate compounds were attached to the Type B particles, and the element composition agreed with that of the heat insulating materials that were used inside the reactor building. From these results, it was presumed that the Type B particles were produced in the following process. First, radioactive cesium adsorbed on the fibrous heat insulating materials composed of silicate compounds that were filled in the reactor building. Then, the insulating materials were contracted, pulverized and scattered by the heat and blast due to the hydrogen explosion, resulting in the formation of the Type B particles.

From now, we will quantitatively analyze the spatial distribution of CsMPs around 1F by utilizing the classification of the particles. In addition, classify the tendency of the element composition and internal structure of CsMPs is expected that it will be helpful to elucidate the situation at the time of the deposition considering the appearance frequency and generation source.

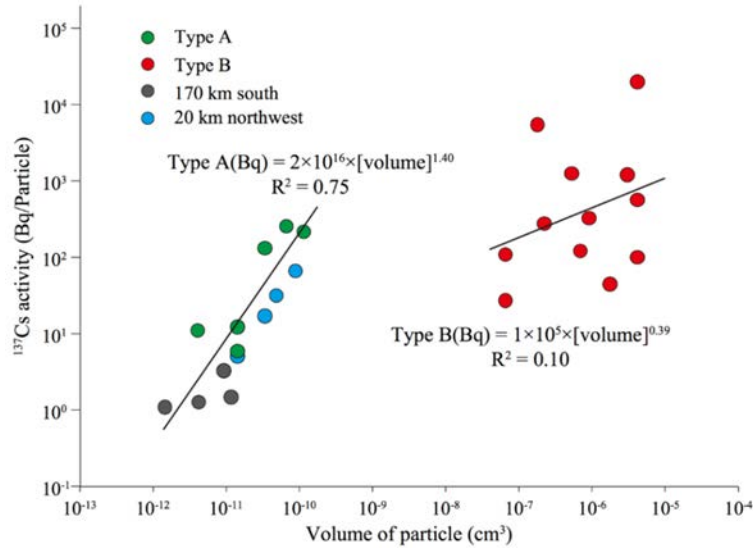


Fig. 2.4-9 Scatter-plot of ^{137}Cs content vs particle volume (Satou et al., 2018)⁴⁹.

The results described in this section were obtained under the project, “Study of Particles Containing Radionuclide Emitted from the Accident of the Fukushima Daiichi Nuclear Power Station, Tokyo Electric Power Company Holdings Inc.” in collaboration with University of Tsukuba, The Jikei University School of Medicine, and Osaka University.

b) Evaluation of physicochemical properties of CsMPs

Next, we investigated the behavior of CsMPs by heating. As a result, the radioactivity of particles gradually decreased with the increase in the temperature above 600°C, and the radioactivity almost lost at 1000°C (Fig. 2.4-10) (Okumura et al., 2018)⁵⁰. The size and spherical shape of CsMPs were almost unchanged after heating, but cesium including radioactive cesium, potassium and chlorine, which were contained in the CsMP before heating, were lost after heating. These results were obtained using by SEM-EDS. (Fig. 2.4-11) (Okumura et al., 2018)⁵⁰. Further, when the CsMPs were heated together with soil, the radioactive cesium released from CsMPs was sorbed by the surrounding soil. From these results, it was shown that radioactivity in CsMPs were lost by heating. Therefore, it is expected that the high radioactivity in the CsMPs will be lost when radioactive waste including CsMPs is burned in incinerators. Furthermore, it was also found that iron, zinc and tin originally dissolved in the glass matrix were crystallized to oxide nanoparticles inside the CsMPs after heating by TEM and electron diffraction analysis. On the basis of these results, it was considered that the SiO_2 matrix of the CsMP and these elements remained in the CsMP after heating, but alkali ions and chlorine containing cesium released from the surface of CsMPs by elemental diffusion (Okumura et al.,

2018)⁵⁰). It is expected that such physicochemical property of CsMPs will become basic data which are useful to eliminate the anxiety about the residual and concentration of cesium with high specific radioactivity originating from CsMP, even when the removing materials in incineration contain CsMP.

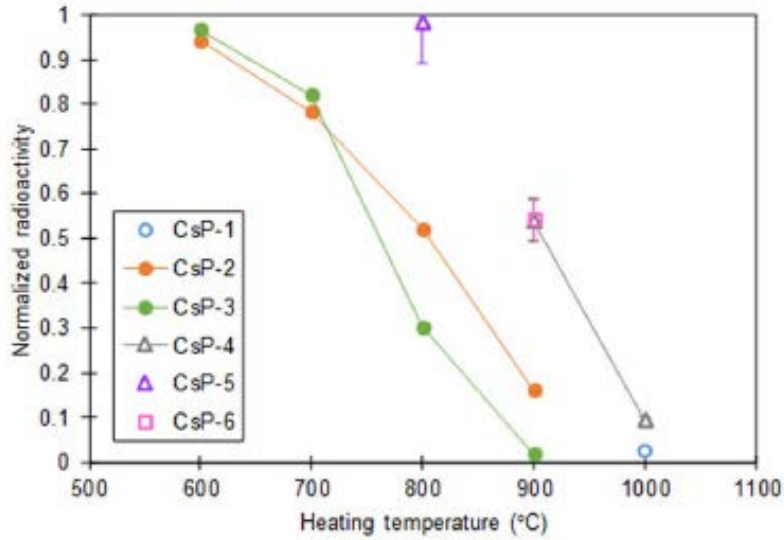


Fig. 2.4-10 Radioactivity change of CsMPs by heating (Okumura et al., 2018)⁵⁰).

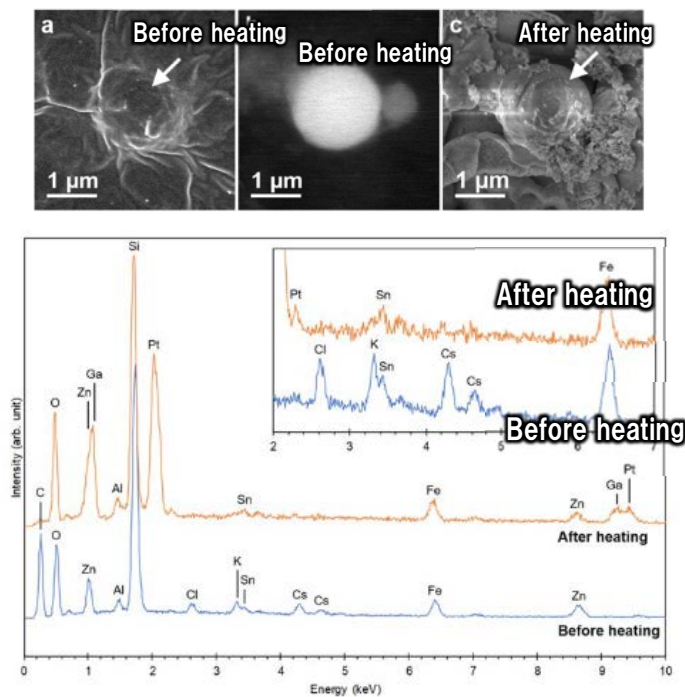


Fig. 2.4-11 Electron microscopy images of CsMP before and after heating (upper photographs) and results of element analysis by SEM-EDS (lower figure). (Okumura et al., 2018)⁵⁰).

The results described in this section were obtained by the entrusted research to the University of Tokyo from JAEA, “Identification of Mineral Phases and Microparticles Adsorbing Radioactive Cesium in Environment of Fukushima and Elucidation of Elusion Process”.

c) Development of the analytical methods for CsMPs

In order to evaluate statistically the physicochemical properties and spatial distribution of the CsMPs emitted from the FDNPP, it is required to establish an efficient methodology for separating a certain amount of CsMPs in future. Therefore, we established a simple method for CsMP isolation from environmental samples (lichens and litter) by combined an organic digestion treatment and electron microscopic analysis with EPMA (Tagomori et al., 2017⁵¹), Dohi et al., 2018⁵²). We obtained CsMPs by applying this method. EPMA observation results show that their shapes were both spherical and non-spherical and their diameters were around several microns (Fig. 2.4-12) (Dohi et al., 2018)⁵²). The elemental compositions in all of them were mainly composed of silicon and oxygen, and contained iron and zinc. Then, the radioactivity ratios of ¹³⁷Cs/¹³⁷Cs on 11 March 2011 of these samples were used for presuming their originated from the Unit 2 and Unit 3 of the reactor. These characteristics of CsMPs in this study, size, elemental compositions and radioactive cesium ratios, were similar to the CsMPs separated from environmental samples without chemical treatments such as soil (Adachi et al., 2013³⁵), Kogure et al., 2016⁵⁵), Yamaguchi et al., 2016³⁷), Furuki et al., 2017⁵⁶), Imoto et al., 2017⁵⁷), Ochiai et al., 2018⁵⁸). Therefore, the digestion treatment is not considered to have influenced the CsMPs characteristics. We proposed to apply the present method as one of the isolation methods for particles. Now we are accumulating the data on the chemical composition of the particles.

In collaboration with the University of Tokyo, we will further combine with the method to determine the location of CsMP using marker samples supposing the isolation and analysis of CsMP particles from soil samples etc. Also, we will develop a method for the isolation and analysis corresponding to the property of the samples.

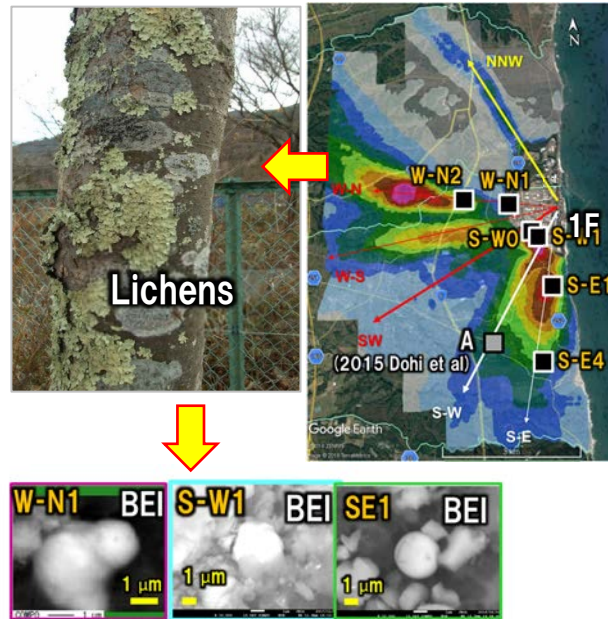


Fig. 2.4-12 Sampling points of lichens near 1F (upper right figure) and electron microscope images of CsMP in lichens (lower photographs).

©2018ZENRIN Image©2018 TerraMetrics

The results described in this section were obtained under the Grant-in-Aid Fund sponsored by the Ministry of Education, Culture, Sports, Science and Technology, “Estimation of radionuclides inventory of on-site area in the FDNPP based on the migration characteristics of radionuclides in off-site area” in collaboration with National Museum of Nature and Science, Kyoto University, and Fukushima University. The results were obtained also by the entrusted research to the University of Tokyo from JAEA, “Identification of Mineral Phases and Microparticles Adsorbing Radioactive Cesium in Environment of Fukushima and Elucidation of Elusion Process”.

2.4.4 Future subjects

As to the item (1), we compared the concentration of radioactive cesium (amount of cesium per unit weight) in lichens and amount of deposition in soil (amount of cesium per unit area) in the present study. it will be required to evaluate these two values on the same basis. In the near future, we will compare the amount of radioactive cesium per unit area among lichens, soil and the other environmental samples, and evaluate the radioactive cesium capacity and retention time (environmental half-life) in lichens. Thereby we aim for the practical application of lichens as an indicator of the initial deposition amount.

For the item (2), we will improve the statistical reliability of data and increase the analytical data of radiation dose distribution in mountainous areas. Thereby, we will further evaluate the heterogeneous distribution of radioactive cesium and its factors.

Concerning the item (3) a), the formation process of the Type B particles was presumed in the present study. However, the process of the Type A particles, which is still not clear, will be future subject to be investigated. As to the item (3) b), the elucidation of the dissolution property of CsMPs will be the future subject to be investigated in order to predict the behavior of them as one of cesium forms in environment.

Therefore, we will further investigate the dissolution property of CsMP in various solution expected in various environments such as seawater, pure water and low-pH solution. For the item (3) c), we will plan to check the effect of digestion treatments (e.g. solubility in acid) on the property of CsMPs. Therefore, we will compare their properties before and after the treatment to evaluate the effect.

3 Dynamics in river system

3.1 Outline

Radioactive cesium (^{137}Cs) released in environment by the accident migrates through river system as dissolved form in water (dissolved state) or adsorbed form on organic materials or soil particles (particulate state). The concentration of ^{137}Cs in river system rapidly decreased just after the accident (about one year after the accident). After that, ^{137}Cs has been continuously discharged from catchment accompanied by the decrease in the discharged rate. Radioactive ^{137}Cs in river system is concerned not only as contamination to fishery products but also as a cause of internal exposure by using it as drinking water or agricultural water. Therefore, the future prediction of the ^{137}Cs concentration in river system is an urgent issue that contributes to the judgment for the residents' return and resettlement.

JAEA has been conducting the long-term radiation monitoring in river systems (rivers, reservoirs, and coastal areas, shown in Fig. 3.1-1) in Hamadori District. Thereby, we have been clarifying the factors that determine the amount of ^{137}Cs in river system.

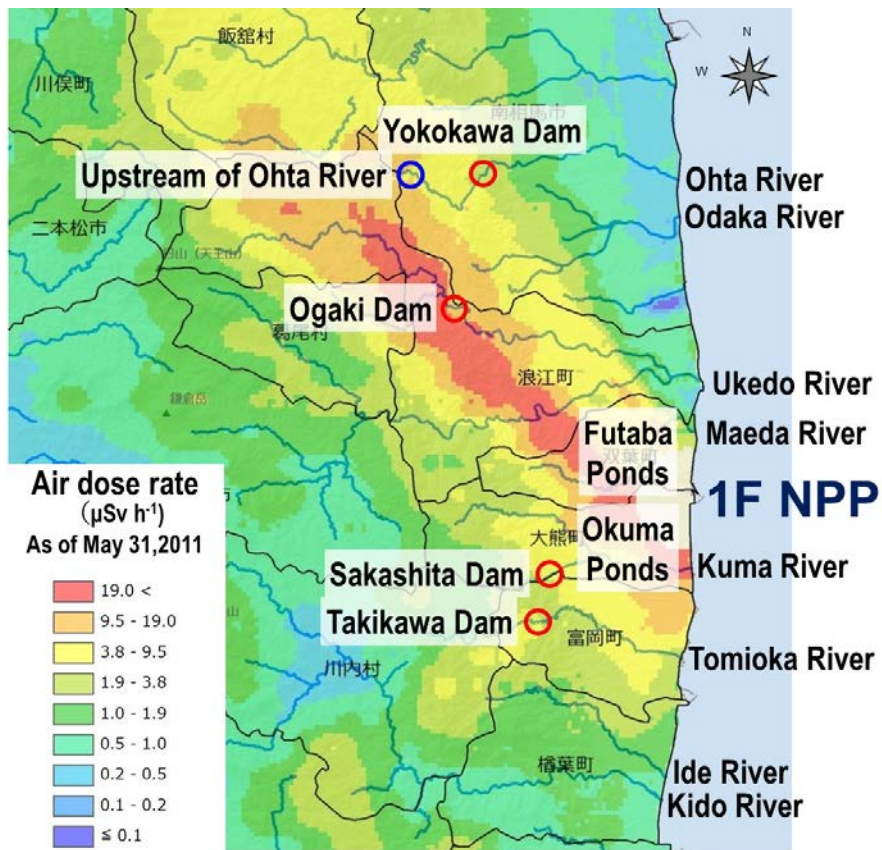


Fig. 3.1-1 Investigation spots.

Deposition map is generated with ArcGIS, based on 5th air-borne monitoring (converted to May 31st, 2011).

It was found that the concentration of ^{137}Cs in rivers and reservoirs has been decreasing with the effective half-life of 2.0-4.4 years since three years after the accident. The decreasing rate of particulate ^{137}Cs concentration in reservoirs was slower than that in rivers, probably due to the effect of resuspending of ^{137}Cs from bottom of the reservoir. On the other hand, we found the seasonal variations for the concentration of dissolved ^{137}Cs both in rivers and reservoirs, that is, the concentration was high in summer and low in winter. From the clear positive correlation between the temperature-dependence of ^{137}Cs concentration and the dissolved organic carbon (DOC), it was considered that the high concentration of dissolved ^{137}Cs in summer was due to the elution of ^{137}Cs by the decomposition of organic materials such as litter. Based on the investigation in the headwaters region, it was suggested that dissolved ^{137}Cs in river water is produced from surface soil or deposited litter after the water spring. Although the concentration of ^{137}Cs in water in rivers and dams was much lower than 1 Bq L^{-1} that in reservoirs in the difficult-to-return zone is still higher than 1 Bq L^{-1} . Therefore, in order to use such water as irrigation water, it would be necessary to implement countermeasures to reduce the concentration of ^{137}Cs .

The ^{137}Cs discharge rate from the catchment area in 2.6 years after the accident estimated from the accumulation amount of ^{137}Cs in the reservoir bottom was about 1.1-1.4% of the initial deposition amount. The ^{137}Cs discharge rate per year for 3-6 years after the accident calculated from the continuous observation results in rivers was less than 0.2% except for FY 2015 that was recorded as unprecedented heavy rain. Based on both results, it was clarified that the outflow rate of ^{137}Cs was decreasing with time. For flood plain, it was found that air dose rate had been decreasing with time because soil particles with low cesium concentration were deposited on the surface with time. This tendency is considered to continue in future. It was suggested that the concentration of ^{137}Cs contained in soil particles discharged from the flood plain was determined not only by the particle size but also greatly by the composition of minerals.

For coastal area, it was found that the closer to the land, the higher the ^{137}Cs concentration. The result indicated that radioactive cesium had been supplied not only from the contaminated water at the initial stage of the accident but also from the land through rivers. In this area, it was revealed that considerable amount of ^{137}Cs existed in the deep region compared with the previously reported results. Therefore, we pointed out the possibility that the amount of radioactive cesium on marine sediment had been underestimated in the former studies. In particular, for cuesta land form with cliffs of about 2-3 m in height difference, the accumulation amount of radioactive cesium showed 1 to 2 orders of magnitude higher value because of the sedimentation environment where fine particles are continuously precipitating due to the decrease in the flow rate. However, since such a concave terrain is limited to about 0.2% of the total seabed surface, the influence on the evaluation of the total accumulation amount at coastal areas is small.

3.2 Headwaters region

3.2.1 Objectives

In the previous studies, the following results were obtained; 1) the concentration of dissolved ^{137}Cs in river water was positively correlated with the Cs deposition amount in the river basin (Tsuji et al., 2014)⁵⁹⁾, 2) the concentration of dissolved ^{137}Cs under storm flow conditions was higher than that under base flow conditions (Shinomiya et al., 2014)⁶⁰⁾ and 3) the concentration of dissolved ^{137}Cs exhibited seasonal variations under base flow conditions (high in summer and low in winter) (Tsuji et al., 2016)⁶¹⁾. Also, it was reported that the concentration of radioactive cesium in litter near rivers was about ten times higher than that in litter deposited on riverbeds (Murakami et al., 2014)⁶²⁾; Sakai et al., 2016⁶³⁾). From the above results, it is considered that dissolved ^{137}Cs is possibly being leached from litter. However, the source and migration behavior of dissolved ^{137}Cs in river system has not yet been clarified.

In the present study, in order to elucidate the source and migration behavior of dissolved ^{137}Cs in stream water in forests, we conducted the investigation and research aiming for the following evaluations; 1) the evaluation of source and source route of dissolved ^{137}Cs by the investigation of headwaters regions, 2) the evaluation of leaching potential of dissolved ^{137}Cs by the degradation on site using litter bags, and 3) the evaluation of the variation tendency (seasonal changes) of dissolved ^{137}Cs concentration by periodical water sampling from the upstream to the downstream in the river basin. The results of the investigation and research are as follows.

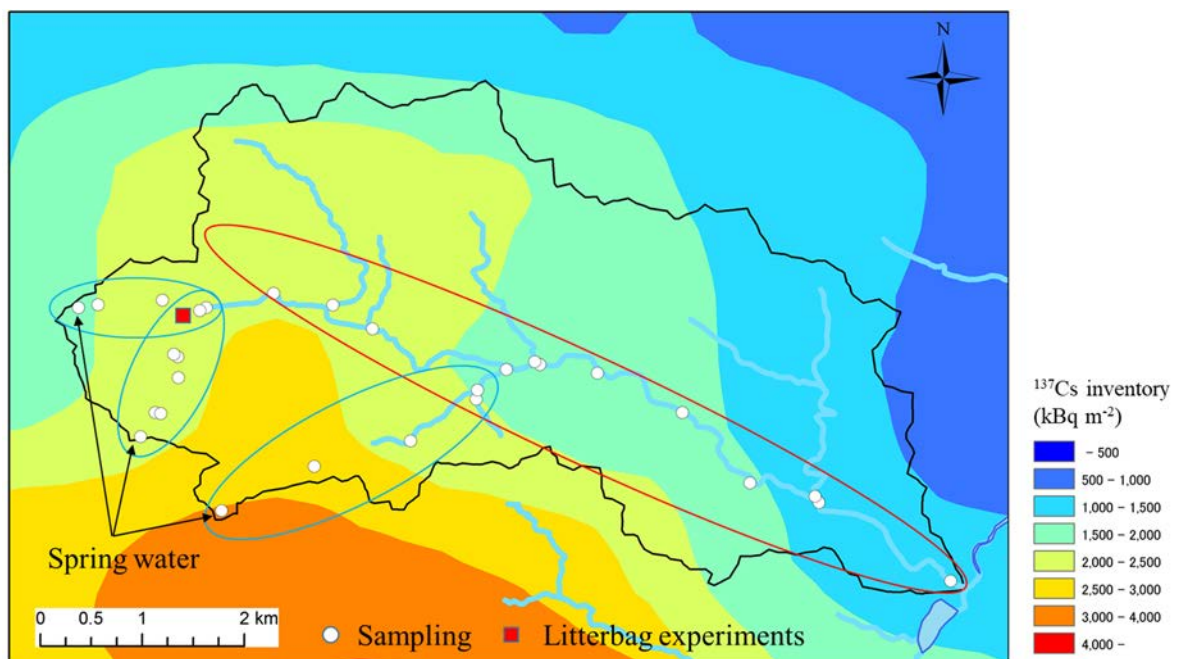


Fig. 3.2-1 Investigated regions.

Closing line in red: The periodic sampling spots in the investigation from the upstream to the downstream.
Closing lines in blue: The areas where the headwaters regions were investigated (November 2016 and August/November 2017).

^{137}Cs inventory is based on 3rd air-borne monitoring (July 8th, 2011).

3.2.2 Methods

The investigated area was the upstream river basin of the Ohta River located in Namie Town, Minamisoma City, Fukushima Prefecture (Fig. 3.2-1). The characteristics of this area are; the area of the river basin was 21 km², the average deposition amount of ¹³⁷Cs was 1.9 MBq m⁻² (calculated from the data of the third aerial radiation monitoring (NRA, 2011)⁶⁴), and more than 90% of the land-use of the area is forest (calculated from the JAXA High Resolution Land-Use and Land-Cover Map, version 14.02 (JAXA, 2014)⁶⁵). The reason that this area was chosen for the investigation was as follows. Firstly, the evaluation can be carried out from the viewpoint of the inflow into dam lake because the area is located in the upstream of the Yokokawa dam in Minamisoma City as described in Chapter 4.6 reporting reservoirs. Secondly, the evaluation can be conducted as a source from forest river basin because almost 100% of the area is occupied by forests. Thirdly, the measurements are relatively easy because the river water contains dissolved ¹³⁷Cs to a certain concentration (higher than 0.1 Bq L⁻¹) due to the high average deposition amount of ¹³⁷Cs.

In order to investigate how dissolved ¹³⁷Cs is generated from the headwaters region, stream water was taken at the position of spring, several meters from the spring, and several points in the downstream at three times (November 2016, August 2017, and November 2017). For clarifying whether the concentration of dissolved ¹³⁷Cs exhibits the seasonal changes or not in the whole river basin and what is the cause of the seasonal changes, water samples had been periodically taken every one or two months from May 2017 at the six spots in the main stream and four spots at the outflow points of the tributary flowing into the mainstream. In order to elucidate how much dissolved ¹³⁷Cs is eluted from litter that is considered to be the source elutes, litter on forest floor of conifer and broad-leaved trees was put in litter bags (size: 40×50 cm, mesh size: about 5 mm), and decomposed on site (Fig. 3.2-2). Then, the samples were brought to the laboratory, and the dissolution tests were conducted. The litter bags were set in June 2017, and collected every three months.



Fig. 3.2-2 Litter bags set on forest floor (litter of conifer).

For headwater, stream water and eluent from litter soil, the sample was filtrated using 0.45 μm membrane, and then the concentration of dissolved ¹³⁷Cs (Bq L⁻¹) was measured by Ge semiconductor detector. In order the measure the water quality, the concentration of the dissolved organic carbon (DOC) was measured using total organic carbon analyzer (Shimadzu Co., TOC-L). The collected samples of litter, soil, and riverbed soil were dried, then the concentration of ¹³⁷Cs was measured by Ge semiconductor detector.

3.2.3 Results and discussion

From the results shown in Fig. 3.2-3, it was found that the concentration of ^{137}Cs in five samples among six samples at the headwater region was lower than the detection limit (0.07 Bq L^{-1}). On the other hand, at the points several meters from the headwater, the concentration of dissolved ^{137}Cs was already in the range from 0.13 to 0.32 Bq L^{-1} . The result suggested that although headwater contains scarcely any dissolved ^{137}Cs , dissolved ^{137}Cs was eluted from surface soil and litter just after the headwater became surface water. Also, it was presumed that the concentration of dissolved ^{137}Cs was determined by the relation between the concentration of dissolved ^{137}Cs in main stream/branch stream water and flow rate depending on the intensity of the inventory.

Concerning the elution potential of dissolved ^{137}Cs by the on-site decomposition using litter bags, the samples were collected at 20 minutes, 2 hours, and 24 hours after the elution as shown in Fig. 3.2-4. As a result, it was revealed that the concentration of dissolved ^{137}Cs in eluted water was 2.26 - 27.8 Bq L^{-1} (mean value: 12.5 Bq L^{-1}) for conifer, and 12.4 - 102 Bq L^{-1} (mean value: 40.2 Bq L^{-1}) for broad-leaved trees. Next, the total amount of ^{137}Cs in litter immersed after the experiment was measured. Also, the elution rate per elution time was obtained by calculating the total amount of ^{137}Cs in the eluted water. As a result, it was revealed that the elution rates of dissolved ^{137}Cs varied depending on the kinds of trees (broad-leaved trees > conifer). The elution rates were 0.15 - 1.25% for conifer (mean value: 0.55%), and 0.81 - 6.64% (mean value: 3.15%) for broad-leaved trees. Further, similar elution tests were conducted by sampling soil just under the litter bags. As a result, it was elucidated that the elution rates were 0.05 - 0.19% (mean value: 0.11%) for soil just under the conifer litter, and 0.17 - 0.94% (mean value: 0.43%) for soil just under the broad-leaved tree litter. That is, it was clarified that the elution rate of dissolved ^{137}Cs from organic soil originating from broad-leaved trees was higher than that originating from conifer, which is similar to the litter case.

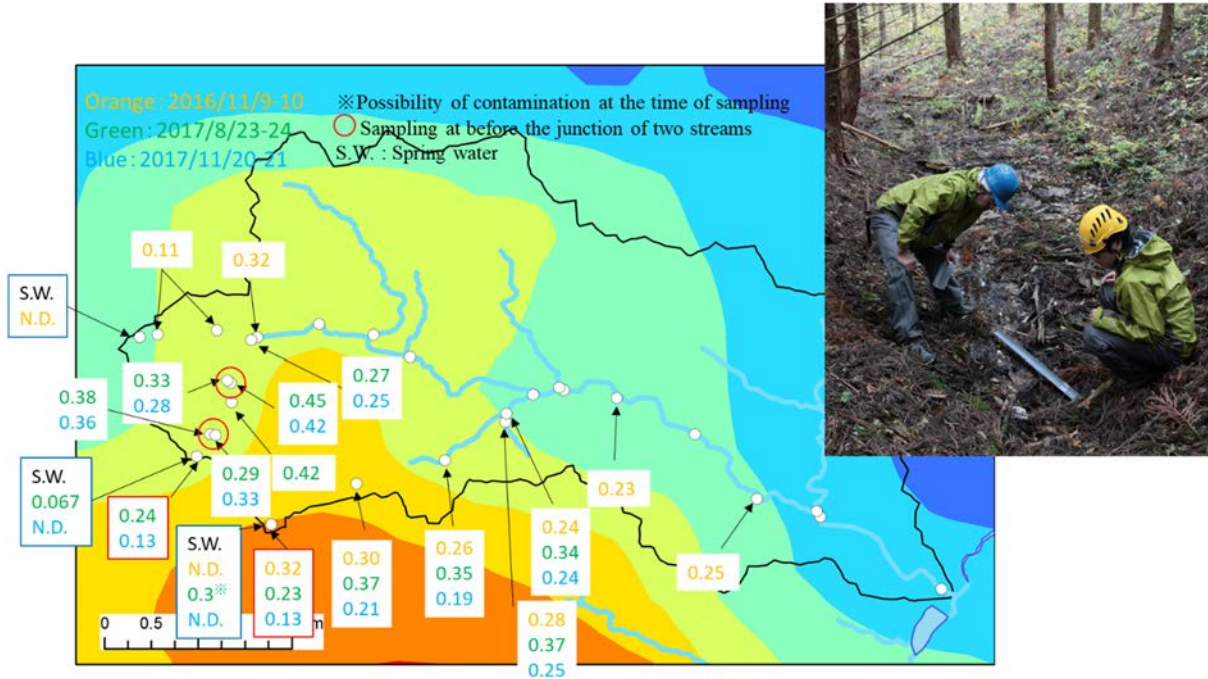


Fig. 3.2-3 Spatial distribution of dissolved ^{137}Cs concentration (Bq L^{-1}) at the spots in the headwaters observation.

Photograph: Sampling of headwater, Blue frame: Headwater, Red frame: Sampling at several meters from the headwater spot

Background map is the same as Fig. 3.2-1.

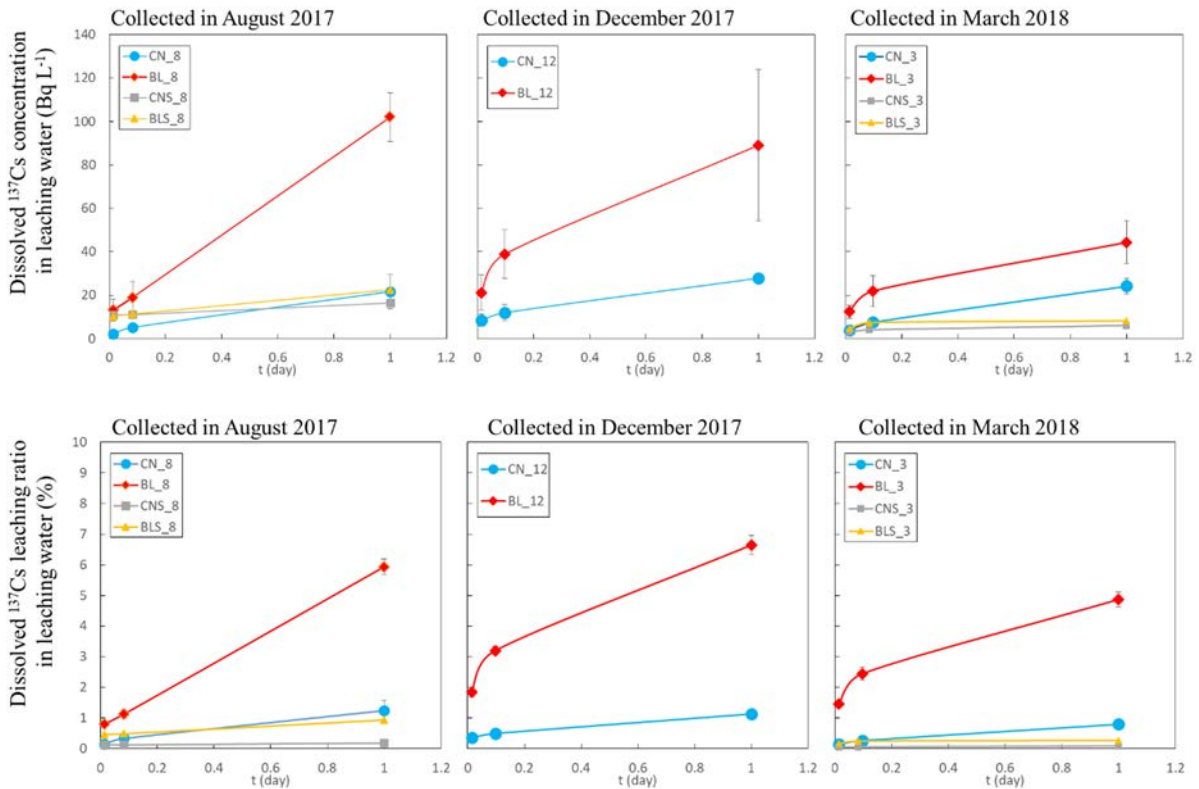


Fig. 3.2-4 Dissolution test of litter and soil.

CN: Conifer, BL: Broad-leaved tree, CNS: Conifer soil, BLS: Broad-leaved tree soil. The suffix represents month of the collection.

Litter and soil were immersed in pure water, then the elute water was collected after 20 minutes, 2 hours, and 24 hours.

The error bars represent the standard deviation of the results in the dissolution tests (n=3). For the dissolution tests of soil, organic soil at the three points just under the litter bag was mixed, then test was conducted for n=1.

From Fig. 3.2-5, it was found that the concentration of dissolved ¹³⁷Cs measured in the longitudinal investigation showed the seasonal variations (high in summer and low in winter) in most of the sampling spots where the samples had been periodically collected, which was similar to the previously obtained results. From Fig. 3.2-6, even for small area in forests, the concentration of dissolved ¹³⁷Cs in river water has positive correlation with the inventory in the river basin ($R^2=0.7821$, $p<0.001$), which was similar to the previously reported results (Tsuji et al., 2014⁵⁹); Yoshimura et al., 2015⁶⁶), etc.). It is considered that various factors such as the difference in vegetation (e.g., area ratio of conifer to broad-leaved trees), topography and soil property would affect the determination of the dissolved ¹³⁷Cs concentration in river water. Among these factors, we consider that the ¹³⁷Cs inventory in river basin is the most important factor. Furthermore, also for forests, it will be possible to conduct analysis using the ¹³⁷Cs inventory distribution obtained by the aerial radiation monitoring. Therefore, in order to evaluate the concentration of dissolved ¹³⁷Cs measured at the different spots in a river basin, we calculated the normalized concentration of dissolved ¹³⁷Cs where the concentration of dissolved ¹³⁷Cs in river water is divided by the deposition amount of ¹³⁷Cs in the respective river basin.

From Fig. 3.2-7, it was revealed that the normalized concentration of dissolved ^{137}Cs showed the positive correlation with the concentration of DOC ($R^2=0.2685$, $p<0.001$). Therefore, it was suggested that the decomposition amount of organic materials (litter) contributes to the concentration of dissolved ^{137}Cs , and the dissolved ^{137}Cs was eluted from organic materials.

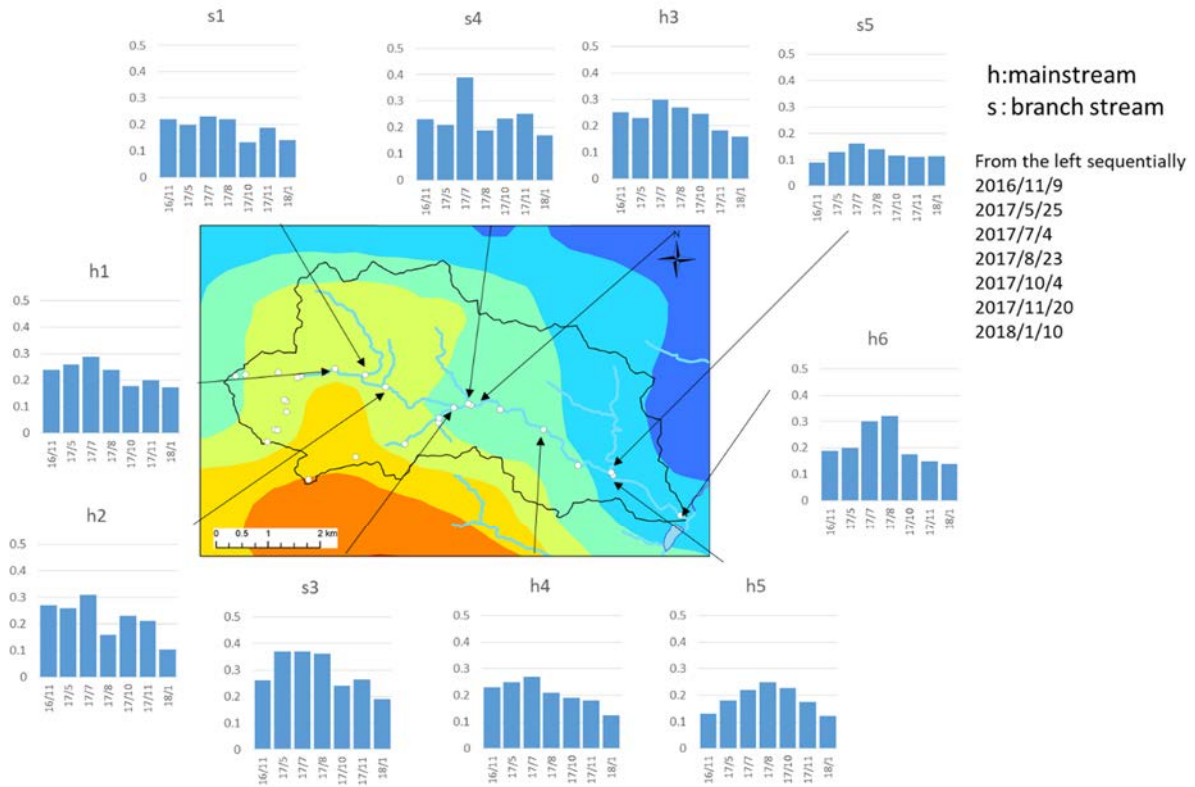


Fig. 3.2-5 Temporal changes in the spatial distribution of dissolved ^{137}Cs concentration (Bq L^{-1}) in the longitudinal investigation along the river.

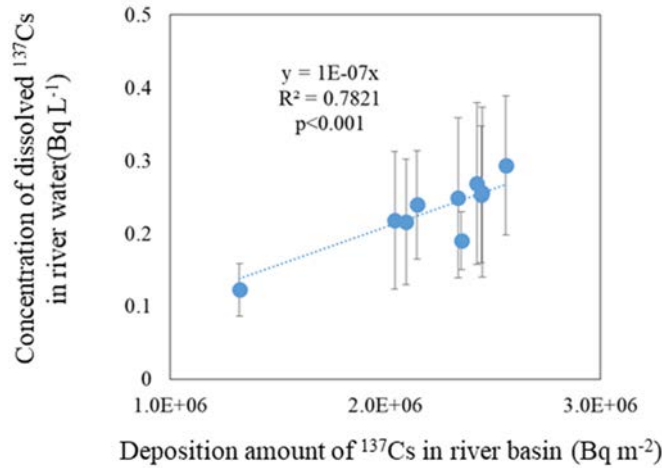


Fig. 3.2-6 Relation between deposition amount of ^{137}Cs in river basin and concentration of dissolved ^{137}Cs in river water.

Deposition amount of ^{137}Cs in river basin: Average deposition amount in the upstream of the respective sampling points (data were taken from the results of the third aerial monitoring). The data on the dissolved ^{137}Cs concentration in river water were taken from the results of temporal changes by the longitudinal investigation along the river. The error bars represent the standard deviation of the data.

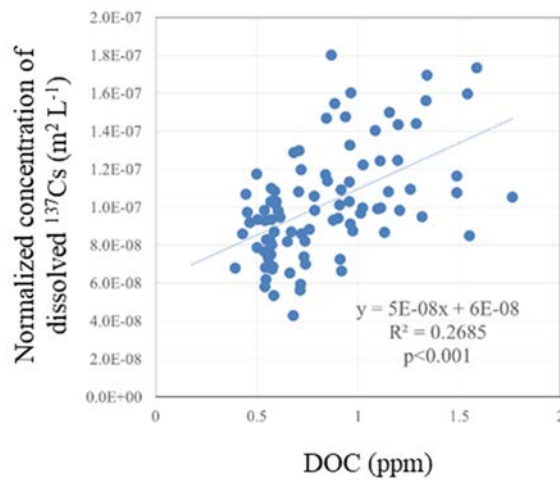


Fig. 3.2-7 Relation between normalized concentration of dissolved ^{137}Cs and concentration of dissolved organic carbon (DOC).

Normalized concentration of dissolved ^{137}Cs ($\text{m}^2 \text{L}^{-1}$) = Concentration of dissolved ^{137}Cs in river water (Bq L^{-1}) \div Deposition amount of ^{137}Cs in the river basin (Bq m^{-2}). In addition to the data of the longitudinal investigation along the river, the data at each sampling point where the deposition amount in river basin can be calculated were used.

3.2.4 Future subjects

In the present study, in order to elucidate the source and migration behavior of dissolved ^{137}Cs in forest stream water, we collected samples from headwater, and conducted the longitudinal investigation and the evaluation of the elution potential from forest litter which may contribute to the dissolved ^{137}Cs . As a result, it was found that the concentration of dissolved ^{137}Cs in headwater was lower than the detection limit (0.07 Bq L^{-1}), but it was $0.13\text{-}0.32 \text{ Bq L}^{-1}$ at several meters from the headwater position. From these results, it was suggested that the surface soil or deposited litter became the ^{137}Cs source after the water spring, and it produced dissolved ^{137}Cs . As the migration behavior, branch stream water that was formed according to the inventory of the river basin in the process of flowing down firstly joined together, and then, dissolved ^{137}Cs was produced based on the relation between the concentration of ^{137}Cs in joined branch stream water and its flow rate. Furthermore, organic materials was expected to considerably contribute to the dissolved ^{137}Cs , because the concentration of dissolved ^{137}Cs was high in summer while it was low in winter, and it has positive correlation with the concentration of DOC. In order to measure the elution potential of organic materials (litter), the litter decomposed on site was brought to the laboratory, and the elution experiment was conducted by immersing the sample. As a result, we found that dissolved ^{137}Cs with extremely high concentration was eluted from conifer and broad-leaved trees ($2.26\text{-}27.8 \text{ Bq L}^{-1}$ for conifer (mean value: 12.5 Bq L^{-1}), and $12.4\text{-}102 \text{ Bq L}^{-1}$ for broad-leaved trees (mean value: 40.2 Bq L^{-1})). From the calculated values of the elution rates, it was revealed that the ^{137}Cs is more easily eluted from broad-leaved trees than conifer ($0.15\text{-}1.25\%$ for conifer (mean value: 0.55%), and $0.81\text{-}6.64\%$ for broad-leaved trees (mean value: 3.15%)). From these results, it would be important to investigate considering the vegetation in river basin as well as the river-basin inventory in future.

Since the litter bags used in the present study can be used in only three elution tests, it is necessary to increase the number of tests. From the results of many tests, we can generalize the elution potential of dissolved ^{137}Cs by evaluating the concentration of dissolved ^{137}Cs using various factors such as temperature and rain fall amount (water content). It is also considered that we will conduct the decomposition on site considering more precise experimental system, e.g, measuring the carbon to nitrogen (C/N) ratio. As to the seasonal variations, we plan to consider whether we can quantitatively explain the changes in dissolved ^{137}Cs concentration or not, using the DOC and fluorescent materials as markers. Although it is considered that the inventory would be the most important factor that determines the concentration of dissolved ^{137}Cs , we intend to also discuss the effect of the difference in vegetation not only by the elution experiments but also at the river basin scale.

3.3 Concentration of dissolved radioactive cesium and its evolution mechanism in rivers

3.3.1 Objectives

Radioactive cesium deposited on land area by the accident is discharging to the living sphere and the ocean through river systems. The amount of discharging radioactive cesium rapidly decreased in one year after the accident. However, radioactive cesium with a certain concentration is still continuously discharging due to the lowering of the decreasing rate (Iwagami et al., 2017)⁶⁷.

According to the results for the Chernobyl nuclear power plant accident, it is expected that the decreasing rate will further become low in coming decades (Smith et al., 2006)⁶⁸. It should be noted that radioactive cesium in dissolved state has especially high bioavailability. Therefore, the prediction of its concentration to evaluate the long-term effects on agriculture, forestry, and fishery products is an urgent subject that contributes to the decision towards the early return of the evacuees and their living reconstruction.

JAEA has been measuring the concentration of dissolved radioactive cesium in eight second-class rivers in Hamadori District since 2014. Since April 2015, the radiation monitoring has been carried out every month. Based on the measurement results, we clarified the decreasing rate of dissolved radioactive-cesium concentration and its seasonal changes. In comparison with the related water quality, the mechanism generating radioactive cesium in dissolved state was investigated.

3.3.2 Methods

Rivers investigated are shown in Fig. 3.3-1. We investigated second-class rivers (the Ohta River, the Odaka River, the Ukedo River, the Maeda River, the Kuma River, the Tomioka River, the Ide River and the Kido River) within 30 km from the 1F. For the Ukedo River, its branch river (the Takase River) that occupies two-thirds of the total flow amount was also investigated. Since these rivers have the same geological background, adsorption/desorption behavior with constituent minerals is considered to be similar. For this reason, these rivers have an advantage that the dynamics of dissolved radioactive cesium can be investigated focusing on the (1) deposition amount and (2) land use.

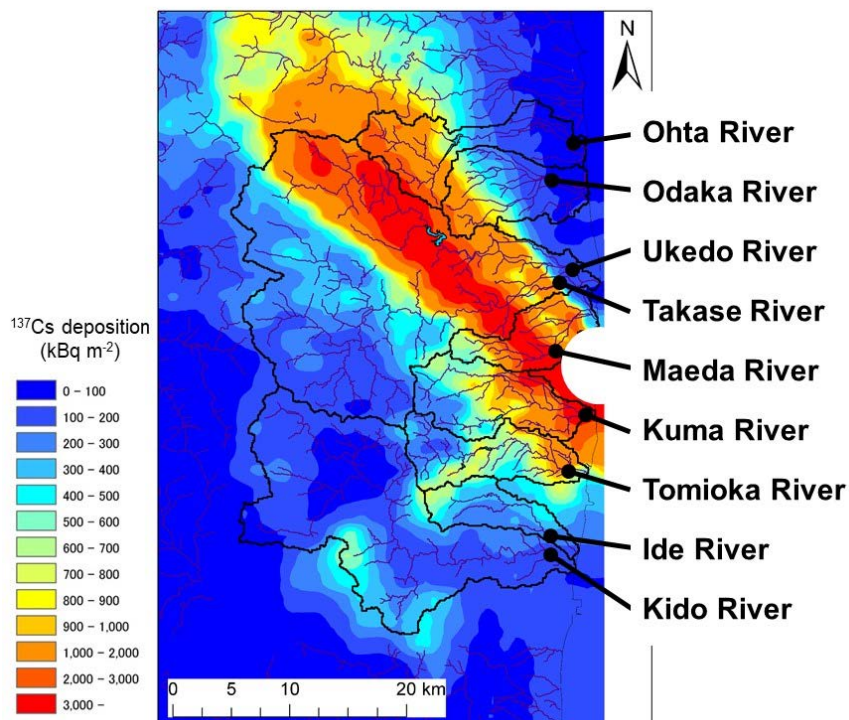


Fig. 3.3-1 Location of rivers investigated.

^{137}Cs deposition is based on 4th air-borne monitoring (November, 2011).

In analyzing the dynamics of dissolved radioactive cesium in rivers, the following three factors were investigated, i.e., (1) concentration of radioactive cesium, (2) concentration of coexisting inorganic ions, and (3) concentration of dissolved organic materials. The contents of the investigation for each factor are as follows.

(1) Concentration of radioactive cesium

Twenty liter of river water was taken from the bridge at the time of normal water level using buckets and ropes. For the Ohta River, the Odaka River, the Ukedo River and the Takase River, the samples have been taken every month from April 2015. For the other rivers, the samples have been collected every month from April 2016. The collected samples were divided into particulate state and dissolved state using membrane filter (pore size: $0.45\ \mu\text{m}$). The particulate component on the filter was dried at 90°C for 90 min, then weighed. For the dissolved component, radioactive cesium was concentrated using nonwoven fabric impregnated with potassium zinc ferrocyanide (Yasutaka et al., 2015)⁶⁹. The concentration of ^{137}Cs in particulate and dissolved samples was determined using Ge semiconductor detector.

(2) Concentration of coexistent inorganic ions

For the dissolved component separated by the above procedure (1), the concentration of the coexistent inorganic ions (F^- , Cl^- , NO_3^- , SO_4^{2-} , Na^+ , K^+ , Mg^{2+} and Ca^{2+}) was measured by high-performance liquid chromatography.

(3) Concentration of dissolved organic materials

For the dissolved component separated by the above procedure (1), the concentration of dissolved organic carbon (DOC) was measured by total organic carbon analyzer. Also, the absorbance was measured by

spectrophotometer. In addition, the fluorescent dissolved organic materials were characterized by three-dimensional fluorescence spectrophotometer.

3.3.3 Results and discussion

Fig. 3.3-2 shows the relation between the distribution of dissolved ^{137}Cs concentration and the deposition amount in the river basin in 2016. As of 2016, the concentration of dissolved ^{137}Cs was lower than 0.3 Bq L^{-1} in the Maeda River and the Kuma River, which are located near the 1F. This value was much lower than the quality standard of drinking water (10 Bq L^{-1}). Also, we observed that the concentration of dissolved ^{137}Cs was correlated with the mean deposition amount of ^{137}Cs in the river basin. Although the similar results were also obtained in the preceding works (Tsuji et al., 2014⁵⁹); Yoshimura et al., 2015⁶⁶); Ochiai et al., 2015⁷⁰), the present results reveal that such correlation also held even five years after the accident.

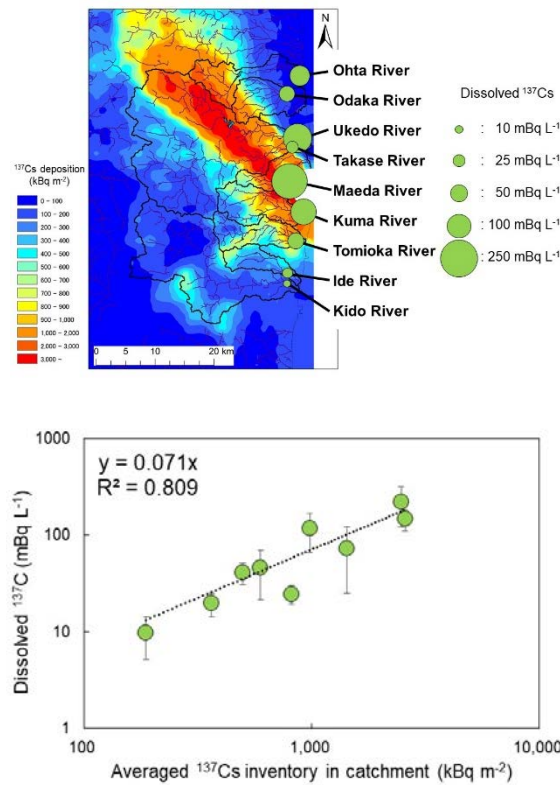


Fig. 3.3-2 Relation between distribution of dissolved ^{137}Cs concentration (left) and mean ^{137}Cs deposition amount in the river basin (right) in 2016.

As described above, the concentration of dissolved ^{137}Cs in river water was correlated with the ^{137}Cs deposition amount in the river basin. In order to further understand the behavior of ^{137}Cs in environment, environmental factors determining the dissolved ^{137}Cs concentration were investigated in addition to the deposition amount. For this purpose, the concentration of dissolved ^{137}Cs (Bq L^{-1}) was normalized by the deposition amount of ^{137}Cs in the river basin (Bq m^{-2}). The normalized value is called “normalized dissolved ^{137}Cs concentration” which is calculated by the following equation,

$$^{137}\text{Cs}_{dis_norm} = C / D$$

where $^{137}\text{Cs}_{dis_norm}$ is normalized dissolved ^{137}Cs concentration ($\text{m}^2 \text{L}^{-1}$), C is dissolved ^{137}Cs concentration (Bq L^{-1}) and D is deposition amount of ^{137}Cs in the river basin (Bq m^{-2}). The relation between the normalized concentration of dissolved ^{137}Cs and the DOC concentration is shown in Fig. 3.3-3. It was found that the normalized dissolved ^{137}Cs concentration has positive correlation with the concentration of SO_4^{2-} , Mg^{2+} and Ca^{2+} ions. These ions are the indication of the elution components from soil originating from river water. Therefore, we considered that dissolved ^{137}Cs tends to easily discharge from the river basin where eluted components easily flow out from soil.

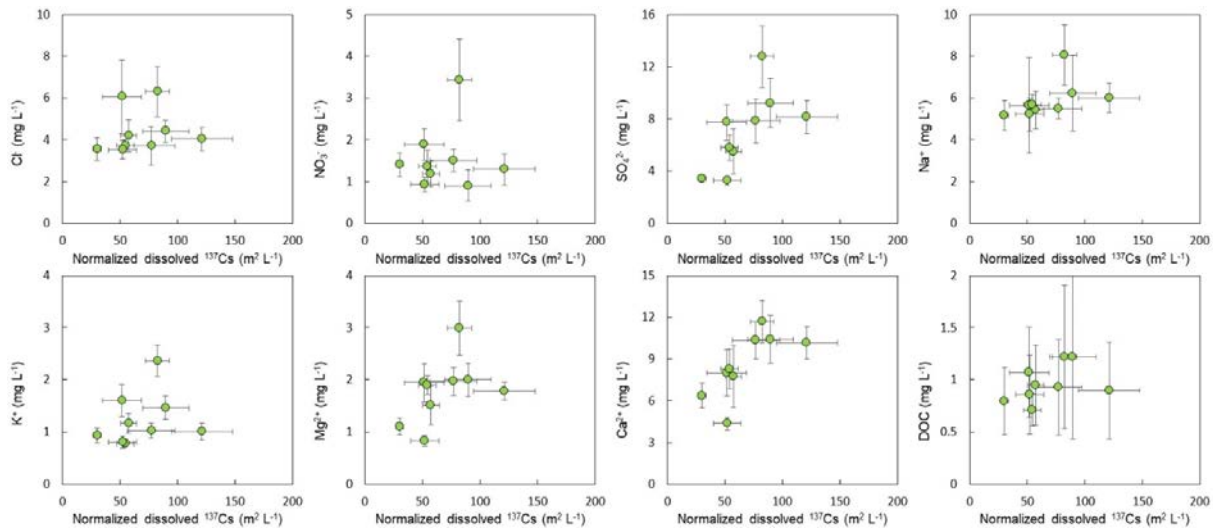


Fig. 3.3-3 Relation between normalized dissolved ^{137}Cs concentration and concentration of coexisting inorganic ions or DOC in 2016.

Fig. 3.3-4 shows the relation between the coverage of forests in river basin and the normalized dissolved ^{137}Cs concentration and SO_4^{2-} , Mg^{2+} , Ca^{2+} ions. Consistent with the above discussion, it is observed that the normalized concentration of dissolved ^{137}Cs and SO_4^{2-} , Mg^{2+} , Ca^{2+} ions tends to be high in the region where the coverage of forests with low outflow from soil is low. From these results, it was considered that the main factor that increased concentration of dissolved ^{137}Cs in river water was the discharge of dissolved ^{137}Cs from places other than forests (e.g. farms). In Fig. 3.3-4, it is also seen that the correlation of the forest coverage with the normalized dissolved ^{137}Cs concentration is low compared with that with coexisting inorganic ions. The result seems to be due to the difference in the ^{137}Cs deposition amount depending on each land-use. Then, we further investigated the relation between deposition rate in forests and the concentration of dissolved ^{137}Cs . The result is shown in Fig. 3.3-5. It is seen that the correlation is better than that observed in Fig. 3.3-4. This means that the discharge effect of dissolved ^{137}Cs from other than forests was more predominant as a factor that increased the concentration of dissolved ^{137}Cs .

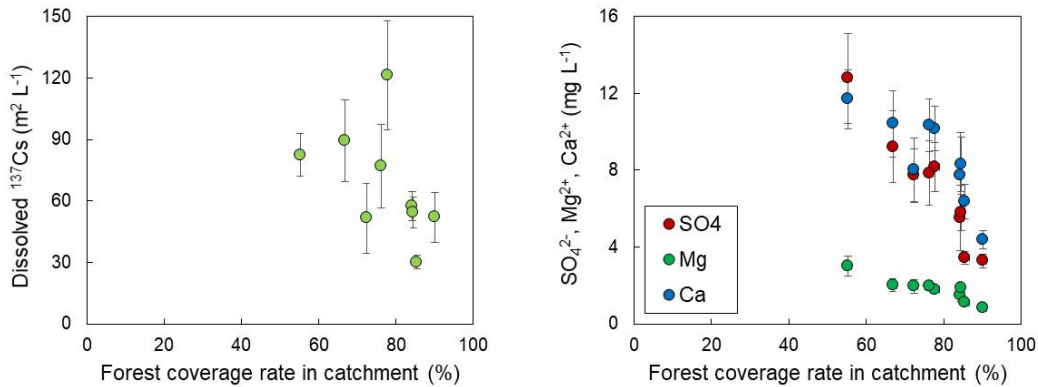


Fig. 3.3-4 Relation between forest coverage and normalized dissolved ¹³⁷Cs concentration and coexisting inorganic ions.

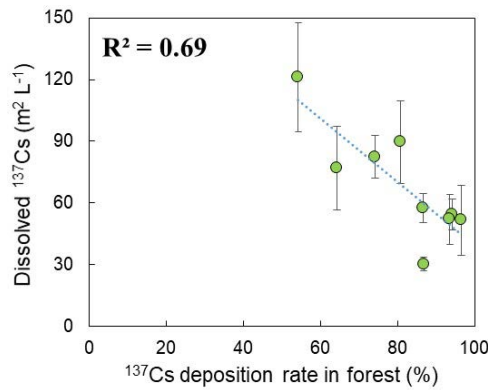


Fig. 3.3-5 Relation between deposition amount of ¹³⁷Cs in forests and normalized dissolved ¹³⁷Cs concentration.

Next, we compared the relation between average rainfall amount in ten days before the sampling and the concentration of dissolved ¹³⁷Cs. The investigation was carried out for the rivers with both high and low ¹³⁷Cs deposition rates in forests. The rivers with high deposition rates are the Ukedo River (87%) and the Takase River (87%). The rivers with low deposition rates are the Kuma River (54%) and the Tomioka River (64%). The results are shown in Fig. 3.3-6. It was observed that the concentration of dissolved ¹³⁷Cs was well correlated with the rainfall amount for the Kuma River and the Tomioka River where the effect of the ¹³⁷Cs discharge from soil was large. Namely, it was revealed that the discharge of dissolved ¹³⁷Cs from places with easy-discharged land use depends on the intensity of the rainfall. On the other hand, such tendency was not observed for the Ukedo River or the Takase River with high deposition rate of ¹³⁷Cs. The result seems to be due to the suppression of the ¹³⁷Cs discharge from soil by litter on forest floor.

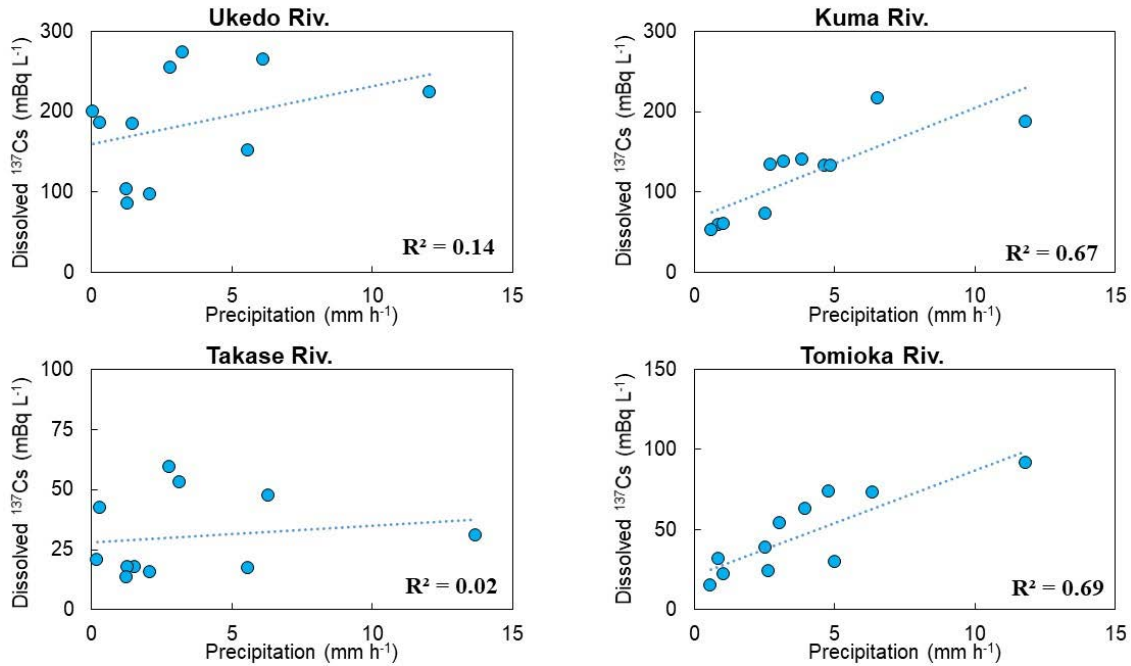


Fig. 3.3-6 Relation between average rainfall amount in ten days and concentration of dissolved ¹³⁷Cs for the Ukedo River, the Takase River, the Kuma River and the Tomioka River.

Fig. 3.3-7 shows the temporal changes in the concentration of dissolved ¹³⁷Cs in the Ohta River, the Odaka River, the Ukedo River and the Takase River where the monitoring had been conducted for more than three years. Since it is known that the concentration of dissolved ¹³⁷Cs exponentially decreases based on experience (Smith et al., 2006)⁶⁸⁾, the results of the curve fitting by simple exponential decreasing function are also shown in Fig. 3.3-7. From the coefficients of the exponential function, the environmental half-lives of dissolved ¹³⁷Cs concentration could be estimated to be 2.5-4.4 years. However, the concentration of dissolved ¹³⁷Cs was seasonally fluctuating in each river, i.e., the concentration tended to be high in summer while it tended to be low in winter. Such seasonal fluctuation was also observed in the other rivers (Tsuji et al., 2016)⁶¹⁾; Muto et al., 2017⁷¹⁾). As pointed out by Tsuji (Tsuji et al., 2016)⁶¹⁾, such seasonal changes in the ¹³⁷Cs concentration depended on the temperature (Fig. 3.3-8). Therefore, the litter at riversides is considered to be the source of dissolved ¹³⁷Cs.

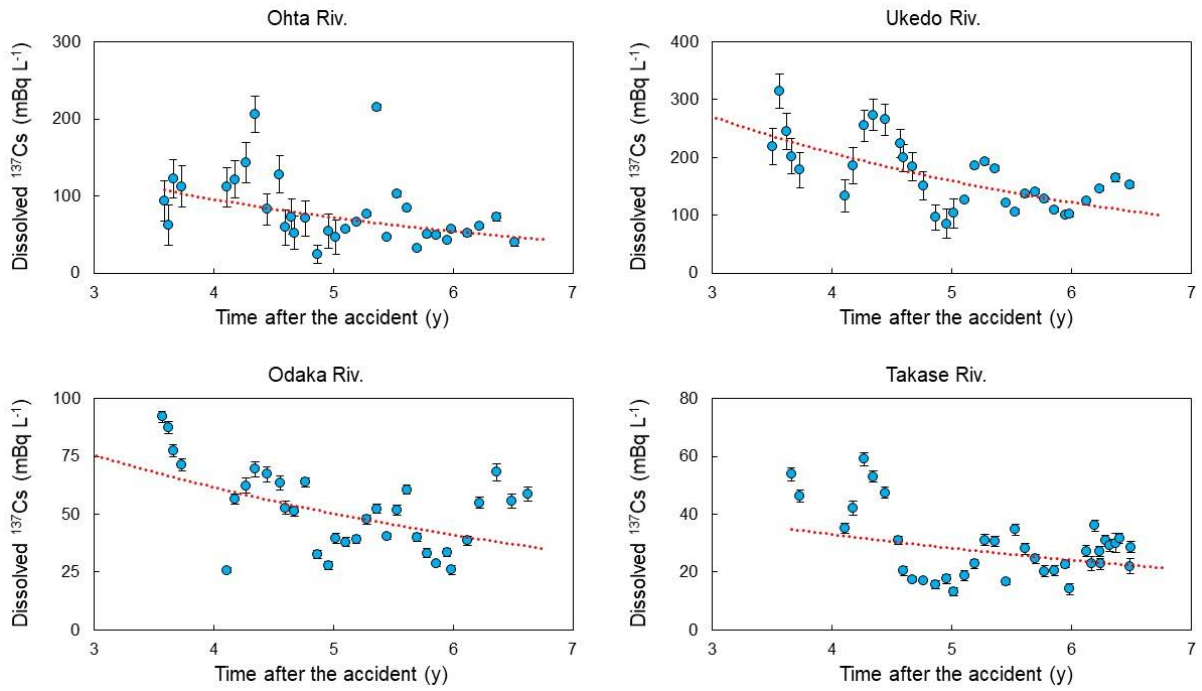


Fig. 3.3-7 Temporal change in concentration of dissolved ^{137}Cs in the Ohta River, the Odaka River, the Ukedo River and the Takase River.

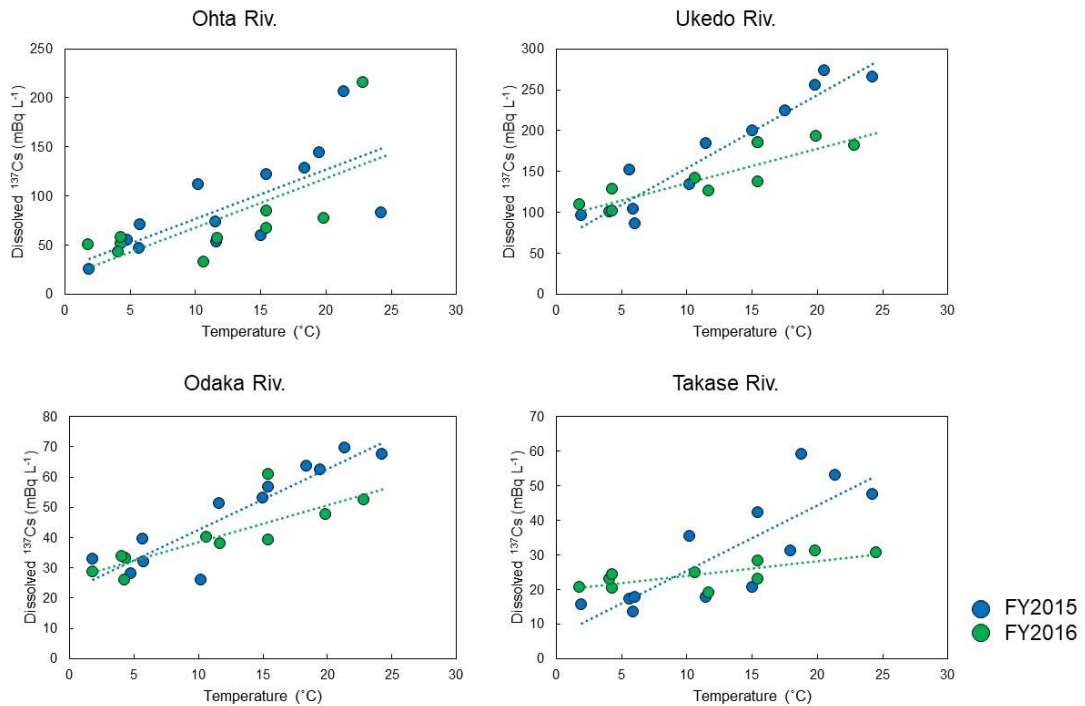


Fig. 3.3-8 Relation between temperature and concentration of dissolved ^{137}Cs in the Ohta River, the Odaka River, the Ukedo River and the Takase River.

On the other hand, Fig. 3.3-7 shows that the concentration of dissolved ^{137}Cs scarcely decreased in winter. This means that the source of dissolved ^{137}Cs in winter did not depend on the temperature, and its decreasing rate was low. As one of the possible ^{137}Cs sources, ^{137}Cs adsorbed on mineral soil in river bottom could be considered. According to the results of radiation monitoring in river system for public use by Ministry of the Environment Government of Japan⁷³⁾, the concentration of ^{137}Cs on river bottom at the Murohara bridge, the Ukedo River and the JR railway bridge in the Ohta River had scarcely decreased since the autumn of 2015, and the environmental half-lives of ^{137}Cs concentration were as long as 12-15 years. Such long half-lives are in good agreement with the changing tendency of the dissolved ^{137}Cs concentration, which was observed in the present study.

From the present investigation results, the decreasing rate of temporal changes in the dissolved ^{137}Cs concentration was divided into the abovementioned two components. The results are shown in Fig. 3.3-9. The decreasing rates of the seasonal-change components due to the litter decomposition are indicated as green dotted lines. The half-lives of the decreasing rate were estimated to be 1.1-1.9 years. These half-lives coincide with the environmental half-life of outflowing water from litter (Koarashi et al., 2016)⁷²⁾. The results show that the ^{137}Cs discharging from litter newly accumulated in forest floors and riversides did not affect so much. This means that ^{137}Cs deposited on litter just after the accident is influencing the concentration of dissolved ^{137}Cs in rivers even at the present, i.e., after more than six years since the accident. However, if we assume that the concentration of dissolved ^{137}Cs will decrease with the present half-life, it is presumed that the influence will become so small that the seasonal fluctuation disappears in a few years. On the other hand, for winter (shown as gray dotted line), we could not quantitatively evaluate the decreasing rate of the ^{137}Cs concentration, but we roughly estimated the half-life to be longer than 10 years.

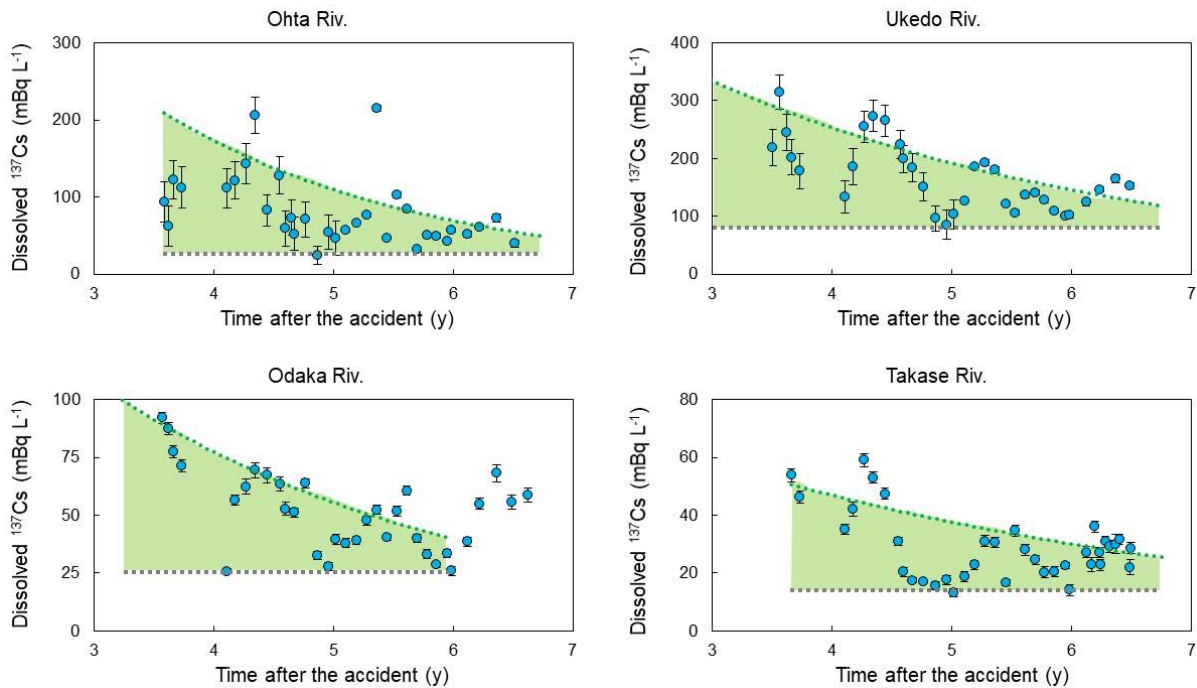


Fig. 3.3-9 Temporal changes in concentration of dissolved ^{137}Cs in the Ohta River, the Odaka River, the Ukedo River and the Takase River (two components).

3.3.4 Future subjects

On the basis of the present investigation results, it was shown that ^{137}Cs originating from winter components will possibly dominate the concentration of dissolved ^{137}Cs in river water from ten years after the accident. Accordingly, we can predict that the concentration of ^{137}Cs will change within the same level as the present concentration for the coming few decades. It would be necessary to continue the observation for the rivers where the concentration of ^{137}Cs in fresh water fish exceeds the shipment reference value (100 Bq kg^{-1}) at present.

3.4 Changes in concentration of particulate radioactive cesium in rivers and its migration and sedimentation behavior

3.4.1 Objectives

Radioactive cesium deposited in land due to the accident is outflowing to the living sphere and the ocean through river systems. The discharge rate rapidly decreased in a year after the accident. However, radioactive cesium with a certain concentration is still continuously discharging due to the lowering of the decreasing rate (Iwagami et al., 2017)⁷⁴). It is known that most of radioactive cesium discharging from a river basin is adsorbed on particulate materials (particulate state). Therefore, in order to know the migration behavior of radioactive cesium in environment, it is necessary to understand the dynamics of particulate radioactive cesium. In addition, there is a concern that air dose rate in the living sphere will rise again and radioactivity will transfer to marine products due to the accumulation of particulate radioactive cesium in the downstream of rivers and the ocean.

JAEA has been continuously observing particulate radioactive cesium as well as dissolved one in eight rivers in Hamadori District, Fukushima Prefecture since 2014 (refer to Section 3.3). Among them, the flux of the particulate radioactive cesium has been observed for six rivers by setting apparatuses for measuring the water level and the turbidity. Further, we have investigated the temporal changes in radioactive-cesium deposition and air dose rates in the flood plains. Based on the observation results, we have elucidated the decreasing rate and migration amount of particulate radioactive cesium. In addition, we have investigated the deposition and migration mechanism of particulate radioactive cesium.

3.4.2 Methods

The rivers investigated in the present study are shown in Fig. 3.4-1. The investigation was carried out for rivers (the Ohta River, the Odaka River, the Ukedo River, the Maeda River, the Kuma River, the Tomioka River, the Ide River and the Kido River) which are located within 30 km from the 1F. For the Ukedo River, its branch river (the Takase River) that occupies two-thirds of the total water discharge amount was also investigated. Since these rivers have the same geological background, adsorption/desorption behavior with constituent minerals is considered to be similar. For this reason, these rivers have an advantage that the dynamics of dissolved radioactive cesium can be investigated focusing on the three points, i.e., (1) deposition amount, (2) land use, and (3) existence of dams.

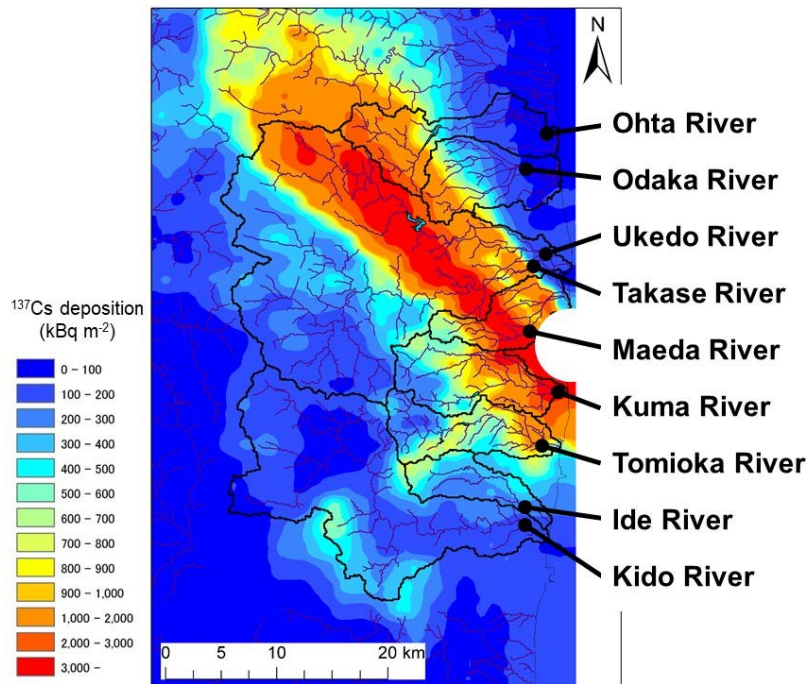


Fig. 3.4-1 Location map of the investigated rivers.

¹³⁷Cs deposition is based on 4th air-borne monitoring (November, 2011).

As the investigation on the dynamics of particulate radioactive cesium in rivers, we conducted four kinds of observation, i.e., (1) continuous observation on water-level/turbidity and observation on water flow-rate, (2) measurement on radioactive-cesium concentration in river water, (3) measurement on depth distribution of radioactive-cesium concentration in flood plain, and (4) measurement on air dose rate on flood plain. The contents of each observation are as follows.

(1) Continuous observation on water-level/turbidity and observation on water flow-rate

The continuous river measurement instrument composed of water level gauge, turbidity meter, and automatic water sampler had been set in the six rivers (the Ohta River, the Odaka River, the Ukedo River, the Maeda River, the Kuma River and the Tomioka River) since April 2014. The water level and the turbidity were recorded at every 10 minutes interval. When the water level became higher than a certain value, 2-liter river water was taken twelve times at one hour interval. Also, the flow rate was measured at the time of normal water level and flooding. Based on these measurements, the equation of relation between water level and flow rate (H-Q equation) was made, and the observed water level was converted to the flow rate.

(2) Measurement on radioactive-cesium concentration in river water

At the time of normal water level, 20-liter river water was taken from the bridge using buckets and ropes. The sampling has been carried out once per month since April 2015 for the Ohta River, the Odaka River, the Ukedo River and the Takase River. For the other rivers, the sampling has been conducted once per month since April 2016. Also, the same sampling procedure has been carried out at the time of flooding every year. For the collected samples, the particulate and dissolved components were separated using membrane filter (pore size: 0.45 μm). The particulate component on the filter was dried at 90°C for 90 min, then weighed. For the dissolved component, radioactive cesium was concentrated using nonwoven fabric impregnated with

potassium zinc ferrocyanide (Yasutaka et al., 2015)⁶⁹). The concentration of ^{137}Cs in particulate and dissolved components was determined using a Ge semiconductor detector. For the samples taken in the procedure (1) at the time of flooding, the measurable amount of dissolved ^{137}Cs component could not be obtained. So, only particulate ^{137}Cs on the filter was measured.

(3) Measurement on depth distribution of radioactive-cesium concentration in flood plain

At the fixed point in the flood plain of each river, soil was taken in the depth direction at 1 cm interval by the scraper-plate method. The sampling has been conducted once a year after the flood season. The concentration of ^{137}Cs in the sampled soil was measured by a Ge semiconductor detector.

(4) Measurement on air dose rate on flood plain

Five side lines were set at the direction perpendicular to the water flow in the flood plain of each river. The interval of the lines was about 10 m. The air dose rate at 1 m height was measured along the side line at 1-2 m interval using gamma plotter H (Mimura et al., 2012)⁷⁵). The results were recorded together with the location information obtained by GPS. The measurements were conducted at the same time with soil sampling from the flood plain.

3.4.3 Results and discussion

Fig. 3.4-2 shows the temporal changes in the concentration of particulate and dissolved ^{137}Cs for the Ohta River, the Odaka River, the Ukedo River and the Takase River. Since the present measurement was started after 3 years or more from the accident, the data before that were cited from the references (Tsuji et al., 2014⁵⁹); Yoshimura et al., 2015⁶⁶); Ochiai et al., 2015⁷⁰), 2016⁷⁶); Eyrolle-Boyer et al., 2016⁷⁷); Naulier et al., 2017⁷⁸). The data on the concentration of particulate and dissolved ^{137}Cs presented here are limited to those obtained after one year or more from the accident. Hence, we consider that the data do not contain those just after the accident where the concentration of ^{137}Cs rapidly decreased. Therefore, the data were fitted by simple exponential decreasing function, which are shown in Fig. 3.4-2 together with the effective half-lives. For all rivers, it was revealed that the decreasing rates of the concentration of particulate ^{137}Cs were higher than those of dissolved ^{137}Cs . As described in Section 3.3, the source of dissolved ^{137}Cs may be moving to the components with low decreasing rate. However, it was shown that the concentration in the particulate ^{137}Cs sources has been decreasing at a constant rate even though six years have passed since the accident. As a possible source of particulate ^{137}Cs , surface soil due to the soil runoff and litter decomposition products are considered (Naulier et al., 2017⁷⁸); Muto et al., 2017⁷¹). It is known that ^{137}Cs in litter and surface soil is gradually migrating to deeper region with time (Mishra et al., 2016⁷⁹); Imamura et al., 2017⁸⁰). Namely, it is presumed that the ^{137}Cs concentration in the source is still decreasing with time even now. Therefore, we can predict that the concentration of particulate ^{137}Cs in river water will decrease accompanied by the concentration decrease in the source. On the other hand, as described in Section 3.3, there is a possibility that the contribution rate of the ^{137}Cs source with low decreasing rate like dissolved ^{137}Cs will increase with time, and thereby the decreasing rate will also become low.

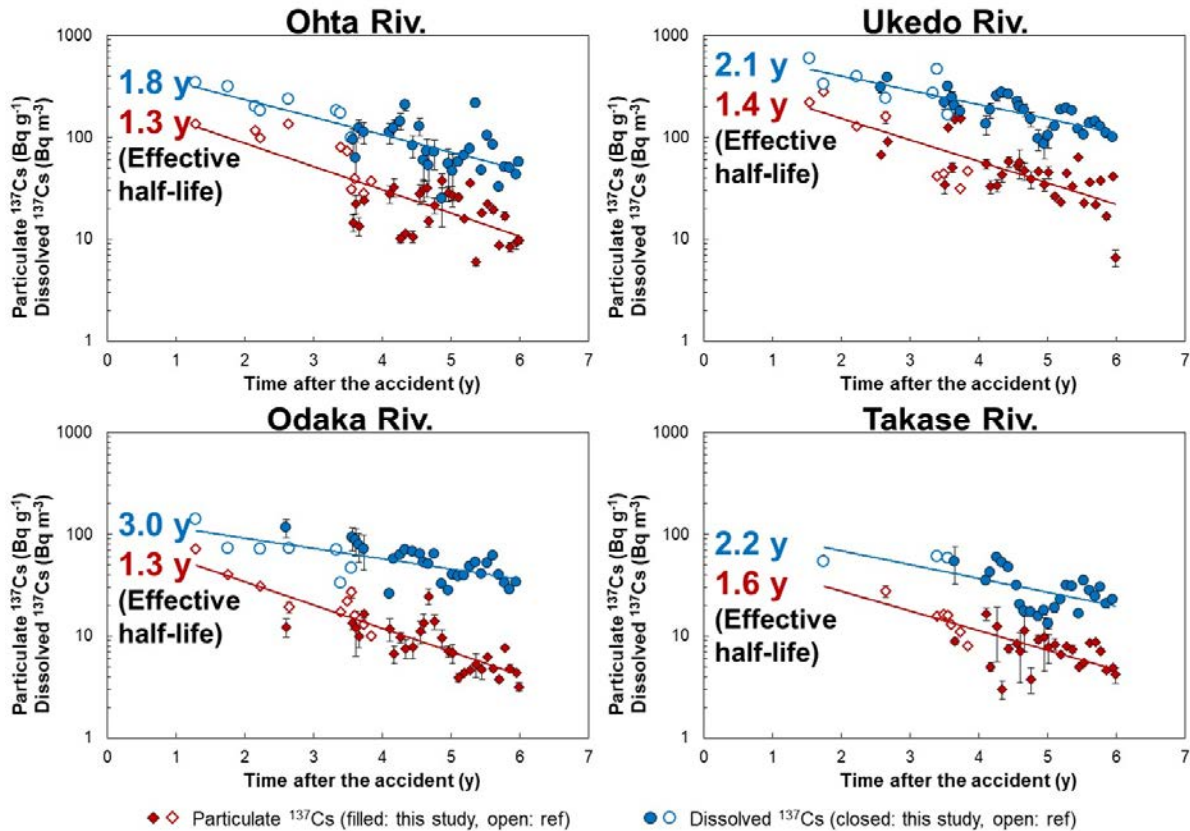


Fig. 3.4-2 Temporal changes in concentration of particulate and dissolved ^{137}Cs in the Ohta River, the Odaka River, the Ukedo River and the Takase River.

From the results of the particulate/dissolved ^{137}Cs concentration and the observation by the continuous river measurement instrument as well as the H-Q equation, the discharge rates of ^{137}Cs from the river basins per year were calculated for the Ohta River, the Odaka River, the Ukedo River, the Takase River, the Maeda River, the Kuma River and the Tomioka River from FY2014 to FY2016. The results are shown in Fig. 3.4-3. The ^{137}Cs outflow rates per year in the observation period were 0.04-0.5% of the ^{137}Cs deposition amount in the river basin. Except for FY2015 which recorded the unprecedented heavy rain, the ^{137}Cs outflow rates were lower than 0.2%. In the case of the Ukedo River, the Ohta River and the Tomioka River with dams in the midstream, the ^{137}Cs outflow rates were low compared with those in the other rivers. The increase in the outflow rates from these rivers in FY2015 (about 1.5 times) were also lower than those from the other rivers (2-4 times). This is because much ^{137}Cs was deposited with particulate materials on the bottom of the dam lakes. Furthermore, for the rivers with dam, the contribution rate of dissolved ^{137}Cs to the ^{137}Cs outflow rate per year became high accompanied by the ^{137}Cs deposition. The discharge of particulate ^{137}Cs happened mostly at the time of flooding. Thus, the contribution rate of dissolved ^{137}Cs exceeds 50% at present. From the results in Fig. 3.4-2, it is considered that this tendency will become clearer in the future.

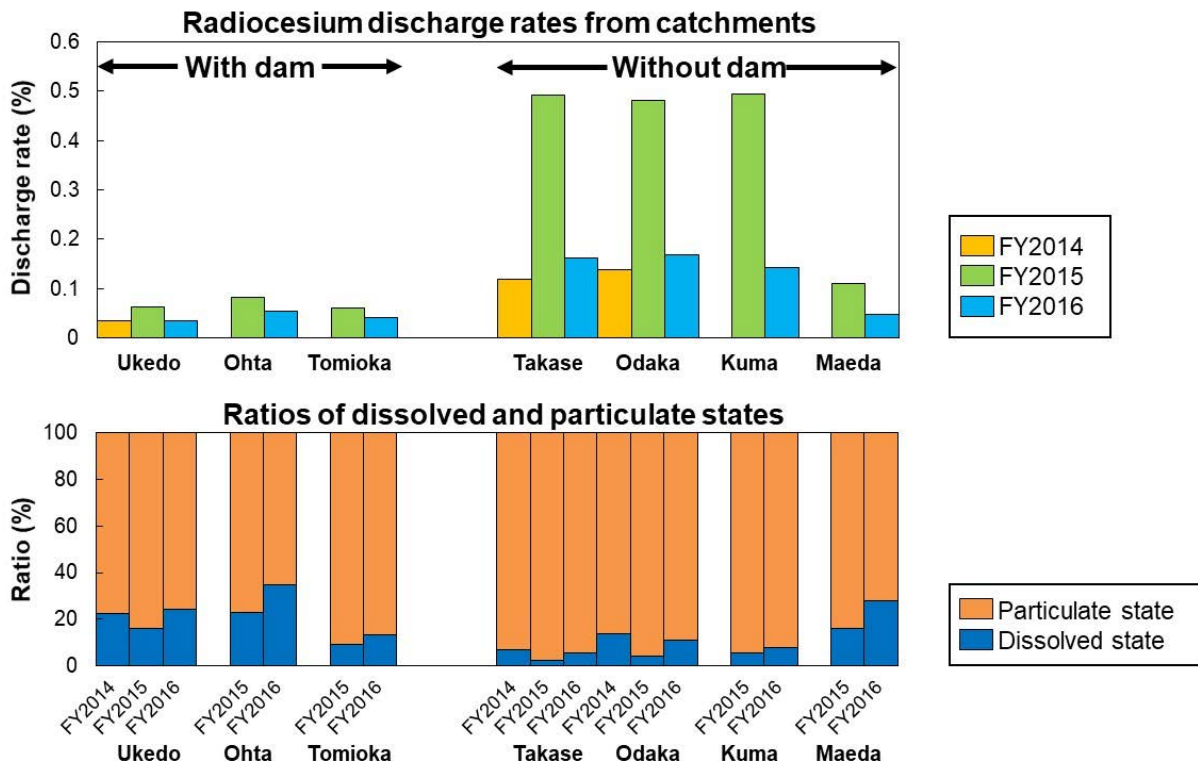


Fig. 3.4-3 Outflow rate of ¹³⁷Cs per year for the Ohta River, the Odaka River, the Ukedo River, the Takase River, the Maeda River, the Kuma River and the Tomioka River.

Among the results of the air dose rate distribution that had been continuously observed since 2013, the temporal changes in the average air dose rates at high-water channel and bank were summarized for the Ukedo River, the Takase River and the Kuma River. The results are shown in Fig. 3.4-4. The air dose rates in the surrounding areas measured by the aerial monitoring are also shown in the figure. Since the bank is not flooded, the air dose rate³⁾ at the bank for each river showed about the same value as that in the surroundings, and it decreased faster than the decreasing rate estimated from the physical decay of radioactive cesium. The fast decrease in the air dose rates at the bank is considered to be due to the shielding effect where radioactive cesium is gradually permeated into soil with time. On the other hand, the air dose rates at the high-water channel that had been flooded were varied depending on the river. The air dose rates at the high-water channel were lower than those at the bank for the Kuma River where the average air dose rates in the river basin were low compared with the surrounding measurement area. On the other hand, for the Takase River with high average air dose rates in the river system, the air dose rates at the high-water channel were higher than those at the bank. These results showed that the air dose rates at the high-water channel were influenced by the concentration of radioactive cesium in soil particles transferred from the upstream. In the case of the Ukedo River with dams in the midstream, the air dose rates at the high-water channel were not so different from those at the bank, because the migration of soil particles was prevented by the dams. Further, in the Takase River and the Ukedo River where there was a high water discharge at the time of heavy rain in Kanto-Tohoku district in September 2015, the rapid decrease in air dose rates were observed at that time.

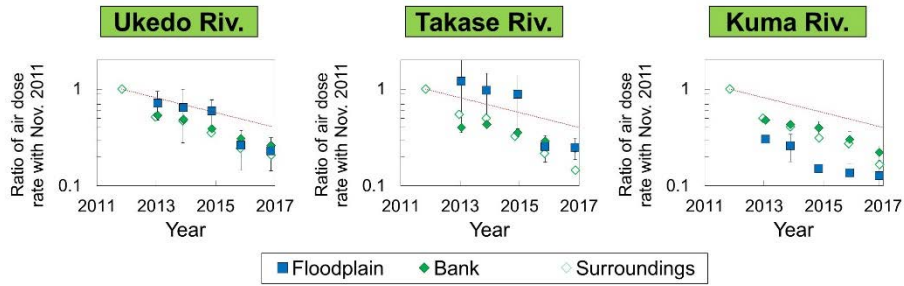


Fig. 3.4-4 Temporal changes in air dose rates for the Ukedo River, the Takase River and the Kuma River.

The values were normalized by the air dose rate (surrounding area) on November 5, 2011 as unity. The dotted lines in red represent the decreasing rate calculated by the physical decay of ¹³⁷Cs.

Figure 3.4-5 shows the results of sediment transfer amount for the Ukedo River system on September 8-13 in 2015 at the time of water discharge caused by the heavy rain in Kanto-Tohoku district. The data were obtained with the automatic observation apparatuses that were set in the river. It is seen that the transfer and deposition amount of sediment in the Takase River without dam in the upstream was larger than that in the Ukedo River with dams. At that time, the amount of sediment transfer in the Takase River was more than 80% of the total transfer in a year (in the case of the Ukedo River, it was about 50%). On the basis of the comparison of the results among the automatic observation apparatuses set in the same river, it was revealed that about 10-20% of outflowing radioactive cesium was deposited on flood plain.

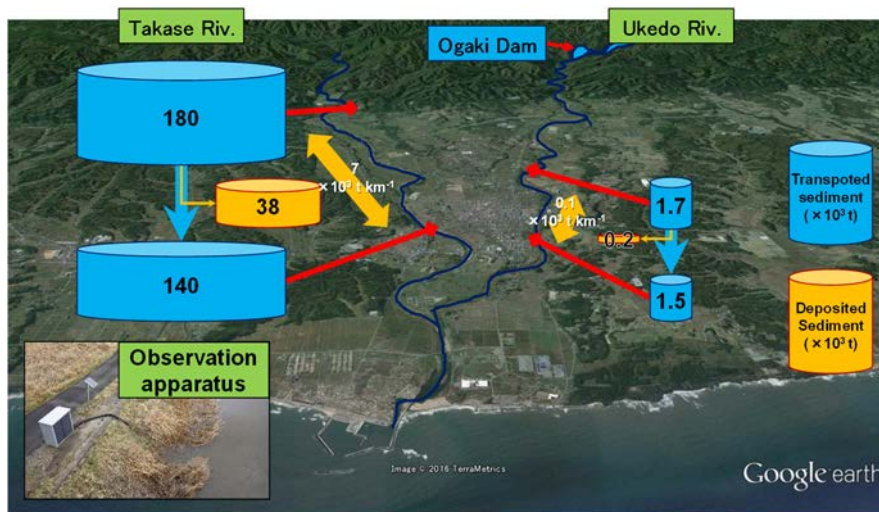
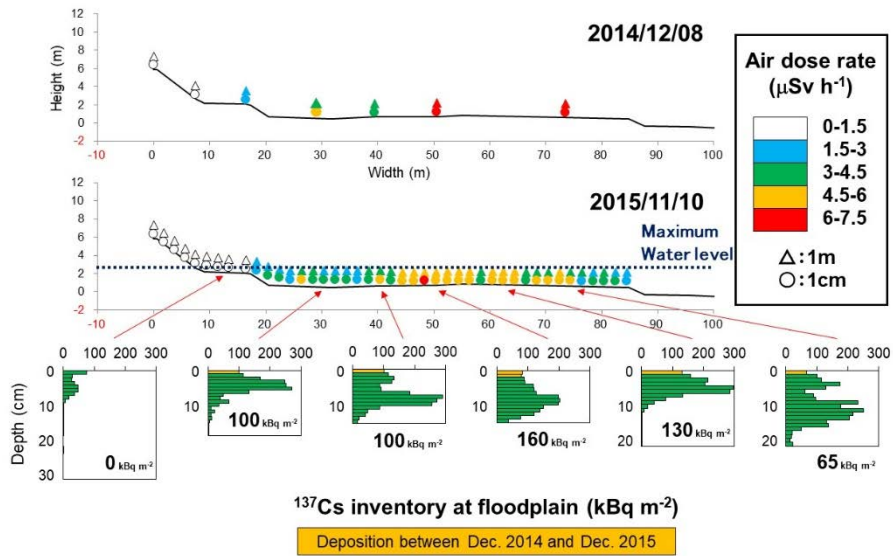


Fig. 3.4-5 Amount of sediment transfer in September 2015 at the time of water discharge caused by the heavy rain in Kanto-Tohoku district.

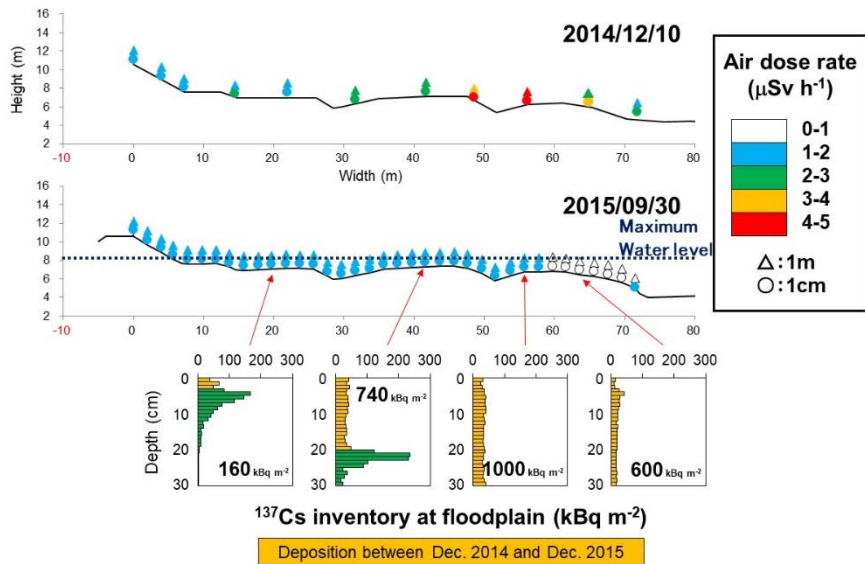
Data were obtained with the automatic observation apparatuses.

Google earth, Image©2016, TerraMetrics.

We have investigated the changes in the deposition amount of radioactive cesium on flood plain in the downstream and the air dose rates at the flood plain, which were induced by the unprecedented heavy rain. When compared the air dose rates at the flood plain in winter 2014 with those in autumn 2015, it was found that those at the high-water channel in the Ukedo River were lower by 10-20%, and those in the Takase River were lower by 30-70% than the respective air dose rates at the banks that had not been flooded (Fig. 3.4-6). The results showed that the decreasing rates of the air dose rates were considerably higher than those estimated by the physical decay of ^{137}Cs in this period (about 10%). Similar to the air dose rate, we also clarified the amount of sediment and radioactive-cesium deposition in this period from the difference in the depth distribution of radioactive cesium between the data in winter 2014 and those in autumn 2015. The results are shown in Fig. 3.4-6. It was found that the thickness of sediment deposited in the flood plain was 1-2 cm for the Ukedo River and 30 cm or more for the Takase River. For both rivers, the concentration of radioactive cesium in the deposited sediment was relatively lower than that in sediment that had been deposited in the past. The result showed that the air dose rate at the high-water channel decreased. When the obtained amount of deposited radioactive cesium per unit area was multiplied by the area of the high-water channel, it was confirmed that the amount of radioactive-cesium deposition was almost the same as that evaluated by the observation apparatuses. In this way, we have quantitatively clarified the migration and deposition behavior of radioactive cesium in rivers by evaluating with multiple methods.



(a) The Ukedo River



(b) The Takase River

Fig. 3.4-6 Temporal changes in air dose rate distribution at the cross section of flood plain and depth distribution of radioactive cesium.

3.4.4 Future subjects

From the present investigation results, we can predict that air dose rates on flood plain will decrease with time in future, because soil particles with low radioactive-cesium concentration are deposited, or soil particles with high radioactive-cesium concentration discharged due to the soil erosion. However, it can be also predicted that air dose rate at some points in flood plain may increase due to the temporal deposition of clay sediment with high cesium concentration. Therefore, it is necessary to make measures to eliminate anxiety about the increase in radiation exposure by evaluating air dose rates in the entire flood plain.

3.5 Riverbed soil

3.5.1 Objectives

Migration of radioactive cesium in river system is affected by various factors such as particle size, distribution coefficient (K_d), amount of clay minerals, and amount of organic materials in sediment. The concentration of radioactive cesium generally increases as the particle size decreases (e.g., He and Walling, 1996)⁸¹). In addition to the particle size, kinds of minerals of suspending materials related to the K_d and especially clay minerals affect the migration of radioactive cesium, because these materials have different Cs-adsorption ability (Facchinelli et al., 2001⁸²); Korobova and Chizhikova, 2007⁸³). It was reported that the low-concentration of radioactive cesium is strongly adsorbed on micaceous minerals (Sawhney, 1970)⁸⁴), so the amount of smectite is also one of the factors to affect the radioactive cesium migration (Facchinelli et al., 2001)⁸²). Mukai et al. (2014)⁸⁵) showed that radioactive cesium is uniformly adsorbed on weathered biotite taken in Fukushima Prefecture. However, it has not yet been clarified what kinds of minerals are involved in the migration of radioactive cesium as a medium. If the transfer medium of radioactive cesium can be specified, the results will contribute to predicting future movement of radioactive-cesium distribution in rivers and elucidating the sorption/desorption mechanism of radioactive cesium on minerals.

In the present study, we investigated the sediment in the Tomioka River, Fukushima Prefecture, from the upstream dams to the downstream sea in order to discuss the relation between radioactive cesium concentration per particle size and mineral composition.

3.5.2 Methods

For the investigation positions, we chose the Tomioka River basin among second-class rivers flowing from the northern Abukuma Mountains to the Pacific sea. Fig. 3.5-1 shows the location of the investigation and sampling. In the Abukuma mountain region, the hinterland of the Tomioka River, granodiorite from Cretaceous period to Miocene period is widely distributed. The granodiorite with medium-to-coarse grain contains amphibole and biotite. In the coastal region, sediment in Quarternary period is distributed (Editorial committee of TOHOKU, part 2 of regional geology of Japan, 1989)⁸⁶). The inventory of ^{137}Cs was 600-1,000 kBq m⁻² in the upstream region, and 1,000-3,000 kBq m⁻² in the downstream region. Riverbed soil was taken from the upstream dam, riverbed and seabed sediments. In total, six samples were collected. The samples were taken at sites A and B in the upstream, at the sites C-E in the downstream, and at the site F in the sea. The samples had been collected at the time of normal water level from 2012 to 2014. The samples in dam and sea were taken with grab sampler. For riverbed soil, the surface sediment of 1 cm was collected using a scoop in the range of 10 cm×10 cm. For the collected samples, the measurement of particle size distribution, the X-ray diffraction (XRD) analysis, the radioactivity analysis, and the separation of minerals were conducted.

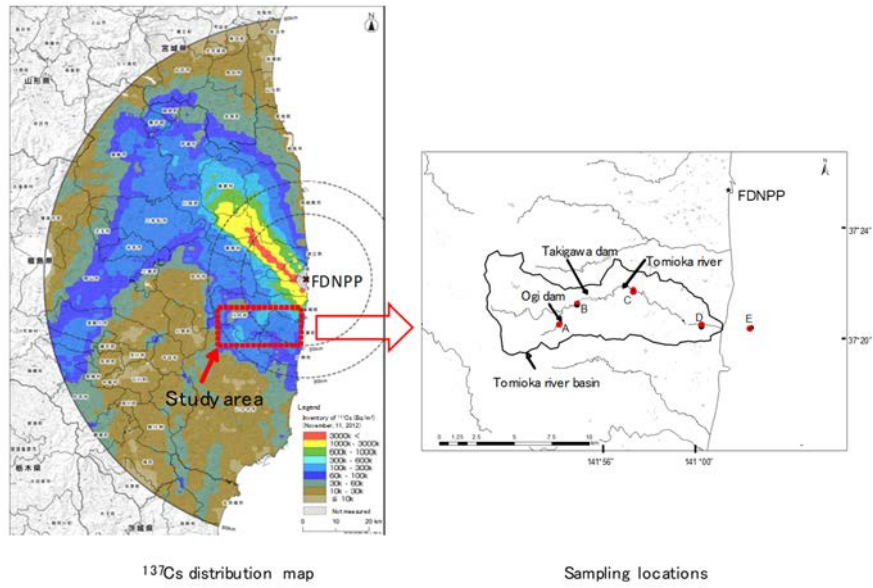


Fig. 3.5-1 Sampling position in the Tomioka River.

FDNPP: Fukushima Dai-ichi Nuclear Power Plant

^{137}Cs deposition is based on 6th air-borne monitoring (November 16th, 2012).

3.5.3 Results and discussion

Fig. 3.5-2 shows the relation between the concentration of ^{137}Cs and the particle size fraction of sediment at the sites A-F. It was found that the concentration of ^{137}Cs in particle fraction smaller than 20 μm was higher than that in particle fraction larger than 20 μm . It was also elucidated that the concentration of ^{137}Cs in particle fraction with clay-size (2 μm) was 3 to 9 times higher than that in particle fraction with silt-size (63-20 μm).

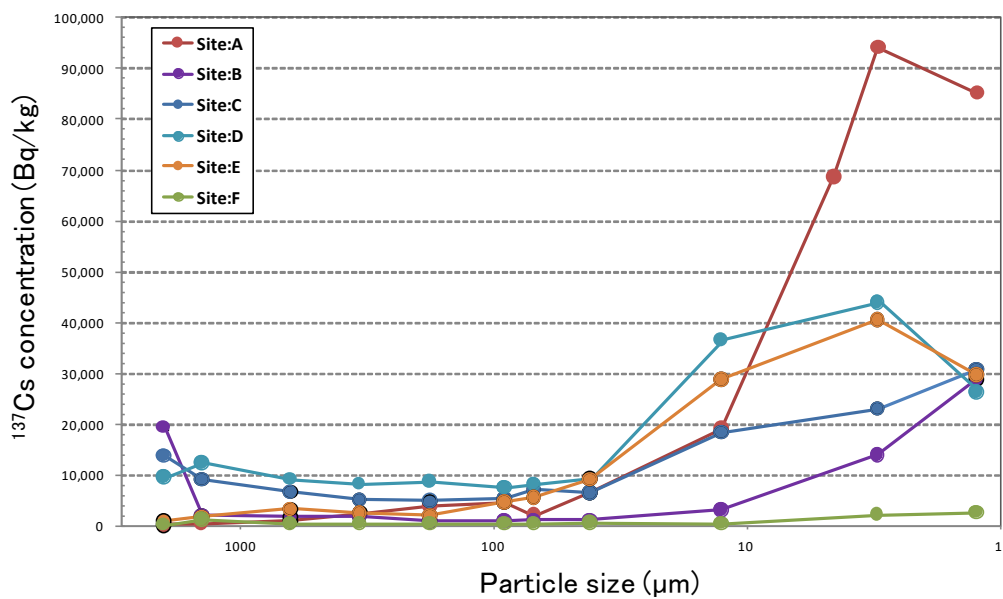


Fig. 3.5-2 Relation between ^{137}Cs concentration and particle size fraction.

The contribution of each particle size fraction to the total radioactivity in bulk sediment was obtained from the concentration of radioactivity and the weight based on the method by Tanaka et al. (2015)⁸⁷⁾ (Fig. 3.5-3). It is seen that the radioactivity in the particle size fraction of 250-106 μm was high at the sites B, C, D and E. The contribution of each particle size fraction to the total radioactivity in bulk sediment was 45.6% at the site B, 20.2% at the site C, 43.0% at the site D and 28.7% at the site E, respectively. For the site A, the particle size fraction of 20-5 μm was dominant. In the case of the site F, the ^{137}Cs concentration in particle fraction of 75-63 μm was higher than that in particle fraction with the other size. From these results, it was revealed that radioactive cesium remains in fine-grained sand (250-106 μm) on riverbed of the Tomioka River system.

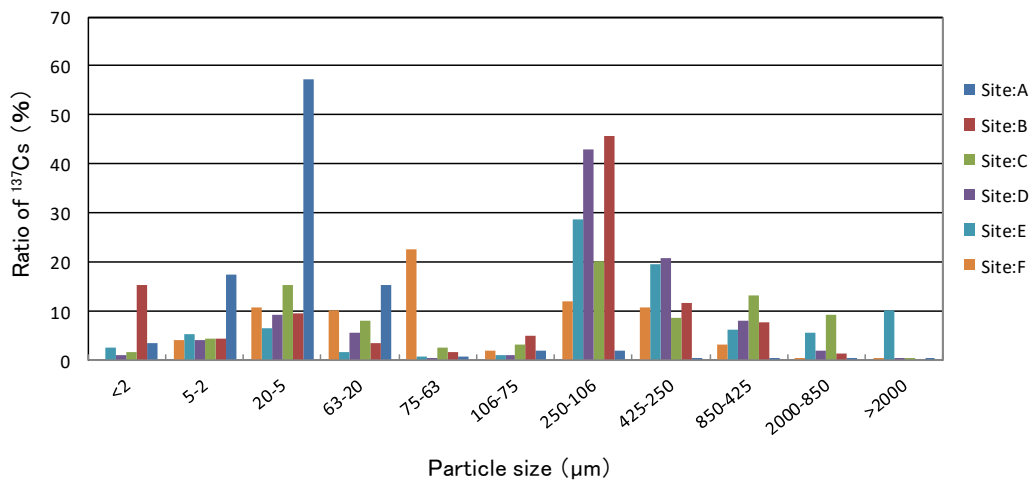


Fig. 3.5-3 Proportion of ^{137}Cs per particle size fraction.

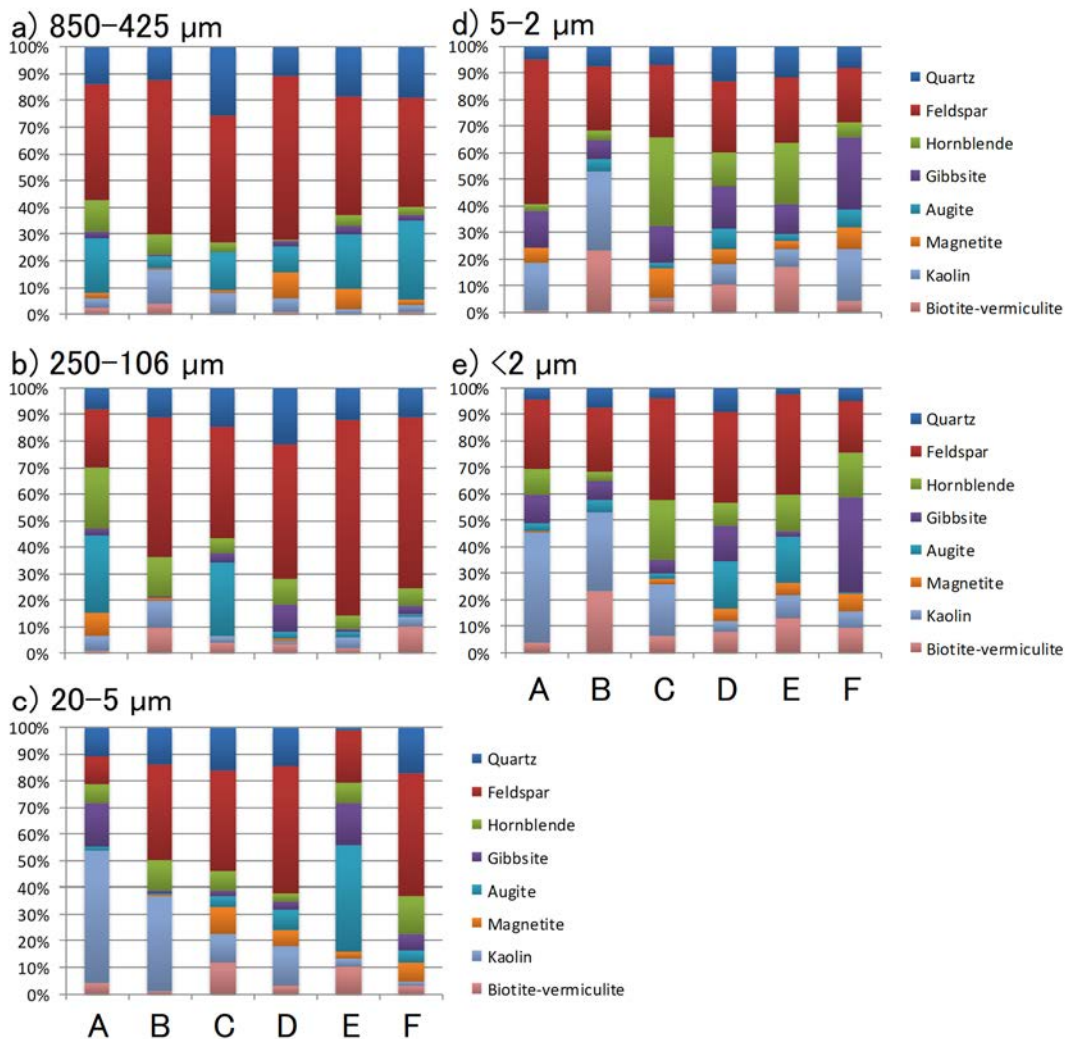


Fig. 3.5-4 Proportion of mineral composition per particle size fraction.

The sediment is composed of quartz, feldspar, amphibole, gibbsite, augite, magnetite, kaolin minerals biotite, and vermiculite from the upstream to the downstream (Fig. 3.5-4). Among the five particle size fraction, quartz and feldspar were dominant in coarse particle fraction (850-425 μm). For fine particle fraction (250-106 μm), quartz, feldspar and amphibole occupied more than 50%. For silt (20-5 μm) and clay particle fraction (< 2 μm), clay minerals occupied 50% in the upstream, and 12-53% in the downstream. The amount of clay minerals became smaller as the downstream.

Fig. 3.5-5 shows the results of classifying mica minerals, colorless minerals and colored minerals in 250-106 μm fraction according to the shape and mineralogy. The results of the quantitative analysis for respective minerals are presented in Table 3.5-1. For colorless minerals, quantitative volume of the downstream riverbed (site D) was larger than that in the upstream dam (site A), also the amount of mica minerals and colored minerals became small in the downstream.

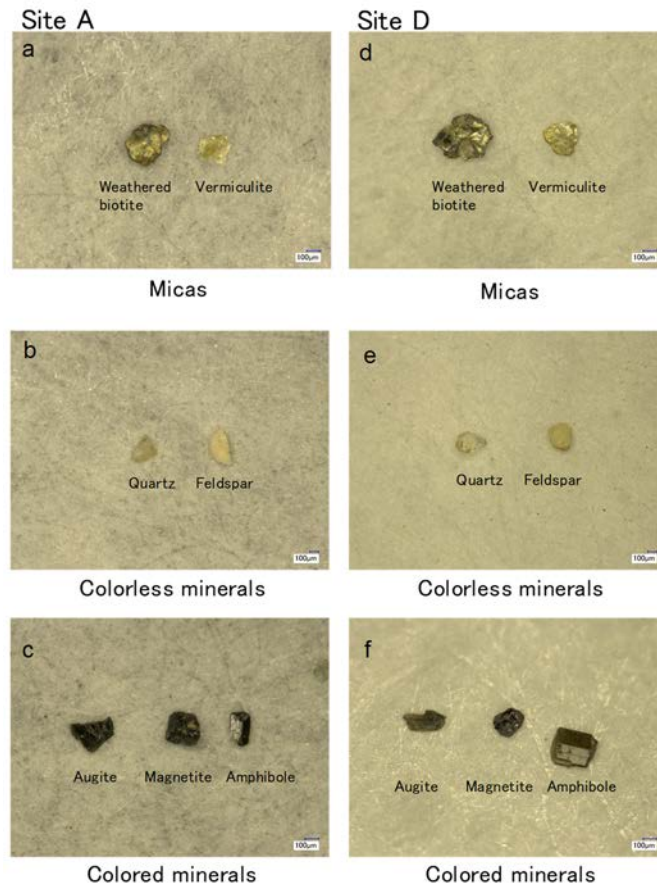


Fig. 3.5-5 Separation results of minerals from 250-106 μm fraction at the sites A and D.

(a) and (d): Mica mineral (the left and right photographs show weathered biotite and vermiculite, respectively). (b) and (e): Colorless mineral (the left and right photographs show quartz and feldspar, respectively.) (c) and (f): Colored mineral (the left, middle and right photographs show augite, magnetite and amphibole, respectively.)

The ^{137}Cs concentration in minerals of 250-106 μm fraction at the sites A and D is shown in Fig. 3.5-6. The ^{137}Cs concentration in mica minerals and colored minerals was higher than that in colorless minerals. The ^{137}Cs concentration in colored minerals was 1.2-2.2 times higher than that in mica minerals, and that in colorless minerals was 1/3-1/5 times of that in mica minerals.

Table 3.5-1 Results of separation and quantitative analysis of 250-106 μm fractions at the sites A and D.

Separated minerals	Replicates	Site A		Site D	
		wt (%)		wt (%)	
		Average	SD	Average	SD
Micas	3	28.1	7.7	11.1	7.8
Felsic	3	40.2	8.1	78.0	7.8
Mafic	3	31.7	1.9	10.9	3.9

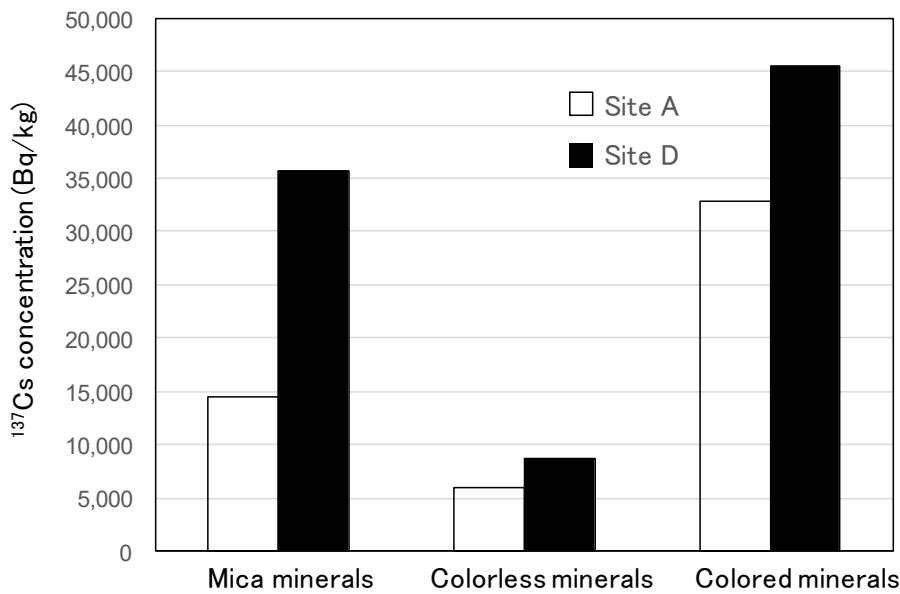


Fig. 3.5-6 Concentration of radioactivity in respective minerals at the sites A and D.

From these results, it was found that even for similar sized particles the concentration of ^{137}Cs are different depending on the kind of minerals and the quantity. In particular, it was revealed that the amount of mica minerals, colored minerals, and colorless minerals could be the indication to know radioactive cesium dynamics in river basin. It was newly found that colored minerals contain equivalent or larger amount of radioactivity compared with mica minerals. Also, we elucidated that ^{137}Cs is contained in colorless minerals. It should be noted that biotite and vermiculite can also become transfer media of ^{137}Cs . In the previous study, it was reported that biotite (<50 μm) in which a part became vermiculite is easy to adsorb radioactive cesium compared with the other clay minerals (Mukai et al., 2016)⁸⁸⁾. There is a possibility that amphibole and magnetite among colored minerals adsorb ^{137}Cs . While there was another report presenting that amphibole contains ^{137}Cs of about one-third that of mica minerals, because the K_d value is higher than that of the other colored minerals (Allard et al., 1985)⁸⁹⁾. On the other hand, since ^{137}Cs is hardly sorbed in magnetite at pH lower than 8.5 (Granizo and Missana, 2006)⁹⁰⁾, the contribution of magnetite to ^{137}Cs migration would be low. Since it is known that the K_d value of feldspar is higher than that of the other colorless minerals (Allard et al.,

1985)⁸⁹⁾, and that of quartz is two orders of magnitude lower than that of mica minerals (Akiba et al., 1989⁹¹⁾; Allard et al., 1985⁸⁹⁾), there is a possibility that mica minerals, amphibole and feldspar contribute to the ¹³⁷Cs migration in the Tomioka River. For sand fraction in river system, not only mica minerals but also colored minerals and colorless minerals can become transfer media of ¹³⁷Cs. On the other hand, also for clay fraction, the present results suggested that not only mica minerals but also kaolin minerals were involved (Ohnuki and Kozai, 2013)⁹²⁾ in the ¹³⁷Cs migration.

3.5.4 Future subjects

Since the details of the quantitative mineral distribution in the whole river system are not clear, it is important to estimate the quantity and amount of radioactive cesium for respective mica minerals, colored minerals, and colorless minerals.

3.6 Reservoir

3.6.1 Objectives

Radioactive cesium (¹³⁷Cs) released by the accident migrates in terrestrial and river systems in the state of being dissolved in water (dissolved state) and in the state of being adsorbed on organic materials and soil particles (suspended state). It was reported that the concentration of dissolved and suspended ¹³⁷Cs had rapidly decreased in the early stage after the accident (about one year after the accident). However, considering from the case of the Chernobyl nuclear power plant accident, it is expected that the decreasing rate of ¹³⁷Cs concentration would become lower in one year or more after the accident. In Hamadori District, Fukushima Prefecture, lots of reservoirs are installed for securing irrigation water. These reservoirs may play a role in accumulating ¹³⁷Cs supplied from the upstream basin. On the other hand, it is considered that the reservoirs may also play a role in the outflowing source of ¹³⁷Cs to the downstream. Therefore, reservoirs are the important investigation spots in evaluating the dynamics of ¹³⁷Cs in whole river basins. In this chapter, we present the investigation results of water quality and bottom sediment, which had been conducted in order to clarify the migration and deposition behavior of ¹³⁷Cs in reservoirs.

3.6.2 Methods

(1) Observation spots

The investigation was conducted for four dams (Yokokawa, Ogaki, Sakashita and Takigawa dams) in Hamadori District, Fukushima Prefecture and nine small reservoirs in Okuma Town and Futaba Town, where the air dose rates are high. The location of the investigated spots are shown in Fig. 3.6-1.

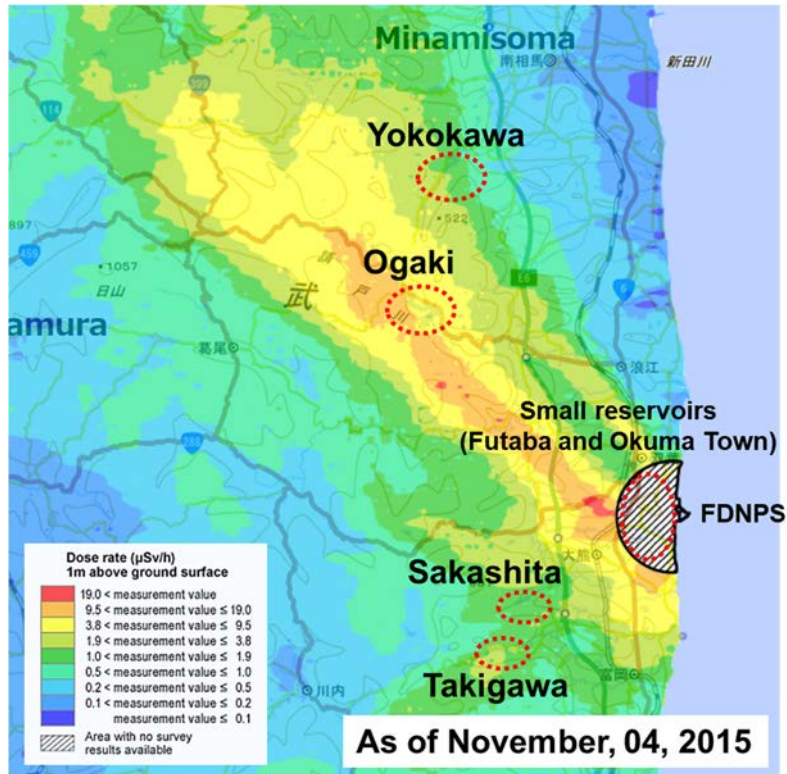


Fig. 3.6-1 Location of the investigated spots.

Dose rate is based on 10th air-borne monitoring (November 4th, 2015).

(2) Contents of the investigation

1) Investigation of water quality

Reservoir water had been collected using a van-Dorn water sampler or a dipper once a month from April 2014. The collected water was separated into dissolved and suspended components by filtrating using membrane with 0.45 μm pores. For the dissolved component after the filtration, the samples taken in Sakashita and Takigawa dams were concentrated using nonwoven fabric impregnated with potassium zinc ferrocyanide (Yasutaka et al., 2015)⁶⁹ or coprecipitated using phospho-ammonium molybdate. For the samples taken in Yokokawa and Ogaki dams, the filtrate was treated by evaporative concentration around 70 °C. The radioactivity in respectively treated samples were measured by a Ge semiconductor detector. On the other hand, the suspended component on the filter was dried at 90 °C for 90 min, and weighed, then the radioactivity was measured by a Ge semiconductor detector.

2) Investigation of bottom sediment

Here, we report on the results of the investigation of bottom sediment conducted at Ogaki dam, Namie Town in FY2013. The bottom sediment samples were collected using an underwater vibration-type core sampler and an undisturbed columnar bottom sampler. The sample was cut to columnar shape at 1 cm or 2 cm interval using a scraper. Then, the sample was put in a U8 container after being dried, and the concentration of the radioactivity was measured by a Ge semiconductor detector. For columnar samples taken at the Ogaki dam, particle-size distribution was measured by a laser diffraction particle size analyzer

(Shimadzu Co. SALD-3100) in order to know the property of particle size of the bottom sediment at the sampling spot. For a part of bottom sediment, the sample was divided by the particle size using a sieve and an elutriation process, then the concentration of radioactivity for each particle size was measured by a Ge semiconductor detector. The particle size was classified into seven groups according to Wentworth et al. (1922)⁹³, that is, clay (<2 μm, 2-4 μm), mud (4-16 μm, 16-63 μm), sand (63-500 μm, 500-2000 μm) and gravel (>2000μm).

3) Investigation by sediment trap

A sediment trap (Nichiyu Giken Kogyo Co. Ltd.) was set at the lake bottom near the water intake of the dam (the sampling intake was 60 cm height from the bottom of the lake). Using the sediment trap, sedimentary particles had been periodically collected since April 2014. The collected sample was put in a U8 container after being dried, then the concentration of the radioactivity was measured by a Ge semiconductor detector. Like the bottom sediment samples, the sedimentary samples were divided by the particle size using a sieve and an elutriation process, then the concentration of radioactivity for each particle size was measured by a Ge semiconductor detector.

3.6.3 Results and discussion

(1) Water quality

1) Temporal changes in the concentration of dissolved and suspended ¹³⁷Cs

The concentration of dissolved ¹³⁷Cs in Sakashita dam and Takigawa dam had been changing below 0.1 Bq L⁻¹, and that in Ogaki dam and Yokokawa dam had been changing below 1 Bq L⁻¹. In Okuma Town and Futaba Town which locate in the difficult-to-return zone, the concentration of dissolved ¹³⁷Cs in reservoirs was approximately less than 1 Bq L⁻¹ (Fig. 3.6-2). It was observed that the concentration of dissolved ¹³⁷Cs increased in summer, while it decreased in winter. However, on the basis of the four-year continuous observation from 2013, it was clarified that such seasonal fluctuation of the ¹³⁷Cs concentration did not induce changes in ¹³⁷Cs concentration at the order level through the year.

The concentration of suspended ¹³⁷Cs was approximately in the range from 10⁴ to 10⁶ Bq kg⁻¹ (Fig. 3.6-3). However, we could not confirm any clear seasonal fluctuation in contrast to dissolved ¹³⁷Cs.

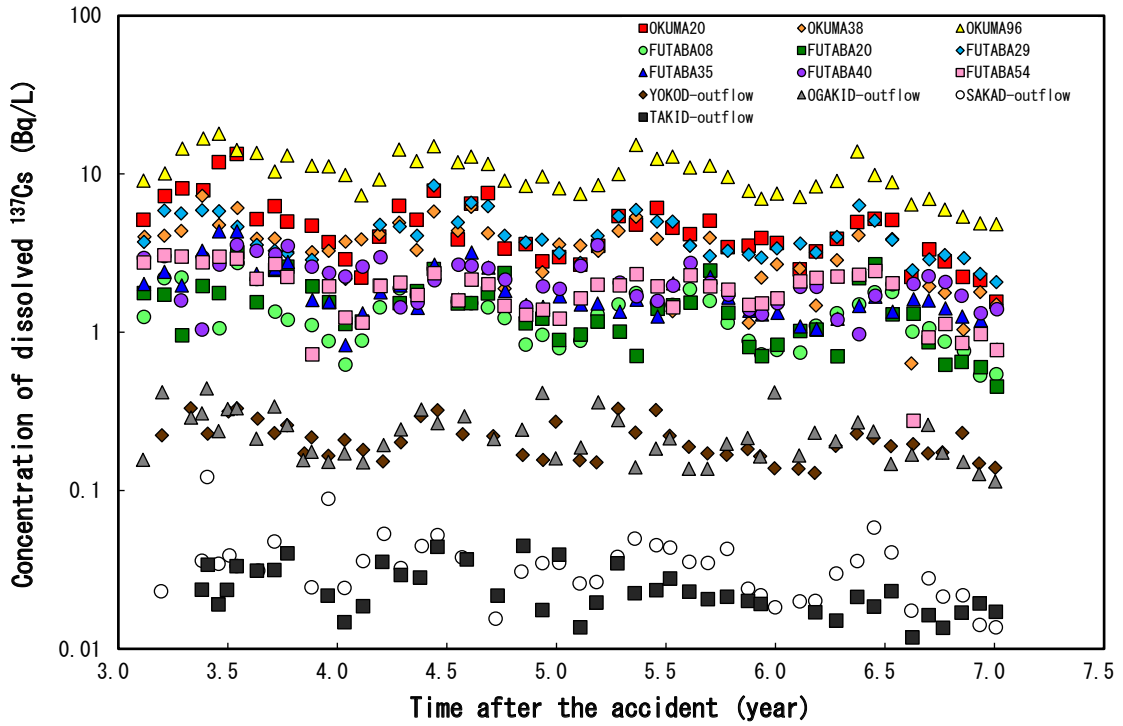


Fig. 3.6-2 Temporal change in concentration of dissolved ^{137}Cs .

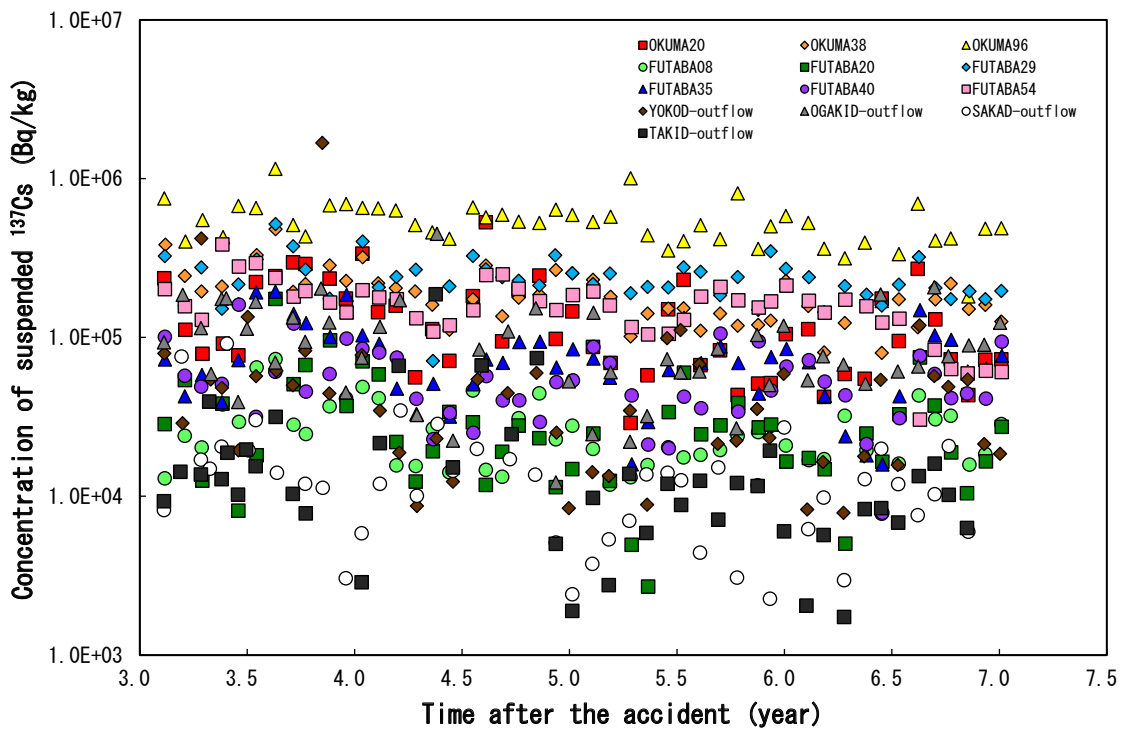


Fig. 3.6-3 Temporal change in concentration of suspended ^{137}Cs .

We started the measurements on the concentration of dissolved and suspended ^{137}Cs after 3 years or more from the accident. Therefore, it is considered that our observation does not include the period of rapid decrease in the ^{137}Cs concentration just after the accident. For this reason, in this section, the changes in the ^{137}Cs concentration were fitted by a simple logarithmic approximation curve with one component shown below,

$$T_{\text{eff}} = \ln 2 / \lambda_{\text{eff}} \quad (1)$$

$$A_t = A_0 \exp(-\lambda_{\text{eff}} t) \quad (2),$$

where T_{eff} is the effective half-life, λ_{eff} is the decay component, A_t is the ^{137}Cs concentration in the year (t) that has passed after the accident, and A_0 is the initial ^{137}Cs concentration just after the accident. Table 3.6-1 summarizes the effective half-life of the concentration of dissolved and suspended ^{137}Cs in each reservoir, the decay component, and the initial ^{137}Cs concentration just after the accident. The effective half-life of the concentration of dissolved and suspended ^{137}Cs could be estimated to be 1.95-3.22 years and 1.83-3.51 years, respectively. Comparing these results with the effective half-lives of the concentration of dissolved and suspended ^{137}Cs in rivers shown in Section 3.4.3, it was revealed that the decreasing rate of the dissolved ^{137}Cs concentration was hardly different from that in rivers, while the concentration of suspended ^{137}Cs in reservoirs decreased more slowly than that in rivers. One of the plausible reasons of this fact is that suspended ^{137}Cs in reservoirs does not come from the upstream like rivers, but suspended state with high ^{137}Cs concentration is continuously produced due to the effect of refloating of sediment in the reservoir.

Table 3.6-1 Effective half-life and decay component of dissolved and suspended ¹³⁷Cs concentration in each reservoir in four years (from 3 years to 7 years after the accident), and the initial ¹³⁷Cs concentration just after the accident.

measurement spot	dissolved state			suspended state		
	A_{0_d}	λ_{eff_d}	T_{eff_d}	A_{0_p}	λ_{eff_p}	T_{eff_p}
	Bq L ⁻¹		year	kBq kg ⁻¹		year
OKUMA20	13.97	0.233	2.15	340	0.229	2.17
OKUMA36	12.63	0.284	1.95	476	0.195	2.33
OKUMA96	24.16	0.177	2.42	1050	0.144	2.63
FUTABA08	2.83	0.161	2.52	42	0.113	2.87
FUTABA20	4.15	0.226	2.18	55	0.164	2.50
FUTABA29	5.69	0.080	3.22	306	0.060	3.51
FUTABA35	4.51	0.191	2.35	121	0.122	2.80
FUTABA40	4.10	0.138	2.67	92	0.122	2.80
FUTABA54	4.47	0.189	2.36	517	0.246	2.10
Yokokawa dam	0.36	0.108	2.92	108	0.223	2.19
Ogaki dam	0.39	0.117	2.84	121	0.082	3.19
Sakashita dam	0.08	0.180	2.41	53	0.320	1.83
Takigawa dam	0.07	0.213	2.24	44	0.268	2.01

2) Apparent distribution coefficient in reservoir

We calculated the apparent distribution coefficient based on the concentration of dissolved and suspended ¹³⁷Cs by the following equation,

$$\text{Apparent distribution coefficient (L kg}^{-1}\text{)} = \frac{\text{Concentration of suspended } ^{137}\text{Cs (Bq kg}^{-1}\text{)}}{\text{Concentration of dissolved } ^{137}\text{Cs (Bq L}^{-1}\text{)}} \quad (3)$$

Fig. 3.6-4 shows the apparent distribution coefficient in each reservoir, which had been obtained in the period of the investigation. The apparent distribution coefficients in small reservoirs in Okuma Town and Futaba Town were approximately in the order from 10⁴ to 10⁵ L kg⁻¹, and those in dams were approximately in the order from 10⁵ to 10⁶ L kg⁻¹. These values were one to two orders of magnitude larger than those reported by foreign countries (Konoplev et al., 2016)⁹⁴). From this result, it is understood that the concentration of dissolved ¹³⁷Cs in reservoir water is kept considerably low because ¹³⁷Cs is strongly adsorbed on suspended particles such as clay minerals in the investigated reservoirs in Fukushima Prefecture. From now on, we plan to clarify the difference in the apparent distribution coefficient in each reservoir by investigating the details of organic material content that is considered to contribute to the production of mineral species at the bottom and dissolved species.

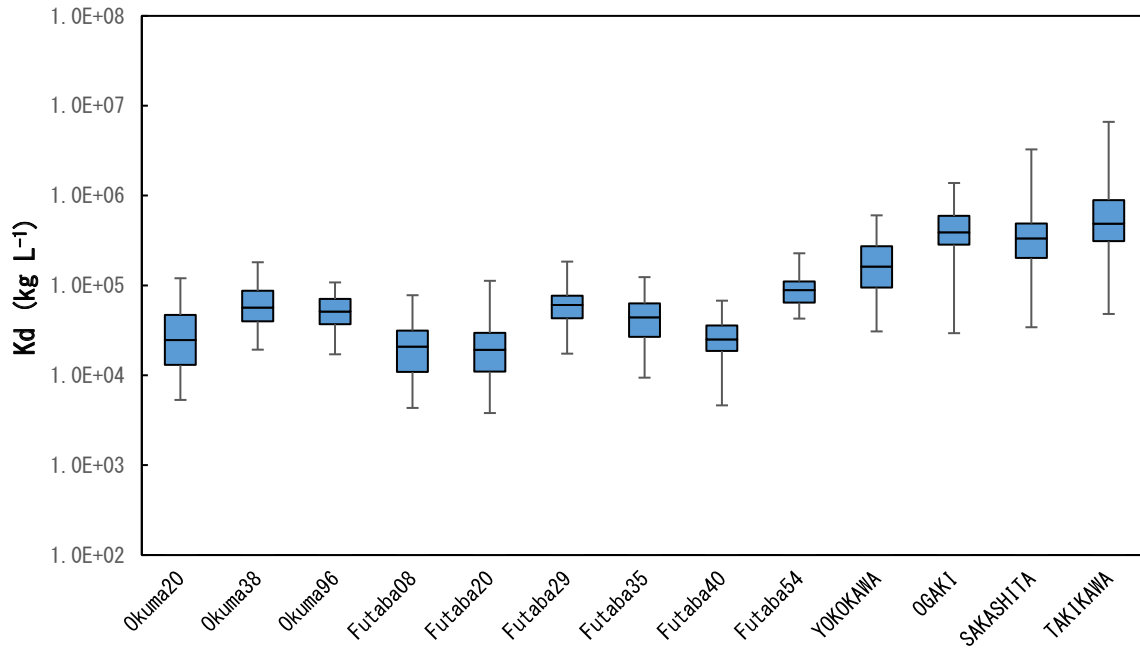


Fig. 3.6-4 Apparent distribution coefficient in each reservoir.

(2) Bottom sediment

Fig. 3.6-5 shows the measurement spot of bottom sediment in Ogaki dam. In FY2013 when the investigation was conducted, the downstream region was designated as the evacuation-order area. Therefore, the water level was managed to be low, because there was no schedule to be used for irrigation water. The bottom sediment samples were collected at nine spots along the water route of the reservoir.

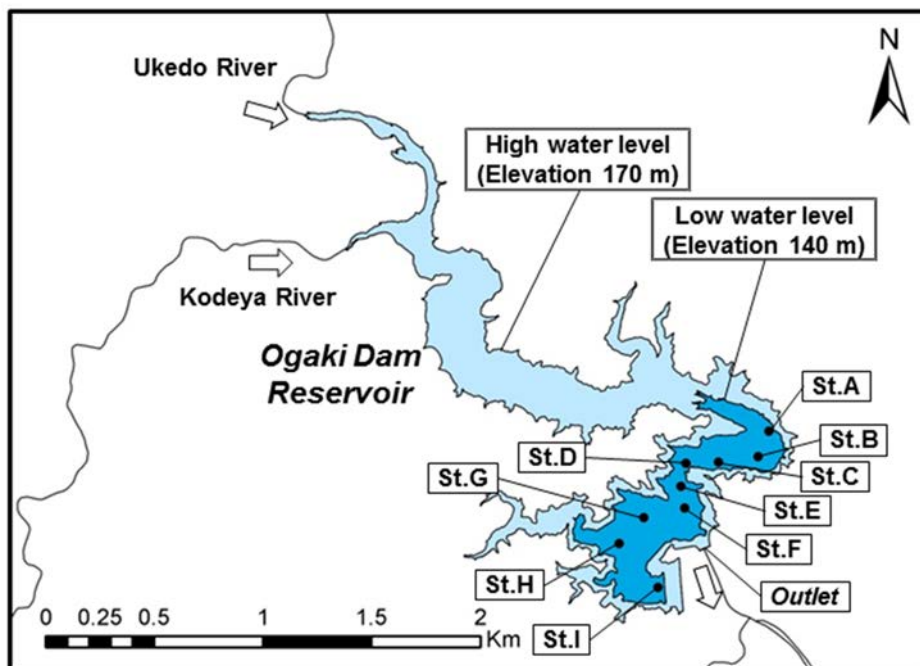


Fig. 3.6-5 Sampling spots of bottom sediment in Ogaki dam.

1) Estimation of accumulation and outflow amount of ^{137}Cs to bottom sediment

Table 3.6-2 shows the deposition amount and deposition rate of ^{137}Cs in each sampling spot. Fig. 3.6-6 presents and vertical distribution of ^{137}Cs concentration and particle size of bottom sediment in each spot. In most of the sampling spots, the layer with high ^{137}Cs concentration was clearly observed in the lower part of the contaminated bottom sediment. It is considered that this layer was formed by the deposition of suspended particles with high ^{137}Cs concentration at the relatively early stage after the accident. Therefore, this layer is the important indication to estimate the deposition rate of bottom sediment.

Table 3.6-2 Deposition amount and deposition rate of ^{137}Cs at each sampling point in Ogaki dam.

sampling spot	sampling date	water depth (m)	length of sample (cm)	deposition amount of ^{137}Cs (MBq m ⁻²)	deposition rate (g cm ⁻² y ⁻¹)
A	2013/11/1	18	68	28.5	12.9
B	2013/11/5	21	31	15.4	4.2
C	2013/11/1	24	48	28.6	7.8
D	2013/11/5	21	43	21.4	6.1
E	2013/10/31	25	11	4.8	0.4
F	2013/10/28	21	10	7.0	0.7
G	2013/10/25	13	8	5.0	0.4
H	2013/10/24	12	9	6.9	0.7
I	2013/10/29	10	8	5.9	1.1

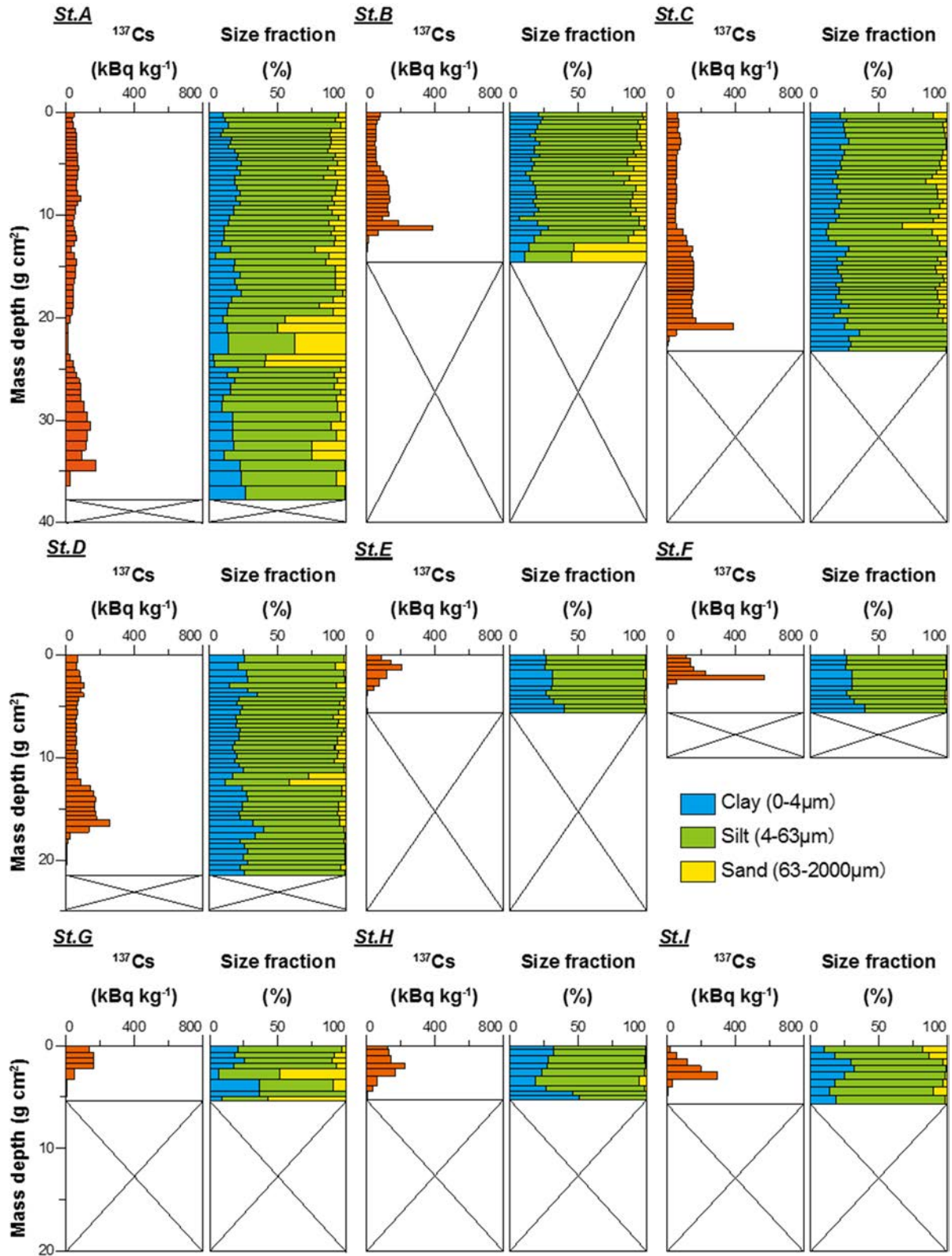


Fig. 3.6-6 Vertical distribution of ^{137}Cs concentration and particle size of bottom sediment in Ogaki dam.

It was observed that the deposition amount of ^{137}Cs in bottom sediment was 4.8-28.6 MBq m⁻², which was higher than the initial deposition amount in land soil around the reservoir (3.2 MBq/m²; MEXT, 2011⁹⁵). It was also found that the accumulation amount of ^{137}Cs in the St. A~D located at the upstream side of the reservoir was larger by 2-6 times than that in the St. E~I located at the downstream side. In addition, the deposition rate of bottom sediment in the upstream side after the accident (4.2-12.9 g cm⁻² y⁻¹) was considerably higher than that in the downstream (0.4-1.1 g cm⁻² y⁻¹). The bottom sediment is mainly composed of clay fraction (about 20%) and silt fraction (about 70%). From the results of particle-size analysis of bottom sediment, it was revealed that the bottom sediment in the upstream side contains sand fraction. Especially, gravel fraction was found in addition to sand fraction at the depth of 19.8-24.8 g cm⁻² in the St. A. The ^{137}Cs concentration in the upper layer (new layer) on this coarse-grained layer was lower than that in the lower layer. For the columnar samples taken in the St. B~D, the similar coarse-grained layer was interbedded, and it was revealed that the concentration of ^{137}Cs in the upper region of this coarse-grained layer tended to be lower than that in the lower region. It is considered that this coarse-grained layer that is specific to the upstream region was formed by the flood due to the heavy rain at the time of typhoon. On the other hand, in the case of St. E and St. F that are close to the outlet works in the downstream side, the bottom sediment consists of clay fraction and silt fraction, but neither sand fraction nor gravel fraction was observed. From these results, it is presumed that among the sediment flowing from the upstream region, only relatively fine fraction (clay fraction and silt fraction) was transported to the vicinity of the outlet work, and a part of this fraction is outflowing to the downstream region.

The Tohoku Regional Agricultural Administration Office has been measuring the concentration of suspended materials in influent and effluent at Ogaki dam since September 2012. Based on the observed ^{137}Cs concentration in the suspended materials, they estimated the inflow and outflow of ^{137}Cs into reservoirs. As a result, they reported that among ^{137}Cs flowing into a reservoir, about 90% tended to be accumulated in the reservoir without flowing to the downstream of the reservoir (MAFF, 2016)⁹⁶. Considering the total balance of ^{137}Cs in the Ukedo River basin, it is considered that Ogaki dam pooled ^{137}Cs that came from the upstream, and the dam played a role in considerably reducing its outflow to the downstream.

Based on the accumulation amount of ^{137}Cs in bottom sediment of the reservoir, we estimated the outflow amount of ^{137}Cs from the upstream. As a result, it was suggested that about 3.0×10^{12} - 3.9×10^{12} Bq was supplied as the outflow for about 2.6 years from the accident to the date of the investigation. Since this amount corresponds to about 1.1-1.4% of the initial deposition amount in the upstream region (2.8×10^{14} Bq), we considered that the amount of the outflow was appreciably small (Funaki et al., 2018)⁹⁷. In the previous studies (Yoshimura et al., 2015⁹⁸); Hayashi et al., 2016⁹⁹); Niizato et al., 2016⁹); Tsuji et al., 2016⁶¹); Iwagami et al., 2017⁶⁷), it was also reported that amount of ^{137}Cs outflow in forests and rivers was considerably small, and ^{137}Cs will remain in forests for a long time. We obtained the results that are in good agreement with the previously reported ones.

3.6.4 Future subjects

The Tohoku Regional Agricultural Administration Office fertilized potassium (content of exchangeable potassium: 25 mg/100 g dry soil) in paddy fields after the decontamination in FY2015, and conducted test cultivation using water in the Ukedo River discharged from Ogaki dam. As a result, they found that the concentration of radioactive cesium (total of ^{134}Cs and ^{137}Cs) in all brown rice was appreciably lower than the standard value for food safety (100 Bq kg^{-1}). Thus it was revealed that there is no problem in using water discharged from the dam as irrigation water (Tohoku Agricultural Administration Bureau., 2016)⁹⁶. On the other hand, since the concentration of dissolved ^{137}Cs in reservoirs in the difficult-to-return zones is still higher than 1 Bq L^{-1} , it would be necessary to implement countermeasures to reduce the concentration of dissolved ^{137}Cs in order to use it as irrigation water.

3.7 Estuary and coastal area

3.7.1 Objectives

It is presumed that radioactive cesium adsorbed on soil flowing from mountain forests into estuaries and coastal areas through rivers would be deposited in the region where the water depth is relatively shallow. In the preliminary analysis using the ROMS, it was suggested that most of soil particles corresponding to silt with a particle size of 0.02 mm was deposited in the region shallower than about 30 m within 5 km from the coast (Itakura, 2013: private communication). However, most of the previous studies were conducted for seabed sediment and sea water deeper than 50 m, so there has been few data on sediment and water in the region shallower than 30 m (Otosaka and Kobayashi 2012¹⁰⁰); Kusakabe et al., 2013¹⁰¹); Black and Buesseler 2014¹⁰²); Ono et al., 2015¹⁰³), etc.). Therefore, in the investigation of estuaries and coastal areas by the F-TRACE (Long -term Assessment of Transport of Radioactive Contaminant in the Environment of Fukushima), the purpose of the research was to understand the migration behavior of radioactive cesium in the sea shallower than about 30 m. Through the understanding of the migration behavior of radioactive cesium, it will be possible to estimate the contribution of radioactive cesium supplied from rivers and to present information on the basic future prediction of “place” where marine products are living.

3.7.2 Methods

It has been considered that the main pathway of radioactive cesium produced by the accident of the nuclear power station into estuaries and coastal areas are; 1) fallout from the atmosphere, 2) direct release from the nuclear power station, and 3) supply from rivers (Tsumune et al., 2012)¹⁰⁴). It was observed that the concentration of radioactive cesium in seabed sediment at the estuary and coastal area near the nuclear power station is relatively higher than that in offshore and the estuaries of the other rivers. This fact is considered to be due to the direct release from the nuclear power station (Kusakabe et al., 2013¹⁰¹); Misumi et al., 2014¹⁰⁵). This means that the distribution of radioactive cesium in estuaries and coastal areas was determined by various factors such as, 1) the initial effect due to the direct release just after the accident, 2) the supply from rivers, and 3) the secondary re-movement due to the waves and coastal currents at the estuary and coastal area. Therefore, in order to clarify the significant factors that determine the cesium distribution, we tried to understand the characteristics of the environmental features at the estuary and coastal area by firstly conducting the investigation and research to know the distribution of radioactive cesium. Based on the results, we conducted the investigation and research on the factors that determined the changes in the distribution of radioactive cesium. The main results obtained so far are summarized in Table 3.7-1.

Table 3.7-1 Significant investigation items that has been conducted so far at the estuaries and coastal areas.

Year	Significant investigation items	Main target area
FY 2013	<ul style="list-style-type: none"> ●Bathymetric survey and sonic prospecting ●Sediment sampling (grab sampler and core sampler) ●Nautical survey (flow direction and velocity, wave height, turbidity etc.) 	<ul style="list-style-type: none"> ●Near the mouth of Odaka, Ukedo and Kuma River ●Near the mouth of all rivers ●Near the mouth of Ukedo River
FY 2014	<ul style="list-style-type: none"> ●Bathymetric survey and sonic prospecting ●Sediment sampling (grab sampler) and sea water sampling 	<ul style="list-style-type: none"> ●Near the mouth of Maeda and Tomioka River ●Near the mouth of all rivers
FY 2015	<ul style="list-style-type: none"> ●Bathymetric survey and sonic prospecting ●Sediment sampling (core sampler) and sea water sampling ●Nautical survey (flow direction and velocity, turbidity etc.) 	<ul style="list-style-type: none"> ●Near the Fukushima Daiichi Nuclear Power Plant ●Near the mouth of all rivers ●Near the mouth of Ukedo River
FY 2016	<ul style="list-style-type: none"> ●Sediment sampling (core sampler) ●Nautical survey (flow direction and velocity, turbidity etc.) 	<ul style="list-style-type: none"> ●Near the mouth of all rivers ●Near the mouth of Ukedo River
FY 2017	<ul style="list-style-type: none"> ●Sediment sampling (core sampler) and sea water sampling ●Nautical survey (flow direction and velocity, turbidity etc.) 	<ul style="list-style-type: none"> ●Near the mouth of all rivers ●Near the mouth of Ukedo River

As to the investigation on the distribution of radioactive cesium, we conducted the inspection of seabed sediment distribution and seafloor topography, the sampling of seabed sediment and sea water, etc. Concerning the investigation on the factors that determine the distribution of radioactive cesium, we conducted the mooring survey, towing survey, etc. The results are shown in the followings.

3.7.3 Results and discussion

(1) Results of investigation and research on the distribution of radioactive cesium

1) Distribution of radioactive cesium in seabed sediment

① Distribution of seabed sediment and seafloor topography

Radioactive cesium is strongly adsorbed on clay minerals, and the larger the specific surface area is, the higher the abundance per unit area is. This means that the finer the particle is, the higher the concentration of radioactive cesium is (Ambe et al., 2014)¹⁰⁶⁾. Therefore, it is necessary to clarify the particle size distribution of seabed sediment. In addition, the seafloor topography would affect the particle size distribution of seabed sediment. Considering these factors, we have conducted the investigation on seabed sediment distribution and seafloor topography in the estuaries and coastal areas of the main rivers. The results are shown in Fig. 3.7-1.

As a result of the investigation on seabed sediment distribution, it was elucidated that bedrock (Alternated layer of sandstone and mudstone in Sendai layer group; Geological Survey of Japan, Kubo et al., 1994¹⁰⁷⁾) was widely distributed in the region from the Ohta River to the Tomioka River. The distribution ratio of the bedrock in the investigated area corresponded to about 52% of the seabed area. At the north side of 1F, seabed sediment tended to be distributed from the front side to the south side of the estuary, while it tended to be distributed on a straight line from the estuary at the south side of 1F. For the region from the Odaka River to the Ukedo River and the region from the Kuma River to the Tomioka River, we also confirmed the sandbank-

shaped distribution extended to the northern northeast direction with a width of about 1 km to several hundred meters. The thickness of the sediment layer was as thin as 2 to 3 m at the maximum, and we confirmed the region where the bedrock is partly exposed. Seabed sediment was mainly composed of fine to medium grain sand, and the distribution of silt composed of fine particles was limited.

For seafloor topography, the shallow lowland was spread from the front side to the south side of the estuary at the north side of 1F, while it was spread on a straight line from the estuary at the south side of 1F. Seabed sediment tended to be distributed on the lowland. It is understood that the abovementioned sandbank-shaped distribution of seabed sediment exists at the base (near the junction of layered surface and cliff slope) of the cuesta terrain (produced by the selective erosion along the alternated layer of sandstone and mudstone in Sendai layer group : Mii, 1962¹⁰⁸⁾ ;Hoshino, 1971¹⁰⁹⁾) with cliffs of relative height difference of 2 to 3 m. Based on the measured wave height (described later), we calculated the critical water depth for sediment motion by the method proposed by Uda et al. (2002)¹¹⁰⁾. As a result, we obtained that the depth is about 10 m.

Among seabed sediment, fine soil particles corresponding to silt tended to be distributed in semicircular depression made by the collapse of a part of cliff among cuesta terrain (Fig. 3.7-2).

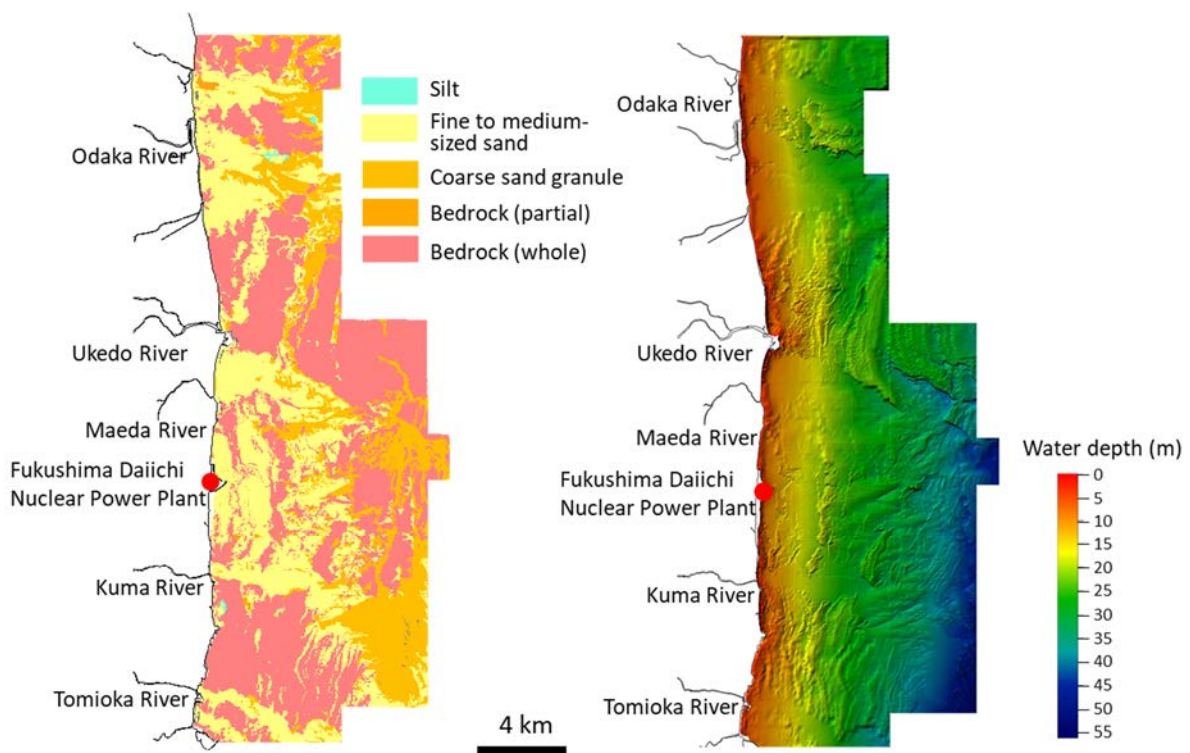


Fig. 3.7-1 Predicted seabed sediments map (left) and Bathymetric map (right).

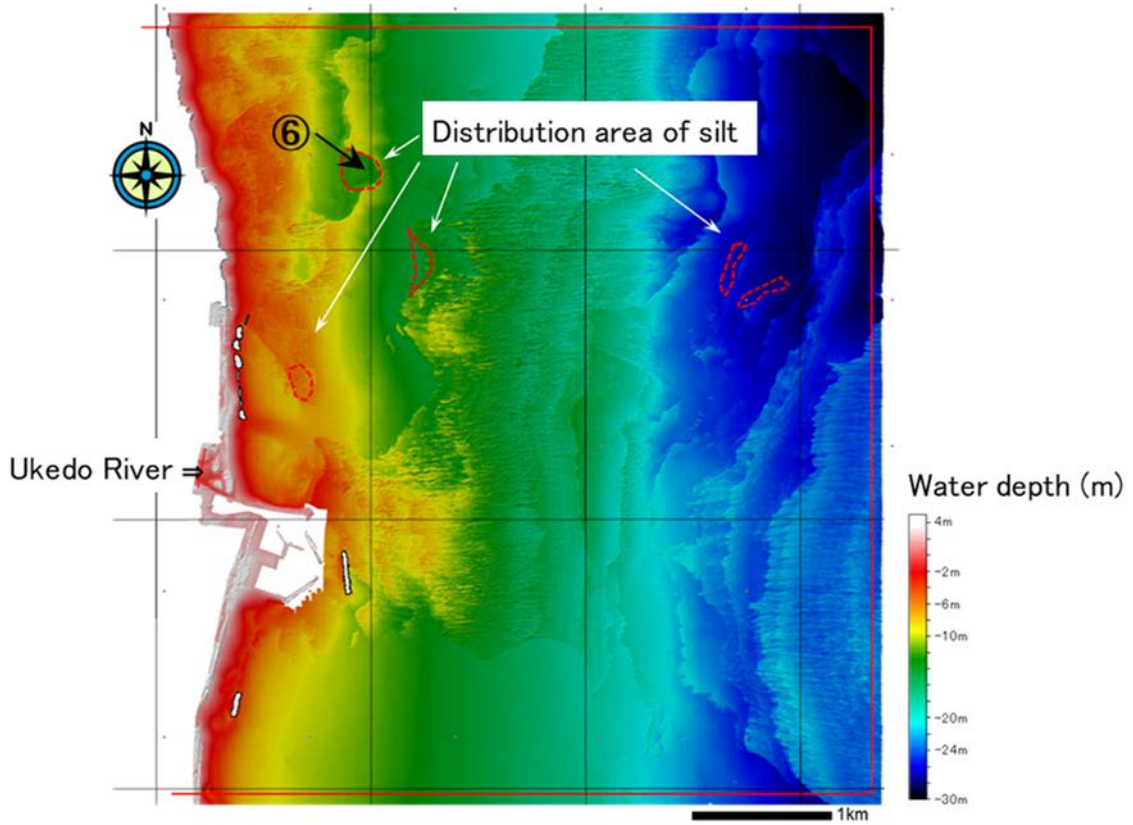


Fig. 3.7-2 Bathymetric map and distribution of silt particles near the mouth of the Ukedo River.

“⑥” shows the sampling position of columnar samples (vibration core system) (refer to the text).

② Distribution of radioactive cesium in seabed sediment

Figs. 3.7-3 shows the relation between the distance from the coast and the ^{137}Cs concentration in seabed sediment. Fig. 3.7-4 presents the relation between the distance from the coast and the ^{137}Cs inventory.

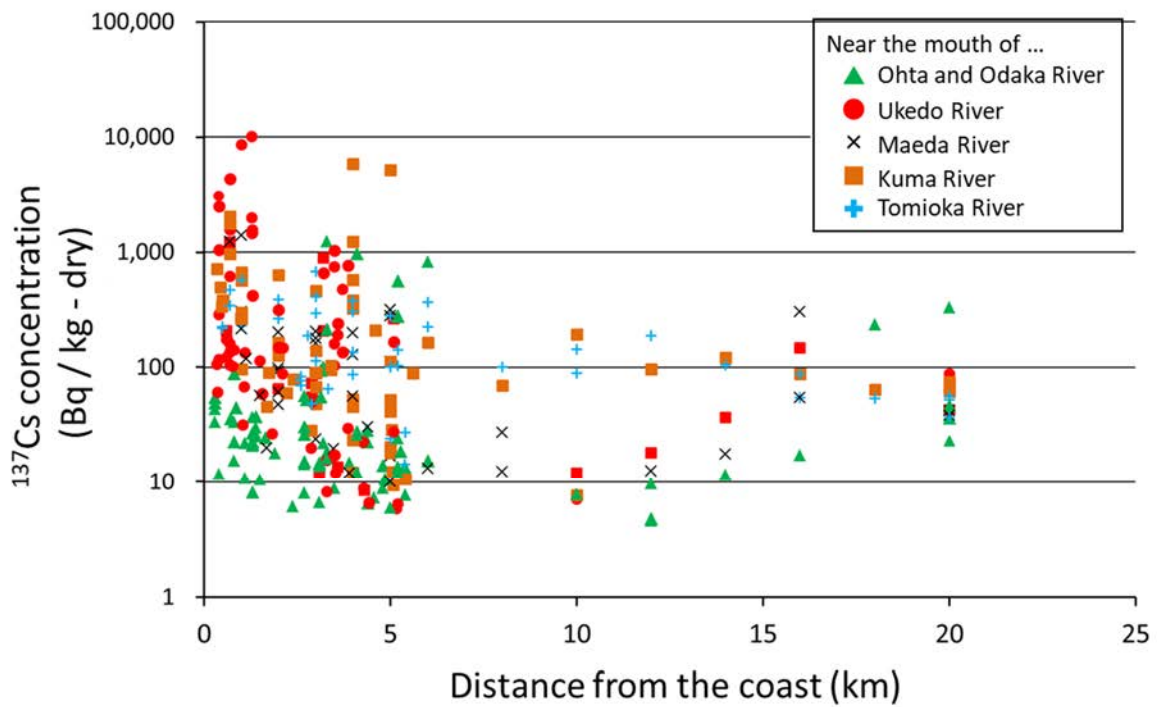


Fig. 3.7-3 ¹³⁷Cs concentration as a function of the distance from the coast (from FY2013 to FY2016). For columnar samples, the average concentration in the surface region (maximum depth: 10 cm) is shown.

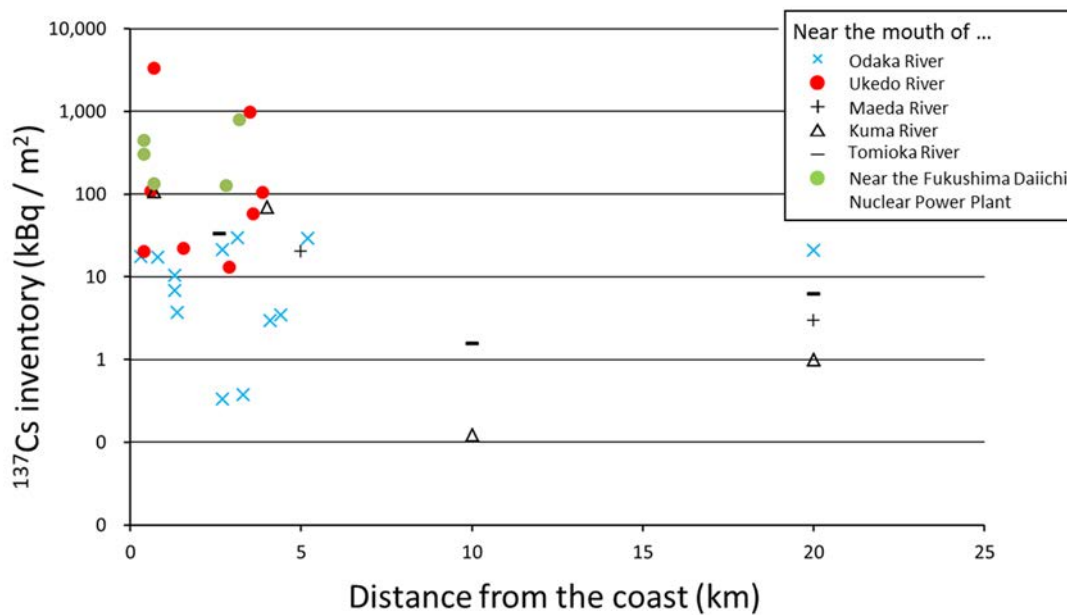


Fig. 3.7-4 ¹³⁷Cs inventory as a function of the distance from the coast (from FY2013 to FY2016). Among the columnar samples, data are shown only at the positions where the lowest depth of ¹³⁷Cs was confirmed.

It is seen that the most of the ^{137}Cs concentration was around several hundred Bq/kg. This value is lower by two to three orders of magnitude than the ^{137}Cs concentration in sediment of reservoirs and rivers. Although the inventory of ^{137}Cs was distributed mostly around tens of kBq m^{-2} , we can observe some places where it exceeded 100 kBq m^{-2} . Accordingly, the observed ^{137}Cs inventory was significantly higher (Tsuruta et al., 2017)⁽¹¹¹⁾ than the previously observed results at the places shallower than 30 m (Otosaka and Kato, 2014⁽¹¹²⁾; Black and Buessler, 2014⁽¹⁰²⁾). We also confirmed many places where the ^{137}Cs concentration and its inventory were high in the region of 5 km from the coast. However, these values decreased when the distance becomes larger than 5 km. Therefore, the distribution of ^{137}Cs and its inventory showed that sediment with high ^{137}Cs concentration supplied from rivers was deposited in shallow sea region near the coast. This is in good agreement with the preliminary analysis.

Fig. 3.7-5 shows the vertical distribution of radioactivity of ^{137}Cs ($\text{kBq m}^{-2} \text{ cm}^{-1}$) and the median grain size for seabed sediment collected using vibrocoring, in which a core tube is driven into the seabed sediments by using the force of gravity enhanced by vibrational energy, in the estuary of the Ukedo River (Tsuruta et al., 2017)⁽¹¹¹⁾.

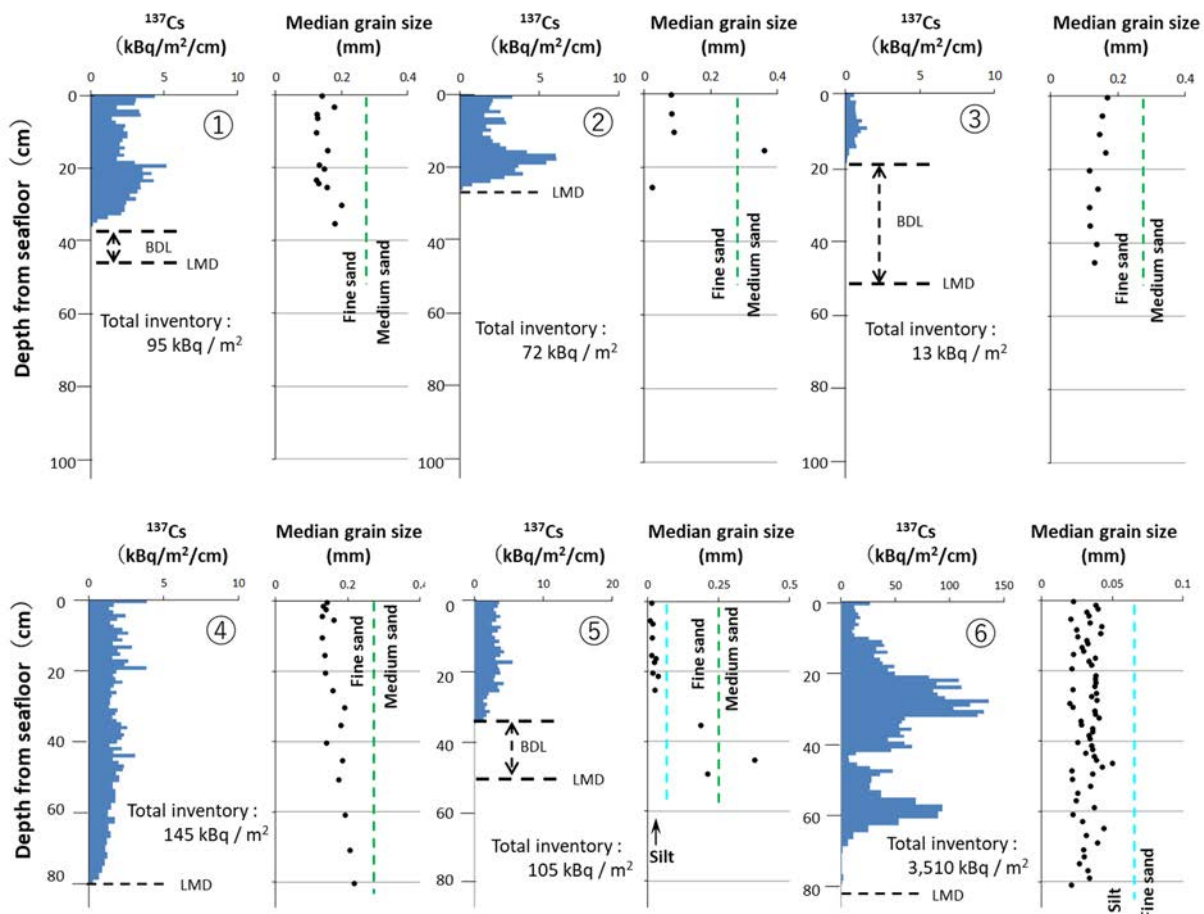


Fig. 3.7-5 Vertical distribution of ^{137}Cs in seabed sediment (near the mouth of the Ukedo River).

The samples were collected using vibrocoring (FY2013).

BDL: below detection limit, LMD: lowermost core depth.

The columns from ① to ③ in Fig. 3.7-5 show the results for the samples collected in near the Ukedo River mouth at the spots where the distribution region of the sediment is relatively wide. The columns from ④ to ⑥ in Fig. 3.7-5 presents the results of ^{137}Cs in seabed sediment distributed at the base of the cliff in cuesta terrain described above. The samples shown in ①-③ were mainly composed of sandy particles. The content of ^{137}Cs per 1 m^2 in these samples was lower by one to two orders of magnitude than that in flood plain of the Ukedo River (Nakanishi, 2014)¹¹³⁾. On the other hand, the samples shown in ④-⑥ were mainly composed of fine particles corresponding to silt, and the content of ^{137}Cs per 1 m^2 was higher than that in ①-③ samples. In particular, the ^{137}Cs content per 1 m^2 in sample ① was about $3,500\text{ kBq m}^{-2}$, which was comparable to the ^{137}Cs content in the flood plain of the Ukedo River. With respect to the vertical distribution, it was found that the particle size of the samples taken in the observation spots scarcely changed, and fine silt particles were continuously deposited. We have measured the flow velocity directly above the observation spots, and calculated mean shear stresses (N m^{-2}) from the measured flow velocity. The results are presented in Fig. 3.7-6. For the position shown in ⑥, the mean shear stresses was small and its width was narrow compared with those at the other positions. From these results, it was revealed that since the flow velocity decreases at the semicircular depression due to the cliff made of bedrock, fine particles are continuously deposited at the spot. As a result, fine particles with high ^{137}Cs concentration accumulated in this region (Tsuruta et al., 2017)¹¹¹⁾. The investigation of seafloor topography showed that the region of semicircular depression is limited to be about 0.2 % of the total seabed area. Therefore, these spots are considered to be abnormal places from the viewpoint of ^{137}Cs distribution.

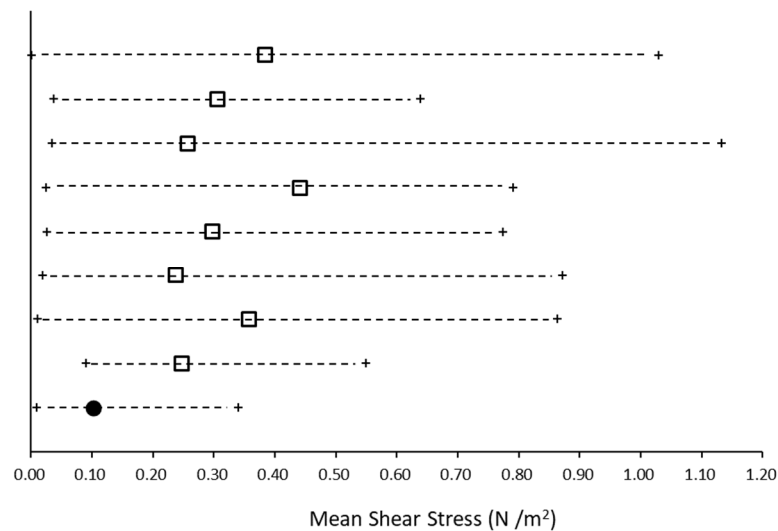


Fig. 3.7-6 Mean shear stresses at the bottom layer.

The mark “●” shows the data for ⑥, and the marks “□” represent the data for the other places.

③ Changes in radioactive cesium in seabed sediment

Fig. 3.7-7 shows the temporal changes in ^{137}Cs concentration in seabed sediment. The decreasing rate of the ^{137}Cs concentration was higher than that estimated from the physical decay. When the average concentration in FY2013 was compared with that in FY2016, the apparent half-life was about 2.65 years. It was presumed that such fast decrease in the ^{137}Cs concentration is due to; 1) migration of cesium to the lower

layer of seabed sediment by biological disturbance and diffusion, 2) re-suspension of particles and their migration to the ocean, and 3) dissolution to sea water (Otosaka, 2017)¹¹⁴.

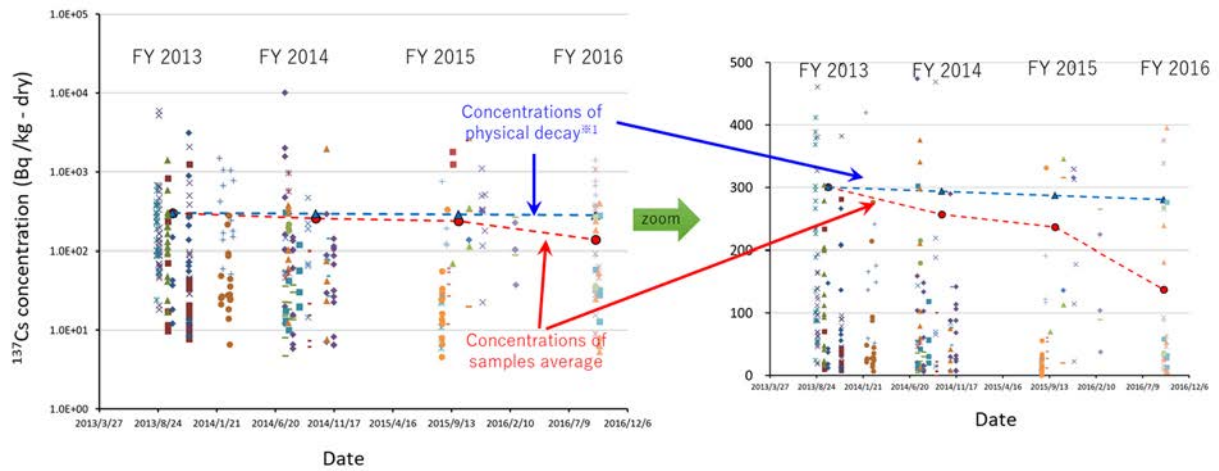


Fig. 3.7-7 Temporal changes of ¹³⁷Cs in seabed sediment.

the red dotted lines show the average value per fiscal year.

※1 Concentration when the average concentration in FY2013 is taken as the initial concentration.

It is seen that the ¹³⁷Cs concentration had considerably decreased from FY2015 to FY2016. At present, the cause of this decrease cannot be identified. However, one of the plausible causes is that the ¹³⁷Cs concentration in seabed sediment was diluted by large amount of sediment supplied from the land due to the heavy rainfall in Kanto-Tohoku district in September 2015.

2) Distribution of radioactive cesium in seawater

Fig. 3.7-8 and Fig. 3.7-9 show the concentration of dissolved and particulate ¹³⁷Cs, respectively, in seawater. For dissolved ¹³⁷Cs, seawater was filtrated by a filter with 0.45 μm pores, then it was condensed by ammonium molybdate treatment, and the concentration of ¹³⁷Cs was measured. For particulate ¹³⁷Cs, the radioactivity of the particles on the filter was measured for long time (70-100 hours).

It was observed that the concentration of dissolved ¹³⁷Cs was in the order of 10⁻² Bq L⁻¹ in the region from the coast to 1 km offshore. On the other hand, the concentration of dissolved ¹³⁷Cs was in the order of 10⁻³ Bq/L at the offshore more than 1 kilometer from the coast, and it gradually decreased with the distance from the coast. For the estuaries and coastal regions of the Ukedo River and the Kuma River, the clear difference in the concentration of dissolved ¹³⁷Cs was not confirmed. It was also found that the concentration of dissolved ¹³⁷Cs was slightly high near the 1F (within 1 km from the harbor) among the regions around the coast. Since the concentration of dissolved ¹³⁷Cs in rivers ranged in the order from 10⁻² to 10⁻¹ Bq L⁻¹, it was shown that the concentration of dissolved ¹³⁷Cs in seawater was one or two orders of magnitude lower than that in rivers. Further, it was confirmed that the concentration of dissolved ¹³⁷Cs in seawater tended to decrease with year (×(FY2014)→△(FY2015)→○(FY2016)→□(FY2017)).

For particulate ^{137}Cs , the concentration in seawater ranged approximately from several hundreds to 2,000 Bq kg^{-1} , and we did not observe any tendency of its clear changes with the distance from the coast or year. For the abovementioned semicircular depression, the concentration of suspended ^{137}Cs tended to be high, and it was lower by about one order than that in rivers (generally higher than 10,000 Bq kg^{-1}).

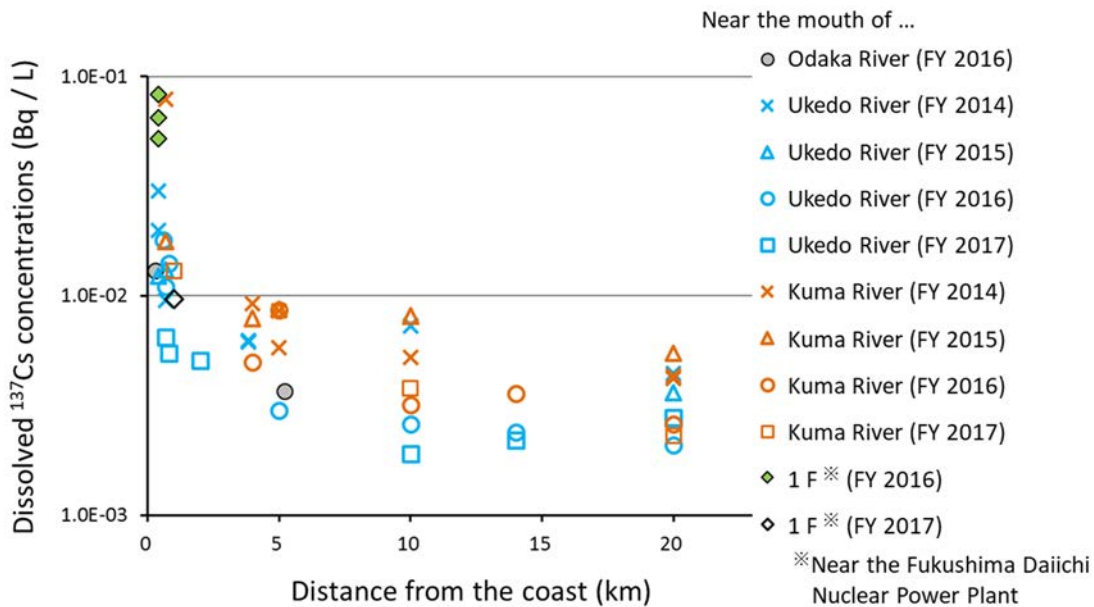


Fig. 3.7-8 Concentration of dissolved ^{137}Cs (FY2014-FY2017).

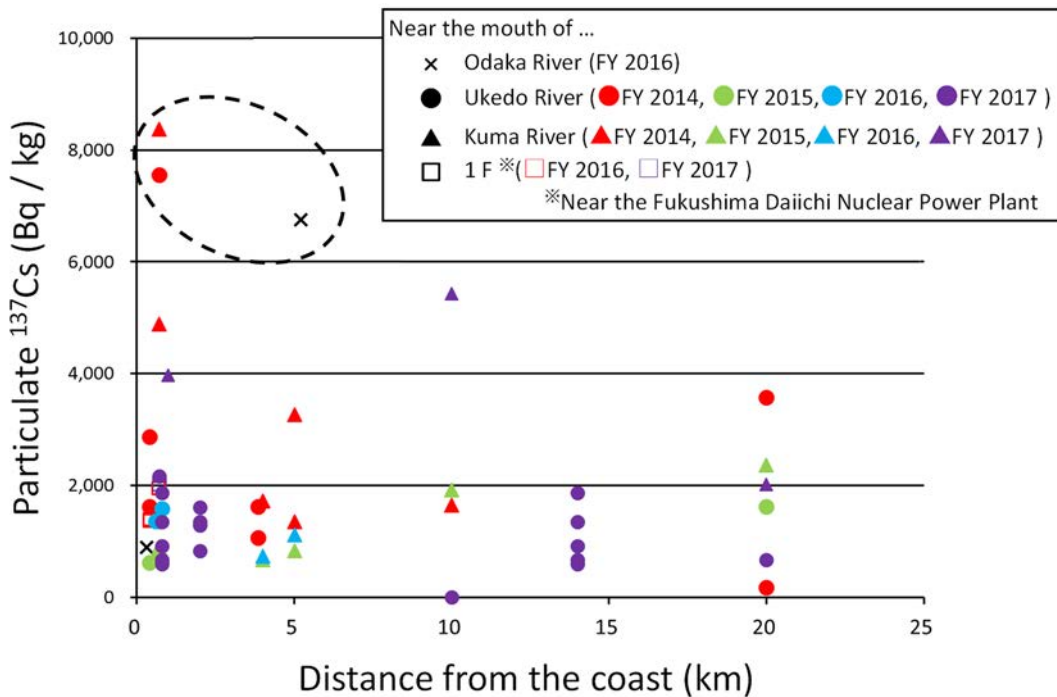


Fig. 3.7-9 Concentration of particulate ^{137}Cs (FY2014-FY2017).

Dotted circle: samples from the just above of semicircular depression areas

3) Summary

From the investigation results obtained so far, we were able to clarify the distribution of radioactive cesium and its tendency in seabed sediment and seawater in the region of relatively shallow water depth (shallower than about 30 m). It was observed that the concentration of radioactive cesium in seabed sediment and seawater became higher as the distance from the coast decreases. As the cause of this tendency, the following two factors were presumed, i.e., ① the effect of the contaminated water at the initial stage of the accident (Tsumune et al., 2012¹⁰⁴); Misumi et al., 2014¹⁰⁵, etc.), and ② the effect of river water with high ¹³⁷Cs concentration supplied from the land. As to the former factor, there was a possibility that the clear vertical changes in ¹³⁷Cs amount shown in ⑥ of Fig. 3.7-5 reflected the ¹³⁷Cs supply related to the increase of river water (Tsuruta et al., 2017)¹¹¹). From the vertical ¹³⁷Cs distribution shown in Fig. 3.7-5, we clarified that ¹³⁷Cs existed at a deeper region under the seabed compared with the previous investigation results. Further, we could point out the possibility that the amount of cesium in seabed sediment was underestimated in the previous investigation. In addition, we showed that it is necessary to clarify the distribution of bedrock and seabed sediment in order to know the amount of cesium in seabed sediment because the area of bedrock occupies more than half of the seabed in the region of estuaries and coastal areas within 5-8 km from the coast.

(2) Results of investigation on the factors controlling the changes in the distribution of radioactive cesium

Radioactive cesium in seabed sediment and seawater sinks, deposits and re-migrates (suspension, traction, etc.) by nearshore current and ocean wave as the driving force. Therefore, in order to predict the future distribution of radioactive cesium, it is necessary to quantitatively evaluate; 1) where and how much radioactive cesium supplied from rivers will deposit in the estuary and coastal regions, and 2) by what kind of event and to what extent it will move again. Since it is expected that the extent and characteristic of nearshore current and ocean wave are different depending on the season, weather condition, distance from estuary/coast, seafloor topography, etc., it is necessary to know the width of temporal and spatial parameters. Therefore, in order to obtain the temporal parameters originating from the difference in the season and weather condition at the investigation spot, the moored survey was conducted. The towing survey was also carried out for obtaining the spatial parameters under the specific weather condition.

1) Moored survey

The investigation position and measurement layout for moored survey are shown in Fig. 3.7-10. The moored survey consisted of two parts. One was the measurement of water and current measuring system where the re-migration of particles from seabed sediment was measured. The other was the sediment trap system in which the deposition amount of particles was measured. The moored survey meters were set at three points in the Ukedo River at about 1 km (FP-A), 2 km (FP-B) and 14 km (FP-C) from the river mouth. The measurements had been carried out from February 2017 to February 2018. In order to know the radioactive cesium supplied from the river and the response among the respective measurement positions, the sampling of river water and analysis of radioactive cesium were conducted near the estuary of the Ukedo River in the period of setting the sediment traps (about 10 days per one time, and seven times in total).

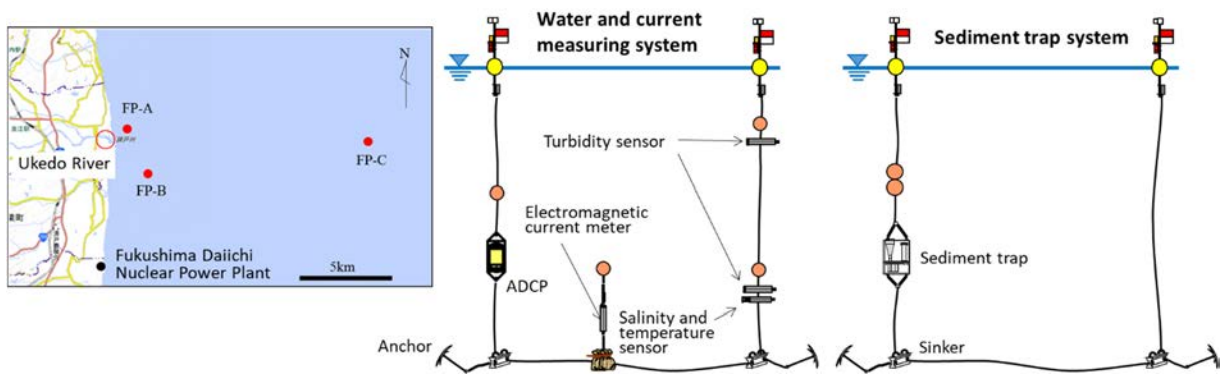


Fig. 3.7-10 Investigation position and measurement layout for moored survey.
 Marine map: Geospatial Information Authority of Japan.

Fig. 3.7-11 shows mass and ^{137}Cs flux at FP-A and FP-B in February 2017. The fluctuation of the deposition amount of ^{137}Cs at FP-A was large depending on the measurement date. However, it was found that the observed deposition amount of ^{137}Cs at 1 km offshore (several hundreds to 2,500 Bq m^{-2} per one day) was about three orders of magnitude larger than that at the position of about 870 m depth and about 100 km from the coast (Otosaka et al., 2014)¹¹². Therefore, it was suggested that most of ^{137}Cs was deposited within the region of several km offshore. At present, we are analyzing the collected samples, and conducting analysis of the obtained measurement data. We will continue the analysis through the comparison of flow condition data and river samples.

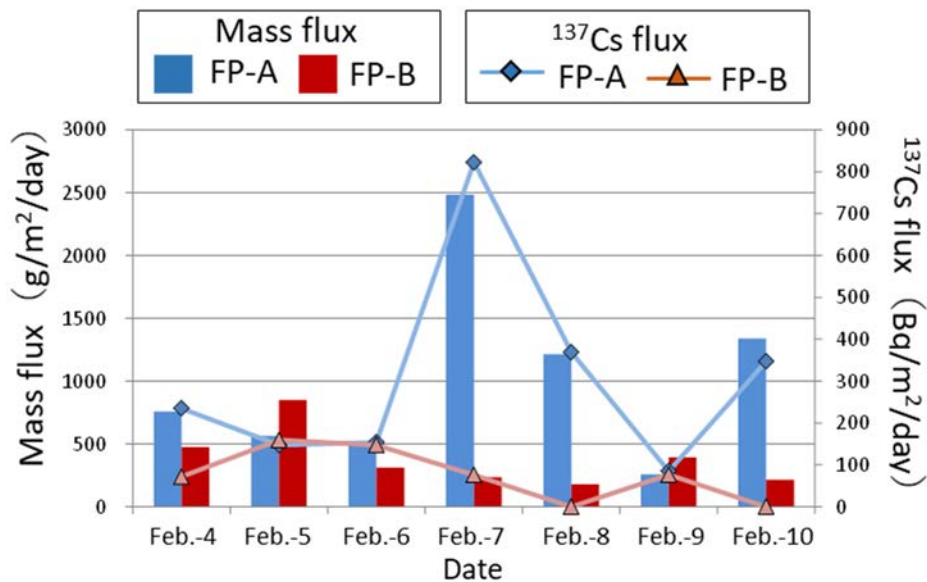


Fig. 3.7-11 Deposition amount of sediment (left) and deposition amount of ^{137}Cs (right) from February 4 to 10 in FY2017

2) Towing survey

The towing survey had been conducted at eight times from August 2014 to December 2014. The measurements were carried out for flow velocity and flow direction using the ADCP (Acoustic Doppler Current Profiler). As a separate measurement, 2 liter seawater was collected, and the suspended solids (SS) were measured. Fig. 3.7-12 shows the results of the suspended material transport at the time of normal water level and high water level. For the transport of suspended materials, the results were obtained by multiplying the flow velocity by the SS. The results are shown by dividing in the direction of north-south/east-west based on the flow direction.

For the transport in the north-south direction, it is seen that the suspended materials were transported to the south direction on the whole at the time of both normal water level and high water level. Although the transport to the north direction became dominant in the narrow region in front of the estuary at the time of high water level, the strong transport to the south direction was observed on the whole. For the transport in the east-west direction, the large flow to the west direction (direction to the shore) was generally seen at the time of normal water level, but the flow changed to the east direction (direction to the offshore) at the time of high water level. It is considered that the change in the flow direction was caused because the flow in the offshore direction became strong due to the water outflow from the river. For both north-south and east-west directions, the transport amount of suspended materials at the time of high water level increased to several times of that at the time of normal water level. Therefore, it is considered that radioactive cesium migrated accompanied by the transport of large amount of suspended materials at the time of high water level. At present, we are analyzing the transport amount of cesium from the amount of radioactive cesium and the flow rate.

3) Summary

It was clarified that the transport of suspended materials in the south direction and offshore direction was dominant in the flooded season. The result supports the previous investigation and analytical results (Tsumune et al., 2012¹⁰⁴); Misumi et al., 2014¹⁰⁵, etc.).

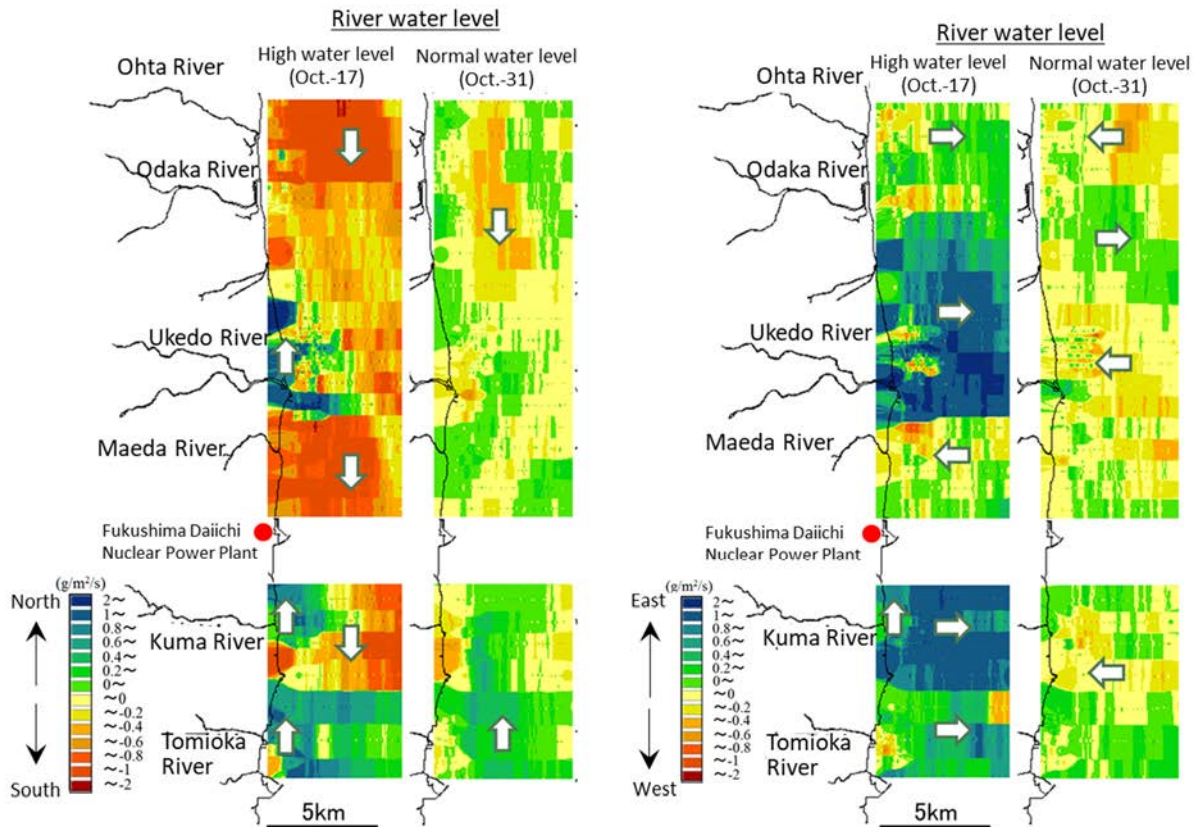


Fig. 3.7-12 Results of sediment flux based on the towing survey.
North to south direction (left), east to west direction (right)

3.7.4 Future subjects

As future subjects, we plan to analyze results of the mooring survey shown in 1) of Section 3.7.3. Thereby, we will conduct quantitative analysis of the deposition/re-migration behavior of radioactive cesium supplied from rivers in estuaries and coastal regions. Also, we will continue to investigate the distribution of seabed sediment, which was proved to be effective for clarifying the migration behavior of radioactive cesium. Also, we intend to collect columnar samples that can prove the existence of radioactive cesium in deeper region under the seabed. By combining these studies, we will continue to clarify the distribution of radioactive cesium and its changes with high accuracy. In particular, in order to verify the discussion proposed by Otosaka (2017)¹¹⁴⁾ concerning the re-migration of ^{137}Cs in seabed sediment and the changes in the amount of radioactive cesium, it would be necessary to periodically confirm the existence of radioactive cesium in the deeper region under the seabed.

4 Urban area

4.1 Outline

People stay in urban area for long time, so the effect of radiation exposure in urban area would be larger than that in the other environment. Therefore, it is important to clarify the temporal and spatial changes in air dose rate and deposition amount of radioactive cesium in urban area in order to evaluate/predict the future radiation exposure and make measures for reducing it. In the present study, as a monitoring method for the surface distribution of air dose rate in urban area, we investigated the applicability of unmanned helicopter survey (AUH survey) that can monitor wide region. Also, we evaluated the distributions and temporal changes in air dose rate and radioactive cesium based on the observation at the fixed points.

Comparison between the results of AUH and ground-based surveys revealed that even for urban area composed of various components such as buildings and paved surfaces, the AUH survey can provide measurement accuracy comparable to that for flat land such as grassland. It was also clarified that the accuracy is largely affected by the patchy and local distribution of ambient dose equivalent rates on the ground and differences in the fields of view, rather than land-uses. The air dose rate in urban area decreased more rapidly than that in the other land-use. The amount of radioactive-cesium deposition on the surfaces specific to urban area (paved surface etc.) is decreasing more rapidly than that on soil surface such as grassland. This fact is considered to have contributed to the rapid decrease in air dose rate in urban area. With respect to the outflow of radioactive cesium from urban area, it was suggested that the migration of dissolved radioactive cesium was predominant. However further study will be needed to clarify the outflow process of radioactive cesium.

4.2 Investigation of monitoring methods

4.2.1 Objectives

The AUH survey can rapidly evaluate the surface distribution of air dose rate in wide are. The present method is composed of three processes, i.e., ① the measurement from the sky, ② the correction of altitude dependence of the count rate, and ③ conversion of the count rate to the air dose rate. In the previous method, the processes ② and ③ have been applied supposing the flat soil areas such as grasslands (Sanada and Torii, 2015)¹¹⁵). On the other hand, urban area generally consists of buildings like houses and paved surface like asphalt in addition to grasslands. There is a possibility that such structures specific to urban area would affect the processes ② and ③. The objectives of the present study was to confirm the applicability of the AUH survey to the urban area and evaluate the measurement accuracy.

4.2.2 Methods

Investigation was carried out for urban area (about 1-1.5 km²) located in Okuma Town and Tomioka Town (Fig. 4.2-1) in December 2014. The air dose rate in the measurement area was evaluated by AUH survey, and ground-based survey using KURAMA-II system (Kyoto University RAdiation Mapping-II System; Ando et al, 2015¹¹⁶).

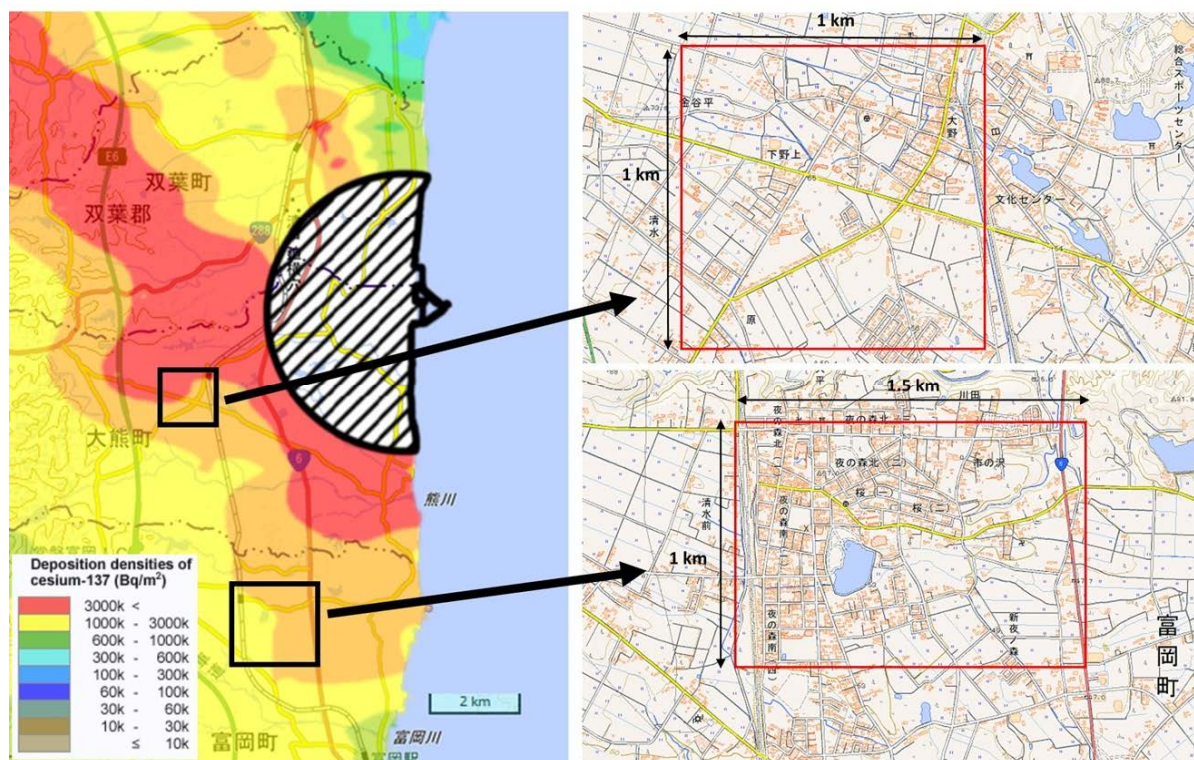


Fig. 4.2-1 Study sites.

Map was obtained from Geospatial Information Authority of Japan.

(<https://maps.gsi.go.jp/development/ichiran.html>)

Distribution of the ¹³⁷Cs deposition amount was obtained by the results of the fourth airborne monitoring survey by MEXT (MEXT, 2011)³).

The flight condition of the AUH survey was as follows. The aircraft used was an unmanned helicopter of self-sustaining flight type (RMAX G1, Yamaha Motor Co., Ltd.). Both the flight height and interval of the measurement lines were 80 m, and flight velocity was 8 m s⁻¹. As a radiation detector, the LaBr₃ : Ce scintillation detector was used. The measurements were carried out by counting one time per second in the energy range from 0 to 3,000 keV. In the analysis, the count rates in the energy range of 50-1,600 keV were used.

The counting rate generally decreases with the flight height. Therefore, it is necessary to correct the measured count rate to that at a standard height using a height-correction coefficient defined as decreasing rate of the count rate with height. The height-correction coefficients were obtained at three sites in the measurement area by fitting a first-order exponential approximation curve to the relation between height and count rate (Fig. 4.2-2). As a result, it was obtained that the average height-correction coefficient was 0.0081 (±0.0002 (coefficient of variation (CV) =2%)). The measured count rate was corrected to that at 80 m as a standard height using the obtained height-correction coefficient. In addition, air dose rates were measured at the three sites, and the ratio of the air dose rate to the count rate at the standard height (conversion factor) was obtained. The average conversion factor to the air dose rate was 2441 (±661) cps hr μSv⁻¹ (CV=27%). As to the further details of the monitoring condition, experimental apparatuses, and analytical methods, please refer to Sanada and Torii (2015)¹¹⁵⁾, and Yoshimura et al. (2019)¹¹⁷⁾.

For the ground-based survey, a person carried a KURAMA-II system on the back, and measured the air dose rate in 10 km stroke in the measurement area with logging interval of three seconds. In the ground-based way, there are roadways, agricultural roads, parks, etc. In order to compared the data of the AUH survey with those of the ground-based survey, the obtained data were converted to the mesh data as the average values in the mesh based on the mesh data for land use (mesh size of 100 m square), which is presented by the Ministry of Land, Infrastructure and Transport using a Geographic Information System (ArcGIS.10.4, ESRI).

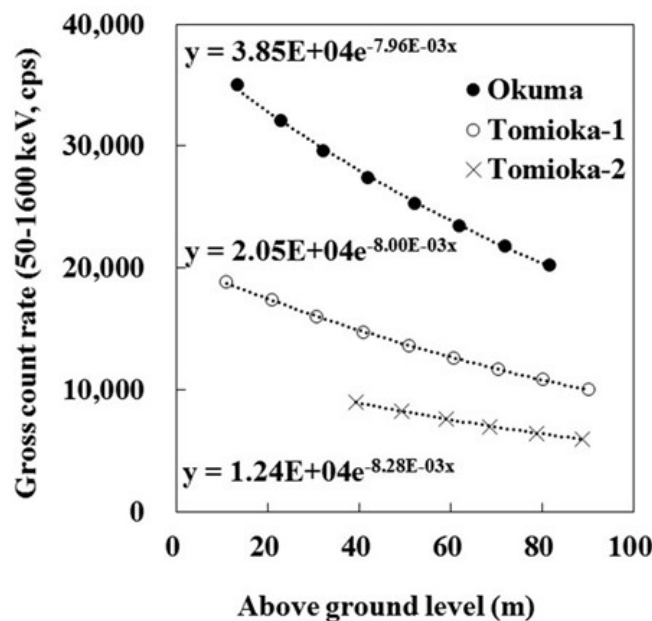


Fig. 4.2-2 Evaluation of the height conversion factor (decreasing of count rate with height).

4.2.3 Results and discussion

Fig. 4.2-3 shows the distribution map of the air dose rate obtained by the AUH survey and the ground-based survey. It was found that the north side of Okuma Town and the east side of Tomioka Town showed the several times higher air dose rate compared with those at the respective counter sides. The large gradient of air dose rate was also observed in the limited areas of 1-1.5 km². Such tendency of the distribution was also obtained by the AUH survey. On the other hand, the localized high and low air dose rate was observed in the regions at 100 m scale by the ground-based survey, but such fluctuation was not observed by the AUH survey. The distribution map obtained by the AUH survey showed the distribution where the data obtained by the ground-based survey were spatially averaged. That is, it was revealed that the AUH survey could obtain the planar averaged air dose rate under the present flight condition but could not obtain its localized distribution at 100 m scale.

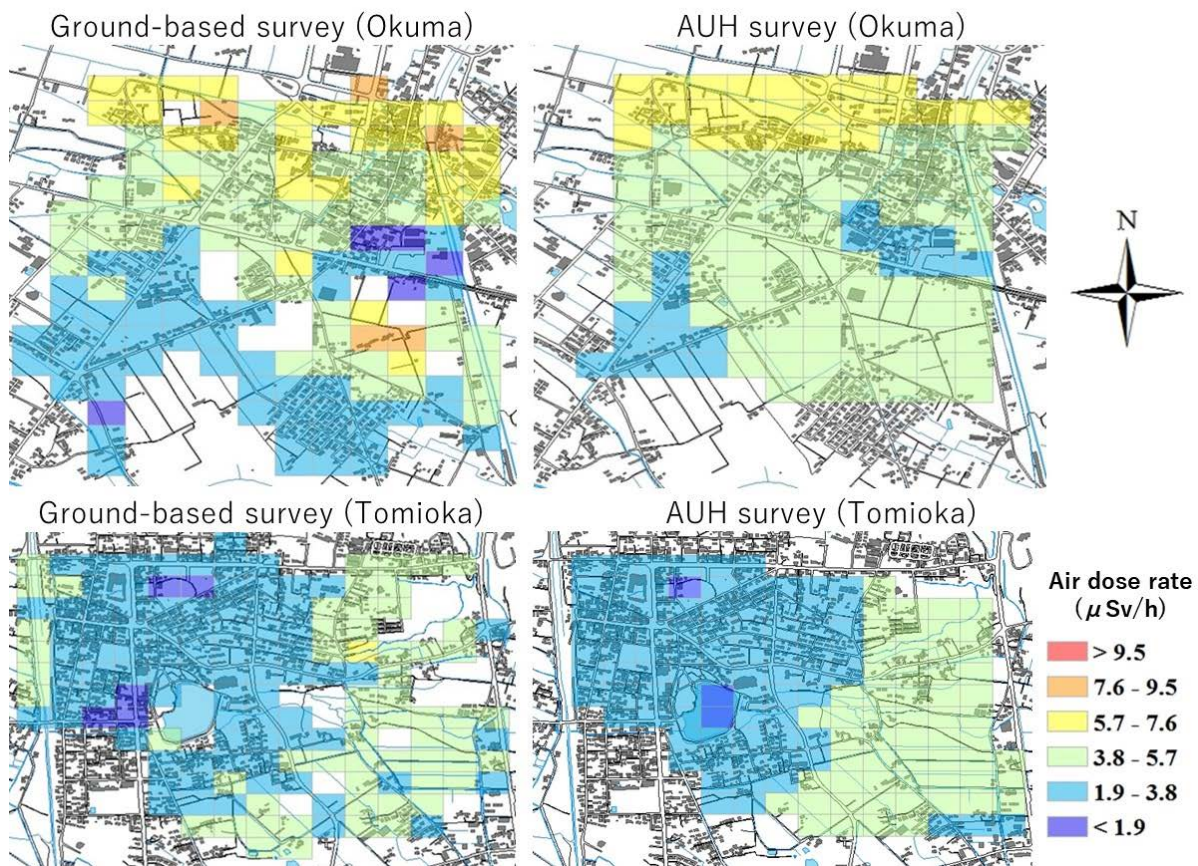


Fig. 4.2-3 Distribution map of air dose rate.

Fig. 4.2-4 presents the results for comparison of the air dose rate obtained by AUH survey with that obtained by ground-based survey. The air dose rate obtained by the AUH survey was within 0.5-2.0 times of that obtained by the ground-based survey, and its Root Mean Square Percentage Error (RMSPE) was 24.4%. This measurement accuracy was the same as that for flat soil land such as grassland obtained by the AUH survey (Sanada and Torii, 2015)¹¹⁵⁾. The results that the similar measurement accuracy was obtained for urban area composed of building/asphalt and flat soil land suggested that factors other than the land use (structures and materials on the ground) would influence on the accuracy of the AUH survey.

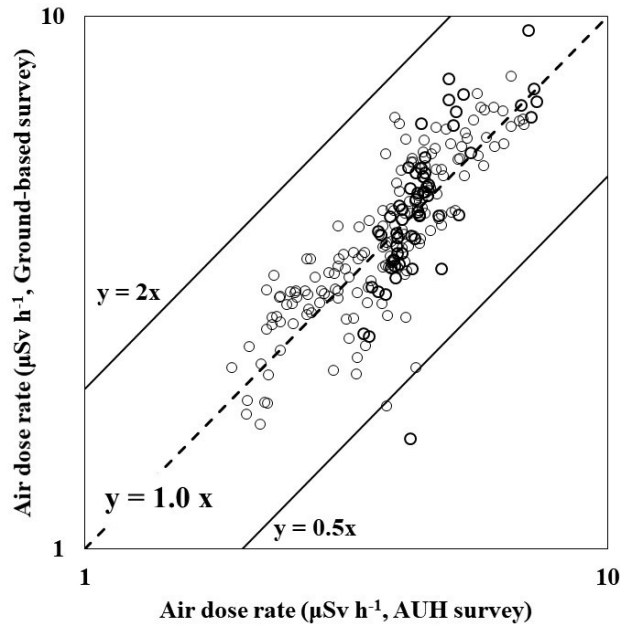


Fig. 4.2-4 Comparison of the air dose rate obtained by ground-based survey and AUH survey.

In order to obtain the air dose rate from the count rate measured by the AUH survey, two processes are necessary, i.e., the above-mentioned correction of the height dependency and the conversion from count rate to air dose rate. The CVs of the height-correction coefficient and the conversion factor were 2% and 27%, respectively, as mentioned above. So the conversion factor to the air dose rate includes large uncertainty compared with that for the height-correction coefficient. In order to evaluate the spatial variation of the conversion factors, the conversion factor of each mesh was obtained as the ratio of the count rate measured by the AUH survey to the air dose rate obtained by the ground-based survey (Fig. 4.2-5). As a result, it was revealed that the average conversion factor was $2,458 \text{ cps hr } \mu\text{Sv}^{-1}$, showing almost the same as the coefficient used in the present study. The CV of the conversion factor, however, was 24%, which was almost the same as the RMSPE obtained by the air dose rate measurements by the AUH survey. These results mean that the spatial variation of the conversion factor considerably affected the measurement accuracy of the AUH survey.

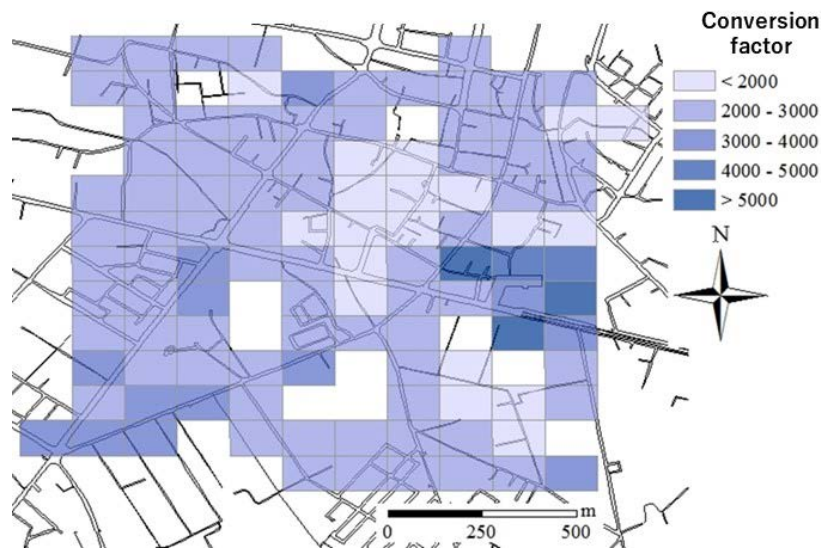


Fig. 4.2-5 Spatial distribution of conversion factor (for Okuma Town).

In order to evaluate the relation between the accuracy of AUH survey and spatial resolution, the data obtained by the AUH survey was compared with those obtained by the ground-based survey for the mesh size of 300 m and 500 m (Fig. 4.2-6). When the spatial resolution increased from 100 m to 300 m, the value of RMSPE considerably decreased from 24.4 % to 14.0 %. On the other hand, even when the spatial resolution was increased to 500 m, the RMSPE was not improved. These results suggested that the results surveyed at 80 m height in the present study reflected the radiation within the area with diameter of 300 m just below the survey point. This area size agreed to the simulation results by Malins et al. (2015)¹¹⁸⁾. From these results, it was considered that the measurement accuracy of the AUH survey was considerably dependent on the difference in the spatial resolution (field of view) between airborne and ground-based survey.

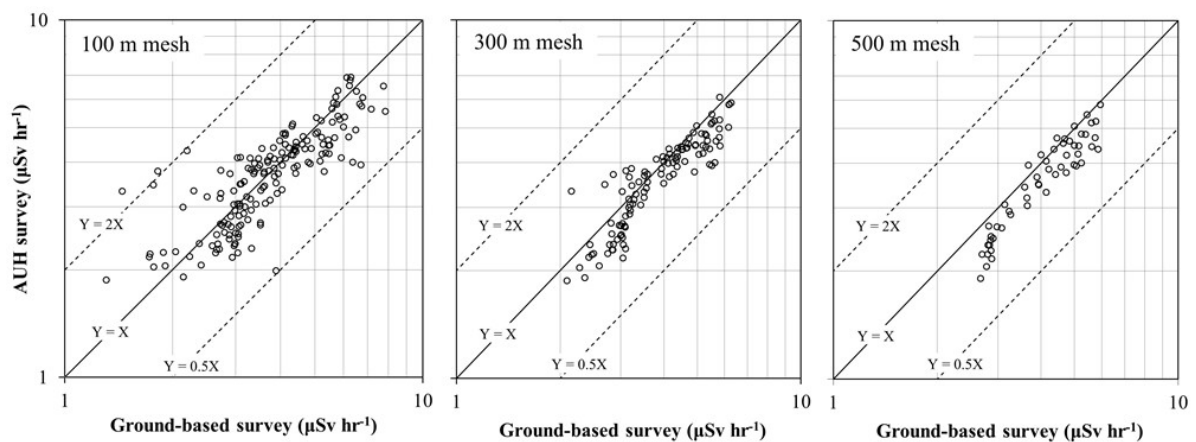


Fig. 4.2-6 Mesh size and uncertainty of the results of AUH survey.

4.2.4. Future subjects

From now, in order to evaluate the environmental dynamics of radioactive cesium, it will be necessary to develop a method to evaluate the distribution of radioactive cesium concentration on the ground surface (Bq m^{-2}) in urban area using the AUH survey in addition to the air dose rate.

4.3 Decreasing tendency of the air dose rate

4.3.1 Objectives

Temporal decrease in air dose rate after the accident have been well studied and reported by the various investigations such as wide-range aerial monitoring (JAEA, 2017)¹¹⁹). In particular, the tendency of the changes in air dose rate after the decontamination is important information to estimate and reduce the future external radiation exposure to the residents and consider the residents' return. The objective of the present study is to know the tendency of the decrease in air dose rate after the decontamination. For this purpose, we conducted long-term measurement of air dose rate for the regions where the decontamination had been carried out based on the Decontamination Pilot Project, thereby, the decreasing tendency of air dose rate after the decontamination was evaluated.

4.3.2 Methods

(1) Study sites

The investigation was conducted in six places where the decontamination was carried out from November 2011 to April 2012 in the Decontamination Pilot Project (Fig. 4.3-1). Among these places, Yamakiya District in Kawamata Town and Kainosaka District in Kawauchi Village were the areas where the residence was restricted, while Tsushima District in Namie Town, Yonomori District in Tomioka Town, Shimonogami District in Okuma Town, and Ottozawa District in Okuma Town were designated as the difficult-to-return zone. The decontamination at the investigation place was carried out in the following procedures. For soil surface, top soil (3-15 cm) was stripped. For asphalt pavement, the surface was cut (-5 mm) by various methods. In the case of forest, litter layer were eliminated (5-10 cm), a part of trees was pruned up to 10 m in height, and the bark was washed and scraped (Japan Atomic Energy Agency, 2013)¹²⁰). The investigation was conducted at 170 points in forest roads, streets, parks, playgrounds, housing sites, fields, grasslands, forests, and their surroundings.

(2) Investigation methods

Sodium iodide (NaI) scintillation survey meter (Hitachi Aloka Medical, Ltd., TCS-172B) was used for the measurement of radiation. In the case of four measurement points where the air dose rate exceeded $30 \mu\text{Sv h}^{-1}$, the survey meter with ionization chamber (Hitachi Aloka Medical, Ltd., ICS-323B) was used. The air dose rate D was measured just above the measurement point four times. The surface dose rate D_s was measured three times for each point in the range of 15 cm radius from the measurement point.

The investigation had been carried out about four years from November 19, 2012 to November 2, 2016. In this period, the measurements had been conducted 1-3 times per month.

(3) Analytical method

The decreasing rate of D and D_s were defined as λ and λ_s (day^{-1}), respectively. The values of D and D_s were obtained by fitting the following equation by the least squares method,

$$D(t) = D(0)e^{-\lambda t} \quad (1)$$

$$D_s(t) = D_s(0)e^{-\lambda_s t} \quad (2),$$

where t (day) is the time from the measurement start, $D(0)$ and $D_s(0)$ are the values of D and D_s ($\mu\text{Sv h}^{-1}$), respectively, at $t = 0$ obtained by fitting in the above equations.

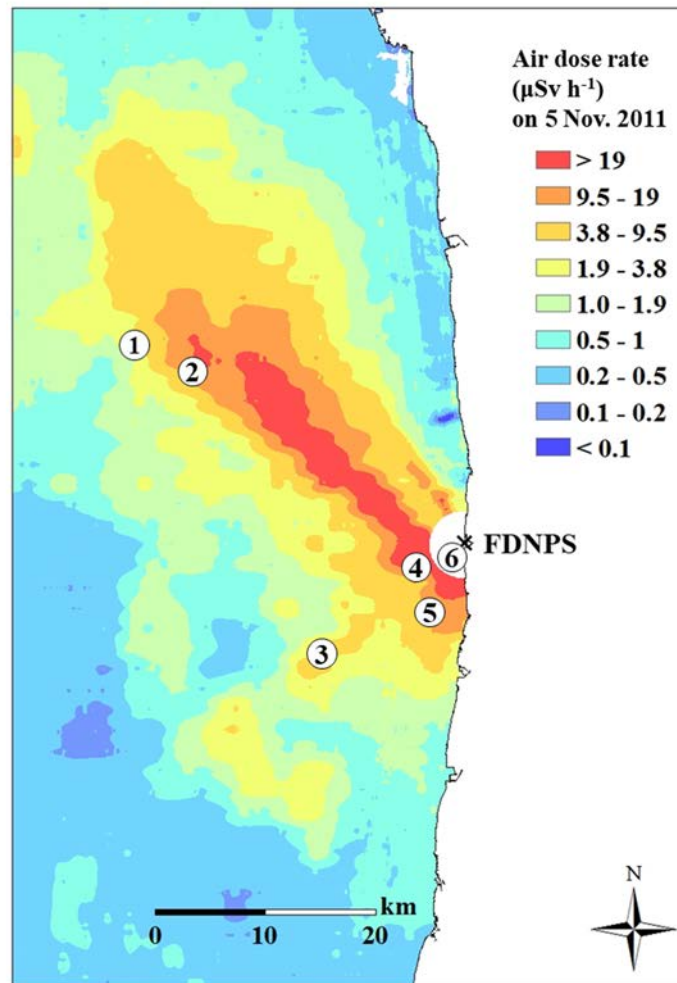


Fig. 4.3-1 Investigation points (displayed on the results of the fourth airborne monitoring survey by MEXT (2011)³).

- ① Yamakiya District, Kawamata Town
- ② Tsushima District, Namie Town
- ③ Kainosaka District, Kawauchi Village
- ④ Yonomori District, Tomioka Town
- ⑤ Shimonogami District, Okuma Town
- ⑥ Ottozawa District, Okuma Town

4.3.3 Results and discussion

(1) Distribution of λ

Fig. 4.3-2 shows the histogram of the λ . The values of λ in the total 170 measurement points were distributed in the range of 4.7×10^{-4} - $8.8 \times 10^{-4} \text{ day}^{-1}$ (Nakama et al, 2018)¹²¹⁾. On the other hand, the λ resulted by physical decay of radioactive cesium (^{134}Cs and ^{137}Cs) was estimated to $4.5 \times 10^{-4} \text{ day}^{-1}$. As a result, all of the measured values of λ were larger than that due to physical decay, suggesting that the decrease in D was resulted by not only the physical decay but also the other factors.

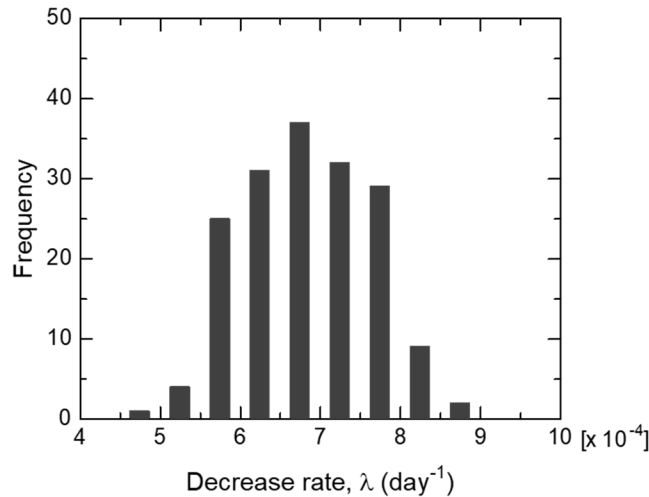


Fig. 4.3-2 Histogram of λ at the 170 measurement points that had been analyzed and evaluated.

(2) Difference in the decreasing rate relating to ground surface properties

In the previous study, it was reported that the decreasing rates of air dose rate were depending on ground surface properties (i.e. asphalt pavement and soil surface) (Kakamu et al, 2013)¹²²⁾. This study separately analyzed the λ for both soil surface (n=103) and asphalt pavement (n=67), and the distribution of λ was compared (Fig. 4.3-3). It was found that the median value of λ was $6.4 \times 10^{-4} \text{ day}^{-1}$ for soil surface, and $7.5 \times 10^{-4} \text{ day}^{-1}$ for asphalt pavement, and the λ for asphalt pavement was significantly larger than that for soil surface (Nakama et al., 2018)¹²¹⁾. As same as the λ , the λ_s showed significantly higher values for asphalt pavement more than soil surface, and the centered value of λ_s was $6.4 \times 10^{-4} \text{ day}^{-1}$ for soil surface and $7.6 \times 10^{-4} \text{ day}^{-1}$ for asphalt pavement (Fig. 4.3-4) (Nakama et al., 2018)¹²¹⁾.

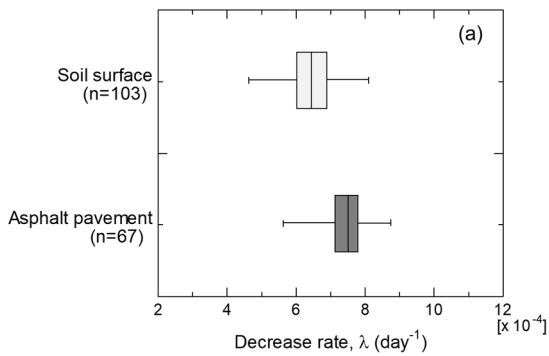


Fig. 4.3-3 Decreasing rate of air dose rate.

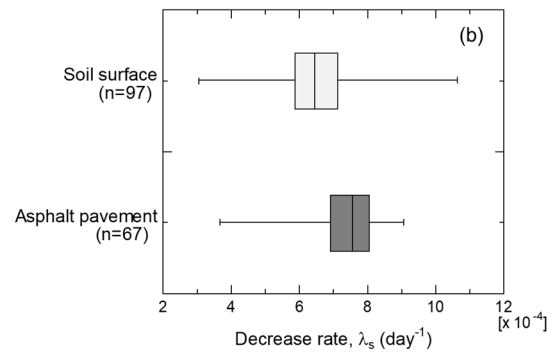


Fig. 4.3-4 Decreasing rate of surface dose rate.

The air dose rate was affected by radiation emitted from both ground surface just beneath the measurement point and surrounding environment. To clarify the effect of the ground surface properties just beneath the measurement point on the λ , we confirmed whether λ_s reflects λ or not using λ/λ_s ratio (Fig. 4.3-5). As a result, it was found that the λ/λ_s ratio in the open places, where the ground surface is flat and there are no buildings, trees, etc. within 10 m radius from the measurement point ($n=54$), was distributed in the range from 0.8 to 1.2. Similarly, we also evaluated the λ/λ_s distribution at the places ($n=110$) except for the open places, i.e., the places where buildings and trees exist around the measurement point. As a result, it was obtained that most of the λ/λ_s ratio was also distributed in the range from 0.8 to 1.2 (Nakama et al., 2018)¹²¹⁾. These results indicate that the radiation emitted from the ground surface just beneath measurement point was reflected in the air dose rate, and it was confirmed that the decreasing of the air dose rate was fast on the asphalt pavement.

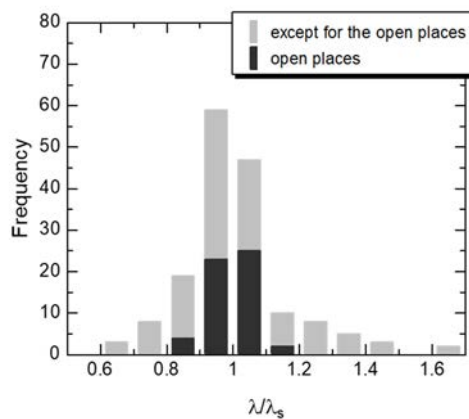


Fig. 4.3-5 Frequency distribution of λ/λ_s .

(3) Effect of local migration of radioactive cesium on air dose rate

From Fig. 4.3-5, it was found that most of the values of λ/λ_s were in the range of 0.8-1.2, but the data considerably exceeded this range at some measurement points. In order to clarify what factors would influence on the fluctuation of the λ/λ_s values, the distributions of λ and λ_s at these measurement points were compared with the median values of all data (Fig. 4.3-6). For the data where λ/λ_s was less than 0.8 or larger than 1.2, the values of λ were close to the median value of all data, but the λ_s values considerably deviated from the median value (Nakama et al, 2018)¹²¹⁾. These results showed that decreasing rate of the surface dose

rate greatly varied depending on the place, while the variation did not influence the decreasing rate of air dose rate.

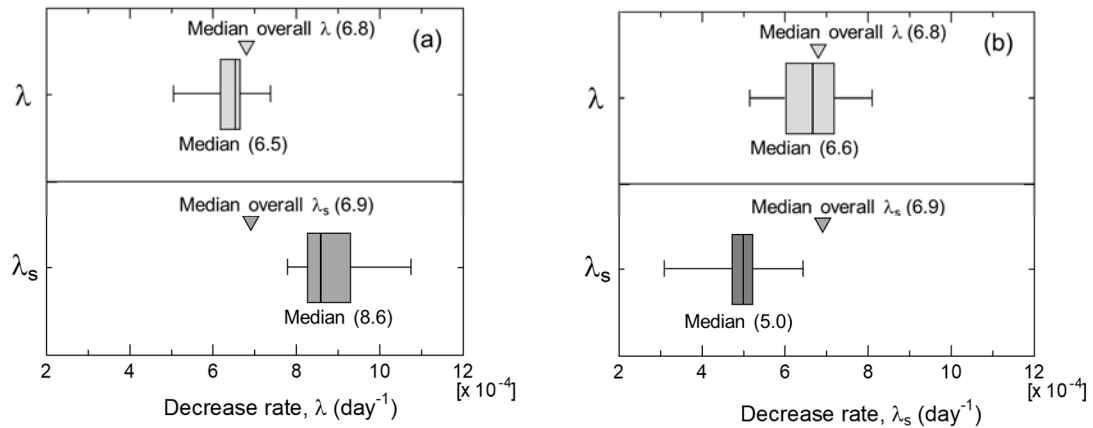


Fig. 4.3-6 Comparison of the distribution of λ and λ_s .

(a) The measurement points where λ/λ_s was less than 0.8.

(b) The measurement points where λ/λ_s was larger than 1.2.

The measurement points where λ/λ_s was less than 0.8 are located at the slope, and soil erosion was observed near the point (Fig. 4.3-7(a) and (b)). Namely, it is considered that the large λ_s was resulted by the wash-off of radioactive cesium-contaminated soil. On the other hand, the measurement points where λ/λ_s was larger than 1.2 are located at the slope edge. Therefore, the measurement point is located at the concave place into which soil flows from the upside of the slope. Actually, soil flow into these points was confirmed (Fig. 4.3-7 (c) and (d)). Namely, it is considered that the value of λ_s became small due to the accumulation of radioactive cesium-contaminated soil. Such measurement points where the soil migration at the ground surface was large has not been observed in the place where λ/λ_s was in the range of 0.8-1.2. Therefore, it was revealed that the local migration of soil contributed to the variation of λ_s , but did not influence the decreasing rate of air dose rate.



Fig. 4.3-7 Photographs around the measurement points.

(a) and (b): Slopes where soil erosion was confirmed around the measurement point. (c): Soil inflow from the upside of the slope was confirmed at the slope edge. (d): Soil flow into the concave place from the surroundings was confirmed.

(4) Effect of forests at the flat place

In the previous studies (Andoh et al., 2015)¹¹⁶⁾, it was reported that the decreasing rate of the D values in forests was low compared with the other land uses. Then, we compared the values of λ among the dataset obtained on soil surfaces in forests ($n=6$), near trees ($n=44$) and open places ($n=53$) (Fig. 4.3-8). It was observed that the median value of λ was $5.8 \times 10^{-4} \text{ day}^{-1}$ for forests, $6.2 \times 10^{-4} \text{ day}^{-1}$ for near trees and $6.9 \times 10^{-4} \text{ day}^{-1}$ for open places. From these results, it was confirmed that the values of λ in forests were small even after the decontamination, while the λ values were large in open places far from forests. The slow decrease in air dose rate on the forest floor and near the forest can probably be explained by changes in the spatial distribution of radioactive cesium in the forest, such as vertical migration from the canopy to the forest floor. It has been reported that a part of the radioactive cesium trapped into the canopy gradually transferred to the forest floor owing to throughfall, stemflow, and litterfall (Niizato et al., 2016)⁹⁾. Radioactive cesium on the forest floor penetrated vertically into the soil over the course of time, and most of it was retained in the forest floor with a slight wash-off (Niizato et al., 2016)⁹⁾. A part of the radioactive cesium which remained in the canopy would have gradually transferred onto the floor during our period of monitoring, and could be an additional radiation source, resulting in slower decrease in air dose rate on the forest floor and near the forest.

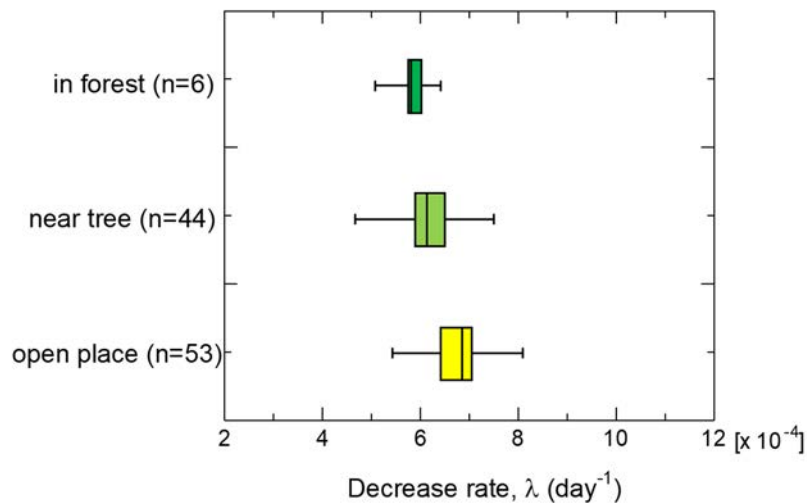


Fig. 4.3-8 Comparison of the distribution of λ in forest, near tree, and in open land.

4.3.4 Future subjects

In the present study, we statistically evaluated the effects of the ground surface properties and forests as the factors that influences the decreasing rate of air dose rate. On the other hand, the relation between the radioactive cesium migrations and decreasing trend of air dose rate needs further study in the future.

4.4 Distribution and migration of ¹³⁷Cs

4.4.1 Objectives

In order to understand the factors that decrease the air dose rate in urban areas and to reflect the knowledge to the planning of decommissioning and the prediction of future radiation exposure, it is necessary to clarify the distribution and migration of radioactive cesium which is major radiation source after the accident. The urban areas are composed of not only the permeable surfaces such as farms and grasslands but also various elements such as paved surface like roads and artificial structures like buildings. Therefore, the properties of the ¹³⁷Cs distribution and migration in urban areas are considerably different from that in the other environments such as forests (IAEA, 2006¹²³; Yoshimura et al., 2017¹²⁴), thereby the investigation focusing on urban areas is necessary. In the present study, we evaluated the distribution of ¹³⁷Cs on components in urban areas such as roofs and roads. We also evaluated the ¹³⁷Cs migration through drainage system.

4.4.2 Methods

(1) Deposition amount of ¹³⁷Cs for each component of urban area

The ¹³⁷Cs activity per unit area (Bq m⁻², hereafter deposition amount) had been measured for components of urban area for eleven buildings in the difficult-to-return zone of Okuma Town and Tomioka Town from January 13 to 23, 2015, and from January 12 to 22, 2016.

The ¹³⁷Cs deposition amount on pavements and permeable surfaces was in-situ measured by a portable Ge semiconductor detector (Falcon-5000, CANBERRA). For the pavements, the surface count rate (cpm) was also measured by a Geiger-Müller (GM) survey meter (TGS-146, Hitachi Aloka Medical, Ltd.), and the ¹³⁷Cs

deposition amount-surface count rate conversion factor was obtained (Fig. 4.4-1).

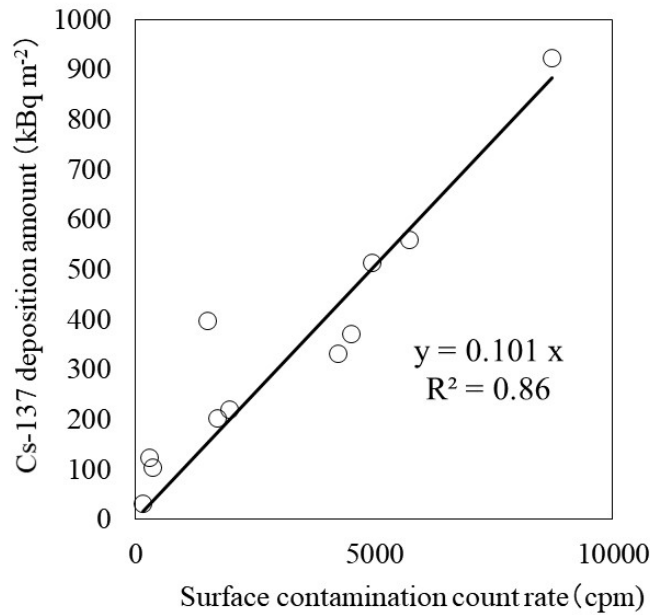


Fig. 4.4-1 Relation between surface count rate and ¹³⁷Cs deposition amount.

The ¹³⁷Cs deposition amount on the other urban components was obtained using the surface count rate measured by the GM survey meter and the above-mentioned conversion factors. Table 4.4-1 summarizes the components measured by the GM survey meter and the list of the number of the data. The measurements were conducted at 1-12 points of four sides of east, west, north and south corresponding to the area of the component. The number of the measurement points by GM survey meter was 1,119 in total. Since the conversion factor depends on the ¹³⁴Cs/¹³⁷Cs ratio, the conversion factor on the measurement date considering the physical decay was used. For the details of the investigation and measurement methods, please refer to Yoshimura et al. (2017)¹²⁴.

Table 4.4-1 Investigated objects and the number of data.

Structure* ¹	Roof	Roof floor* ²	Gutter	Wall	Window	Eaves	Entrance, Porch	Berm* ³	Pavement* ⁴
1. W-2	19	—	—	42	9	6	8	15	—
2. W-1	—	4	—	55	9	3	1	—	10
3. W-1	—	6	—	39	7	3	—	—	6
4. W-1	27	3	—	38	15	—	9	17	—
5. RC-1	—	—	—	46	17	—	6	3	1
6. W-1	34	—	1	33	15	—	3	12	7
7. W-1	32	—	—	30	10	—	6	12	—
8. RC-1	—	9	—	52	15	—	12	7	9
9. RC-2	32	6	35	47	15	—	6	—	18
10. RC-3	34	10	16	37	19	—	—	—	39
11. RC-3	—	9	—	49	8	9	—	—	7
total	178	47	52	468	139	21	51	66	97

*1 wooden (W)-, reinforced-concrete (RC)-number of stories (1-3).

*2 made of resin panel (2, 3, 4), made of water-proof sheet (8, 9, 10), made of concrete (11).

*3 made of concrete.

*4 paved road and parking place.

For the flat permeable surface, it was reported that the ¹³⁷Cs wash-off accompanied by soil erosion was considerably small (Mikami et al., 2015)¹²⁵. Therefore, we estimated the initial ¹³⁷Cs deposition amount on the permeable surface by considering only the physical decay in the deposition amount measured in the present study. The initial deposition amount of ¹³⁷Cs on the permeable surface near the investigated eleven buildings ranged from 2.0 to 3.7 MBq m⁻². In order to compare among the measurement objects with different initial ¹³⁷Cs deposition amount, this study evaluated relative ¹³⁷Cs deposition amount, which are defined as the relative values of ¹³⁷Cs deposition amount on each component to that on a nearby permeable plane field.

In the present study, in order to evaluate the temporal changes of the ¹³⁷Cs deposition amount from the initial stage after the accident, the data obtained by the Decommissioning Pilot Project (JAEA, 2014)¹²⁰ were included in the analysis. The details of the data are reported by Yoshimura (2018)¹²⁶.

(2) Evaluation of ¹³⁷Cs migration through drainage system

The investigation was conducted at the two catchments located in the urban area of the difficult-to-return zone (Fig. 4.4-2). The investigation had been carried out from December 2014 to June 2017. Since the drainage system in the study sites is separate system and located in difficult-to-return zone, there was no ¹³⁷Cs migration via domestic wastewater. The flow rate (m³ min⁻¹) in the drainage system at the end of the catchment and the concentration of sediment (g m⁻³) was estimated based on the water level and turbidity that had been continuously measured. The run-off coefficient (ratio of flow amount to rainfall amount) was used to estimate defective data of the flow amount.

The drainage water sample was collected by an automatic water sampler. The collected water was filtrated by membrane (pore size: 0.45 μm), and the particulate fraction were separated from the dissolved fraction.

The concentration of the particulate and dissolved fractions were measured by a Ge semiconductor detector (GMX40P4-76 germanium detector, Seiko EG&G ORTEC). The ^{137}Cs fluxes of particulate and dissolved fractions were calculated by multiplying the flow amount or discharged amount of sediment by the ^{137}Cs concentration.

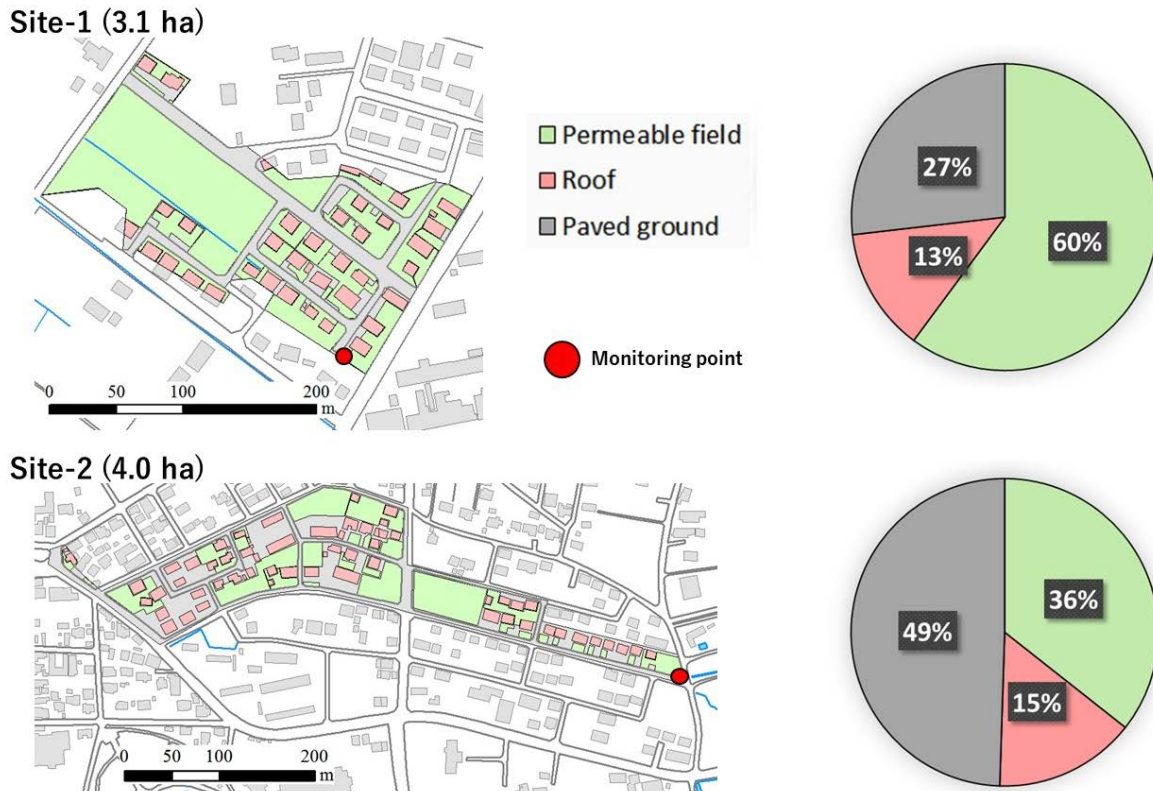


Fig. 4.4-2 Catchment to be investigated.

4.4.3 Results and discussion

(1) ^{137}Cs deposition amount per each component of the urban area

Table 4.4-2 shows the relative ^{137}Cs deposition amount in 2015 obtained for each component. The relative ^{137}Cs deposition amount on the paved surface was 0.18 as of 2015, which was considerably low compared with that on the permeable surface. The relative deposition amount at the component such as roof, wall and window was low, less than 0.1, which showed that the contamination level on the surface of urban areas is limited after four years from the accident.

Table 4.4-2 Relative ¹³⁷Cs deposition amount on components in 2015.

Components	¹³⁷ Cs relative inventory		
	Mean	SD ^a	Range
Roof	0.02	0.02	<0.01–0.06
Roof floor	0.09	0.15	<0.01–0.32
Eavestrough	0.04	0.02	0.02–0.05
Wall	0.01	<0.01	<0.01–0.01
Window	<0.01	<0.01	<0.01
Tiled porch	0.01	0.01	<0.01–0.03
Scarcement	0.08	0.06	0.01–0.16
Paved ground	0.18	0.06	0.07–0.23
Permeable plane field	0.92	–	–

^a SD denotes the standard deviation.

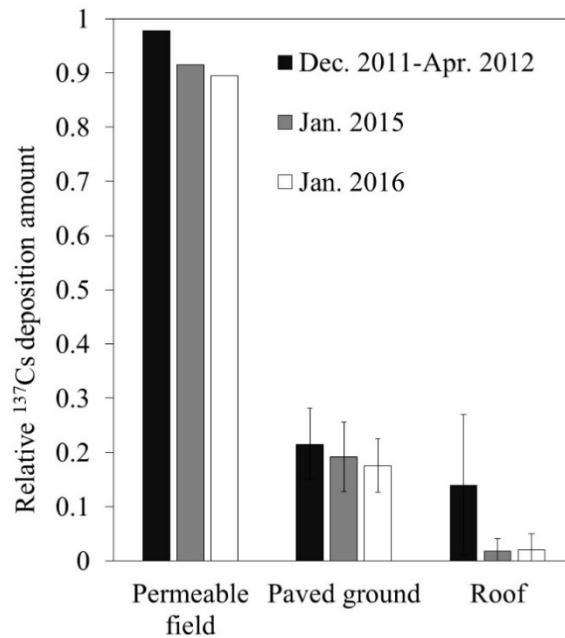


Fig. 4.4-3 Temporal changes in relative ¹³⁷Cs deposition amount at permeable surfaces, paved surfaces and roofs.

Fig. 4.4-3 shows the temporal changes in the relative ¹³⁷Cs deposition amount at the permeable surfaces, paved surfaces and roofs. The relative ¹³⁷Cs deposition amount at the paved surfaces and roofs from 2011 to 2012 were 0.22 and 0.14, respectively, which were same degree of values from 2015 to 2016. It was reported that the ¹³⁷Cs deposition attributed to the 1F accident occurred through wet process (Morio et al., 2011)¹²⁷⁾. Therefore, the present results suggests that most of the ¹³⁷Cs deposited on the paved surfaces and roofs rapidly removed by wash-off at the time of initial deposition, in addition to the weathering effect following to the deposition, and the initial wash-off critically decided the ¹³⁷Cs distribution in urban area.

Studies in Europa after the Chernobyl nuclear accident also reported that most of ¹³⁷Cs on paved surfaces and roofs washed-off at the time of the initial deposition and the following weathering effect (IAEA, 2006)¹²³⁾.

These results are in good agreement with the present results. The decreasing rate of the relative ^{137}Cs deposition amount on the permeable surfaces, paved surfaces and roofs from 2011 to 2016 were 8%, 18% and 85%, respectively. The results suggested that ^{137}Cs washed-off rapidly from paved surfaces and roofs compared with permeable surfaces due to the weathering effect after one year from the accident. There is a possibility that the rapid decrease in radioactive cesium from the components specific to an urban area contributed to the rapid decrease in the air dose rate in the urban area. From now, it will be necessary to quantitatively analyze the relation between the decrease in radioactive cesium and the decrease in the air dose rate in order to obtain the effective knowledge for predicting the future air dose rate etc.

(2) Evaluation of ^{137}Cs migration through drainage system

Table 4.4-3 shows the flow rate and the flux of sediment and ^{137}Cs observed from July 2016 to June 2017. The washed-off rate of ^{137}Cs to the deposition amount in the catchment area, which is estimated from the results of fourth airborne monitoring survey by MEXT, was 0.02-0.05%. These value are the same as or larger than those of the forest area. However, there is a possibility that the estimation of the deposition amount in urban area by the aerial monitoring includes the large uncertainty. Therefore, in order to estimate the accurate ^{137}Cs wash-off rate, further evaluation will be needed especially concerning on the deposition amount.

The ^{137}Cs migration flux in the above-mentioned period was 0.17-0.29 $\text{kBq m}^{-2} \text{yr}^{-1}$ for particulate, and 0.38-0.65 $\text{kBq m}^{-2} \text{yr}^{-1}$ for dissolved frations, which showed that 57-79% of ^{137}Cs migrated as dissolved phase. The fact that ^{137}Cs migrated predominantly as dissolved phase suggested that the wash-off process of the ^{137}Cs from urban area was different from that from the other environment, and the urban area would possibly become the main bioavailable ^{137}Cs source.

Table 4.4-3 List of the measurement results.

	Okuma Town	Tomioka Town
Total flow amount ($\text{m}^3 \text{yr}^{-1}$)	7,741	15,762
Total sediment outflow amount (kg yr^{-1})	23	17
Total ^{137}Cs outflow amount (kBq yr^{-1})	20,743	32,754
Outflow amount of particulate ^{137}Cs (kBq yr^{-1})	8,872	6,905
Outflow amount of dissolved ^{137}Cs (kBq yr^{-1})	11,871	25,849
Ratio of dissolved state (%)	57	79
Deposition amount of ^{137}Cs in river basin (MBq)	94,023	65,440
Outflow rate (%)	0.02	0.05

4.4.4 Future subjects

From now, it is important to investigate a method to evaluate the deposition amount in river basin. Also, it will be important to evaluate the mass balance between the decrease in the ^{137}Cs deposition amount measured on the ground and the ^{137}Cs migration amount through drainage, and quantitatively evaluate the weathering effect that is specific to the urban area on the air dose reduction.

5 Modeling research on environmental dynamics

5.1 Outline

The objectives of the modeling research are to deductively confirm the phenomena that have been estimated by the investigation as well as to predict future distributions of radioactive cesium and air dose rate in the environment and consider necessary countermeasures. In an analytical method using a model, a future situation is generally predicted with statistical approach where past monitoring results are extrapolated to the future by the statistical treatments. However, such statistical approach is difficult to be applied to our project, because we intend to evaluate and predict the effect of countermeasures such as decontamination and migration suppression of radioactive materials. Accordingly, the modeling with phenomenological approach was mainly adopted in this project.

In forests, radioactive cesium is circulated in trees, litter layers, and soil layers. A part of radioactive cesium is incorporated into wild vegetable and wild birds and beasts, and another part flows out to rivers. In rivers and dam lakes, radioactive cesium flows out in adsorbed state on suspended materials or in dissolved state. A part of flowing cesium is deposited on river beds, lake beds and flood plains, or refloats to the surface and migrates to the downstream. In soil, radioactive cesium deposited on the surface slowly migrates to the deep region with time. Therefore, air dose rates on soil generally decrease faster than those estimated by the physical decay of radioactive cesium. The subjects of the modeling research comprehensively cover the behavior of radioactive cesium in forests/land and its migration process from forests/land to the ocean through rivers and dam lakes. However, it is difficult to develop a single model to comprehensively represent whole phenomena in these wide regions. Also, it should be noted that the modeling is in principle to clarify the essence of a phenomenon by simplification. Considering these natures of modeling, it is not desirable to develop a too much complicated model. Therefore, we are developing and preparing multiple models with different advantages, while using appropriate models depending on the respective magnitude and phenomenon of the subjects. As indices of the future prediction and countermeasures, our research subjects cover from dose rates corresponding to external radiation exposure to the concentration of radioactive cesium in agricultural, forest and fishery products which corresponds to the internal exposure.

The main research subjects that have been targeted so far by the analytical research are as follows.

- Medium-to-long term prediction of the distribution of radioactive cesium and air dose rate.
- Evaluation of the amount of radioactive cesium flowing out from rivers into the ocean.
- Evaluation of the behavior of radioactive cesium in rivers and dams at the time of heavy rain, and evaluation of the changes in dose rate by the deposition of radioactive cesium.
- Evaluation of the behavior of radioactive cesium in dissolved state with high bioavailability.
- Evaluation of the effect of radioactive-cesium dynamics in environment on its concentration in agricultural, forest and fishery products.

The main analytical models that have been prepared so far to correspond to the above subjects are summarized in Table 5.1-1 and Fig. 5.1-1. The models can be roughly classified into the terrestrial dynamics model, the river system dynamics model, the dose rate evaluation model, the depth migration model, and the evaluation model for migration to agricultural, forest and fishery products. We are evaluating by selecting and flexibly combining these models corresponding to the purposes. For example, as to the prediction of the distribution of radioactive-caesium and air dose rate in wide region and outflow of radioactive caesium into the sea, the terrestrial dynamics model is used. On the other hand, both the terrestrial dynamics model and the river system dynamics model are used in combination concerning the dynamics of radioactive caesium and sediment at the time of heavy rain (Fig. 5.1-2).

The analysis by the terrestrial dynamics model covers the dynamics of radioactive caesium at river-basin scale from land such as forests to rivers, lakes and the sea. We are preparing the SACT (Soil And Cs Transport model) that analyzes the year-averaged dynamics based on the USLE (Universal Soil Loss Equation), and the GETFLOWS (GEneral purpose Terrestrial fluid-FLOW Simulator) that analyzes the dynamics of water, sediment and radioactive caesium at short-time events such as heavy rain in detail. The SACT was independently developed by JAEA after the accident, and the GETFLOWS was developed by the Geosphere Environmental Technology Corp.

The river system dynamics model is a method to analyze the dynamics of water flow, sediment and radioactive caesium in rivers, lakes, and the sea. We are preparing from one to three dimensional models corresponding to the scale of time and space to be analyzed. The terrestrial dynamics model also analyzes the phenomena in river system, but the analysis is rather simple. On the other hand, the area dealt with by the river system dynamics model is specified only to the river system region, thus the scale and precision of the model are different from those analyzed by the terrestrial dynamics model (Fig. 5.1-3). The one dimensional TODAM (Time-dependent, One-dimensional Degradation And Migration model) and the three dimensional FLESCOT (Flow, Energy, Salinity, Sediment Contaminant Transport model) were developed by the PNNL (Pacific Northwest National Laboratory). The two dimensional iRIC/Nays2D was developed by the Hokkaido University (iRIC/Nays2D analyzes water flow and sediment transportation but does not directly analyze the dynamics of radioactive caesium). The ROMS (Regional Ocean Modeling System) is being developed as an open source to analyze the sea, and the analysis considering ocean wave and ocean current becomes possible in combination with the SWAN (Simulating Waves Nearshore). The JAEA model is being developed independently by JAEA based on the know-how in the abovementioned models with a view to high-speed and large-scale calculation.

The depth migration model, mDSF (modified Diffusion-Sorption-Fixation model), analyzes the one-dimensional depth migration of radioactive caesium in soil. It was developed independently by JAEA as an advection and dispersion model considering reversible/irreversible sorption and desorption.

Radiation dose evaluation model, ADRET (Air Dose Rate Evaluation Tool), analyzes the radiation dose rate distribution on the basis of radioactive caesium distribution in soil or in buildings at flat land. The dose conversion coefficients in this model are obtained by the PHITS (Particle and Heavy Ion Transport code System) which is separately being developed by JAEA. The 3D-ADRES(3D-Air Dose Rate Evaluation

System) is a system to produce geometrical model of the rough terrain and structure on ground such as buildings and trees, and to construct input data for the PHITS.

The evaluation model for migration to agricultural, forest and fishery products, CMFW (Compartment Model for Forest and Water), is a simple compartment model that combines the dynamics of radioactive cesium at river-basin scale with agricultural, forest and fishery products. It analyzes the global mass-balance of radioactive cesium at river-basin scale and its effects on agricultural, forest and fishery products. The model is being developed independently by JAEA in order to clarify the effects of environmental dynamics of radioactive cesium at river-basin scale dealt with in this project on agricultural, forest and fishery products.

In the following sections 5.2-5.7, the outline and results are described for each model. The examples of combining multiple models are described in the section 5.8, and future subjects are described in the final section 5.9.

The subjects to be investigated (or social needs) have been changing with time after the accident, thus we have prepared and improved the models according to the situation. For four or five years after the accident, we had been focusing on the evaluation of the behavior of radioactive cesium adsorbed on sediment, which played a major role in the migration of radioactive cesium in environment. However, with the progress in the research on the dynamics of radioactive cesium adsorbed on sediment, we had shifted the research subjects to the behavior of dissolved radioactive cesium originating from non-decontaminated forests, which might influence the bioavailability (sorption/desorption behavior on organic materials and soil). Also, for the evaluation of radiation dose rate, we had firstly been analyzing the depth distribution, dose rate and evaluation of the decontamination effects only for flat lands without buildings. However, the analysis had been upgraded to consider more complicated topography and structures on land. We plan to flexibly promote the development and improvement of the models along with the progress in the investigation and changes in social needs.

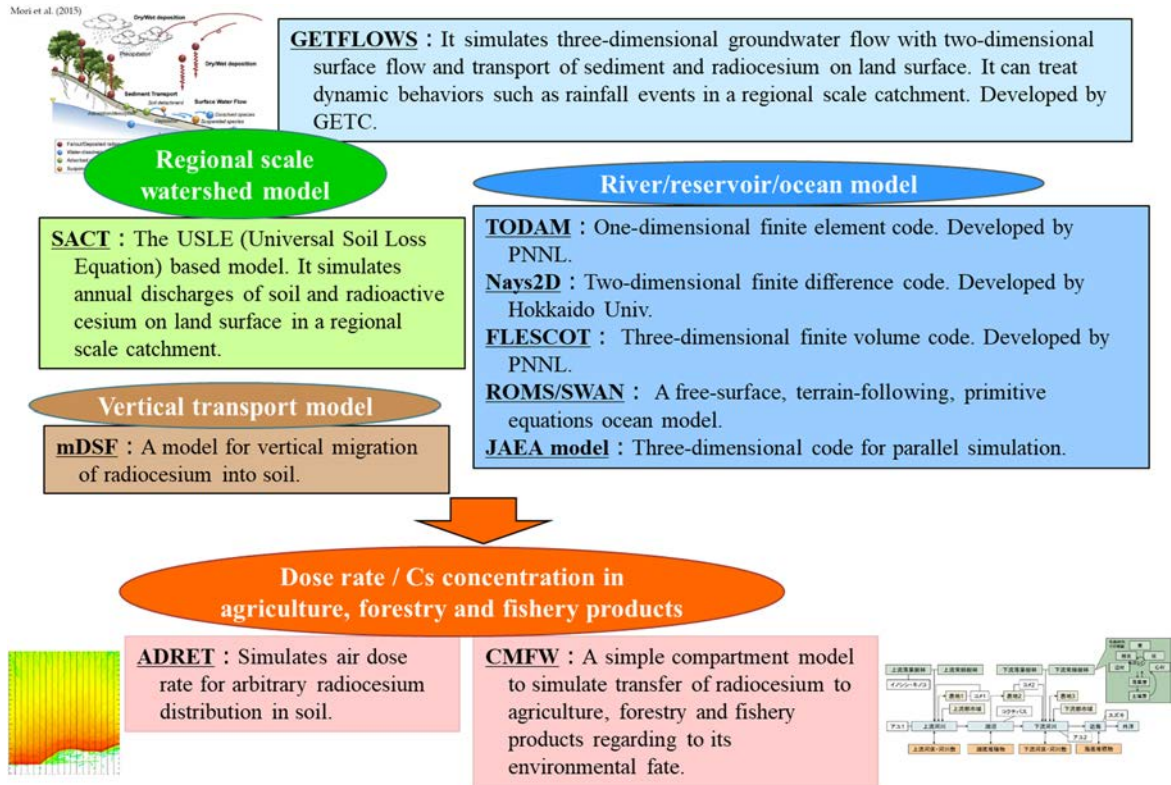


Fig. 5.1-1 Analytical models and their scopes of application.

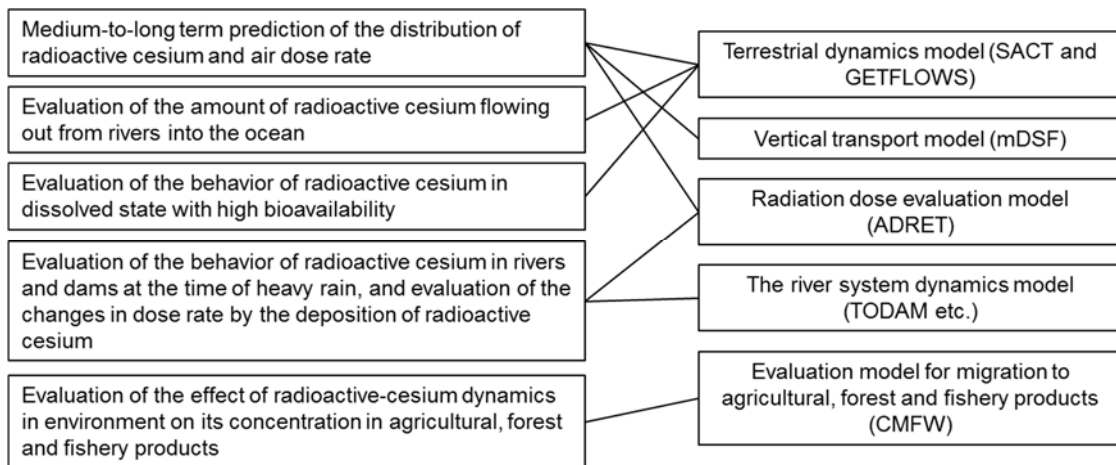


Fig. 5.1-2 Main subjects and examples of the model application.

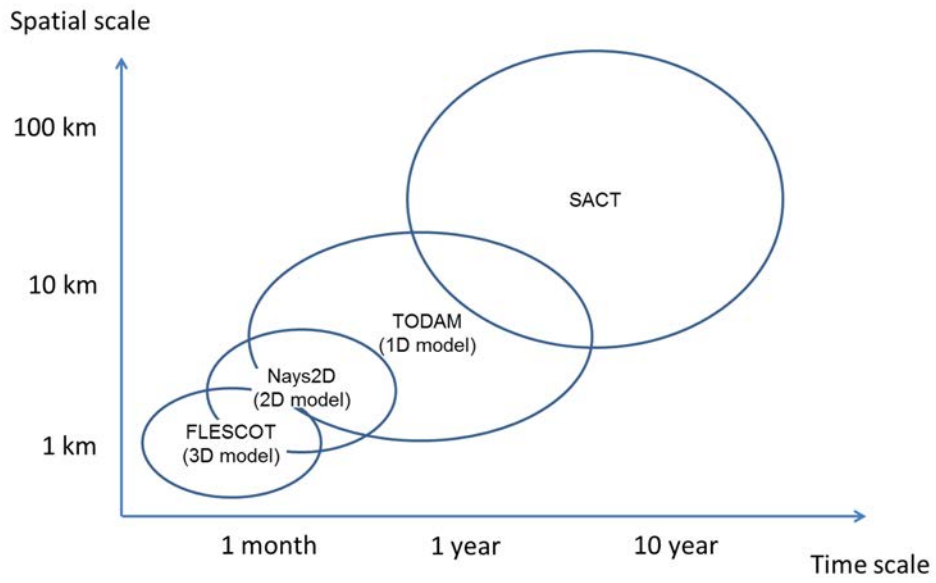


Fig. 5.1-3 Scale of time and space studied by the terrestrial/river-system dynamics models (cited from Kurikami et al. (2015)¹²⁹⁾ with modification).

Table 5.1-1 List of analytical model.

Name	Outline/Example of application	Developer	Reference
Terrestrial dynamics model			
SACT (Soil And Cs Transport model)	Model for wide area based on the USLE (Universal Soil Loss Equation). It analyzes soil erosion on ground surface and associated dynamics of radioactive cesium in a year scale	JAEA	Yamaguchi et al. (2013) ¹²⁹⁾ , Yamaguchi et al. (2014) ¹³⁰⁾ , Kitamura et al. (2014) ¹⁾
GETFLOWS (General purpose Terrestrial fluid-FLOW Simulator)	Three-dimensional finite difference program for river basin equipped with the analysis of rainfall, evapotranspiration, surface/underground water flow, soil erosion, sedimentation, dynamics of radioactive cesium. It analyzes short-term outflow behavior such as heavy rain.	Geosphere Environmental Technology Corp.	Tosaka et al. (2000) ¹³¹⁾ , Mori et al., (2015) ¹³²⁾
River system dynamics model			
TODAM (Time-dependent, One-dimensional Degradation And Migration model)	One-dimensional finite element program. It analyzes the dynamics of soil composed of three components with different particle size, dissolved radioactive cesium, and radioactive cesium adsorbed on soil, in rivers and lakes.	Pacific Northwest National Laboratory (PNNL), UAS	Onishi et al. (2007) ¹³³⁾ , 2014 ¹³⁴⁾
iRIC/Nays2D	Two-dimensional finite difference program. It analyzes the dynamics of soil in rivers and lakes. It evaluates the amount of spatial sedimentation in lake beds and flood plain.	Hokkaido University	Shimizu (2003) ¹³⁵⁾ , Shimizu et al. (2012) ¹³⁶⁾
FLESCOT (Flow, Energy, Salinity, Sediment Contaminant Transport model)	Three-dimensional finite volume program. It analyzes the dynamics of soil composed of three components with different particle size, and dissolved radioactive cesium, and radioactive cesium adsorbed on soil, in lakes and estuaries.	Pacific Northwest National Laboratory (PNNL), UAS	Onishi et al. (1993) ¹³⁷⁾ , 2014 ¹³⁸⁾
ROMS (Regional Ocean Modeling System)	Model for analyzing the ocean equipped with free surface, terrain following, and primitive equation group. It is being used in various field in scientific community. It analyzes the behavior of radioactive cesium flowing out from rivers into estuaries.	ROMS Community	e.g. Haidvogel et al. (2000) ¹³⁹⁾
JAEA model	Under development with a view to fast and large-scale calculation	JAEA	
Depth migration model			
mDSF (modified Diffusion-Sorption-Fixation model)	One-dimensional finite-element depth migration model. It analyzes advection and dispersion considering the reversible/irreversible sorption and desorption associated with the time delay to soil.	JAEA	Kurikami et al. (2017) ¹⁴⁰⁾
Radiation dose evaluation model			
PHITS (Particle and Heavy Ion Transport code System)	Monte-Carlo calculation model simulating various behavior of radiation in every material using nuclear reaction model, nuclear data, etc.	JAEA etc.	Sato et al. (2018) ¹⁴¹⁾
ADRET (Air Dose Rate Evaluation Tool)	Model analyzing air dose rate originating from arbitral radioactive cesium in soil for flat land. The dose conversion coefficients are calculated from the PHITS.	JAEA	Malins et al. (2016) ¹⁴²⁾
3D-ADRES (3D-Air Dose Rate Evaluation System)	System to make geometrical model for considerably undulating land and structures on land such as buildings and trees. It constructs the input data for PHITS.	JAEA	Kim et al. (2018) ¹⁴³⁾
Evaluation model for migration to agricultural, forest and fishery products.			
CMFW (Compartment Model for Forest and Water)	Compartment model for dynamics at river-basin scale considering the migration to agricultural, forest and fishery products. It analyzes global mass balance of radioactive cesium at river-basin scale and its effects on agricultural, forest and fishery products.	JAEA	Kurikami et al. (2017) ¹⁴⁴⁾

5.2 Terrestrial dynamics model at river-basin scale (evaluation of year-average dynamics)

5.2.1 Objectives

The objective of analytical research using SACT, which evaluates year-average dynamics among the terrestrial dynamics models at river-basin scale, is mainly to predict medium-to-long term distribution of radioactive cesium and air dose rate distribution, and evaluate the amount of radioactive cesium flowing out from rivers into the ocean.

5.2.2 Methods

The SACT (Yamaguchi et al., 2013¹²⁹), 2014¹³⁰) is a model to analyze year-average dynamics of radioactive cesium at the river-basin scale from land to rivers, lakes and the sea based on the USLE which was developed mainly by the U.S. Department of Agriculture. The details of the model, analytical conditions, and analytical results were reported in the references (Yamaguchi et al., 2013¹²⁹), 2014¹³⁰), Kitamura et al., 2014¹). In this section, the outline of the model is described.

As shown in Fig. 5.2-1, the calculation by SACT mainly consists of the following four steps.

In the first step, the soil erosion potential is calculated for each square cell whose east-west and north-south sides are 100 meter using the USLE. In the USLE, the average amount of sediment $A(\text{t ha}^{-1} \text{y}^{-1})$, which is eroded in a year, is calculated by the product of the following five coefficients,

$$A = R \cdot K \cdot LS \cdot C \cdot P \quad (5.2-1)$$

where R is the rainfall coefficient, LS is the topography coefficient, C is the product coefficient, and P is the maintenance coefficient. Each coefficient is determined from the data presented by the government such as rainfall amount, altitude data, land use data and soil data.

In the second and third steps, the soil flux actually flowing out from the cell into the downstream and erosion/sedimentation flux at the cell are calculated based on the soil erosion potential calculated in the first step. In the calculation by the SACT, three components, i.e., sand, silt and clay, are considered. In the case of nonadherent sand, the maximum amount of the downward flow $G_S(\text{t y}^{-1})$ for floating sand is first calculated by the Du Boys' equation (Vanoni, 1975)¹⁴⁵). Then, the flux of the downward flow $Q_S(\text{t y}^{-1})$ is calculated by comparing the result with the sum of the sand flux $Q_{S0}(\text{t y}^{-1})$ flowing out from the upstream of the cell and the erosion flux $E_S(\text{t y}^{-1})$ calculated by the USLE for the cell. The calculation procedure is expressed as the following equation

$$Q_S = \begin{cases} Q_{S0} + E_S & \text{if } Q_{S0} + E_S < G_S \\ G_S & \text{if } Q_{S0} + E_S \geq G_S \end{cases} \quad (5.2-2).$$

On the other hand, the flux $Q_m(t y^{-1})$ of adherent silt and clay flowing out from the cell to the downstream is calculated in the following equation, considering the relation between the erosion flux $E_m(t y^{-1})$ obtained from the USLE/Pathemoneades-Krone's equation (Vanoni, 1975)¹⁴⁵⁾ and sedimentation flux $D_m(t y^{-1})$ obtained from the Pathemoneades-Krone's equation,

$$Q_m = \begin{cases} 0 & \text{if } Q_{m0} + E_m \leq D_m \\ Q_{m0} + E_m - D_m & \text{if } Q_{m0} + E_m > D_m \end{cases} \quad (5.2-3).$$

In the fourth stem, the behavior of ^{137}Cs adsorbed on sediment is analyzed. Supposing that the depth profile of ^{137}Cs in soil be exponential and all ^{137}Cs be adsorbed on soil, ^{137}Cs is then distributed to sand, silt and clay corresponding to their specific surface area. The calculation is performed by sorbing ^{137}Cs on migrating soil for each particle size, which was calculated up to the third step.

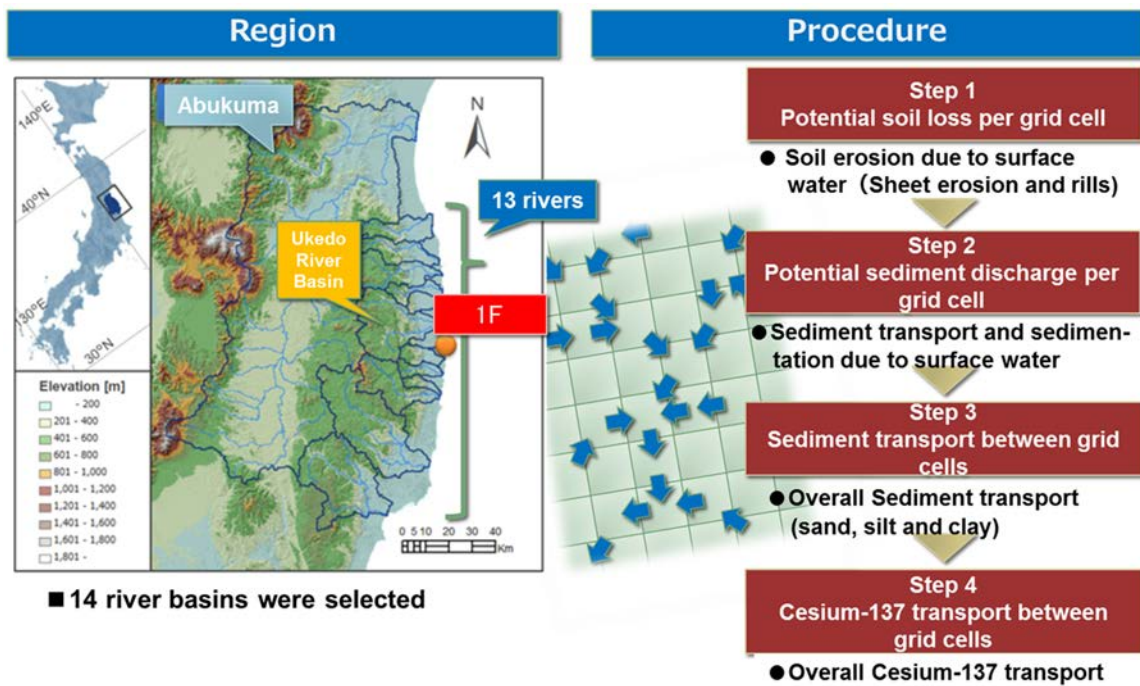


Fig. 5.2-1 Analytical process in SACT.

5.2.3 Results and discussion

The analysis was conducted for 14 river basins; the Abukuma River, the Uda River, the Mano River, the Niida River, the Ohta River, the Odaka River, the Ukedo River, the Maeda River, the Kuma River, the Tomioka River, the Ide River, the Kido River, the Natsui River, and the Same River (Yamaguchi et al., 2013¹²⁹); Yamaguchi et al., 2014¹³⁰); Kitamura et al., 2014¹).

Table 5.2-1 summarizes the total amount of soil and ¹³⁷Cs flowing out from each river basin into the sea in a year after the fallout. The total amount of ¹³⁷Cs flowing out from 14 river basins was estimated to be 8.4 TBq. It was confirmed that this value is almost consistent with that estimated from the observed results (Kitamura et al., 2014)¹). However, it was supposed that the results vary from 0.7 TBq to 10.2 TBq based on the sensitivity analysis considering the uncertainty of the parameters (Yamaguchi et al., 2014)¹³⁰). The outflow amount of soil and ¹³⁷Cs was the largest in the Abukuma River, because it has the largest river basin area among the abovementioned 14 rivers. On the other hand, although the river basin area of the Ukedo River is less than one-tenths of that of the Abukuma River, the outflow of ¹³⁷Cs was comparable to that of the Abukuma River, because the deposition amount of ¹³⁷Cs in the Ukedo River was appreciably large.

Table 5.2-2 shows the outflow amount of soil and dynamics of ¹³⁷Cs complied depending on the respective land use. The area of fields occupies only about 10 % of the total area. However, the fields account for about 58 % of the total outflow of soil, and about 47 % of the total outflow of radioactive cesium. The area of forests is about 64 % of the total area (forests: 5,329 km², total area: 8,370 km²), but the contribution of forests to the dynamics is relatively small, such that forests account for about 24% of the soil erosion amount (erosion in forests: 2.9×10⁵ t, total amount of erosion: 1.2×10⁶ t), and about 41% of the outflow of radioactive cesium. This is because the ground of forests is covered with trees, undergrowth and litter layer, so the erosion is suppressed. When the decontamination is conducted in a forest, the forest will become wasteland because the coating layers are lost. Such situation may possibly result in the increase in the outflow rate of soil and radioactive cesium. The outflow rate of radioactive cesium from forests was estimated to be about 0.3 % in a year (outflow of ¹³⁷Cs: 3.0×10¹² Bq, amount of ¹³⁷Cs initial deposition: 9.2×10¹⁴ Bq), which is almost in agreement with the measured results.

Table 5.2-1 Total amount of soil and ¹³⁷Cs flowing out from river basin into the sea in a year after the fallout.

Name of river	River basin area (km ²)	Amount of sediment outflow into the sea (t y ⁻¹)	Amount of ¹³⁷ Cs outflow into the sea (Bq y ⁻¹)	Average concentration of ¹³⁷ Cs adsorbed on sediment (Bq kg ⁻¹)
Abukuma River	5423	2.4×10 ⁵	3.0×10 ¹²	1.2×10 ⁴
Ukedo River	420	2.7×10 ⁴	2.0×10 ¹²	6.2×10 ⁴
Niida River	261	1.6×10 ⁴	1.1×10 ¹²	6.5×10 ⁴
Maeda River	48	1.6×10 ⁶	4.0×10 ¹¹	2.5×10 ⁵
Kuma River	6.4	2.5×10 ³	2.8×10 ¹¹	1.1×10 ⁵
Ohta River	6.9	1.7×10 ³	2.7×10 ¹¹	1.6×10 ⁵
Mano River	167	5.5×10 ³	2.0×10 ¹¹	3.7×10 ⁴
Kido River	260	1.5×10 ⁴	1.4×10 ¹¹	9.0×10 ³
Odaka River	67	2.5×10 ³	1.3×10 ¹¹	5.3×10 ⁴
Tomioka River	63	2.0×10 ³	1.1×10 ¹¹	5.8×10 ⁴
Natsui River	685	4.2×10 ⁴	1.1×10 ¹¹	2.6×10 ³
Same River	592	5.1×10 ⁴	8.9×10 ¹⁰	1.7×10 ³
Ide River	40	3.0×10 ³	6.9×10 ¹⁰	2.3×10 ⁴
Uda River	16.3	2.4×10 ³	6.4×10 ¹⁰	2.6×10 ⁴
Total	8352	4.2×10 ⁵	8.4×10 ¹²	2.0×10 ⁴

Table 5.2-2 Amount of soil outflow and dynamics of ¹³⁷Cs for each land use.

Land use	Area (km ²)	Average amount of soil erosion (t ha ⁻¹ y ⁻¹)	Total amount of soil erosion (t y ⁻¹)	Total ¹³⁷ Cs (t=0 y) (Bq)	Total ¹³⁷ Cs (t=1 y) (Bq)	Amount of ¹³⁷ Cs decrease in a year (Bq y ⁻¹)	Amount of ¹³⁷ Cs decrease by the physical decay (Bq y ⁻¹)	Amount of ¹³⁷ Cs decrease by the outflow (Bq y ⁻¹)
field	852	8.1	6.9×10 ⁵	1.3×10 ¹⁴	1.2×10 ¹⁴	6.6×10 ¹²	3.0×10 ¹²	3.5×10 ¹²
forest	5329	0.6	2.9×10 ⁵	9.2×10 ¹⁴	9.0×10 ¹⁴	2.4×10 ¹³	2.1×10 ¹³	3.0×10 ¹²
river system	156	-	-	1.1×10 ¹³	1.2×10 ¹³	-2.7×10 ¹¹	2.5×10 ¹¹	-5.7×10 ¹¹
rice field	1157	1.5	1.7×10 ⁵	1.6×10 ¹⁴	1.5×10 ¹⁴	4.5×10 ¹²	3.5×10 ¹²	9.7×10 ¹¹
city area	457	0.1	5.4×10 ³	6.8×10 ¹³	6.7×10 ¹³	1.5×10 ¹²	1.6×10 ¹²	-8.6×10 ⁹
others	147	1.0	1.5×10 ⁴	1.7×10 ¹³	1.7×10 ¹³	3.9×10 ¹¹	3.9×10 ¹¹	-9.7×10 ⁸
road and railway	67	0.2	1.6×10 ³	1.0×10 ¹³	1.0×10 ¹³	2.5×10 ¹¹	2.3×10 ¹¹	2.1×10 ¹⁰
wasteland	152	3.9	5.9×10 ⁴	1.6×10 ¹³	1.5×10 ¹³	6.5×10 ¹¹	3.6×10 ¹¹	3.9×10 ¹¹
golf course	47	0.6	2.9×10 ³	3.5×10 ¹²	3.4×10 ¹²	9.0×10 ¹⁰	6.9×10 ¹⁰	1.1×10 ¹⁰
sand	1	0.2	15	1.9×10 ¹¹	1.9×10 ¹¹	4.2×10 ⁹	4.3×10 ⁹	-6.0×10 ⁷
total	8370		1.2×10 ⁶	1.3×10 ¹⁵	1.3×10 ¹⁵	3.8×10 ¹³	3.0×10 ¹³	6.4×10 ¹²

In the SACT analysis, the values of some parameters have not been measured, or the obtained values vary depending on the place and year. Therefore, the maximum and minimum values for the amount of radioactive-cesium outflow into the sea were calculated. Also, a sensitivity analysis was conducted in order to estimate the parameters that have large effects (Yamaguchi et al., 2014)¹³⁰⁾. A list of the cases in the sensitivity analysis is shown in Table 5.2-3. With respect to the basic cases, the changed parameters are shaded in gray. As the parameters to be evaluated, those with high heterogeneity were chosen, such as rainfall coefficient (RAIN-1, 2), critical shear stress (TAU_C-1, 2), distribution of soil particle size (GRAIN), flow rate in dam lake (LAKE_V) and buffer depth of radioactive cesium (CS_PROF).

Fig. 5.2-2 shows the outflow amount of ¹³⁷Cs into the sea in a year for each case calculated by the analysis. Although the outflow amount is different among each case, it was revealed that the outflow rate especially decreased when the critical shear stress in land was large (TAU_C-1). The critical shear stress affected the maximum downward flow calculated by the Du Boys's equation for sand, and erosion/sedimentation flux calculated by the Pathemoneades-Krone's equation for silt and clay. In the present case, it was revealed that the decrease in the erosion flux of silt and clay was especially affected by the critical shear stress. The next highest sensitivity parameter was the buffer depth of radioactive cesium (CS_PROF, α is the reciprocal of the buffer depth). These results show that it is essential to set the critical shear stress and depth distribution of radioactive cesium based on the measurements in order to analyze with higher precision.

Table 5.2-3 Cases in the sensitivity analysis.

Case	Rainfall coefficient	Critical shear stress (sand)		Critical shear stress for re-suspension (silt, clay)		Critical shear stress for precipitation (silt, clay)		Particle size distribution (sand, silt, clay)	Flow rate in lakes	Depth distribution of ¹³⁷ Cs
		river τ_c (Pa)	land τ_{cr} (Pa)	river τ_{ed} (Pa)	land τ_{ed} (Pa)	river τ_{ed} (Pa)	land τ_{ed} (Pa)			
NORMAL	336.6	0.180	0.260	0.060	0.260	0.043	0.260	40:40:20	0.01	1.20
RAIN-1	421.65	0.180	0.260	0.060	0.260	0.043	0.260	40:40:20	0.01	1.20
RAIN-2	198.57	0.180	0.260	0.060	0.260	0.043	0.260	40:40:20	0.01	1.20
TAU_C-1	336.6	0.180	7.000	0.060	7.000	0.043	7.000	40:40:20	0.01	1.20
TAU_C-2	336.6	0.180	0.260	1.300	0.260	0.800	0.260	40:40:20	0.01	1.20
GRAIN	336.6	0.180	0.260	0.060	0.260	0.043	0.260	40:50:10	0.01	1.20
LAKE_V	336.6	0.180	0.260	0.060	0.260	0.043	0.260	40:40:20	0.20	1.20
CS_PROF	336.6	0.180	0.260	0.060	0.260	0.043	0.260	40:40:20	0.01	0.50
MAX	421.65	0.180	0.260	0.060	0.260	0.043	0.260	40:40:20	0.20	0.50
MIN	198.57	0.180	7.000	1.300	7.000	0.800	7.000	40:50:10	0.01	1.20

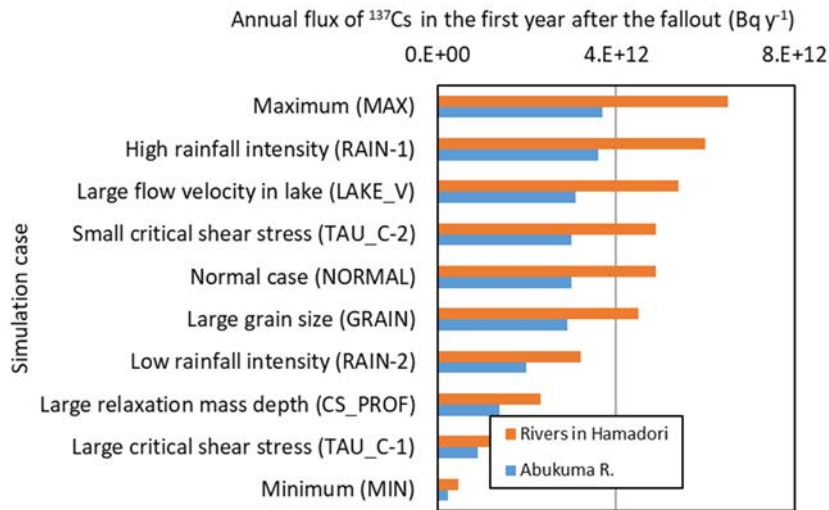


Fig. 5.2-2 Amount of ¹³⁷Cs outflow into the sea in a year, calculated by the sensitivity analysis for each case (cited from Yamaguchi et al. (2014)¹³⁰ with modification).

Fig. 5.2-3 shows the prediction of the changes in the amount of ¹³⁷Cs deposition until 100 years after the fallout in the basic case (NORMAL) described above. Although the contribution of the physical decay was large, it was shown that the reduction of the radioactive-cesium inventory by the erosion and transportation of soil (so called “weathering effect”) is expected.

5.2.4 Future subjects

In response to the recent accumulation of the measured data, the abovementioned analytical results were compared with the measured data on the time-dependence of ¹³⁷Cs concentration in river water. As a result, it was clarified that the decreasing rates of the measured data are higher than those predicted by the analysis. Therefore, we are now proceeding the development of the methods aiming to improve the precision of the prediction by considering the time-dependence of the depth profile and kinetics of sorption/desorption (Liu et al., 2018)¹⁴⁶.

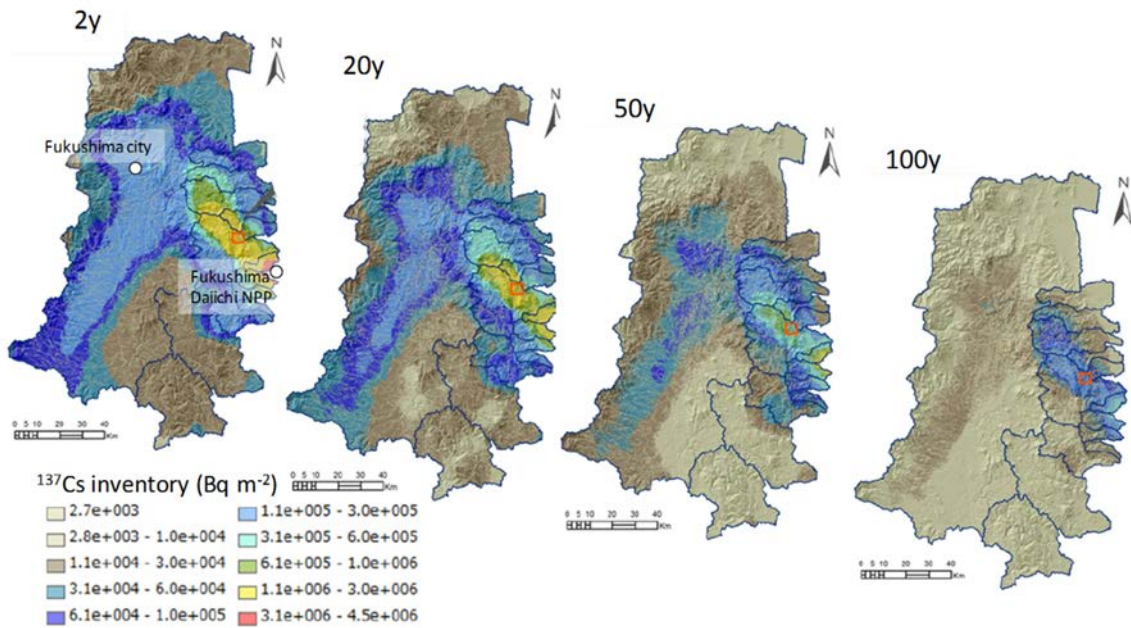


Fig. 5.2-3 Prediction map of ^{137}Cs deposition until 100 years after the fallout for the basic case (cited from Yamaguchi et al. (2013)¹²⁹ with modification).

5.3 Terrestrial dynamics model at river-basin scale (dynamics model for water circulation, sediment and ^{137}Cs)

5.3.1 Objectives

Among the terrestrial dynamics models at river-basin scale, the GETLOWS deals with the correspondences to river flow, and outflow of sediment and radioactive cesium. The objective of the analytical research using the GETLOWS is to elucidate the source of radioactive cesium flowing out mainly from rivers into the sea and evaluate the behavior of dissolved radioactive cesium with high bioavailability.

5.3.2 Methods

In the present study, we have conducted the transportation analysis for sediment and radioactive cesium based on the existing simulator for river-basin water circulation, GETFLOWS (GEneral purpose Terrestrial fluid-FLOW Simulator) (Fig. 5.3-1), which has been developed and applied for over twenty years in Japan.

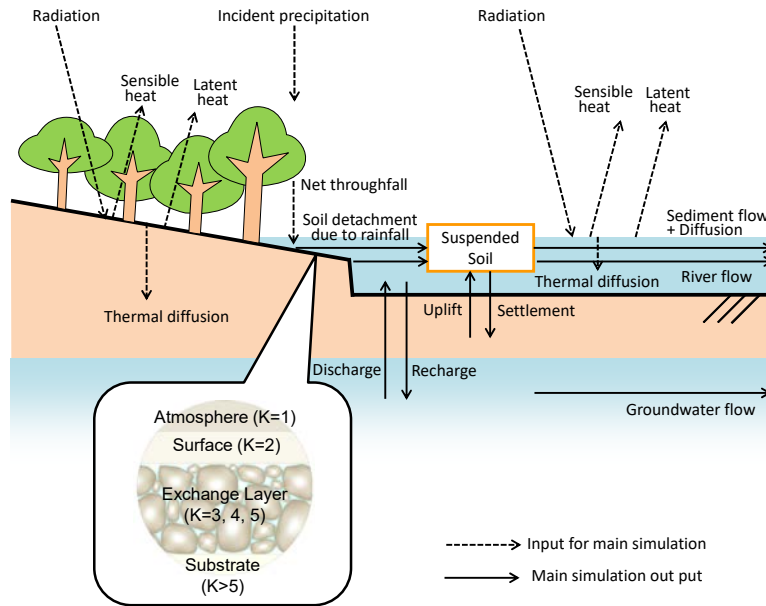


Fig. 5.3-1 Outline of GETFLOWS (modified from Kitamura et al., 2016¹⁴⁷).

The details of the model, analytical conditions, results were described in the references (Kitamura et al. (2016)¹⁴⁷, Sakuma et al. (2017)¹⁴⁸, 2018¹⁴⁹ 150). In this report, the outline of the model is described. In the followings, the equations governing each phenomenon are shown. The equation governing water-air two-phase fluid is expressed as follows,

$$-\nabla \cdot M_p - q_p = \frac{\partial}{\partial t} (\rho_p \phi S_p) \quad (p=\text{water, air}) \quad (5.3-1)$$

where M_p is the mass flux ($\text{kg m}^{-2} \text{s}^{-1}$), q_p is the sink-source term ($\text{kg m}^{-3} \text{s}^{-1}$), ρ_p is the density (kg m^{-3}), ϕ is the effective porosity ($\text{m}^3 \text{m}^{-3}$), S_p is the saturation ratio ($\text{m}^3 \text{m}^{-3}$), and t is the time (s).

The equation governing the sediment transportation in land is presented as,

$$-\nabla (M_w R_{ss,i}) + \nabla \cdot D_{ss,i} \nabla (\rho_w R_{ss,i}) - q_{ss,i} + \frac{m_{ss,i}^{splash} + m_{ss,i}^{erosion}}{d_e} = \frac{\partial}{\partial t} (\rho_w R_{ss,i}) \quad (5.3-2)$$

where M_w is the mass flux of water ($\text{kg m}^{-2} \text{s}^{-1}$), $R_{ss,i}$ is the concentration of suspended sediment with particle size component i , (kg kg^{-1}), $D_{ss,i}$ is the diffusion coefficient of suspended sediment with particle size component i in surface water ($\text{m}^2 \text{s}^{-1}$), $m_{ss,i}^{splash}$ is the erosion amount of suspended sediment with particle size component i by raindrop ($\text{kg m}^{-2} \text{s}^{-1}$), $m_{ss,i}^{erosion}$ is the erosion amount of suspended sediment with particle size component i by surface flow ($\text{kg m}^{-2} \text{s}^{-1}$), d_e is the water depth (m), and $q_{ss,i}$ is the sink-source term of suspended sediment with particle size component i ($\text{kg m}^{-3} \text{s}^{-1}$).

The equations governing the transportation of suspended cesium on ground and dissolved cesium on and under grounds are expressed as,

$$\begin{aligned}
 & -\nabla \cdot (M_w R_{ss,i} R_{cs,i}) + \nabla \cdot D_{ss,i} \nabla (\rho_w R_{ss,i} R_{cs,i}) - q_{ss,i} R_{cs,i} - \lambda \rho_w R_{ss,i} R_{cs,i} \\
 & + \frac{R_{cs,i} m_{ss,i}^{sprash} + R_{cs,i} m_{ss,i}^{erosion}}{d_e} - \rho_w R_{ss,i} m_{ss,i}^{adsorption} = \frac{\partial}{\partial t} (\rho_w R_{ss,i} R_{cs,i})
 \end{aligned} \tag{5.3-3}$$

$$\begin{aligned}
 & -\nabla \cdot (M_w R_{cw}) + \nabla \cdot D_{cw} \nabla (\rho_w R_{cw}) - \rho_w q_w R_{cw} - \lambda \rho_w \phi S_w R_{cw} \\
 & + \rho_w R_{ss,i} m_i^{adsorption} + \rho_{ss,i} (1 - \phi) m_i^{adsorption} = \frac{\partial}{\partial t} (\rho_w \phi S_w R_{cw})
 \end{aligned} \tag{5.3-4}$$

where $R_{cs,i}$ is the concentration of radioactive cesium in suspended sediment with particle size component i (Bq kg^{-1}), R_{cw} is the concentration of dissolved cesium in water (Bq kg^{-1}), D_{cw} is the rheological dispersion coefficient ($\text{m}^2 \text{s}^{-1}$), λ is the decay constant (s^{-1}), and $m_{ss,i}^{adsorption}$ is the sorption/desorption amount between radioactive cesium and component with particle size component i ($\text{Bq kg}^{-1} \text{s}^{-1}$). For the dissolved cesium in equation (5.3-4), the fifth term and sixth term in the left-hand side are applied to cesium on ground surface, and underground cesium, respectively.

In the analysis by GETFLOWS, the generalized Darcy's law for underground fluid (water and air) and Manning law for overland flow are described in the same-type equations, hence both surface water and underground water can be simultaneously calculated. With respect to sediment, equations for suspended sediment with multiple particle size (six divisions) are solved considering the erosion by raindrops and erosion/deposition by surface flow. For surface soil (exchange layer of sediment), the erosion and sedimentation height in river basin region is calculated by saving the results of erosion and sedimentation. Concerning radioactive cesium, the sorption/desorption equations are solved using decay constant and sorption distribution constant K_d for radioactive cesium in dissolved state, in suspended state on suspended sediment etc., and in sorbed/fixed state on soil and rocks. As to the model parameters, the calibration and the validation were conducted for water, sediment, and radioactive cesium based on the measured values. Herewith, the following evaluations were performed by preparing the models with high reproducibility.

5.3.3 Results and discussion

In implementing the outflow analysis of radioactive cesium in river basin, the following four questions are considered as subjects to be solved.

1. What kinds of character among river basins can explain the behavior of radioactive cesium flowing out from the river basin?
2. How is the response of turbidity and radioactive-cesium concentration according to the scale of the flooding?
3. From where and how much radioactive cesium flows out in a small river basin?
4. Can dissolved as well as suspended radioactive cesium be reproduced using K_d model supposing the instant

sorption/desorption equilibrium that is generally used?

In order to answer the above four questions, the analysis was conducted in 1) five river basins close to the 1F (the Odaka River, the Ukedo River, the Maeda River, the Kuma river and the Tomioka River), 2) Oginosawa river basin in Kawauchi Village, Fukushima Prefecture, and 3) the upper river basin of the Ohta River, Fukushima Prefecture (Fig. 5.3-2). For the calculation by the GETFLOWS, it is needed to make a three-dimensional hydrogeological structure model by concentrating various data. In Figs. 5.3-3 to 5.3-5, the geological structure models are presented. The parameters concerning the underground water flow such as absolute permeability were given to each layer in the geological structure model. Also, we set the parameters concerning evapotranspiration and surface flow based on the land use and soil distribution on ground. Herewith, the hydrogeological structure model was constructed.

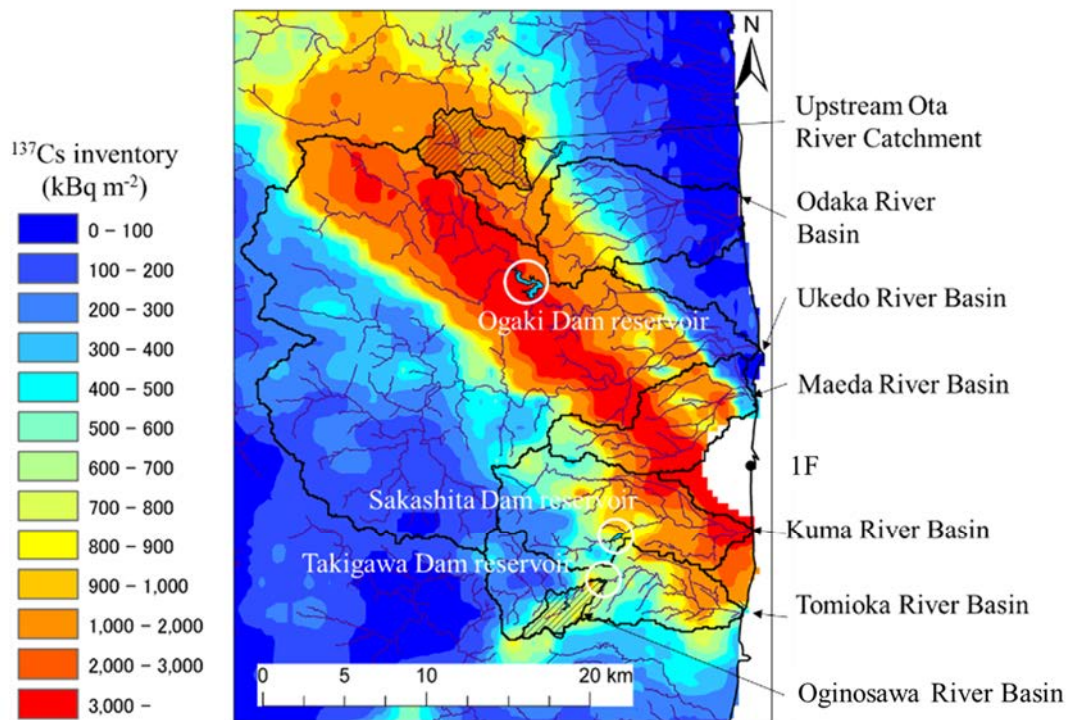


Fig. 5.3-2 Distribution of ¹³⁷Cs deposition in five river basins close to the 1F (the Odaka River, the Ukedo River, the Maeda River, the Kuma River, and the Tomioka River), the upper river basin of the Ohta River, and Oginosawa River basin in Tomioka River basin area (data taken by the fourth airborne radiation monitoring in November 2011).

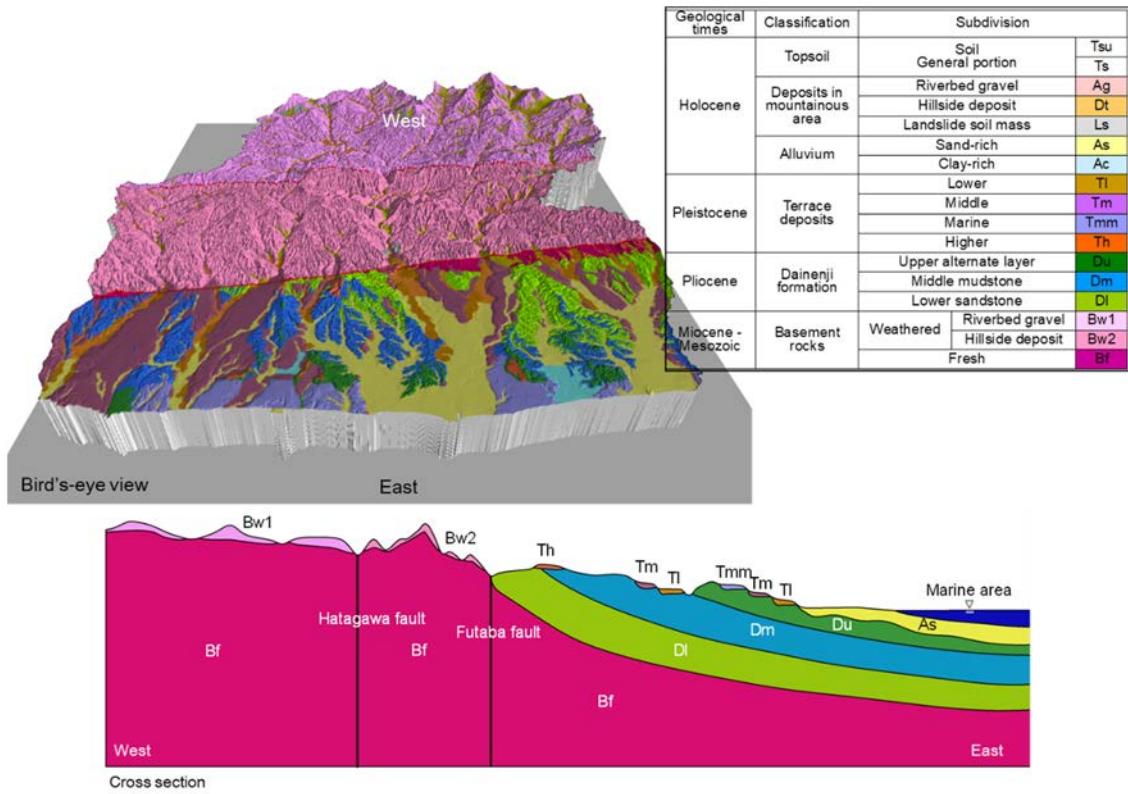


Fig. 5.3-3 Three-dimensional geological structure model (River basin areas of the Odaka River, the Ukedo River, the Maeda River, the Kuma River and the Tomioka River).

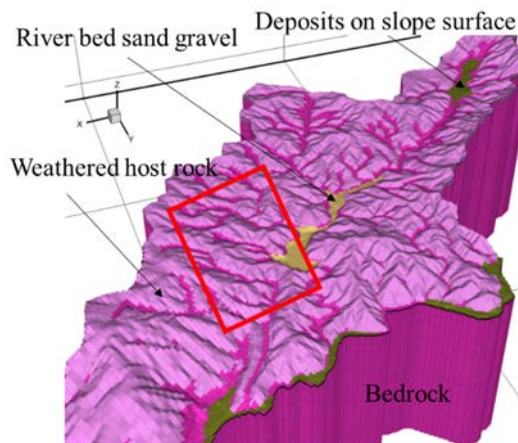


Fig. 5.3-4 Three-dimensional geological structure model (Oginosawa River basin).
Red frame shows the region depicted in Fig. 5.3-9.

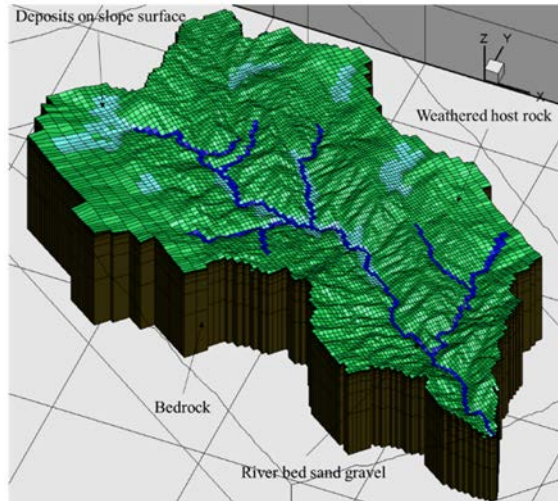


Fig. 5.3-5 Three-dimensional geological structure model (upper river basin of the Ohta River).

As to the region 1) described above, the simulation of rain outflow at different rainfall intensity was conducted for five river basins. Herewith, it was evaluated as to what kinds of features of the river basin contribute to the outflow of radioactive cesium. The features of the river basins to be investigated are summarized in Table 5.3-1. The rainfall events to be analyzed were the typhoon No. 15 in September, 2011 (Roke), the typhoon No. 18 in September 2013 (Man-yi), and the typhoon No. 26 in October 2013 (Wipha).

Table 5.3-1 Features of each river basin.

	Area	Forest	Rice field	Others	Amount of initial deposition (¹³⁷ Cs)
(unit)	km ²	%	%	%	TBq
Odaka River	68	49	26	25	48
Ukedo River	424	57	25	18	833
Maeda River	45	6.5	8	17	6.2
Kuma River	6.5	6.1	14	15	86
Tomioka River	62	6.1	13	16	38
Oginosawa (Tomioka River system)	6.7	92	2	6	5.5
Upper basin of the Ohta River	21	99	0	1	40

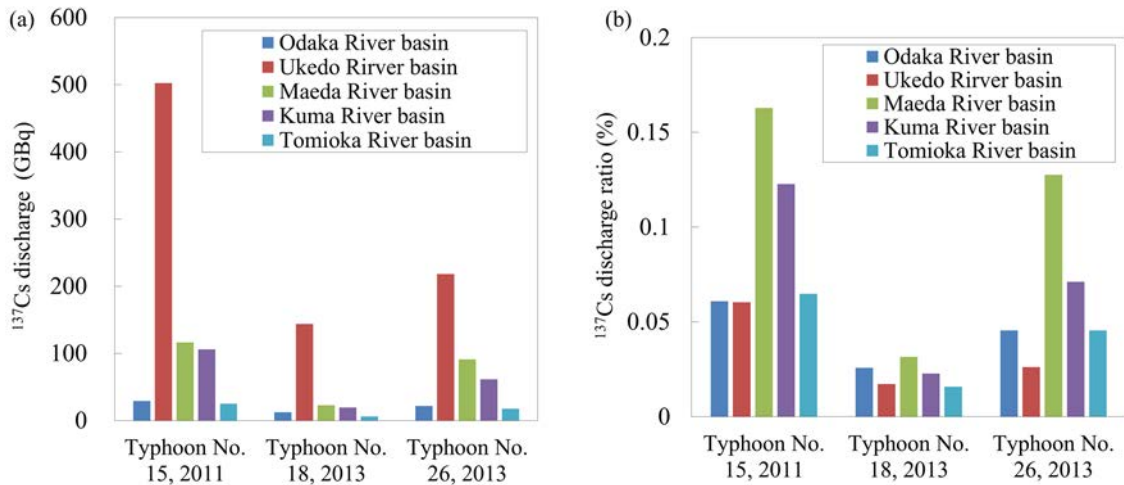


Fig. 5.3-6 (a) Outflow amount and (b) outflow ratio of ¹³⁷Cs from five river basins at heavy rainfall such as typhoon.

As shown on the left side of Fig. 5.3-6, the amount of ¹³⁷Cs outflow (GBq) was the largest in The Ukedo River basin (Table 5.3-1) which has large area and large amount of initial deposition (about 144-503 GBq). Then, the amount of ¹³⁷Cs outflow was in the order of the Maeda River basin (about 23-117 GBq), the Kuma River basin (20-106 GBq), the Odaka River basin (about 12-29 GBq) and the Tomioka River basin (about 6-25 GBq). However, when the outflow amount was evaluated by the outflow ratio obtained by dividing the amount of ¹³⁷Cs outflow by the amount of initial ¹³⁷Cs deposition, it was rather the lowest in the Ukedo River basin (about 0.02-0.06%), and the highest in the Maeda River basin (about 0.03-0.16%). If there is a dam, which has an effect to stop the sediment flow from the upstream, the outflow of suspended cesium to the downstream would be suppressed. Also, if there is a forest where the surface water flow is suppressed, the amount of sediment outflow would also decrease. From these results, it was considered that the outflow of ¹³⁷Cs was suppressed in the Ukedo River basin where large amount of radioactive cesium remained in the upper basin of dam lake, which is mostly composed of forests. As a result, the outflow ratio became small. On the other hand, in the Maeda River basin without dams, a large amount of ¹³⁷Cs was deposited in rice fields where the outflow of sediment is large, consequently the outflow ratio became large. From these results, it was elucidated that the outflow ratio of radioactive cesium from rivers to the sea tended to be low in river basins with dams, while it tended to be high in river basin which is mostly composed of rice fields etc. where a large amount of radioactive cesium was deposited (Sakuma et al., 2017)¹⁴⁸.

Next, we estimated the response of turbidity and radioactive-cesium concentration to various rainfall patterns (Fig. 5.3-7) in dam outlet works and head works by the analysis. The purpose of the estimation is to evaluate the relation of rainfall intensity with turbidity and radioactive-cesium concentration, from the viewpoint of presenting information for making a decision of water-intake control in dam outlet works and head works. The examples of the results are shown in Fig. 5.3-8.

Case	Mountain area	Coastal area	Period (y/m/d)	Cumulative precipitation (mm)		
				Tsushima St.	Namie St.	Average in the simulation
Typhoon in 2011/9	High	High	2011/9/20~2011/9/22	251.0	289.0	263.2
A-1	High	Low	2013/7/26~2013/7/28	96.5	34.0	51.7
A-2			2013/9/14~2013/9/16	143.0	104.5	124.4
A-3			2013/8/5~2013/8/7	45.0	15.5	44.0
B-1	Low	High	2013/10/19~2013/10/21	49.5	102.5	76.2
B-2			2013/10/1~2013/10/3	19.0	44.0	30.4
B-3			2013/10/22~2013/10/24	19.5	33.0	24.5
C-1	High	High	2013/10/15~2013/10/17	124.5	151.0	135.7
C-2			2013/6/14~2013/6/16	76.5	77.5	49.4
C-3			2013/4/2~2013/4/4	56.5	75.0	68.7
Virtual precipitation (large) (intensity equivalent to Typhoon in 2015/9)	High		· Time history trend is equivalent to that monitored at the Namie station in C-1 event. · Cs inventory is based on the airborne survey at 2016/11/18.			370.2
Virtual precipitation (middle) (intensity equivalent to C-1)	Middle					135.7
Virtual precipitation (low)	Low					49.75

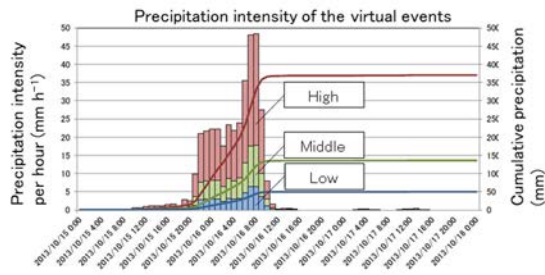
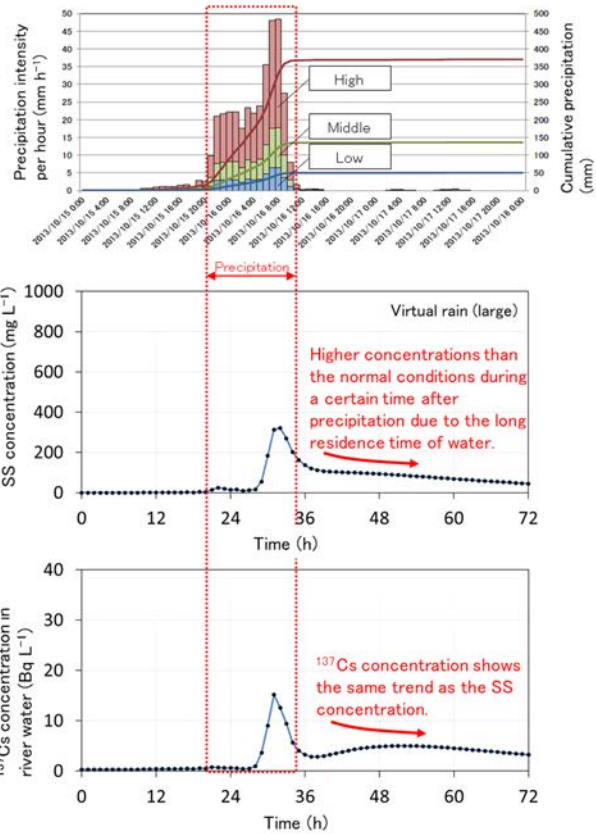
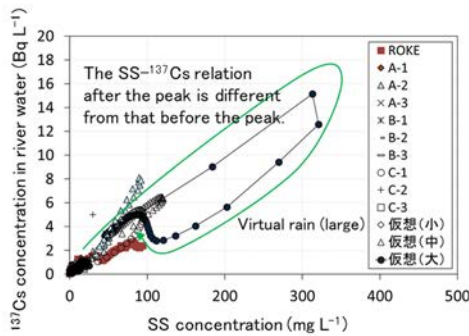


Fig. 5.3-7 Rainfall patterns applied in the analysis.

Outlet of the Ogaki Reservoir

- At the outlet of the Ogaki dam reservoir, both suspended sediment (SS) and ¹³⁷Cs in water have dull peaks of concentrations followed by higher concentrations than the normal conditions during a certain time after precipitation due to the long residence time of water.
- The hysteresis, which is the difference of the SS-¹³⁷Cs relation between before and after the peak, is caused by the mixture of the sediment from different areas in the upstream overland.



The Weir in the Takase River

- The concentrations of SS and ¹³⁷Cs decrease quickly after precipitation because no dam exists in upstream.
- ¹³⁷Cs concentration increases quickly due to the inflow of the highly contaminated sediment from the overland nearby.
- Then the sediment with lower ¹³⁷Cs concentration from upstream areas reaches to the weir.
- It is sometimes difficult to estimate ¹³⁷Cs concentration in water from SS concentration because the origin of the sediment depends on precipitation intensity.

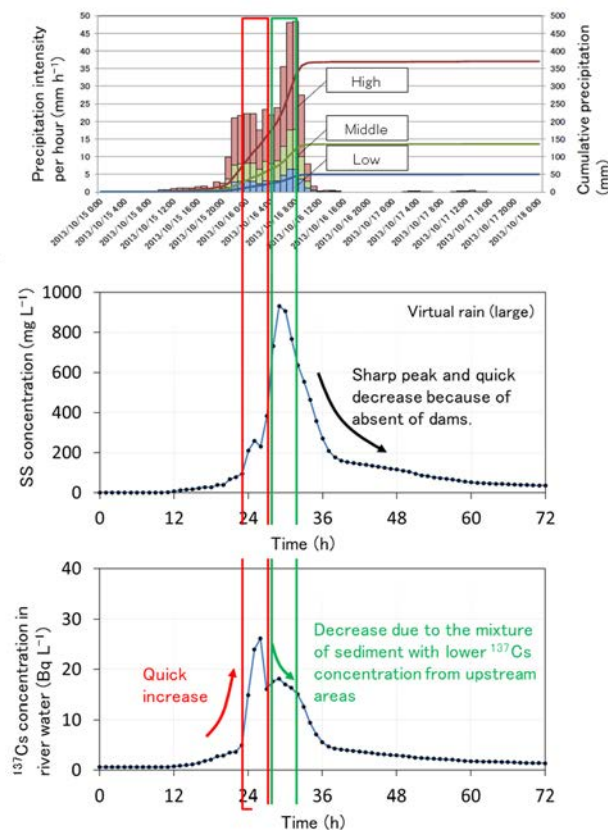


Fig. 5.3-8 Example of analytical results.

For outlet works in Ogaki dam located in the upstream of the Ukedo River, the peaks of suspended sediment and radioactive-cesium concentration became round due to the retention of radioactive cesium in the dam lake. For the time being after the rainfall, their concentration continued to be higher than that at the time of normal flow condition. The relation between the concentration of suspended sediment and radioactive cesium was different between before and after the rainfall period (hysteresis). This is because the source of sediment shifted to the upstream region with time. In the case of the Ogaki dam, the deposition amount of radioactive cesium around the dam was large, while that in the upper river basin was relatively small. Therefore, it was considered that the concentration of radioactive cesium decreased with time, and the graph exhibits clockwise hysteresis. In the Ukedo head works located in the Takase River (tributary of the Ukedo River), the ratio of the concentration of sediment to radioactive cesium was not 1:1 due to the effect of the similar hysteresis, which suggested that it is sometimes difficult to estimate concentration of radioactive cesium in river water only by the concentration of suspended sediment. In addition, it should be noted that the model validation regarding time- varying radioactive cesium concentration is not enough, although we validated the model based on the data in 2013 on several rivers (Kitamura et al., 2016¹⁴⁷), Sakuma et al., 2017¹⁴⁸).

Concerning the river basins shown in 2), the evaluation was conducted for Oginosawa basin in Kawauchi Village, Fukushima Prefecture. Compared with the abovementioned cells, appreciably small square cells (one side is about 10 m) were used. We evaluated from where and how much sediment and radioactive cesium flowed out from the river basin by conducting the outflow analysis for about four and a half years after the accident (May 26, 2011 - December 31, 2015) including at the time of normal water storage and water discharge. The features of the river basins are shown in Table 5.3-1.

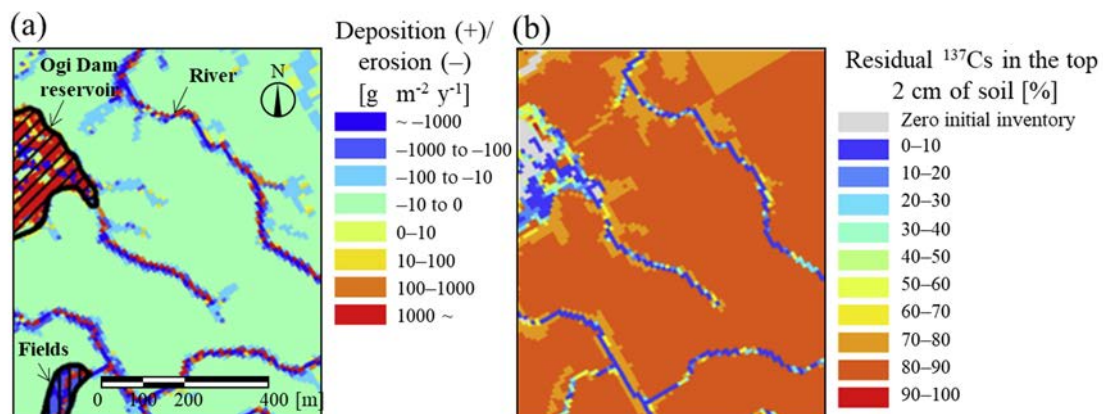


Fig. 5.3-9 (a) Amount of erosion and sedimentation, and (b) ratio of remaining ¹³⁷Cs, in the period from May, 2011 to December, 2015.

As shown in Fig. 5.3-9, the decreasing rates of erosion amount and radioactive-cesium inventory were high near rivers and along stream in forests. While, the erosion almost did not happen in forests far from rivers (total erosion amount: 0.001-0.1 mm), thus the decreasing rate of radioactive cesium inventory was

low. When quantitatively analyzed, it was clarified that the contribution of the vicinity of rivers was about an order of magnitude larger than that of forests far from rivers (Sakuma et al. 2018)¹⁴⁹⁾.

As to the river basins shown in 3), the evaluation was conducted for the upper river basin of the Ohta River, Namie Town, Minamisoma City. We evaluated whether it is possible or not to represent the concentration of dissolved cesium flowing out from forest regions using the precise model reproducing the outflow of water, sediment, and suspended cesium. The features of the river basins are shown in Table 5.3-1, and the set values of the distribution coefficient K_d are presented in Table 5.3-2.

Table 5.3-2 Set values of distribution coefficient K_d .

representative particle size (μm)	Case 1 K_d ($\text{m}^3 \text{kg}^{-1}$)	Case 2 K_d ($\text{m}^3 \text{kg}^{-1}$)
1	200	200
10	200	200
100	200	50
300	200	50
1000	0	0
5000	0	0

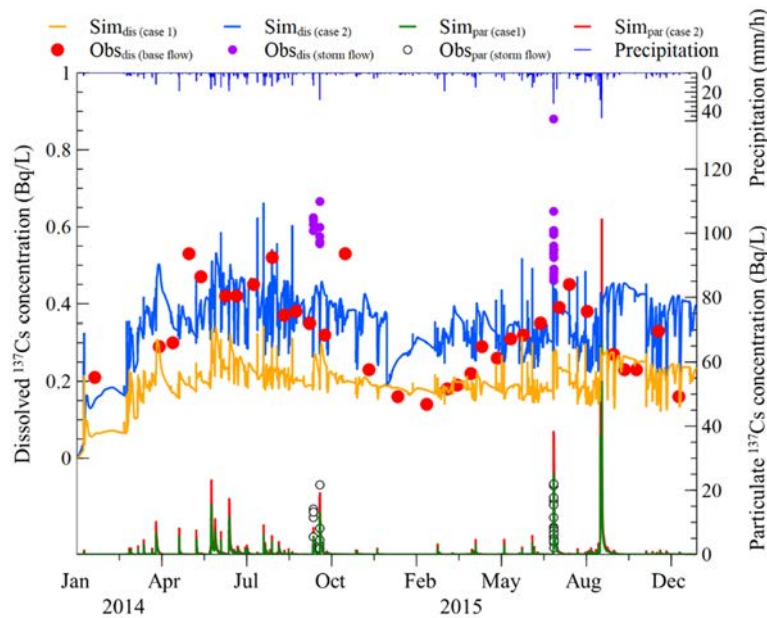


Fig.5.3-10 Comparison between measured data and calculated value for suspended and dissolved cesium.

From Fig. 5.3-10, the measured value of dissolved radioactive cesium in rivers at the time of normal water level was 0.14-0.53 Bq L⁻¹(average: 0.32 Bq L⁻¹). It was found that the mechanism of the outflow can be explained to some extent by considering the difference in cesium sorption property depending on the particle size (Fig. 5.3-10, Simul. Case 2 (average: 0.36 Bq L⁻¹)). However, it was also clarified that it is difficult to represent the seasonal changes in the actually measured concentration of dissolved cesium (the concentration was high in summer, and low in winter) and its changes at the time of rainfall (0.18-0.88 Bq L⁻¹, average: 0.55 Bq L⁻¹) only by the present K_d model. The results suggested that the degradation by microorganism in litter layer contributed to the changes in cesium concentration (Sakuma et al., 2018)¹⁵⁰.

5.3.4 Future subjects

In order to reproduce the concentration of dissolved cesium flowing out from forests, we plan to develop a new model that can express its seasonal changes and increase at the time of water discharge from dams by coupling the forest ecosystem compartment model in the GETFLOWS. Further, we plan to clarify the source of dissolved cesium and its generation path, and obtain parameters for cesium leaching from organic materials. Herewith, we aim to elucidate the mechanism of cesium migration while feeding back to the models.

5.4 River system dynamics model

5.4.1 Objectives

The objective of the analytical research using the river system dynamics model is to evaluate the behavior of radioactive cesium in rivers and dam lakes mainly at the time of heavy rain, and to evaluate the changes in radiation dose rate by the deposition of radioactive cesium.

5.4.2 Methods

For river system dynamics models, we are preparing the multiple one-, two- and three-dimensional models that can correspond to the region and the temporal/spatial scale to be analyzed, which was described in the section 5.1. The methods for numerical analysis are different among these models. Also, the calculation methods for turbulence and equations expressing soil deposition and resuspension are different. However, these models are common in terms of solving the advection/dispersion equations based on the mass conservation law of soil and radioactive cesium in a river system.

Fig. 5.4-1 shows the conceptual image of the river system dynamics model. In the one-dimensional TODAM, three-dimensional FLESCOT, and JAEA model, the transportation in river system is analyzed for three-component soil with different particle size (generally, sand, silt and clay), radioactive cesium adsorbed on these components, and dissolved radioactive cesium. Radioactive cesium flows and disperses on the water current, while repeating sorption/desorption with suspended sediment and riverbed sediment in river system. Suspended sediment sinks to the bottom or rises up to the surface depending on the degree of the shear stress by the water flow. The mass conservation law for sediment and radioactive cesium is expressed by the following equations.

For sediment,

$$\begin{aligned} & \frac{\partial c_i}{\partial t} + \frac{\partial}{\partial x}(uc_i) + \frac{\partial}{\partial y}(wc_i) + \frac{\partial}{\partial z}[(v - v_{si})c_i] \\ & = \frac{\partial}{\partial x}\left(\varepsilon_x \frac{\partial c_i}{\partial x}\right) + \frac{\partial}{\partial y}\left(\varepsilon_y \frac{\partial c_i}{\partial y}\right) + \frac{\partial}{\partial z}\left(\varepsilon_z \frac{\partial c_i}{\partial z}\right) + \left(\frac{s_{ri}}{h} - \frac{s_{di}}{h}\right) + q_{ci} \end{aligned} \quad (5.4-1),$$

for dissolved radioactive cesium,

$$\begin{aligned} & \frac{\partial g}{\partial t} + \frac{\partial}{\partial x}(ug) + \frac{\partial}{\partial y}(wg) + \frac{\partial}{\partial z}(vg) = \frac{\partial}{\partial x}\left(\varepsilon_x \frac{\partial g}{\partial x}\right) + \frac{\partial}{\partial y}\left(\varepsilon_y \frac{\partial g}{\partial y}\right) + \frac{\partial}{\partial z}\left(\varepsilon_z \frac{\partial g}{\partial z}\right) - \lambda g \\ & \quad - \sum_{i=1}^3 K_i (c_i K_{di} g - g_i) - \frac{1}{h} \sum_{i=1}^3 \gamma_i (1-n) d_i K_{bi} (K_{di} g - g_{bi}) \end{aligned} \quad (5.4-2),$$

and for radioactive cesium adsorbed on suspended sediment,

$$\begin{aligned} \frac{\partial g_i}{\partial t} + \frac{\partial}{\partial x}(ug_i) + \frac{\partial}{\partial y}(wg_i) + \frac{\partial}{\partial z}[(v - v_{si})g_i] = & \frac{\partial}{\partial x}\left(\varepsilon_x \frac{\partial g_i}{\partial x}\right) + \frac{\partial}{\partial y}\left(\varepsilon_y \frac{\partial g_i}{\partial y}\right) + \frac{\partial}{\partial z}\left(\varepsilon_z \frac{\partial g_i}{\partial z}\right) \\ & - \lambda g_i - \frac{s_{di}}{h} g_i + K_i(c_i K_{di} g - g_i) + \frac{g_{bi} s_{ri}}{h} + q_i \end{aligned} \quad (5.4-3),$$

where c_i is the concentration of sediment component i (kg m^{-3}), u , w , and v are the flow rate in x -, y - and z -directions, respectively (m s^{-1}), v_{si} is the sedimentation velocity of sediment component i (m s^{-1}), ε_x , ε_y , and ε_z are the dispersion coefficient in x -, y - and z -directions, respectively ($\text{m}^2 \text{s}^{-1}$), s_{ri} is the resuspension flux of the sediment component i ($\text{kg m}^{-2} \text{s}^{-1}$), s_{di} is the sedimentation flux of sediment component i ($\text{kg m}^{-2} \text{s}^{-1}$), h is the water depth (m), q_{ci} is the spring out term of sediment component i ($\text{kg m}^{-3} \text{s}^{-1}$), g is the concentration of dissolved radioactive cesium (Bq m^{-3}), λ is the decay constant (s^{-1}), K_i and K_{bi} are the sorption/desorption rate constants of sediment component i with respect to suspended sediment and river sediment, respectively (s^{-1}), K_{di} is the sorption distribution coefficient of sediment component i ($\text{m}^3 \text{kg}^{-1}$), g_i is the concentration of radioactive cesium adsorbed on suspended sediment component i (Bq m^{-3}), γ_i is the specific gravity of sediment component i (dimensionless), n is the porosity of river sediment (dimensionless), d_i is the particle size of sediment component i (m), g_{bi} is the concentration of cesium in sediment component i in river sediment (Bq kg^{-1}), and q_i is the spring out term of radioactive cesium adsorbed on sediment component i ($\text{Bq m}^{-3} \text{s}^{-1}$). Concerning the flux of sedimentation and resuspension, the Du Boy's equation and Toffaleti's equation (Vanoni, 1975)¹⁴⁵⁾ were used for non-adherent sand, while the Partheniades and Krone's equation (Vanoni, 1975)¹⁴⁵⁾ was used for adherent silt and clay.

The above mass conservation equations were discretized by finite element method in TODAM, and by finite volume method in FLESCOT, respectively. As a JAEA model, we have developed a calculation code that discretizes all directions in three dimensions by difference calculus method using orthogonal grid. In order to precisely represent the topography of the models to be simulated, we are also developing a code that discretizes the horizontal direction by finite element method after dividing into triangular lattices, and discretizes the vertical direction by difference calculus method.

River/reservoir/ocean model

One, two and three dimensional models are available for simulation of radiocesium migration in water column. According to the scale of the issues, appropriate model can be selected.

- Transport of sediment, dissolved contaminant and sediment-sorbed contaminant
- Three sediment-size fractions or sediment types (sand, silt and clay)
- Adsorption and desorption of radiocesium to sediment
- Deposition and resuspension of sediment

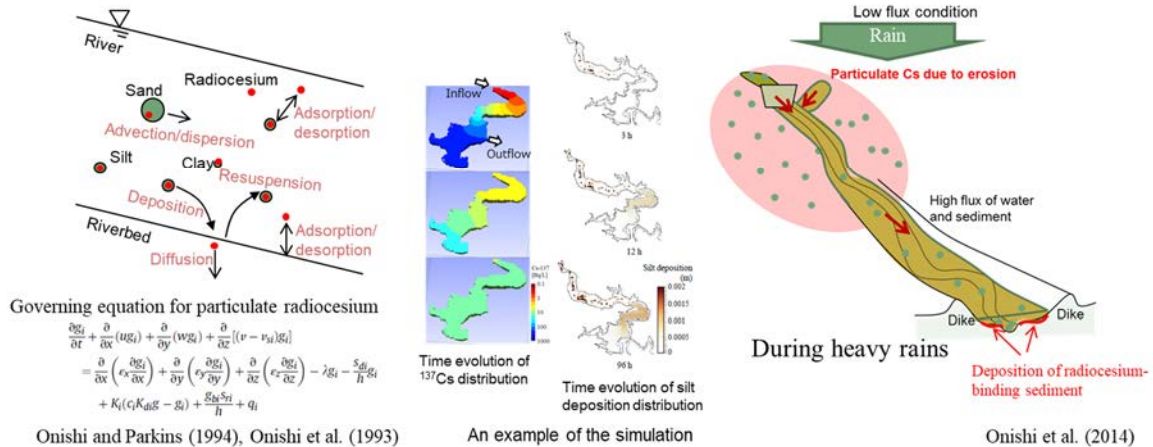


Fig. 5.4-1 Conceptual image of river system dynamics model.

5.4.3 Results and discussion

Since dam lakes have large cross section compared with rivers, the flow rate of river water suddenly decreases when flowing from river into a dam lake. Such decrease in flow rate, i.e., decrease in shear stress, promotes the deposition of suspended sediment and its sedimentation into the lake bottom.

In evaluating the behavior of sediment and radioactive cesium in dam lakes by the analysis, the verification of the model is essential. In order to verify the TODAM, Nays2D, and FLESCOT, we utilized the monitoring data on the flow rates, the concentration of suspended sediment, and the concentration of radioactive cesium in the upstream and downstream of Ogaki dam lake, which were measured at the time of typhoon in September 2013 by the Tohoku Regional Agricultural Administration Office, Ministry of Agriculture, Forestry and Fisheries. Figs. 5.4-2 and 5.4-3 show the measured data and the input values for the analysis by FLESCOT concerning the concentration of suspended sediment, and the concentration of radioactive cesium at the observation spots in the upstream of the dam lake. As a result of the analysis by setting appropriate parameters, the results of the concentration of suspended sediment and the concentration of radioactive cesium (Figs. 5.4-4 and 5.4-5) at the observation spots in the downstream were consistent with the measured data, which confirmed the validity of the model. The similar verification was conducted also for TODAM and Nays2D (Kurikami et al., 2014¹⁵¹); Yamada et al., 2015¹⁵²); Kurikami et al., 2016¹⁵³). Although there were some differences among the models, it was clarified that amount of radioactive cesium

flowing out to the downstream was less than 10% of the total cesium flowing into Ogaki dam lake at the time of rainfall event. At this rainfall event, the water level was intentionally lowered to avoid the breakdown of the dam body by after quakes. Therefore, another analysis was conducted by virtually raising the water level considering the normal water level in operation. As a result, it was elucidated that the outflow rate of radioactive cesium decreased less than half (Table 5.4-1).

Next, the analysis using FLESCOT was conducted for virtual dam lakes with different capacity. We investigated the effect of the differences in strength and duration of rainfall, capacity of dam lakes (or water level), and distribution coefficient of sorption on the outflow rate of the suspended sediment with each particle size and radioactive cesium to the downstream (Kurikami et al., 2016)¹⁵³). An example of the results is shown in Fig. 5.4-6. The figure indicates that the ratio of radioactive cesium flowing out to the downstream tends to increase with the increase in the amount of river water flowing into the dam lake at the time of rainfall. Even with the same inflow amount, it was found that the outflow rate in the short-time heavy rain was higher than that in long-time rainfall. Further, it was elucidated that the higher the water level was (or the larger the dam capacity compared with the inflow amount was), the lower the outflow rate of suspended sediment and radioactive cesium became. At that time, it was also found that the contribution rate of silt with relatively fast precipitation speed decreased, while that of clay with slow precipitation speed increased (Fig. 5.4-7). Fig. 5.4-8 shows the image of the behavior of sediment and radioactive cesium flowing into a dam lake at the time of heavy rain, which had been supposed by the analysis. As a countermeasure against the suppression of the contamination flowing out to the downstream, it was found that the management of the water level was effective. Also, it was suggested that results can be utilized in designing silt fences etc. by specifying the particle size that is easy to migrate.

Table 5.4-1 Outflow rate of suspended sediment and ¹³⁷Cs to the downstream for different water levels in the dam lake.

	At low water level (real condition) E.L. 140m	At middle water level E.L. 155m	At high water level (normal operation condition) E.L. 170m
Outflow rate of sand	0.0%	0.0%	0.0%
Outflow rate of silt	4.5%	2.3%	1.6%
Outflow rate of clay	54%	44%	34%
Outflow rate of ¹³⁷ Cs	9.0%	5.7%	3.5%
Contribution ratio of components adsorbed on silt	40%	25%	18%
Contribution ratio of components adsorbed on clay	60%	6.5%	82%

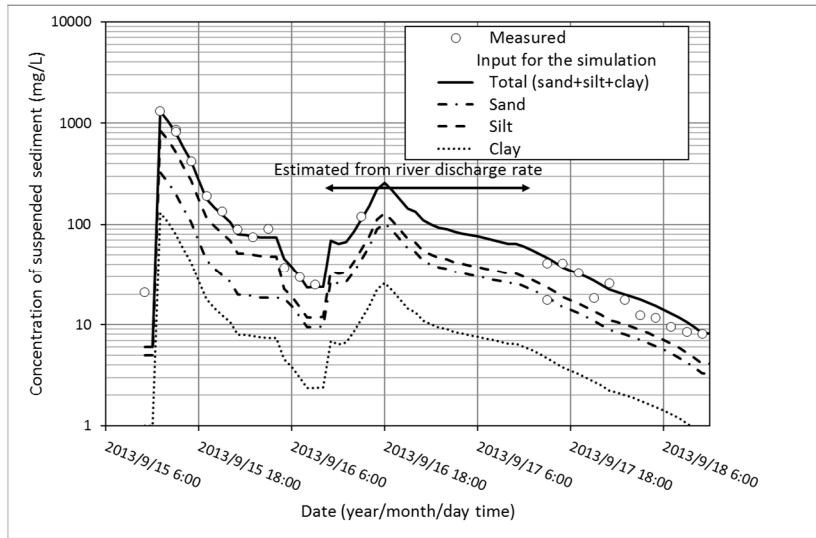


Fig. 5.4-2 Measured values of the concentration of suspended sediment at the observation spots in the upstream of dam lake, and input values in the analysis by FLESCOT (cited from Kurikami et al. (2016)¹⁵³⁾ with modification).

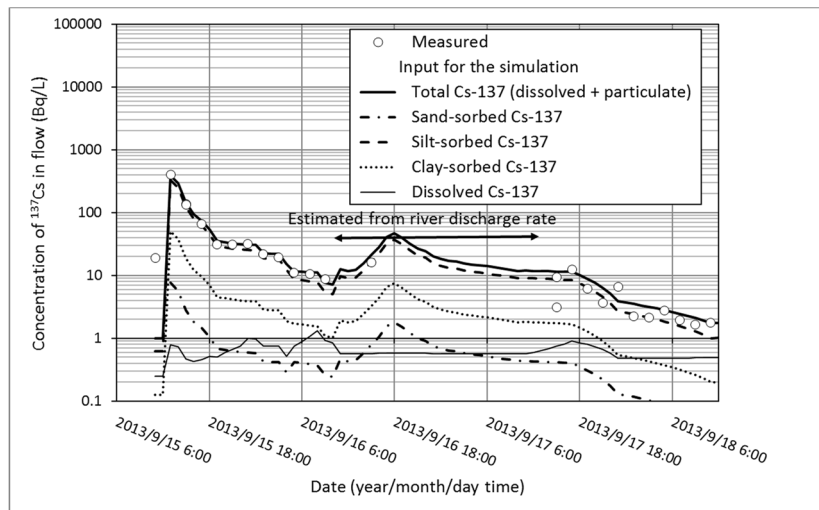


Fig. 5.4-3 Measured values of ¹³⁷Cs concentration at the observation spots in the upstream of dam lake, and input values in the analysis by FLESCOT (cited from Kurikami et al. (2016)¹⁵³⁾ with modification).

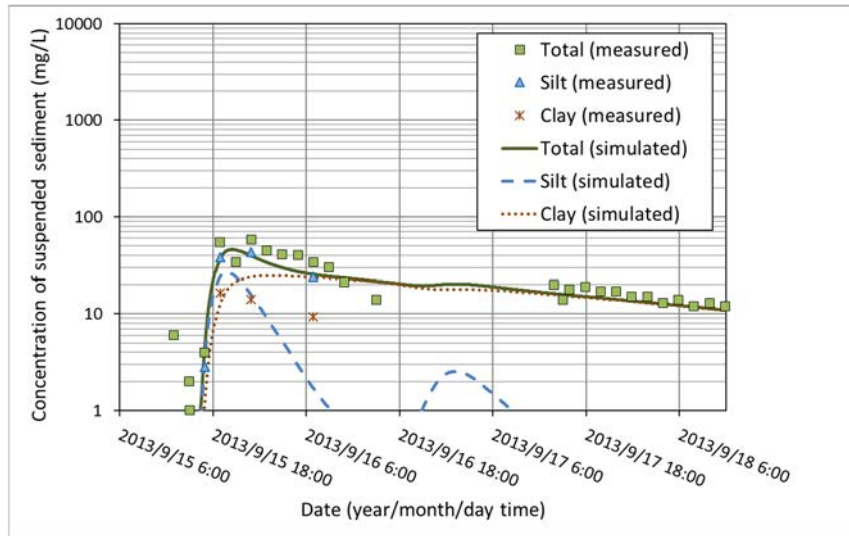


Fig. 5.4-4 Comparison between measured values of the concentration of suspended sediment at the observation spots in the downstream of dam lake and results of analysis by FLESCOT (cited from Kurikami et al. (2016)¹⁵³ with modification).

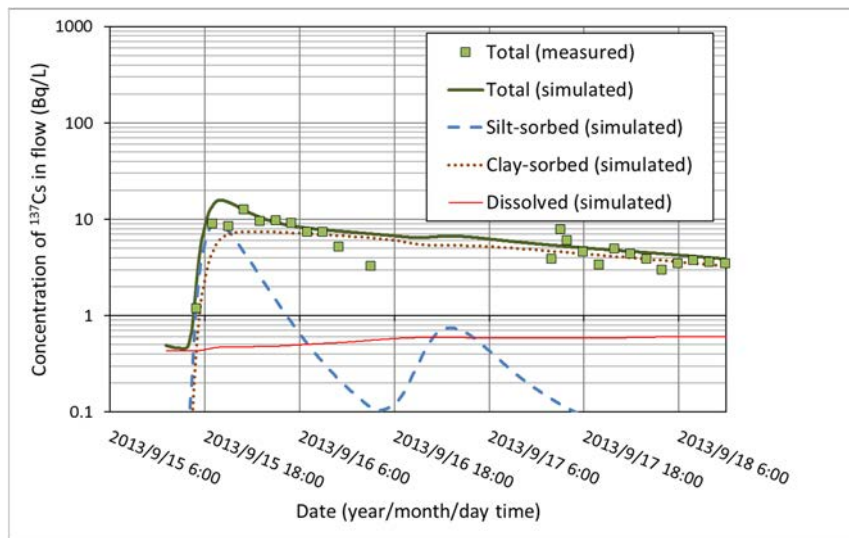


Fig. 5.4-5 Comparison between measured values of ^{137}Cs concentration at the observation spots in the downstream of dam lake and results of analysis by FLESCOT (cited from Kurikami et al. (2016)¹⁵³ with modification).

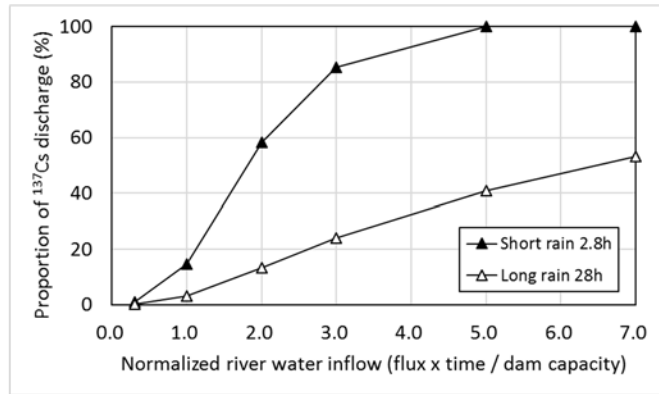


Fig. 5.4-6 Effect of strength/duration of rainfall and capacity of dam on the outflow rate of ¹³⁷Cs to the downstream (cited from Kurikami et al. (2016)¹⁵³ with modification).

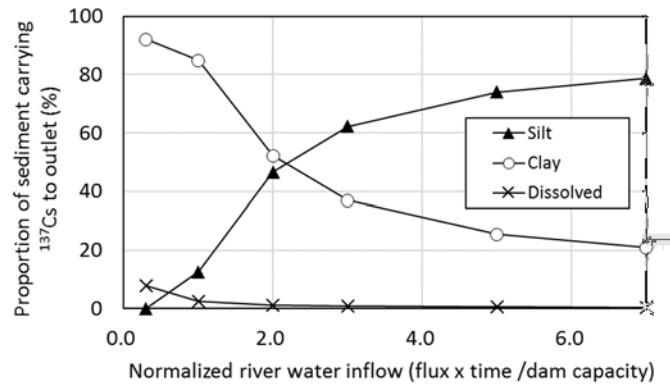


Fig. 5.4-7 Contribution ratio of rainfall scale and each particle size to the outflow of ¹³⁷Cs (long-time rain) (cited from Kurikami et al. (2016)¹⁵³ with modification).

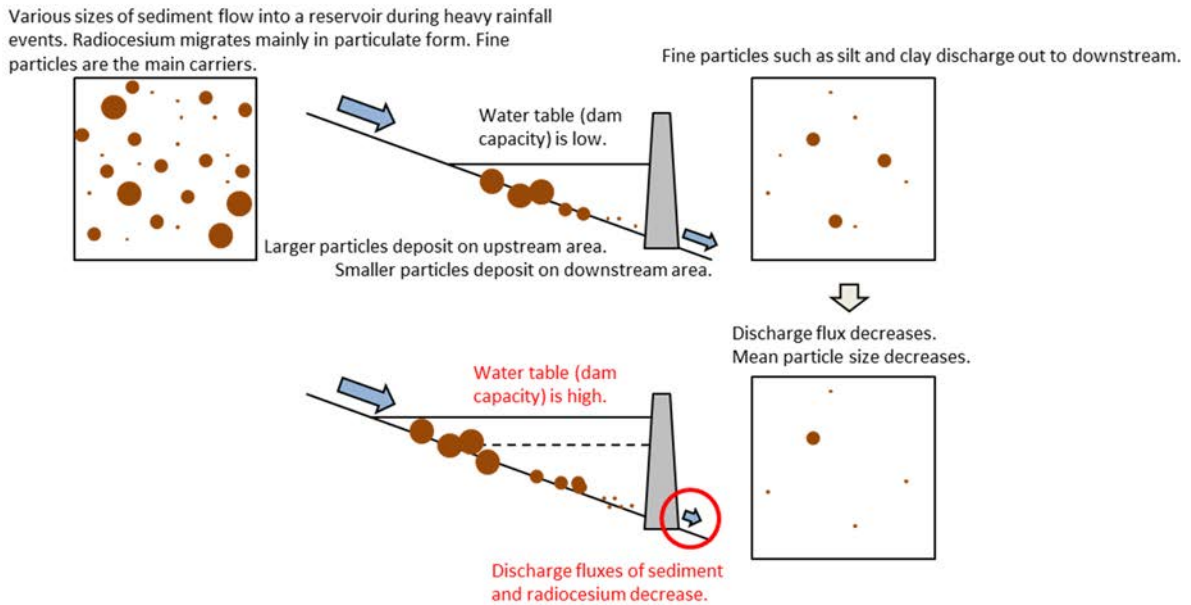


Fig. 5.4-8 Schematic image for the behavior of sediment and radioactive cesium flowing into dam lake at the time of heavy rain.

From the observation, it was confirmed that much sediment adsorbing radioactive cesium was deposited on flood plain located in the downstream of the rivers. Also, it was elucidated that the distribution of the deposited sediment is not homogeneous. In order to understand the mechanism of this phenomenon, the simulation was conducted using the large-scale parallel computer in JAEA by parallelizing the two-dimensional river simulation code Nays2D (Shimizu, 2003¹³⁵), Shimizu et al., 2012¹³⁶) developed by Professor Shimizu of Hokkaido University (Yamada, et. al., 2015)¹⁵⁴).

In order to investigate the mechanism of deposition on flood plain, the simulation was conducted in the region near the estuary of the Ukedo River shown in Fig. 5.4-9, by inputting the typical flow rates and amount of suspended sediment at the time of flood as a boundary condition. The deposition of sediment was evaluated at the cross section near the estuary shown in red ellipse in Fig. 5.4-9. As a result, it was confirmed by the simulation that when water covering the flood plain at the time of flooding drew at the time of water recession, the sediment was deposited on the flood plain (Fig. 5.4-10).

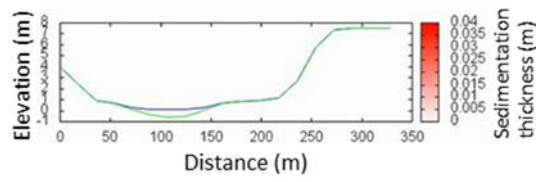
Concerning the heterogeneous distribution of sediment deposition, the deposition amount was calculated by the simulations using the data on flow rates measured in September 2015 at the time of typhoon. Also, the amount of cesium deposition was evaluated using the measured data on the concentration of radioactive cesium adsorbed on suspended sediment in the Ukedo River. The results are shown in Fig. 5.4-11. It can be confirmed that radioactive cesium tended to be deposited in the bent region of the river. For comparison, the distribution of air dose rate measured in 2013 by the unmanned helicopter is shown in Fig. 5.4-12 (Sanada et al., 2013)¹⁵⁵). From this result, we can confirm the tendency that the air dose rate was high in the region where the amount of cesium deposition was large. Therefore, it was considered that the present simulation is one of the excellent methods to evaluate the dynamics of radioactive cesium at the time of flood.



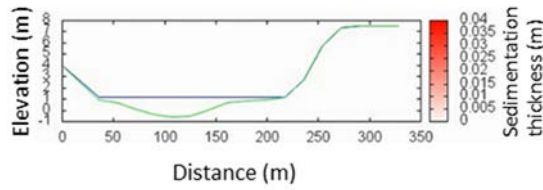
Fig. 5.4-9 Aerial photograph near the estuary of the Ukedo River investigated by the simulation.

Google earth, Image©2013 DigitalGlobe.

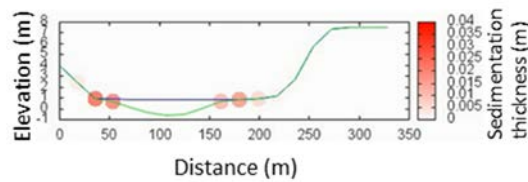
The evaluation of sediment deposition was conducted at the cross section shown in red ellipse.



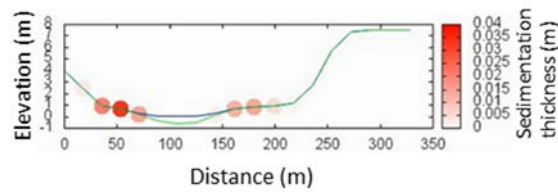
(a) before flood



(b) during flood



(c) at the time of water recession



(d) after the end of flood

Fig. 5.4-10 Deposition amount of sediment at the cross section of red ellipse shown in Fig. 5.4-9. The green lines show the topography, and blue lines display the water level. The red circles represent the deposited position and the shade of red color corresponds to the amount of deposition. It is seen that the deposition was not observed before and during the flood. When the water level decreased due to the water recession, sediment was deposited on the flood plain. After the end of the flood, we can confirm that the deposited sediment remained intact.

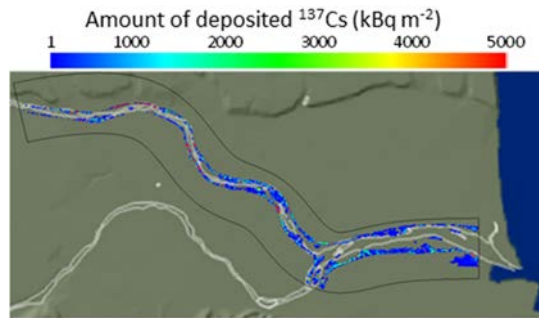


Fig. 5.4-11 The deposition amount of ^{137}Cs at the time of typhoon in September 2015, which was evaluated by the simulation.

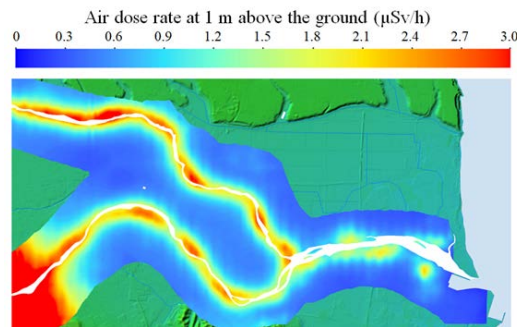


Fig. 5.4-12 Air dose rate measured in 2013 by unmanned helicopter.

Radioactive cesium in dissolved state and adsorbed on sediment, transported to estuary through a river, finally flows into the sea. In this regard, we evaluated the dynamics of radioactive cesium transported by a river at the coastal area by the simulation.

In the JAEA model using the rectangular coordinate system explained in the section 5.4.1, only fresh water is considered. However, it can be also applied to the simulation of the ocean by adding the functions specific to the ocean such as the difference in density between sea water and fresh water, effect of tide, and Coriolis force. In conducting the simulation of the ocean, appreciably wide region has to be analyzed. Hence, it is desirable that the mesh size is as large as possible from the viewpoint of the calculation amount. In contrast, in the region close to the coast where the topography drastically changes, it is necessary to reduce the mesh size in order to accurately represent the topography. However, all regions have to be divided by the same size mesh in the JAEA model. In such case, the calculation is generally conducted using the smallest size mesh considering the precision. Therefore, in the simulation of the ocean in wide region including the coastal area, the calculation is performed using small mesh according to the topographic changes at the coastal area. Namely, the small size mesh has to be also used for the flat ocean region far from the coast, which is unfavorable for the calculation amount. In order to solve this problem, JAEA developed a simulation code with nesting structure, in which the calculation area is firstly divided into multiple blocks considering the topography, then each block is calculated by the JAEA model by giving it an appropriate mesh size. The schematic of this procedure is shown in Fig. 5.4-13.

Using this code, the simulation was performed on the region including the Ukedo River and the 1F, shown in Fig. 5.4-14. The typical flow rate and amount of suspended sediment at the time of flood are virtually

given as boundary conditions. Concerning the meteorological data, we used the observation data on October 13, 2014 when the typhoon approached to the Japanese Islands. Fig. 5.4-15 shows the waterflow in the estuary of the Ukedo River and the Maeda River at the time of the flood. From this result, we can confirm that river water flowing into the sea spread out on the sea surface. We consider that this phenomenon was caused by the fact the density of river water is smaller than that of sea water due to its zero-salinity and higher temperature. On the other hand, the flow direction at the sea bottom was reverse, i.e., water flowed from the offshore to the estuary. From the simulation results, it was confirmed that sediment etc. once flowing out from river into the offshore returned to the estuary.

As the other results, it was also confirmed by the simulation shown in Fig. 5.4-16 and Fig. 5.4-17 that dissolved cesium flowing into the sea went south, and its concentration fairly decreased, but it again flowed into the 1F harbor through the sea bottom. Also, clay and silt flowed into the 1F harbor in the same way, and a part of them was deposited inside of the harbor. These results suggest that the effects of radioactive materials originating from rivers have to be considered in order to evaluate the dynamics of radioactive materials in the 1F harbor.

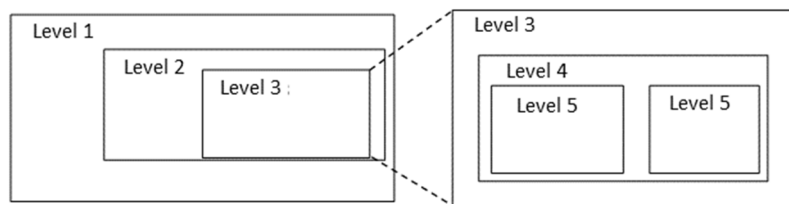


Fig. 5.4-13 Schematic diagram of five-level nest structure.

The regions have nest structure. The calculations for a large region and a small region are conducted using large size mesh and small size mesh, respectively. The calculated results are exchanged at the boundary of them.

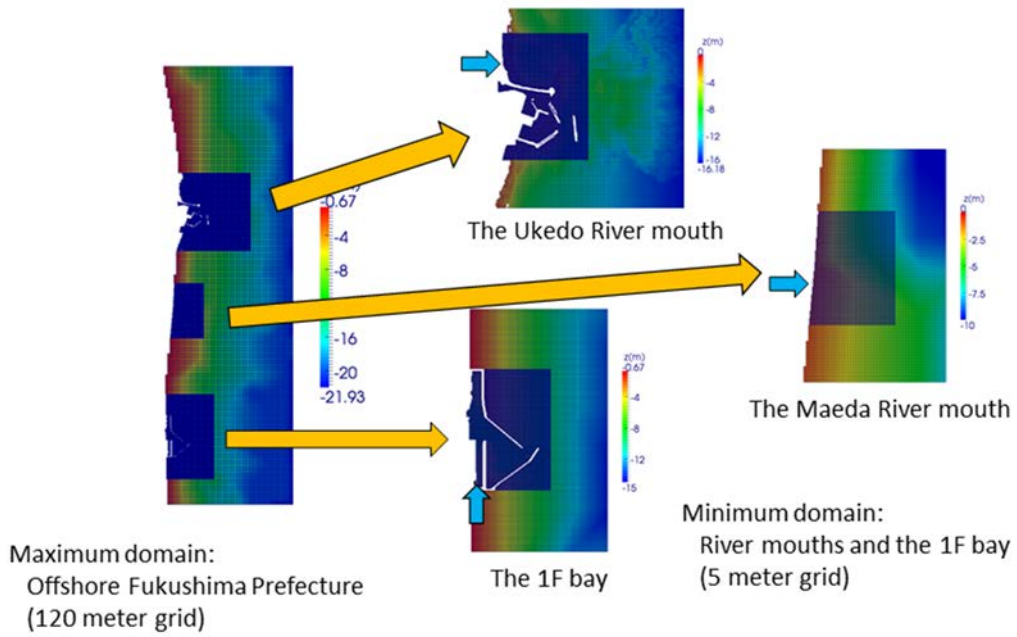


Fig. 5.4-14 Nest structure of the simulation region including the Ukedo River and the 1F.

For the estuaries of the Ukedo/the Maeda Rivers and around the 1F harbor, the calculation was conducted with a mesh size of 5 m. The largest area was calculated with a mesh size of 150 m.

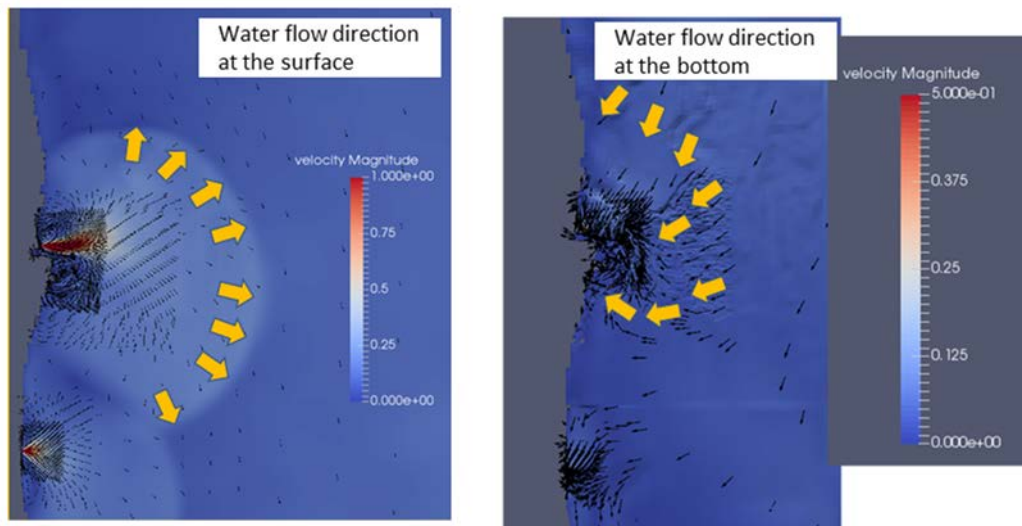


Fig. 5.4-15 Water flow around the estuary at the time of flood.

We can see that water flowing from river spreaded concentrically on the surface, while the reverse flow to the estuary was generated at the bottom.

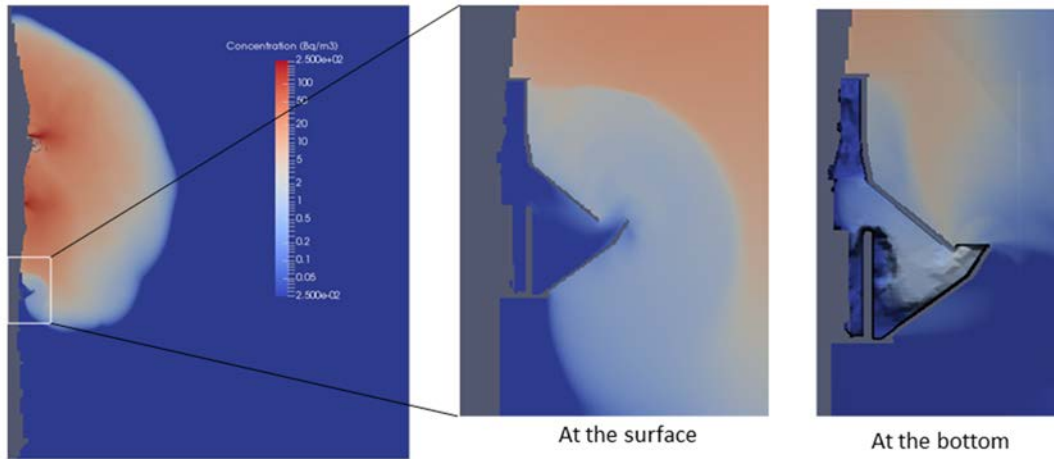


Fig. 5.4-16 Diffusion status of dissolved cesium originating from the river at the time of flood by typhoon.

It is confirmed that cesium flowed from the sea bottom at the entrance of the harbor. It should be noted that the presented data do not necessarily coincide with the real values, because the concentration and amount of dissolved cesium were virtually determined in the simulation.

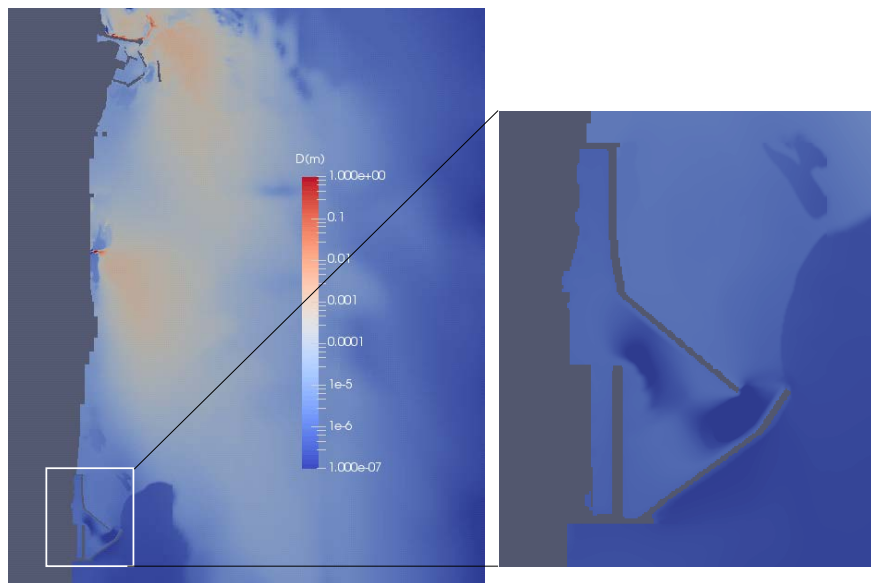


Fig. 5.4-17 Distribution of deposited sediment originating from the river at 30 hours after the end of flood by typhoon.

We can confirm that the sediment was deposited after migrating to the inside of the 1F harbor. It should be noted that the presented data do not necessarily coincide with the real values, because the concentration and amount of suspended sediment were virtually determined in the simulation.

5.4.4 Future subjects

From the analytical results presented so far, we could roughly understand the behavior of radioactive cesium in dam lakes. However, concerning the thermocline in dam lakes, the effect of flocculation of suspended sediment, the generation of dissolved states at the lake bottom, etc., it is still difficult to analytically reproduce the data. Hence, a part of the calculated results does not coincide with the measured values. Since these factors would appreciably affect the outflow of radioactive cesium to the downstream, the improvement of the accuracy in the analysis is a future subject.

From the simulation results presented so far, we could understand the mechanism that sediment adsorbing radioactive cesium was deposited on flood plain and the tendency of the deposited places. However, it should be noted that these calculations were conducted with a mesh size of several meters. Thus, the shape of the wide river channel near the estuary can be correctly reproduced, but there is a possibility that the shape of the narrow river channel far from the estuary cannot be properly reproduced. Therefore, there may remain a problem in the accuracy of the simulation for such narrow river channels. For these reasons, it is needed to develop a simulation method using appropriate mesh whose shape and size fit the topography. However, the problem is that the efficient parallel calculation becomes difficult with the increase in the calculation amount. These problems are future subjects to be solved.

We succeeded in evaluating the behavior of sediment flowing from rivers into the ocean using the developed simulation code. However, the calculation of simulation takes a lot of time at present, because the sufficient parallelization and speeding up of the calculation have not yet been accomplished. Under these circumstances, it is necessary to further parallelize and speed up the computer calculation in order to efficiently perform systematic simulation.

5.5 Depth migration model

5.5.1 Objectives

The objective of the analytical research using the depth migration model is to predict the medium-to-long term changes in the depth distribution of radioactive cesium in soil and air dose rate.

5.5.2 Methods

It is known by the investigation on atmospheric nuclear tests and the fallout by the Chernobyl nuclear accident that radioactive cesium tends to be easily adsorbed on soil, but it migrates slowly to the deep region in the order of several years to decades. The property of migration and sorption/desorption of radioactive cesium in soil not only contributes to the reduction of air dose rate, which is faster than that estimated by the physical decay, but also affects the cesium migration to plants and migration on land such as erosion and sedimentation (He and Walling, 1997)¹⁵⁶⁾. Therefore, it is much important to clarify the physicochemical phenomena related to the migration of radioactive cesium in the depth direction.

The real depth distribution of radioactive cesium exhibits exponential curve at the early stage of the fallout. After that, radioactive cesium slowly migrates to the deep region while maintaining the exponential distribution or the tail of the distribution curve extends to the deep region (for example, see Antonopoulos-

Domis et al., 1995¹⁵⁷); Matsuda et al., 2015¹⁵⁸); Takahashi et al., 2015¹⁵⁹). However, the advection/diffusion model based on the instantaneous equilibrium of sorption/desorption shows that the depth distribution exhibits a normal distribution curve, which cannot represent the real tendency of the depth distribution. As another method, there is the DSF model (Toso and Velasco, 2001)¹⁶⁰ which reproduces the exponential distribution by considering the irreversible sorption. However, even the DSF model cannot explain the slow migration of radioactive cesium after the initial deposition. Accordingly, we considered that the disagreement between the simulation and the real distribution is ascribed to the reversible or irreversible sorption/desorption kinetics, based on the observation results for cesium adsorbed on clay minerals, desorption experiments of soil, and field inspection of cesium migration. Considering these situations, we have developed a new physicochemical model, mDSF (Fig. 5.5-1, Kurikami et al., 2017¹⁴⁰). In the existing DSF model, the kinetics is introduced only to the irreversible sorption, while the instantaneous equilibrium is supposed for the reversible sorption and desorption. On the other hand, the important improvement points in the present mDSF model are; the kinetics is introduced also to the reversible sorption/desorption, and the different reaction rates can be given especially to the sorption and desorption.

The mass conservation equation of the concentration of radioactive cesium in water C_w (Bq m⁻³) in the mDSF model is expressed as,

$$\varepsilon S_r \frac{\partial C_w}{\partial t} = -v \frac{\partial C_w}{\partial z} + D_e \frac{\partial^2 C_w}{\partial z^2} - \rho_d k_r (K_r C_w - C_{sr}) - \rho_d k_i (K_i C_w - C_{si}) - \lambda \varepsilon S_r C_w \quad (5.5-1)$$

where ε is the porosity (dimensionless), S_r is the saturation degree (dimensionless), t is the time (s), v is the Darcy velocity (m s⁻¹), z is the depth coordinate (m), D_e is the effective dispersion coefficient (m² s⁻¹), ρ_d is the dry density of soil (kg m⁻³), K_r and K_i are the sorption distribution coefficients (m³ kg⁻¹) for reversible and irreversible components, respectively, k_r and k_i are the sorption rate constants (s⁻¹) for reversible and irreversible components, respectively, C_{sr} and C_{si} are the concentrations of radioactive cesium in soil (Bq kg⁻¹) for reversible and irreversible components, respectively, and λ is the decay constant (s⁻¹).

For reversible and irreversible sorption/desorption, the following kinetics is considered,

$$\frac{\partial C_{sr}}{\partial t} = k_r (K_r C_w - C_{sr}) - \lambda C_{sr} \quad (5.5-2)$$

$$k_r = \begin{cases} k_{rs} & \text{if } K_r C_w \geq C_{sr} \\ k_{rd} & \text{if } K_r C_w < C_{sr} \end{cases}$$

$$\frac{\partial C_{si}}{\partial t} = k_i (K_i C_w - C_{si}) - \lambda C_{si} \tag{5.5-3}$$

$$k_i = \begin{cases} k_{is} & \text{if } K_i C_w \geq C_{si} \\ 0 & \text{if } K_i C_w < C_{si} \end{cases}$$

where k_{rs} and k_{rd} are the sorption and desorption rate constants, respectively, for reversible component, and k_{is} is the sorption rate constant for irreversible component.

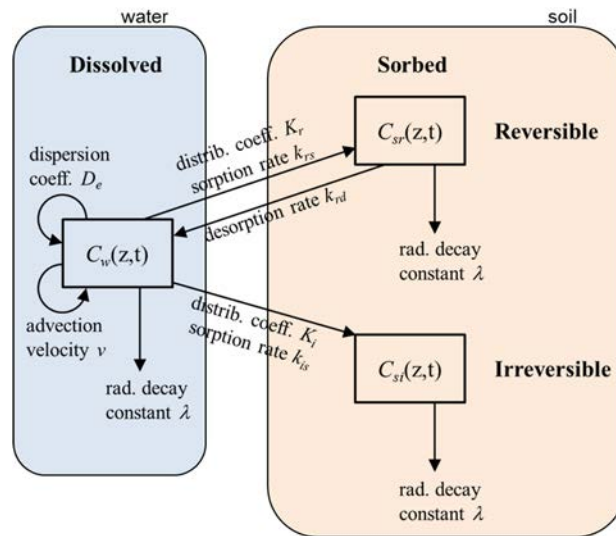


Fig. 5.5-1 Conceptual image of the developed model.

5.5.3 Results and discussion

The depth distribution of radioactive cesium was calculated by the mDSF model using general parameters. The results were compared with the observed data, which is shown in Fig. 5.5-2. In the figure, results calculated by the existing models (simple diffusion model supposing the instantaneous equilibrium, and the DSF model where the kinetics is supposed only for irreversible sorption) are also presented. It is seen that the existing model cannot explain the exponential depth distribution, the tailing at the deep region, or slow migration, while the present model well reproduces the measured distribution.

Further, we investigated the effects of reversible and irreversible sorption/desorption and changes in their rates on the depth distribution of radioactive cesium by changing the parameters in the present model (Fig. 5.5-3). As a result, it was found that the exponential distribution shows up only by considering the kinetics of sorption. This means that the exponential depth distribution at the early stage after the fallout was affected by kinetics of sorption, and the distribution curve was formed in the short time after the fallout. It was also elucidated that the slope of the exponential distribution (or buffer depth) was correlated to the ratio of the sorption rate to the diffusion coefficient. Further, it was presumed that the reason that the tail of the distribution curve extended to the deep region (exhibiting two-step exponential distribution) is that the

desorption slowly proceeded with time in the shallow region, and the sorption slowly continued in the deeper region, due to the small desorption rate compared with the sorption rate. For that reason, the apparent sorption distribution coefficient was suggested to become large in the shallow region. The migration of radioactive cesium to the deep region was supposed to become slow with the progress in the sorption of cesium on irreversible sites, and thereafter the depth profile no longer changed.

Recently, not only the exponential distribution but also unique distribution where the concentration maximum was near the surface region have been often found. We investigated whether such unique depth distribution can be reproduced or not using the present model (Fig. 5.5-4). As a result, it was found that the calculated results deviate from the observed values by considering only the effect of advection, e.g., the peak of cesium concentration moves in proportion to the time duration. On the other hand, the analysis considering the depth dependence of soil properties near the surface well represented the measured phenomena, that is, the depth distribution of radioactive cesium did not change so much although the peak slightly moved. From these trial analyses, it was revealed that unique distribution with the peak maximum near the surface possibly resulted from the depth profile of soil properties such as the depth distribution of sorption property depending on the organic material content.

Fig. 5.5-5 shows the conceptual diagram of the relation between the mechanism of radioactive-cesium migration in the depth direction estimated by the analysis and its depth profile.

5.5.4 Future subjects

We were able to present the physicochemical interpretation to understand the observed depth profile of radioactive cesium by the present model. On the other hand, it should be noted that the migration of radioactive cesium would be affected not only by the physicochemical process considered in the present model but also by the other processes such as biological disturbance, erosion, sedimentation, freezing/melting of soil, and colloid migration (for example, Miyahara et al., 2015¹⁶¹); Konoplev et al., 2016⁹⁴). Therefore, more detailed experiments and observation are indispensable.

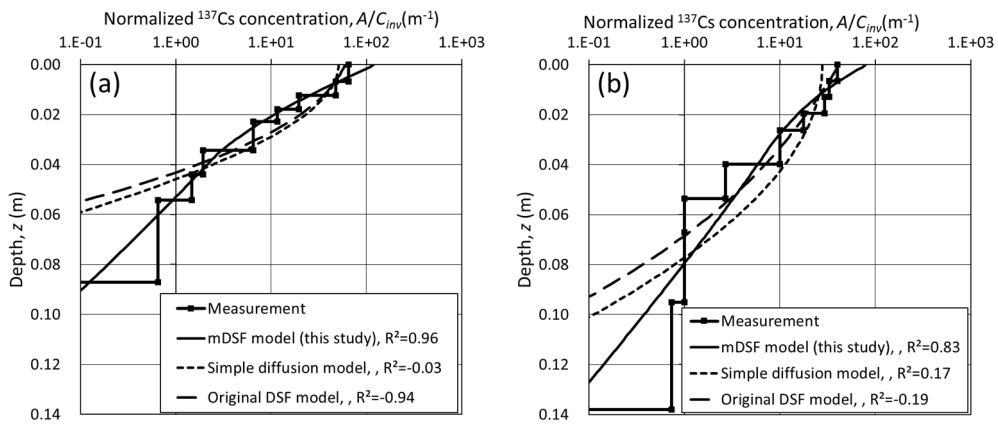


Fig. 5.5-2 Comparison of the results calculated by the present model with the measured values.
 (a) December 2011, and (b) November 2013 (cited from Kurikami et al.(2017)¹⁴⁰ with modification).

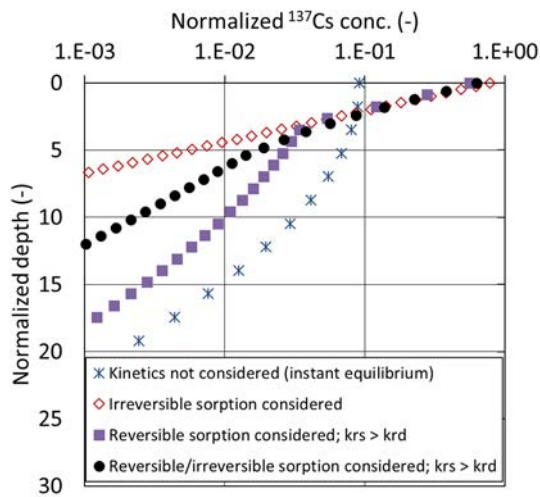


Fig. 5.5-3 Influence of the difference in sorption/desorption parameters on the depth profile of radioactive cesium (cited from Kurikami et al. (2017)¹⁴⁰ with modification).

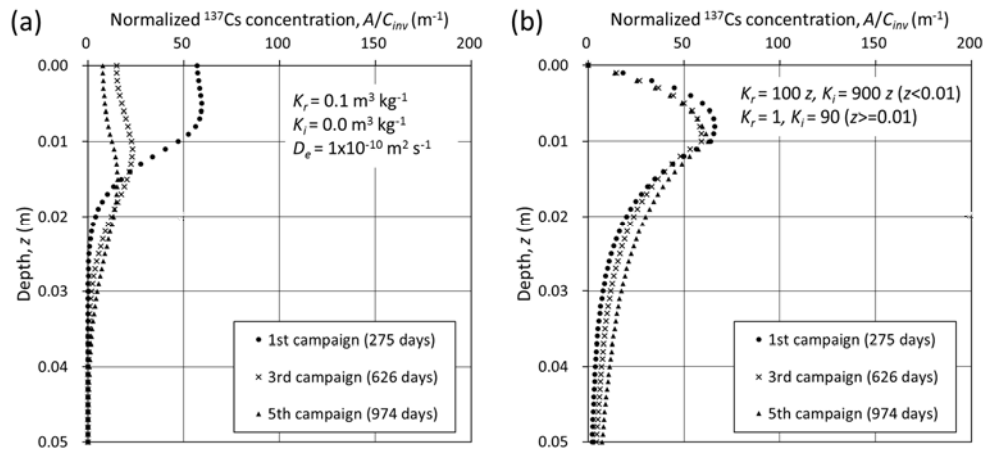


Fig. 5.5-4 Results of the trial analysis reproducing the depth distribution of radioactive cesium with a maximum near the surface region.

(a) Analysis supposing the advection effect, and (b) analysis considering the depth profile of soil property (cited from Kurikami et al. (2017)¹⁴⁰) with modification).

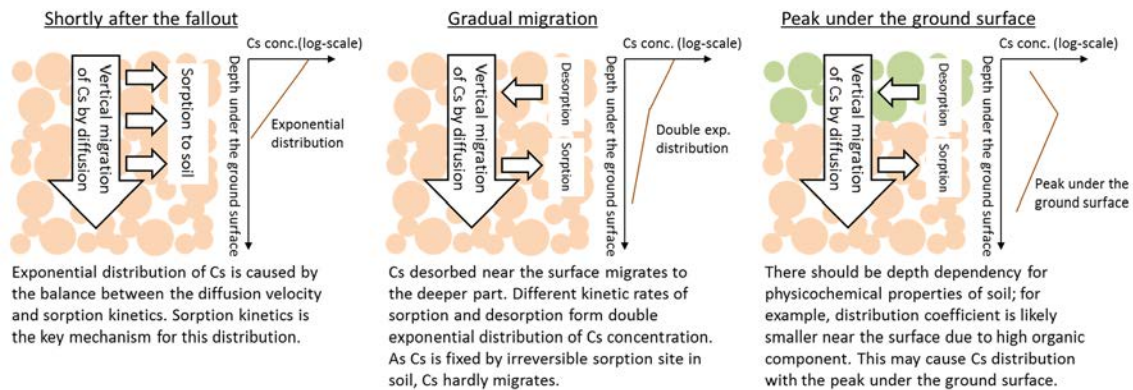


Fig. 5.5-5 Conceptual diagram of the relation between the mechanism of radioactive-cesium migration in the depth direction estimated by the analysis and its depth profile.

5.6 Dose rate evaluation model

5.6.1 Objectives

The objective of the analytical research using the dose rate evaluation model is to predict air dose rate accompanied by the dynamics of radioactive cesium.

5.6.2 Methods

We have developed a tool ADRET that quickly and easily calculates air dose rate on a simple geometry like flat land in order to evaluate various depth distribution and spatial distribution of radioactive cesium and their changes before and after the decontamination (Malins et al., 2016)¹⁴². In this tool, a soil block was

divided horizontally and vertically into grids as shown in Fig. 5.6-1, and then the air dose rate is calculated by giving arbitrary cesium concentration to each grid. The air dose rate in the center of the soil block is calculated by the following equation,

$$\dot{H}^*(10) = \sum_{n,i,j,k} A_{v,n,i,j,k} c_{n,i,j,k} \quad (5.6-1)$$

where $\dot{H}^*(10)$ is the air dose rate, $A_{v,nijk}$ is the concentration of a nuclide n in the ijk -cell (Bq m^{-3}), and c_{nijk} is the dose conversion coefficient ($\mu\text{Sv h}^{-1}$ per Bq m^{-3}). The dose conversion coefficients were obtained in advance by the PHITS. Once the dose conversion coefficients are obtained, the calculation can be finished in less than a few seconds by a normal desktop PC without using large computer.

In flat lands such as open space and farms, the air dose rates are determined by the inhomogeneous distribution of radioactive cesium in the depth direction and horizontal direction. On the other hand, the influence of topography cannot be ignored in mountain region. Fig. 5.6-2 shows the results of dose rates analyzed by the PHITS for simple valley and mountain (Malins et al., 2015)¹⁶². When the concentration of radioactive cesium in soil was the same, air dose rates in mountain were lower and those in valley were higher than those in flat land. It is seen that these tendencies became predominant with the height. In forests, air dose rate is influenced not only by the topography but also by the distribution of adsorption on trees, the distribution of radioactive cesium in litter and soil layer, the shielding effect of trees, etc. In a city area, on the other hand, the distribution of radioactive cesium and the dose rate was inhomogeneous because a city is composed of a mixture of various structures such as large and small buildings, roads and parking lots with asphalt pavement, gardens, and farms.

In order to precisely evaluate the dose rates in forests and city areas, we are developing a tool 3D-ADRES to analyze air dose-rate distribution taking the abovementioned complicated topography and structures on land into consideration. Fig. 5.6-3 shows the conceptual diagram of the modelling method. For topography, the Digital Elevation Model (DEM) was used. Concerning the structures on land, the input files for the PHITS were made by distinguishing buildings and trees using aerial photography. We supposed typical buildings and trees as geometrical models. Using this tool, the analyses were conducted for the forests in Ogi District, Kawauchi Village (Sakuma et al., 2018)¹⁶³, and the city area in Okuma Town and Tomioka Town (Kim et al., 2018)¹⁴³ (Fig. 5.6-4).

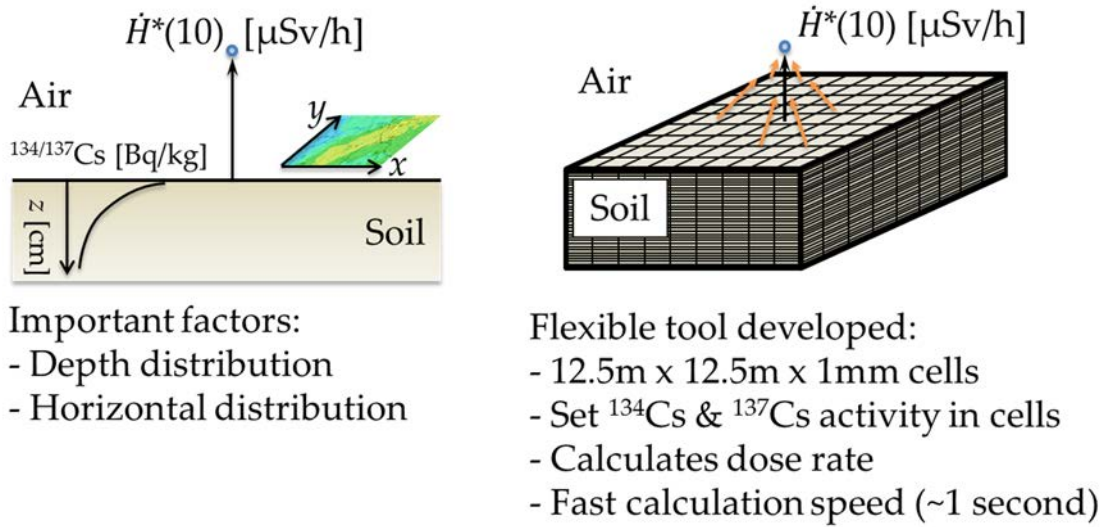


Fig. 5.6-1 Schematic image of the dose evaluation model, ADRET.

Simple Valley and Mountain Model

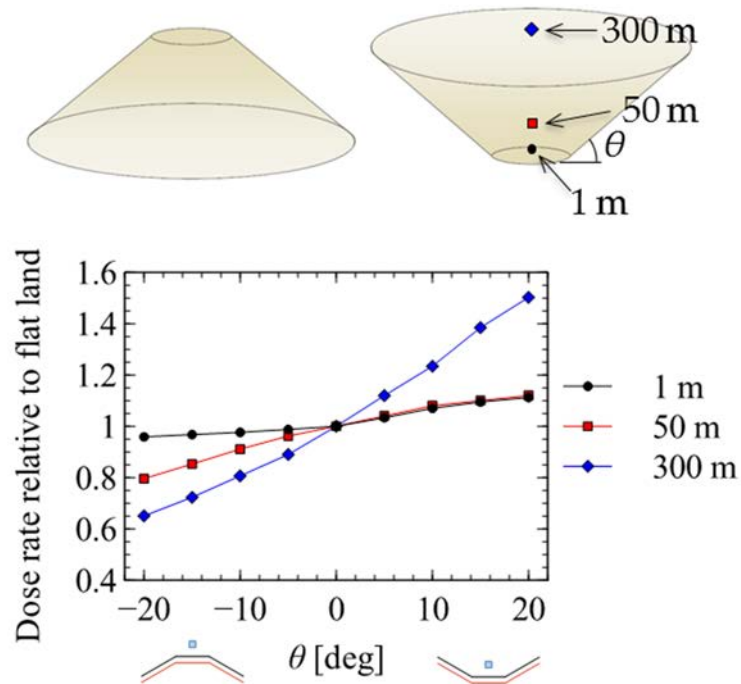


Fig. 5.6-2 Analytical result of radiation dose rate in simple mountain and valley topography (Malins et al., 2015)¹⁶².

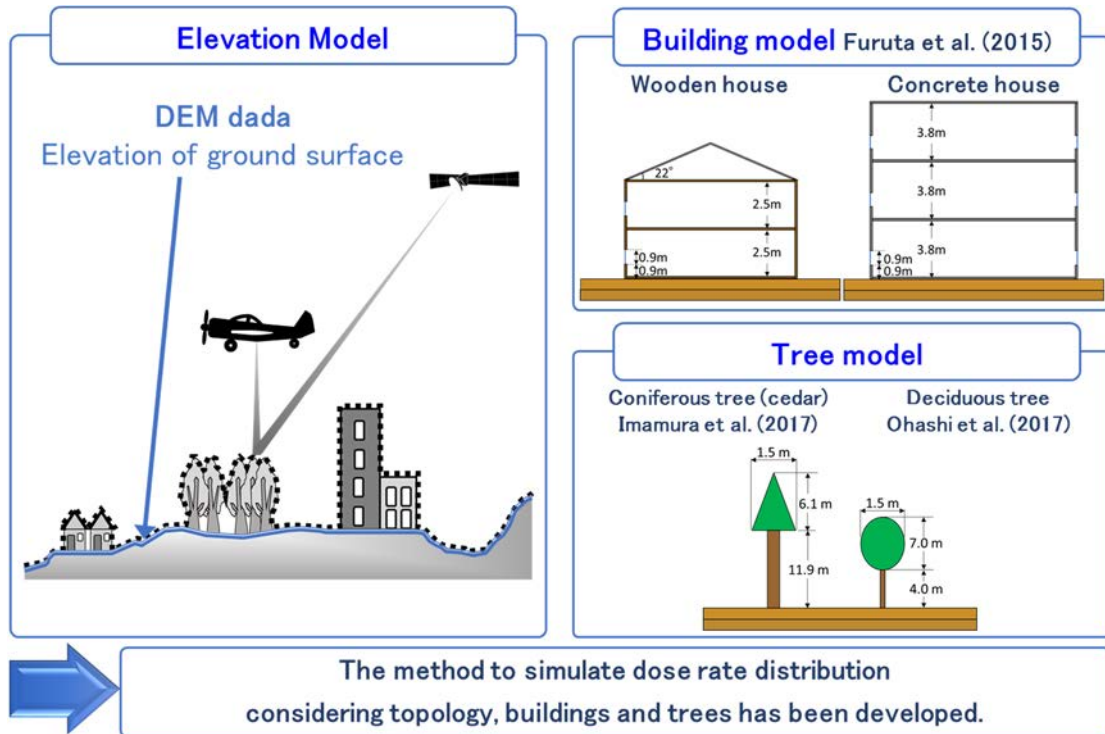


Fig. 5.6-3 Conceptual drawing of geometry-making tool for the PHITS calculation, 3D-ADRES, to evaluate radiation dose rate considering topography and structures on land^{164,165,166}.

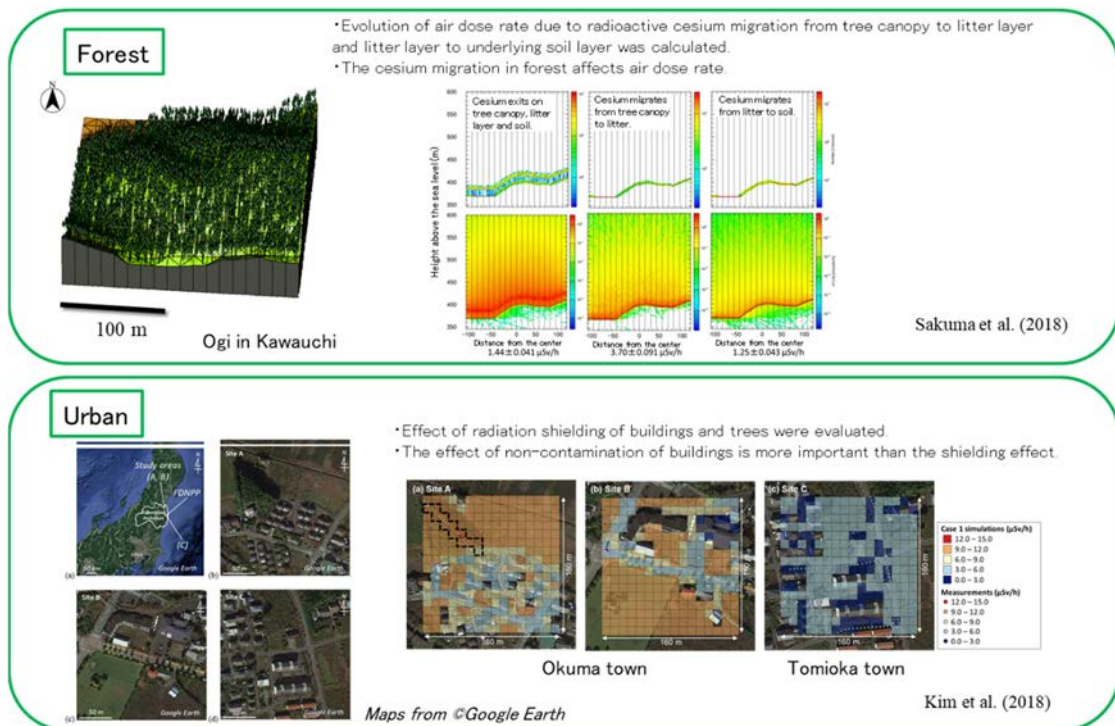


Fig. 5.6-4 Examples of the analysis for the forest in Ogi District, Kawauchi Village (Sakuma et al., 2018)¹⁶³ and city areas of Okuma Town and Tomioka Town (Kim et al., 2018)¹⁴³.

5.6.3 Results and discussion

For flat lands such as open spaces and fields, the air dose rates are determined by the depth profile of radioactive cesium in soil and its horizontal distribution. As a basic analysis, we first conducted the analysis to clarify how far distance the dose rate was influenced under the situation that radioactive cesium was exponentially distributed in flat lands using the PHITS (Fig. 5.6-5). Although the effective distance was a little different depending on the buffer depth, it was understood that about 90% of radiation affecting the air dose rate at 1 meter height originated from radioactive cesium within a radius of 100 meters.

JAEA has been measuring the depth profiles of radioactive cesium and air dose rates at about 80 places in flat area without buildings or trees since December 2011 (Matsuda et al., 2015)¹⁵⁸). Comparing the measured data with the analytical results, it was confirmed that these two values well coincide (Fig. 5.6-6). Further, JAEA has conducted the Decontamination Model Demonstration Project (JAEA, 2012)¹²⁰), and the related analysis was conducted for Otozawa District, Okuma Town where the inhomogeneous horizontal distribution of radioactive cesium was observed in the follow-up investigation of the Project. As a result, it was found that the spatial inhomogeneity of the cesium distribution influenced the variation of air dose rate.

We have also analyzed the effects of the standard decommissioning methods in fields such as topsoil stripping, inversion tillage, and deep plowing, on the reduction of air dose rate. Compared with the results obtained in the Decontamination Model Demonstration Project, it was verified that these methods are effective for reducing the air dose rate. Moreover, we clarified the relation among the depth profile of radioactive cesium, the depth of the decontamination, and the effect of the decontamination (for example, Fig. 5.6-7). Based on these results, we presented the possibility that the decontamination effects lowered with the migration of radioactive cesium to deeper region (Malins, et al. 2016)¹⁶⁷).

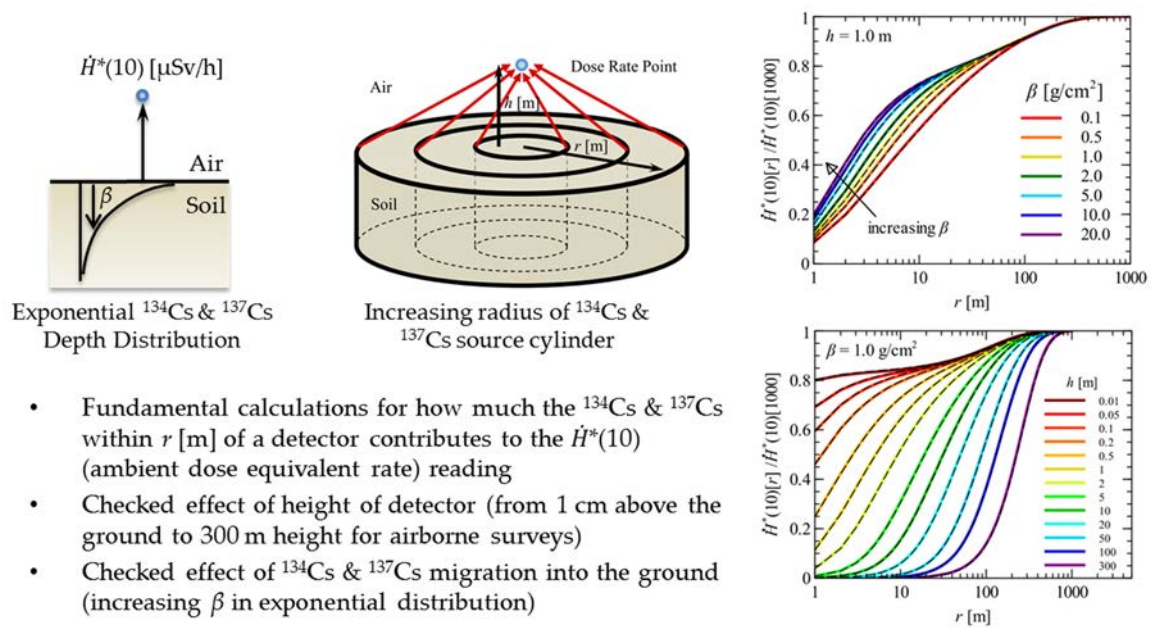


Fig. 5.6-5 Region affected by radiation on flat land.

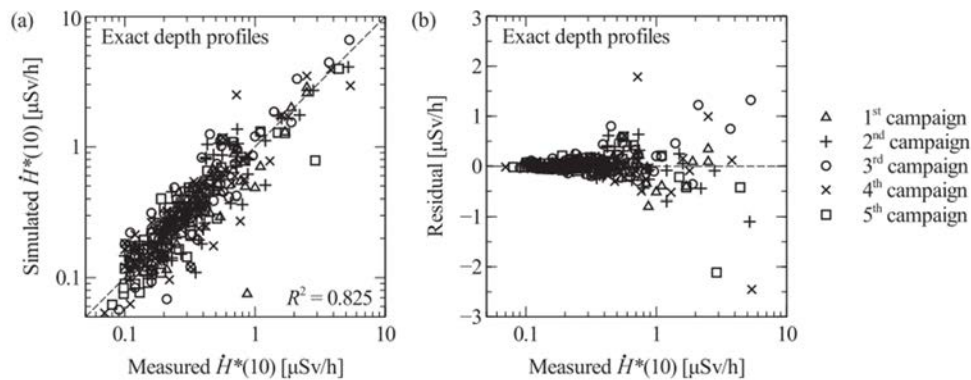


Fig. 5.6-6 Comparison of the analytical results with the measured values (Malins et al. (2016)¹⁴⁸ with modification).

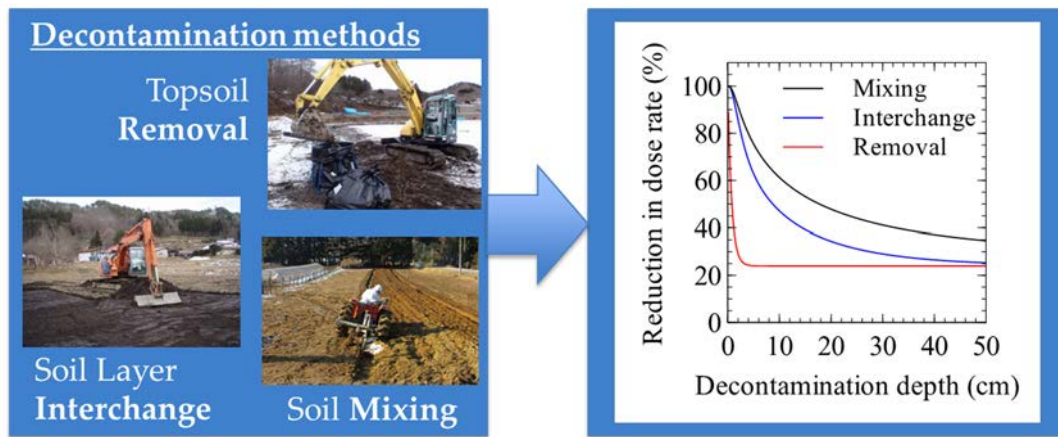


Fig. 5.6-7 Analysis of decontamination effects (cited from Malins et al. (2016)¹⁶⁷ with modification).

For forests, the changes in dose rate by the migration of radioactive cesium from tree crown to forest floor, and from litter to soil layer were analyzed. When radioactive cesium migrated from tree crown to forest floor, the air dose rate at 1 meter height increased because the measured position came near to the radiation source. Also, when radioactive cesium moved from litter to soil layer, the air dose rate decreased due to the shielding effect of the litter and soil layer. The decreasing rate of the measured air dose rate almost coincided with that estimated by the physical decay. It was supposed that this coincidence is due to the offset between the increase by the migration from tree crown to forest bed and the decrease by the migration from litter to soil layer (Sakuma et al., 2018)¹⁶³.

As to the analysis in city area, we investigated the shielding effects of buildings/trees and the effects of non-contaminated region under the buildings on dose rate. These analyses were conducted for the flat area where buildings and trees were virtually eliminated, and for buildings where the radioactive cesium was virtually put under the building at the same amount as the surrounding region. As a result, it was clarified that radiation dose rates in city area with buildings and trees were lower than those without them due to the

shielding effect. It was also found that the radiation dose rates in city area became low because the regions under buildings were not contaminated (Kim et al., 2018)¹⁴³⁾.

5.6.4 Future subjects

The main future subject is to refine the spatial radiation distribution through the verification of radiation dose distribution in forests and city areas.

5.7 Compartment model for river system dynamics considering the migration to agricultural, forest and fishery products

5.7.1 Objectives

The objective of analytical research using the compartment model for river system dynamics considering the migration to agricultural, forest and fishery products is to evaluate the effects of cesium dynamics in environment on radioactive cesium in agricultural, forest and fishery products.

5.7.2 Methods

As described in the section 5.1, the phenomenological modelling approach is the basic idea in this project. We mainly adopt a method for modelling based on the physicochemical mechanism in each region. On the other hand, it is also important to clarify the relation between environmental dynamics and radioactive cesium concentration in agricultural, forest and fishery products, while considering the outline of the behavior of radioactive cesium in forests/lands and the mass-balance/flux of radioactive cesium in the process of migration from forests/lands to the sea through rivers and dam lakes. Therefore, in order to evaluate the effect of environmental dynamics of radioactive cesium at the river-basin scale on the concentration of radioactive cesium in products, we have developed a simple compartment model CMFW considering total river systems (Kurikami et al., 2017)¹⁴³⁾.

Fig. 5.7-1 shows the migration routes considered in the model. The model is divided into the forest region and the surface-water system region. These two regions can be arbitrarily combined. The forest region consists of the compartments of leaves, branches, bark, sapwood, heartwood, litter layer and soil layer. The surface-water region is composed of the compartments of rivers, river beds, flood plain, lakes, sediment on lake bottom, farm lands, city area, inshore, sediment on sea bottom, and the ocean. Fig. 5.7-2 presents the example for the connections among the compartments for the Ukedo River basin.

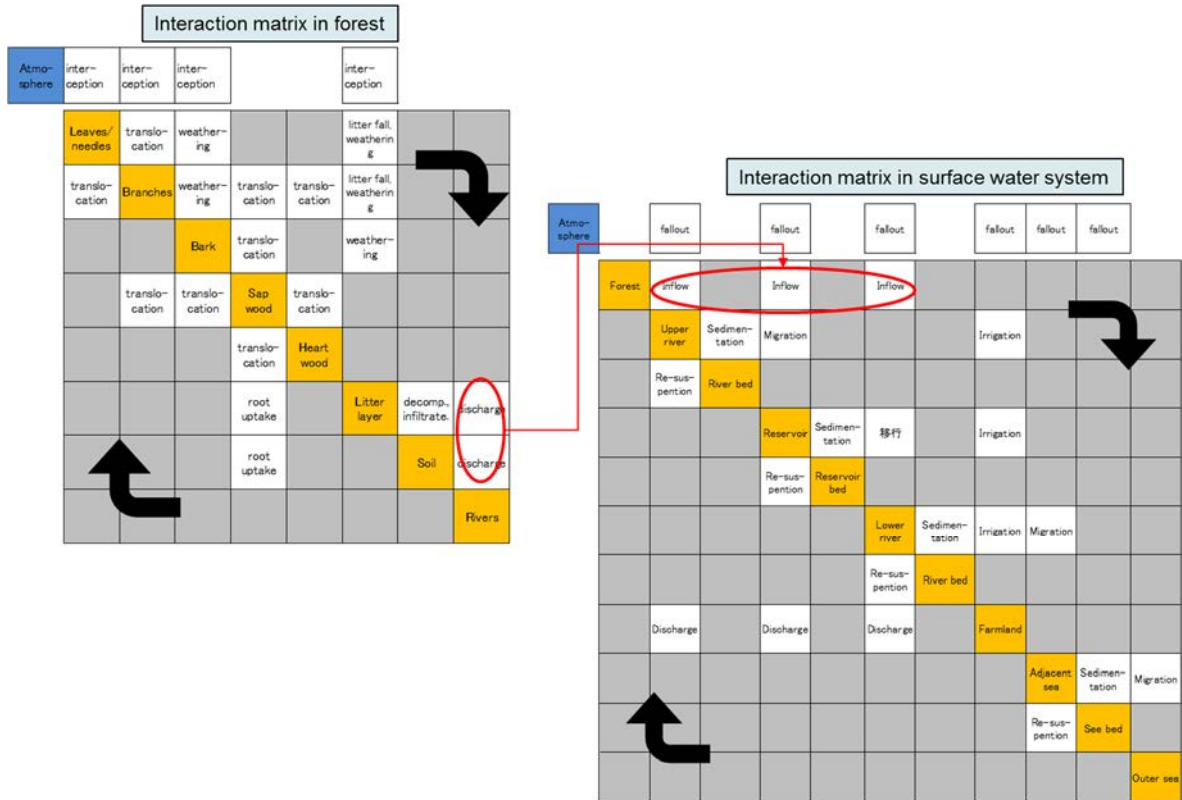


Fig. 5.7-1 Migration route considered in the CMFW (among the dynamic compartments).

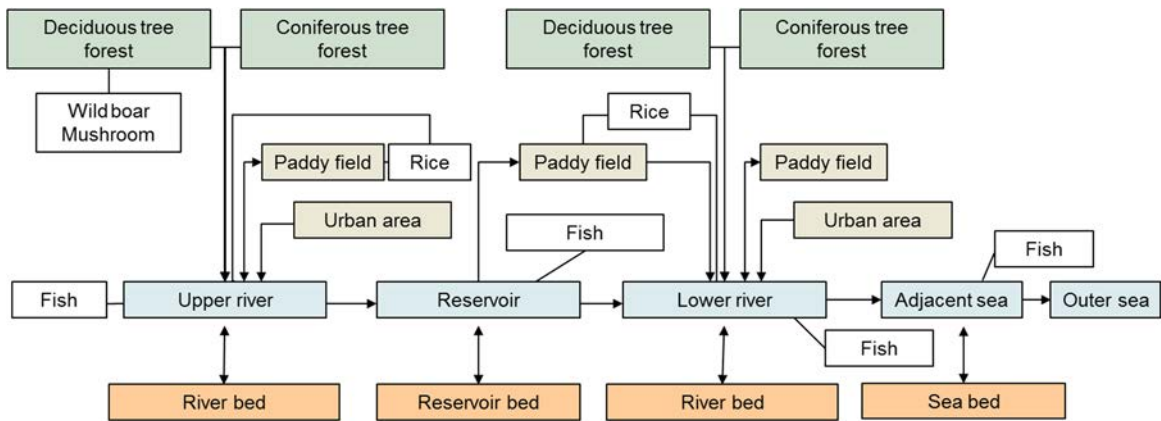


Fig. 5.7-2 Connection among the compartments for the Ukedo River basin.

5.7.3 Results and discussion

For forest, the interception ratios of initial deposition and transfer rates between the compartments were obtained by the inverse analysis. The migration coefficients in the analysis were set so that the coefficients coincide with the measured data on the temporal changes in the radioactive cesium concentration in respective parts of cedar trees in Kawauchi Village and oak trees in Otama Village among the data measured by the Forestry Agency (Forestry Agency, 2015)¹⁶⁸. In the analysis, the migration rate from litter to soil layer

was divided into two components, because the reproducibility of temporal changes was not good if the migration rate was supposed to be composed of one component. As a result, the temporal changes in cesium concentration in respective parts of forests were well fitted with the measured values (Fig. 5.7-3). The blocking rates at the time of fallout were calculated by the rate of the initial deposition amount obtained by the fitting. The results and the tendency of the migration from tree crown to litter layer were in good agreement with the values measured by Kato et al. (2017)¹⁶⁹.

Next, we conducted the trial analysis for the Ukedo River basin, shown in Fig. 5.7-2. The initial value for each compartment was calculated according to the area measured by the aerial monitoring, and the migration rate among the components were set by the reference values. Fig. 5.7-4 shows the stock-flow of radioactive cesium five years after the fallout obtained by the analysis for the Ukedo River basin. It was confirmed that the results for the outflow rate from Ogaki dam and outflow amount to the sea almost coincided with the measured values. Also, it was obtained that the radioactive cesium concentration in river water and sea water was on the order in agreement with the measured values.

In addition, we analytically investigated the effects of each route for direct flow of fallen leaves into river, side flow from litter layer to river, and elution from soil layer to river on the concentration of radioactive cesium in freshwater fish for the upstream region of the Ohta River. Fig. 5.7-5 shows the analytical results of radioactive cesium concentration in freshwater fish for the analysis cases with different cesium inflow route. The measured values were obtained for sweet fish (“Ayu” in Japanese) in the Niida River adjacent to the Ohta River (Japan Fisheries Research and Education Agency, 2017)¹⁷⁰. From these results, it was suggested that both the direct flow of fallen leaves to the river and the flow from litter layer to the river affected the concentration of radioactive cesium in freshwater fish (Kurikami and Sakuma, 2018)¹⁷¹. The specification of such cesium source and migration route is expected to contribute to the prediction of future radiation dose and its countermeasures.

5.7.4 Future subjects

The future subject is to elucidate the source of radioactive cesium incorporated into agricultural, forest and fishery product and the contamination route, and establish the countermeasures to the contamination in products.

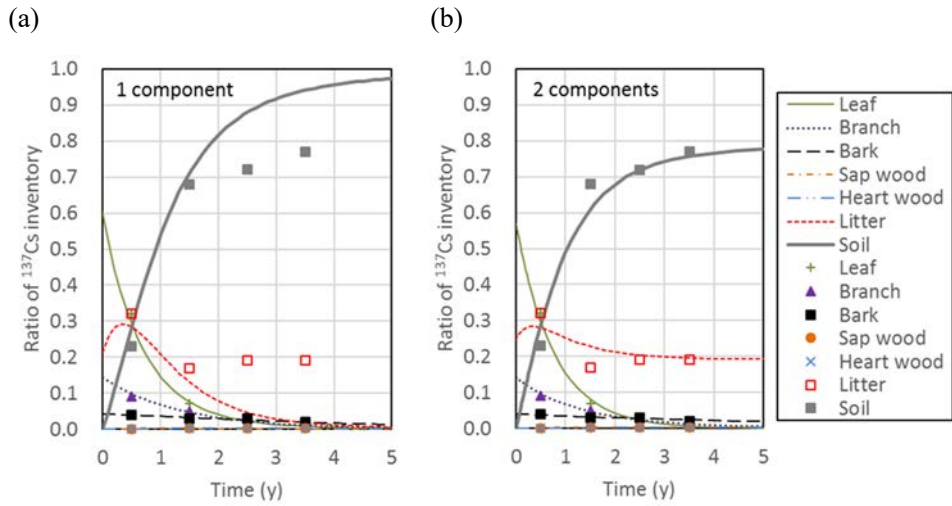


Fig. 5.7-3 Fitting situation of compartments in forest.

(a) The case where only one component was considered, and (b) the case where two components were considered.

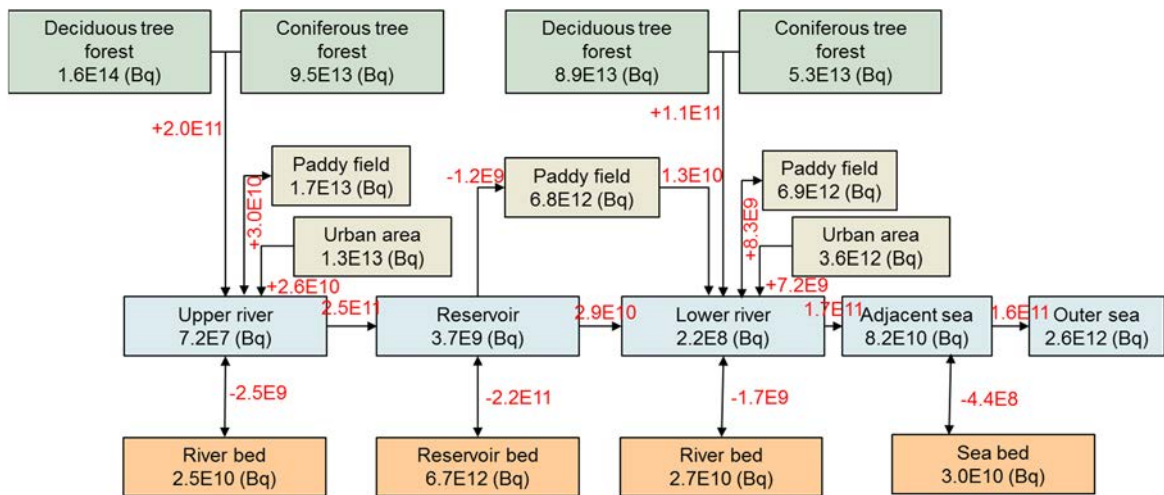


Fig. 5.7-4 Stock-flow of radioactive cesium five years after the fallout for the Ukedo River basin.

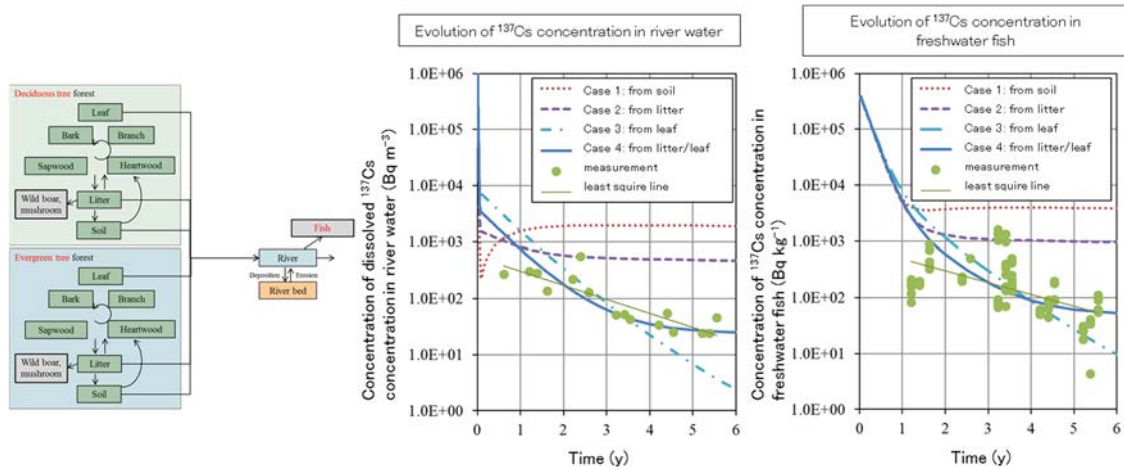


Fig. 5.7-5 Effect of each migration route from forests to rivers on the concentration of radioactive cesium in freshwater fish.

5.8 Example of model integration

5.8.1 Objectives

The models shown in the previous sections have been developed independently. However, it would become possible to complement the models by using them flexibly in combination depending on the purpose. The objective of the work presented in this section is to systematically evaluate the changes in radiation dose rate with the migration of radioactive cesium in the Ukedo River by the combination of the terrestrial and river-system dynamics models. Some of the examples of the model integration will be shown.

5.8.2 Systematic evaluation for the Ukedo River by the combination of the terrestrial and river-system dynamics models

The terrestrial dynamics model analyzes the dynamics of radioactive cesium at river-basin scale. The analyzed area by the terrestrial dynamics model includes the river system such as rivers and dam lakes. However, it simply deals with the dynamics in river system, so it is not suitable for the evaluation in localized regions such as sedimentation on flood plain. On the other hand, in the analysis by the river system dynamics model, sediment and radioactive cesium flowing out from land are indispensable as a boundary condition. This means that two dynamics models are complementary.

As an example for the systematic evaluation of river basin area by the combination of the terrestrial and river-system dynamics models, the outline of the analytical results for the dynamics of radioactive cesium in the Ukedo River basin will be presented in the followings. As shown in the section 5.2, the analysis using SACT has been conducted for wide area including the Ukedo River basin. In this analysis, the outflow flux of radioactive cesium from land to rivers was extracted, and then the values were given to the river system dynamics model TODAM as a boundary condition (Fig. 5.8-1, Onishi et al., 2014¹⁷⁴). Namely, the SACT was used for the analysis in land, while the TODAM was used for the analysis of rivers in river system. From the present analysis results (Fig. 5.8-2), the amount of sediment deposition and the accompanying accumulation of radioactive cesium were estimated for the Ukedo River at the confluence point with the

Takase River (2 km from the estuary) and Ogaki dam (22-27 km from the estuary). In the analysis using only SACT, the deposition in the Ogaki dam lake was partly confirmed, but the deposition with more detailed resolution could not be estimated. Therefore, it was demonstrated that the combination of the terrestrial and river-system dynamics model is important to evaluate the deposition in river beds and flood plain. The more detailed multi-dimensional analysis evaluation was conducted for the Ogaki dam and the confluence point with The Takase River where the possibility of deposition was demonstrated by the SACT-TODAM model, which was already described in the section 5.4.3.

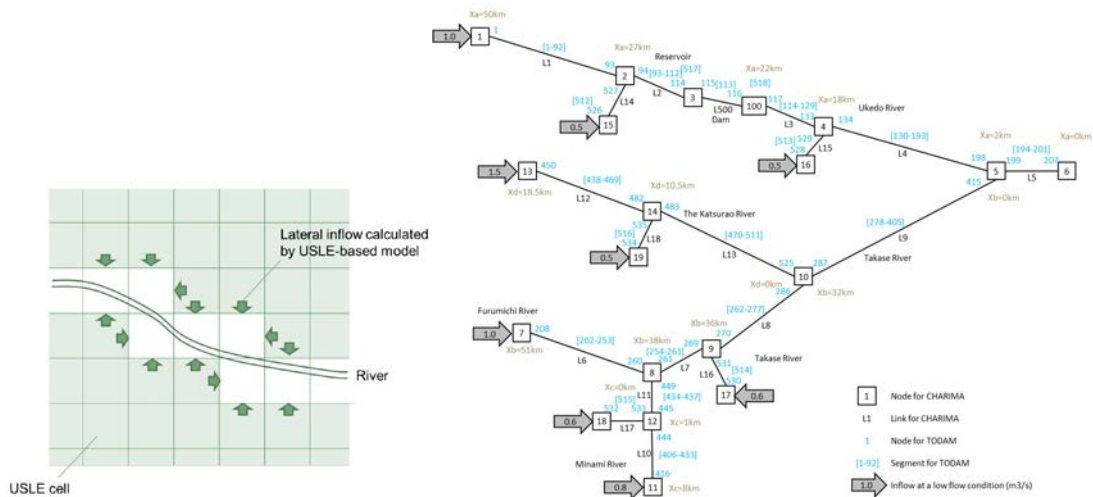


Fig. 5.8-1 Image of application of analytical results obtained by the SACT to the boundary condition of the side inflow in the TODAM (Onishi et al., 2014)¹⁷²).

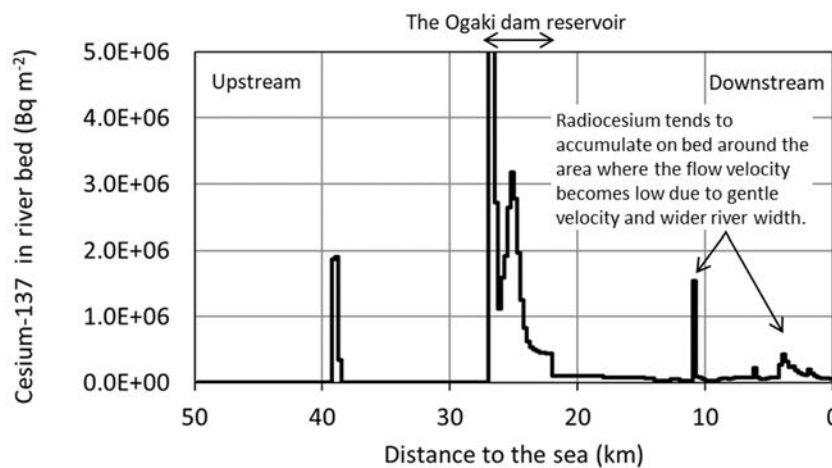


Fig. 5.8-2 Distribution of sediment deposition in dam lake, river beds, and flood plain for the Ukedo River estimated by the SACT-TODAM model.
(cited from Onishi et al. (2014)¹⁷²) with modification).

5.8.3 Changes in radiation dose rate by the migration of radioactive cesium

In this project, the effect of the dynamics of radioactive cesium in environment on radiation dose rate is evaluated. In this evaluation, it is necessary to combine the dynamics model with the dose rate evaluation model.

From the radiation monitoring results conducted so far, it was found that the decreasing speed of air dose rate was faster than that estimated by the physical decay of radioactive cesium (for example, Saito and Onda, 2015¹⁷³). Also, it was clarified that the fast decreasing speed of air dose rate was due to the migration of radioactive cesium into the deep region of soil (Mikami et al., 2015)¹⁷⁴. In order to clarify the cause of these phenomena, we predicted the changes in the air dose rate caused by the migration of radioactive cesium in the depth direction by combining the mDSF model (Kurikami et al., 2017)¹⁴⁰ that analyzes the migration of radioactive cesium in the depth direction shown in the section 5.5 and the dose rate analysis tool ADRET (Malins et al., 2016)¹⁴² described in the section 5.6.1 (Fig. 5.8-3, Kurikami and Malins, 2017)¹⁷⁵. As a result, it was clarified that the decreasing speed of the air dose rate was faster than that determined by the physical decay up to ten years after the fallout, because radioactive cesium migrated into the deep region of soil. Also, it was shown that the decreasing rate became slower due to the progression of the irreversible sorption of radioactive cesium in soil.

Further, we conducted the trial analysis of the spatial changes in radiation dose rate at the time of heavy rain events by combining the analysis of cesium dynamics at river-basin scale or in river by the GETFLOWS and Nays2D shown in the sections 5.3 and 5.4.3 with the dose rate evaluation tool ADRET (Malins et al., 2016)¹⁴² described in the section 5.6.1 (Malins et al., 2015)¹⁷⁶. Figs. 5.8-4 and 5.8-5 show the changes in air dose rate before and after the typhoon attack in September 2011, which was estimated by the GETFLOWS, Nays2D and ADRET. Although the results were not fully verified by comparing with the measured data, we were able to present the analysis process to evaluate the effect of radioactive cesium dynamics at river-basin scale on the changes in radiation dose rate. Incidentally, the analytical results show that there are some places where the dose rates rather increased along the river. This phenomenon was caused by the inflow of sediment with high radioactive cesium concentration to the river from the upstream, and its partial deposition in river beds and flood plain. This tendency was also observed by the dose rate measurements on land or by unmanned helicopter for flood plain around two years after the accident (Sanada et al., 2014¹⁷⁷; Saegusa et al., 2016¹⁷⁸). However, the dose rate tends to rather decrease in recent years, because the concentration of radioactive cesium in sediment flowing down rivers decreased, and sediment with high cesium concentration was buried by sediment with low cesium concentration that was newly deposited on the flood plain (Nakanishi, 2016)¹⁷⁹. The detailed analysis of this point is now in progress.

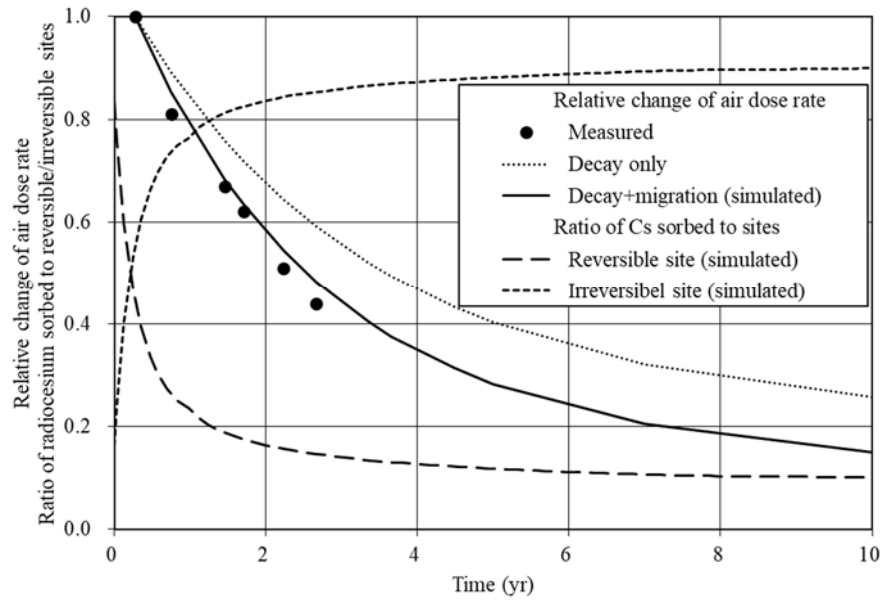


Fig. 5.8-3 Relation between decrease in dose rate caused by the migration of radioactive cesium into deep region and the sorption rate of radioactive cesium on irreversible sites.

The analysis was conducted by the combination of the mDSF and the ADRET models.

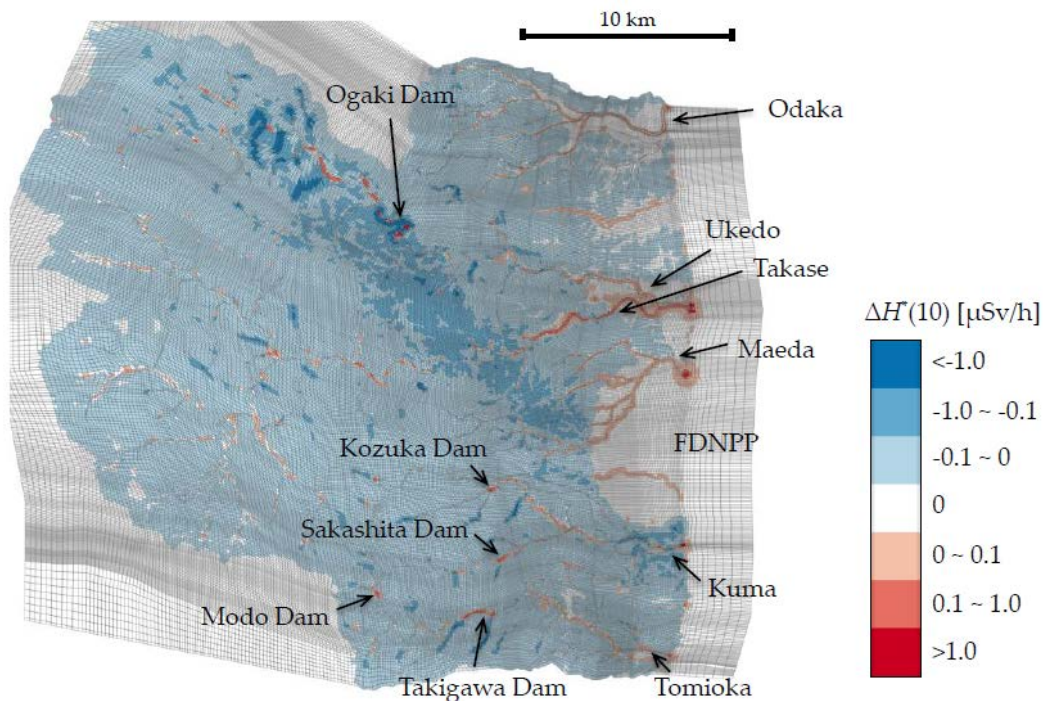


Fig. 5.8-4 Distribution of changes in dose rate before and after the typhoon attack in September 2011.

The data were estimated by the combination of the GETFLOWS and the dose rate evaluation model.

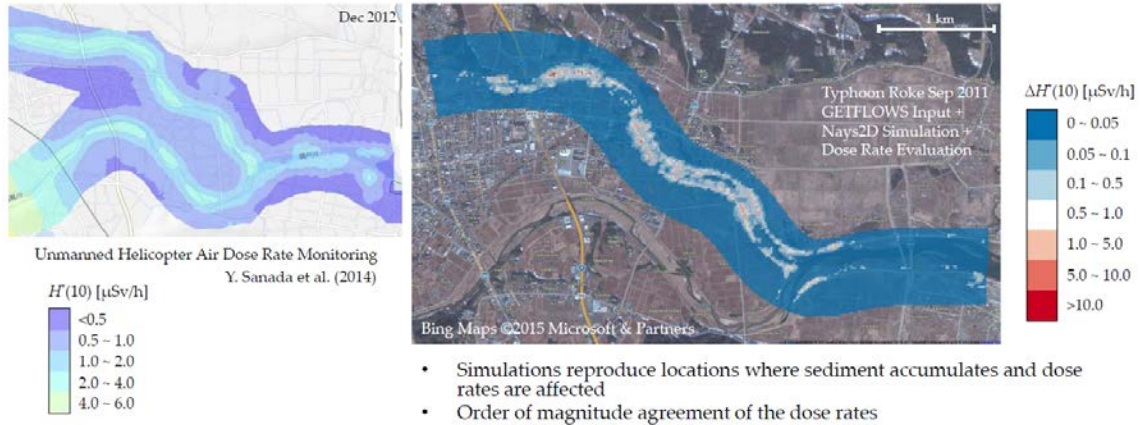


Fig. 5.8-5 Distribution of changes in dose rate around the confluence point of the Ukedo and the Takase Rivers before and after the typhoon attack in September 2011.

The data were estimated by the combination of the GETFLOWS, the Nays2D and the dose rate evaluation model. The left figure shows the results of dose rate measured by the unmanned helicopter in December 2012, Sanada et al, 2014¹⁷⁷).

5.9 Verification of the models

Some of the verification of the models are described in the respective sections. In the analytical research of this project, we aim for modeling with emphasis on the interpretation of the investigated results. Therefore, in this section, the examples of the model verification are again described, especially based on the comparison between analytical results and the measured values.

- Comparison with the measured flux of radioactive cesium flowing out from rivers (terrestrial dynamics model)

The analysis was conducted for river basins of the Abukuma River and rivers in Hamadori District using the terrestrial dynamics model SACT (5.2.2). The analytical results for outflow rate to the sea were compared with the measured values (or evaluated values based on the measurements). As a result, it was confirmed that the analytical results are mostly consistent with the measured values (Kitamura et al., 2014)¹).

The analysis was conducted for five river basins in Hamadori District by the terrestrial dynamics model GETFLOWS (5.3). With respect to the rainfall given as a boundary condition, the analytical results for the amount of river flow, the concentration of suspended sediment, and the concentration of ¹³⁷Cs almost well reproduced the measured values, which confirmed the applicability of the present method (Kitamura et al., 2016¹⁴⁷); Sakuma et al., 2017¹⁴⁸).

- Comparison with the measured concentration of radioactive cesium in river water (terrestrial dynamics model and river system dynamics model)

The behavior of sediment and ¹³⁷Cs was analyzed for Ogaki dam lake at the time of heavy rain by the river system dynamics model TODAM. (5.4.2). From the upstream, the flow amount of river water, the

concentration of suspended sediment, and the concentration of ^{137}Cs were given as boundary conditions. The results obtained by the analysis for the temporal changes in the concentration of suspended sediment and ^{137}Cs at the outlet works were well consistent with the measured values. Similar verification was conducted for the Nays2D and FLESCOT (Kurikami et al., 2014¹⁵¹, 2016¹⁵³); Yamada et al., 2015¹⁵²).

- Comparison with the measurements of the temporal changes in the depth profiles in soil, and accompanying decreasing tendency of radiation dose rate (depth migration model and dose rate evaluation model).

By the combination of the depth migration model mDSF and the dose rate evaluation model ADRET, the shielding effect of gamma-ray accompanied by the permeation of radioactive cesium into the deep region of soil was confirmed by the calculation. The calculated results were in good agreement with the measured values (5.5.3, Kurikami et al., 2017¹⁴⁰; Kurikami and Malins, 2017¹⁷⁵).

- Comparison of the decontamination effect on the reduction of dose rates with the results of the Decontamination Model Demonstration Project (dose evaluation model).

The relation between depth profile of radioactive cesium and air dose rate was analyzed using the dose rate evaluation model ADRET. It was confirmed that the analytical results were well consistent with the measured values. Also, we analyzed the effect of the decontamination methods for fields such as topsoil stripping, inversion tillage, and deep plowing on the reduction of the air dose rates. The effect of the decontamination was demonstrated by comparing the analytical results with the experimental results obtained in the Decontamination Model Demonstration Project (5.6.3, Malins et al., 2016¹⁴²).

- Confirmation of the consistency such as circulation in forests, flow rate from forests to rivers, and concentration of radioactive cesium in rivers (evaluation model for migration to agricultural, forest and fishery products).

The analysis was conducted for circulation in forests, outflow to rivers using the evaluation model for migration to agricultural, forest and fishery product, CMFW (5.7). The results were compared with the measured data of ^{137}Cs circulation in forests (Ministry of Agriculture, Forestry and Fisheries, 2015)¹⁶⁸ and concentration of dissolved ^{137}Cs in river water (Japan Fisheries Research and Education Agency, 2017)¹⁷⁰. It was confirmed that the analytical results were in good agreement with the measured data (Kurikami and Sakuma, 2018)¹⁷¹.

5.10 Future subjects

In the analytical research, we have so far developed and prepared the terrestrial dynamics model, river system dynamics model, dose rate evaluation model, depth migration model, and evaluation model for migration to agricultural, forest and fishery products. These models were properly selected and flexibly combined according to the respective objectives. Herewith, we have conducted; 1) prediction of medium-to-long term distribution of radioactive cesium and air dose rate, 2) evaluation of the flow amount of radioactive

cesium from rivers to the sea, 3) evaluation of the behavior of radioactive cesium in rivers and dam lakes at the time of heavy rain, 4) evaluation of the effect of cesium dynamics in environment on the concentration of radioactive cesium in agricultural, forest and fishery products, and so forth.

The subjects to be investigated (or social needs) have changed with time after the accident. Although the technical problems still remain in some of the models such as insufficient verification, it is necessary to upgrade the model or develop new models in order to correspond to the progress in the investigation and changes in social needs. Specifically, the following subjects are considered.

- Concerning the changes in the concentration of radioactive cesium, there remains gap between the analytical results obtained by the SACT, CFMW, etc. and the measured data. This gap is an important problem in the future prediction of the concentration of radioactive cesium in rivers. The cause of this gap is considered to be that the migration of radioactive cesium into deep region etc. did not reflect on the model. Therefore, the analytical models need to be upgraded.
- The decreasing rates of radioactive cesium in freshwater fish, wild animals and wild plants were slower than those in other things such as agricultural products and marine fish. Therefore, the restrictions and the self-control of shipment still continue. It is necessary to clarify the origin of dissolved radioactive cesium with high bioavailability and the corresponding mechanism of cesium sorption in soil.
- As to the evaluation in dam lakes, we have mainly investigated the buffer effect of radioactive-cesium inflow from the upstream at the time of heavy rain. However, the effect of cesium leaching (internal load) from sediment on the bottom of dam lakes at the time of normal water level has become recently confirmed. Although, this phenomenon has not yet become a serious problem for water use at present, there is a possibility that the cesium leaching will affect the downstream due to the increase in the rate of the internal load if the environment in the river basin changes by the residents' return. In order to investigate the behavior of radioactive cesium at the time of normal water level, it will become necessary to upgrade the river system dynamics models to reproduce the layer of temperature discontinuity, the effect of cesium leaching from sediment on the lake bottom, the flocculation, etc.
- The refinement of the dose rate distribution is important information for the acceleration of residents' return. In the dose rate analysis conducted so far, only simple topography has been considered. However, it will be needed to continue increasing the resolution of the analysis considering the effect of topography and structures on the ground.

The analytical research cannot be conducted only by itself. Thus, it is essential to improve the accuracy of the analysis to solve the problems by repeating the comparison and verification with measured data.

6 Mountain Forest fire

6.1 Outline

As of the end of March 2018, the evacuation zones due to the 1F accident are still designated in the Hamadori District that is coastal plain in the east part of Fukushima Prefecture and Abukuma mountains adjacent to its west, so the access to these areas is severely restricted (Fukushima Prefecture, 2018)¹⁸⁰). Therefore, the probability of wildfires caused by human errors (Goto, 2009)¹⁸¹) is decreasing. On the other hand, accompanied by the access restriction and shipment restriction, the forest tending works (weeding, cutting, pruning and thinning; Nogami, 1992¹⁸²); Ando 1992¹⁸³) or agricultural works around these areas have not been conducted. Hence, the amount of potentially burnable materials at the time of forest fire is increasing.

Since the accident of 1F, three relatively large fires had occurred in Fukushima Prefecture (Radiation Monitoring Unit, Fukushima Prefectural Centre for Environmental Creation, 2017¹⁸⁴); Ministry of Agriculture, Forestry and Fisheries, 2017¹⁸⁵); Forest Planning Division, Fukushima Prefecture, 2018¹⁸⁶); Fig. 8.1.1-1). Among them, the forest fire that occurred in Date City and Minamisoma City from the end of March to the beginning of April in 2016 was put out one or two days after its recognition. The air dose rate around this area had not increases in 1.5 years after the fire. A small amount of radioactive cesium was detected in surface water, but it was hardly observed in mountain stream. Also, radioactive cesium had not been observed in atmospheric floating dust collected around the burnt area (Forest Planning Division, Fukushima Prefecture, 2018)¹⁸⁶).

In the case of the mountain forest fire that occurred in the difficult-to-return zone over Namie Town and Futaba Town from the end of April to the beginning of May 2017, it took more than ten days from its recognition to the putting out after burning about 75 ha (Radiation Monitoring Unit, Fukushima Prefectural Centre for Environmental Creation, 2017¹⁸⁴); Fig. 6.1-1). Although some of the trees were burnt, the fire mainly happened in the litter layer on the forest floor, hence the fire was classified into a small forest fire as an effects of fire on the soil and water systems, ecosystem flora etc. (Ministry of Agriculture, Forestry and Fisheries, 2017)¹⁸⁵). During the forest fire, in addition to the measurement of air dose rate with portable radiation monitoring posts, the sampling of the atmospheric floating dusts and the measurement of radioactive cesium concentration of the dusts were conducted with a high-volume air sampler by Fukushima Prefecture. As a result, it was observed that air dose rate measured with the existing monitoring posts and additional ones did not change. However, changes in the radioactive cesium concentration were observed for the monitoring of atmospheric floating dusts (Fukushima Prefecture, 2018)¹⁸⁷).

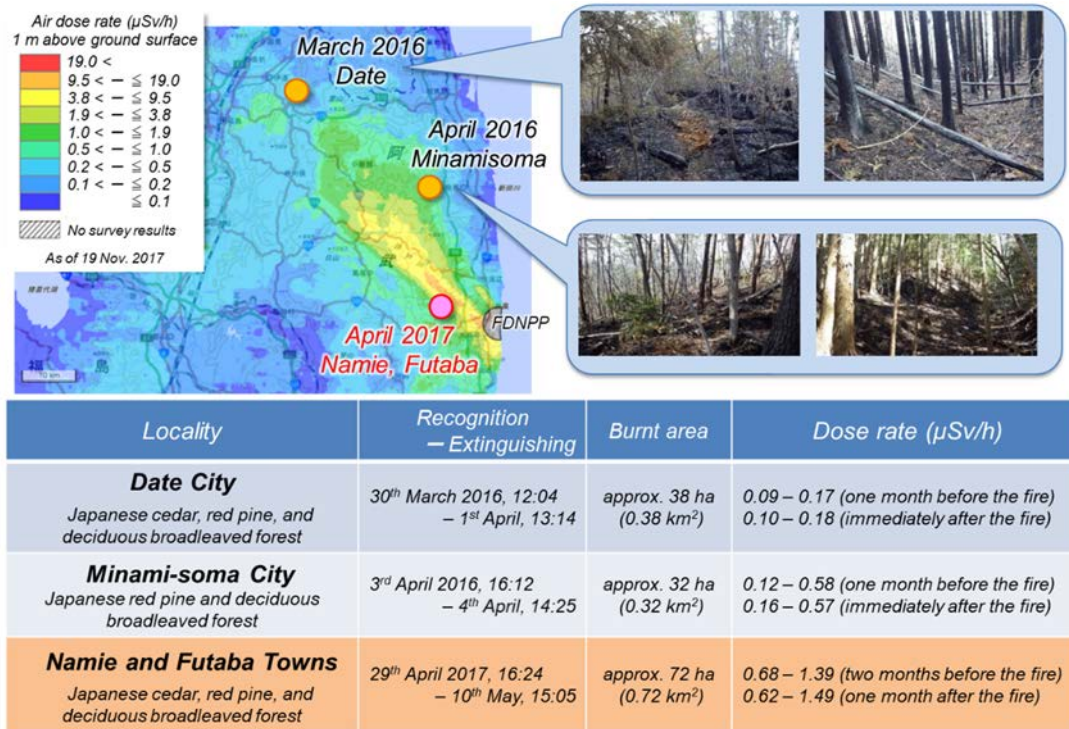


Fig. 6.1-1 Forest fires occurred after the 1F accident.

FDNPP; Fukushima Dai-ichi Nuclear Power Plant.

Distribution map of air dose rate was cited from the Extension Site of Distribution Map of Radiation Dose, GSI Maps.

6.2 Dispersion

6.2.1 Objectives

A mountain fire occurred on April 29, 2017 in Namie Town, Fukushima Prefecture. At that time, the monitoring of the air dose rate was conducted with portable monitoring posts by Fukushima Prefecture. In addition, atmospheric dusts were collected with high-volume air samplers from May 1 to 17, 2017 at three points (“Ishikuma Public Hall”, “Nogami 1st District Meeting Place” and “Yasuragi-So”) around the Mt. Juman within 5 km from the 1F (Fukushima Prefecture, JAEA and NIES, 2017)¹⁸⁸ (Fig. 6.2-1). The radioactive cesium concentration of the dust filters were measured. As a result, it was found that the air dose rate did not change so much in the existing monitoring posts and the additional posts. However, the changes in the radioactive cesium concentration were observed in the atmospheric dust filters. Then, in order to clarify whether or not burning materials containing radioactive cesium were dispersed from the fire site to the surrounding areas, the materials in the dust filters were analyzed in collaboration with the NIES.

For the analysis, the following items were investigated for the samples trapped on the filter; (1) clarification of the existence of radioactive materials, (2) confirmation of the fire-indication materials, (3) relation between the number of the trapped airborne particles in the dust filters and their concentration of radioactive cesium, (4) relationships between wind speed and the number of the trapped airborne particles during fire or normal periods, and (5) observation of IP-photosensitive particles trapped on the filters.

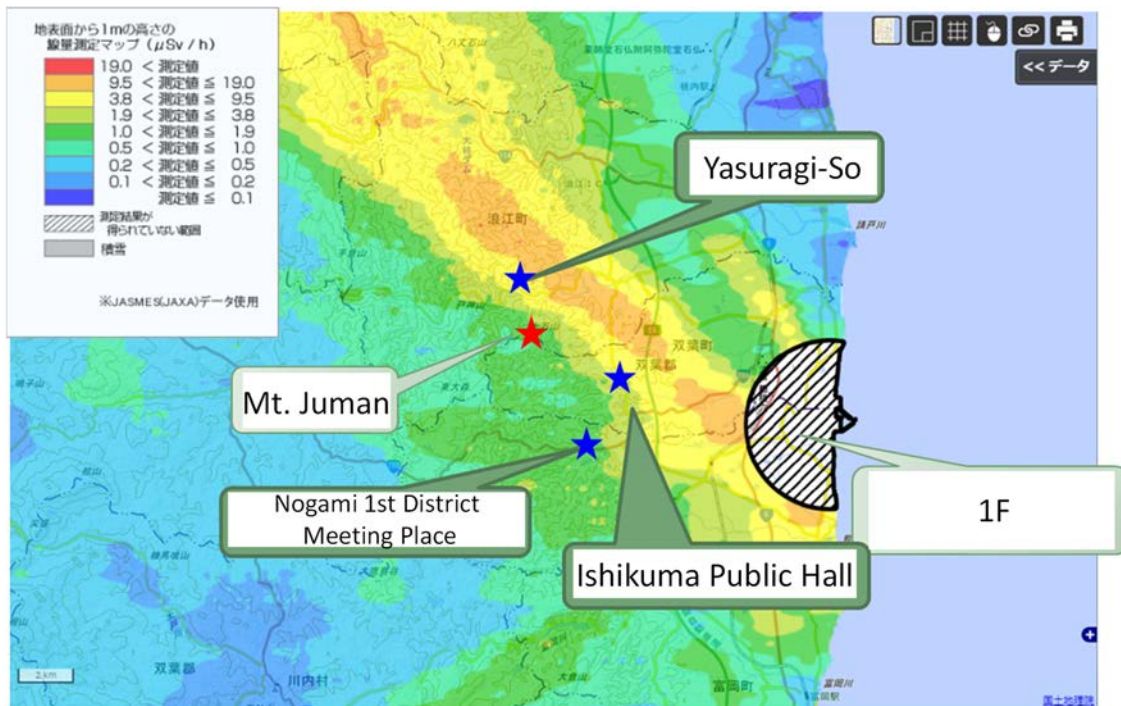


Fig. 6.2-1 Monitoring points of atmospheric dust (Ishii et al., 2018)¹⁸⁹.

(Data on air dose rate: Cited from the Extension Site of Distribution Map of Radiation Dose, as of November 18, 2016. <https://ramap.jmc.or.jp/map/>)

6.2.2 Methods

(1) Clarification of the existence of radioactive materials

The autoradiographs for all filters (total: 50 pieces) (GB-100R, ADVANTEC) were investigated. These filters in U8 container were unfolded one by one to expose them on the imaging plate (IP: BAS-IP, Fuji Film) for 24 hours. After the exposure, IP was analyzed by the laser scanner (Typhoon FLA7000, GE Healthcare). The existence of radioactive materials were determined based on the existence of the photosensitive part (i.e. bright spots distribution on the scanned plate).

(2) Confirmation of the fire-indication materials

After the above procedure (1), the filters were cut in half. The concentration of levoglucosan that can be fire-indication material (atmospheric tracer for higher plants smoke) was analyzed at the NIES using the half of the filter. Furthermore, the changes in the concentration of levoglucosan were investigated during the period of the sampling of atmospheric suspended dust (Fukushima Prefecture, JAEA and NIES, 2017)¹⁸⁸.

(3) Relation between the number of the trapped airborne particles in the dust filters and their concentration of radioactive cesium,

After the measurement of autoradiograph described in (1), image data of the total filters were taken using a digital microscope (VHX-2000, Keyence). Also, in order to obtain the relation between the number of particles trapped in the filters and their concentration of radioactive cesium, the number

of particles under the constant field of view ($1740\ \mu\text{m}\times 1200\ \mu\text{m}$) was counted using a software ImageJ (detection condition: $>3\ \mu\text{m}$ diameter) (hereafter, the particles measured in this method is called “trapped particle”).

(4) Relationships between wind speed and the number of the trapped airborne particles during fire or normal period

The sampling of atmospheric dust was conducted at three points during fire and normal periods. The dust sampling was carried out by three organizations from September 25 to October 2, 2017 as normal period (without effect of the fire) with the same method as the fire in May. The concentration of radioactive cesium in the filters was measured by the Ge semiconductor detector (GMX40, ORTEC). The wind speed data was available of weather-monitoring data in Namie Town by the Meteorological Agency (mean value of one-hour measurement).

(5) Observation of IP-photosensitive particles trapped on the filters

Focusing on the bright spots exposing the IP described in (1), the filters were fragmented to narrow down to 5 mm square the bright spot by repeating the autoradiographs several times. Then, the particles were isolated by the micro-manipulator system (AxisPro FC, Micro support) using a tungsten needle of $1\ \mu\text{m}\Phi$ (Fig. 7.2-2) (hereafter, the particles exposing the IP are called “IP-exposing particles”). The autoradiographs were taken for the fragmented filter before and after the particle isolation to confirm IP-exposing particles were completely isolated. The observation of the particle and elemental analysis were conducted by the electron microprobe analyzer (EPMA: JXA-8530F, JEOL) at the accelerating voltage of 15 kV.

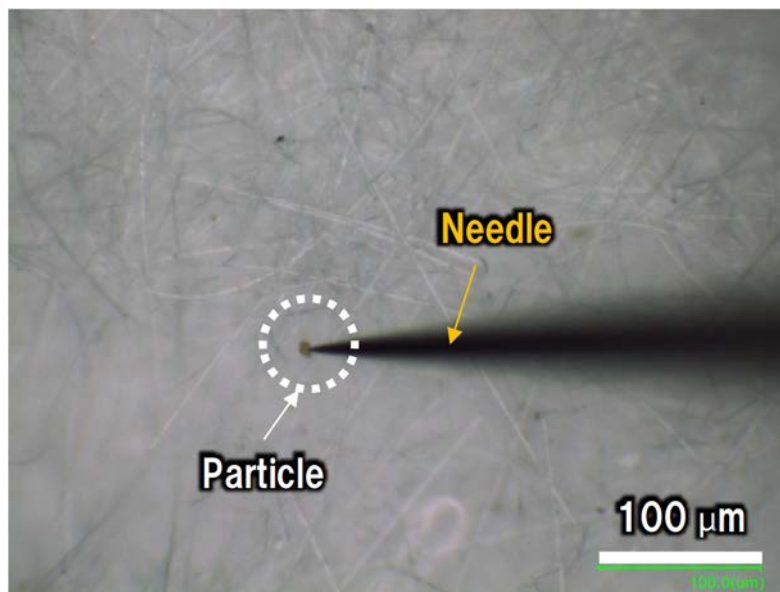


Fig. 6.2-2 Image of particle isolation in filter (Ishii et al., 2018)¹⁸⁹⁾.

6.2.3 Results and discussion

(1) Clarification of the existence of radioactive materials

Among the 50 filters, One or more bright spots (maximum: 3 spots) were detected in 16 filters under 24-hour exposure conditions. From this result, it was considered that the at most three IP-exposing particles were trapped under the condition, and their distribution is heterogeneous in the atmosphere. Then, the concentrations of ^{137}Cs in the dust filters were compared according to the presence or absence of bright spots. As a result, the concentration of ^{137}Cs in the filter with bright spots was ranged from ND (less than the detection limit) to 15.6 ± 0.4 (mBq m^{-3}), while that without bright spots was ranged from ND to 25.5 ± 0.3 (mBq m^{-3}). These results mean that there was not find the difference of radioactive cesium concentrations between in the filters with and without the bright spots. Thus, it was confirmed that the existence of the bright spots did not influence the concentration of ^{137}Cs in the filters.

(2) Confirmation of the fire-indication materials

The concentration of levoglucosan in the atmosphere collected by high-volume air sampler was analyzed at the NIES. As a result, high concentration of levoglucosan was detected in the filters collected during the fire (from May 1 to 9), and it decreased after the fire extinguishment (May 10). The results showed that the changes in the levoglucosan concentration reflected the effect of the forest fire (Fig. 6.2-3) (Fukushima Prefecture, JAEA and NIES, 2017)¹⁸⁸. On the other hand, the clear relationship was not observed between the radioactive cesium concentration and levoglucosan concentration in the filters collected during the fire (Fukushima Prefecture, JAEA and NIES, 2017)¹⁸⁸.

(3) Relation between the number of the trapped airborne particles in the dust filters and their concentration of radioactive cesium

Next, we investigated the relation between the number of trapped particles ($> 3 \mu\text{m}$ diameter) in a constant field of view ($1740 \mu\text{m} \times 1200 \mu\text{m}$) and the concentration of ^{137}Cs in the filter. As a result, it was shown that a good correlation between these two parameters for the filters in all sampling points (Fig. 6.2-4). Also, the number of trapped particles in the filters at three points were compared. The results at the “Ishikuma Public Hall” showed the one-order higher values than those at the other two spots. Furthermore, it was visually confirmed that the degree of coloration and the amount of particles in the enlarged photographs of the filter sampled at the “Ishikuma Public Hall”. These tendency were different from those at the other two sampling spots (Fig. 6.2-5).

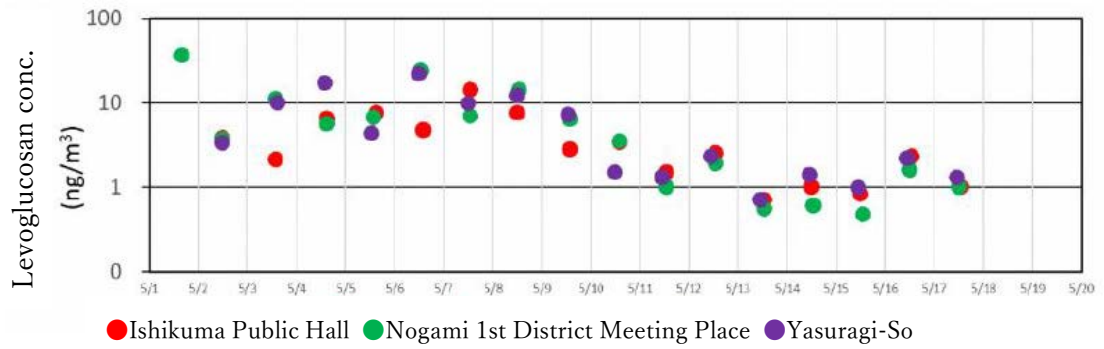


Fig. 6.2-3 Analytical results of levoglucosan (Fukushima Prefecture, JAEA and NIES, 2017)¹⁸⁸.

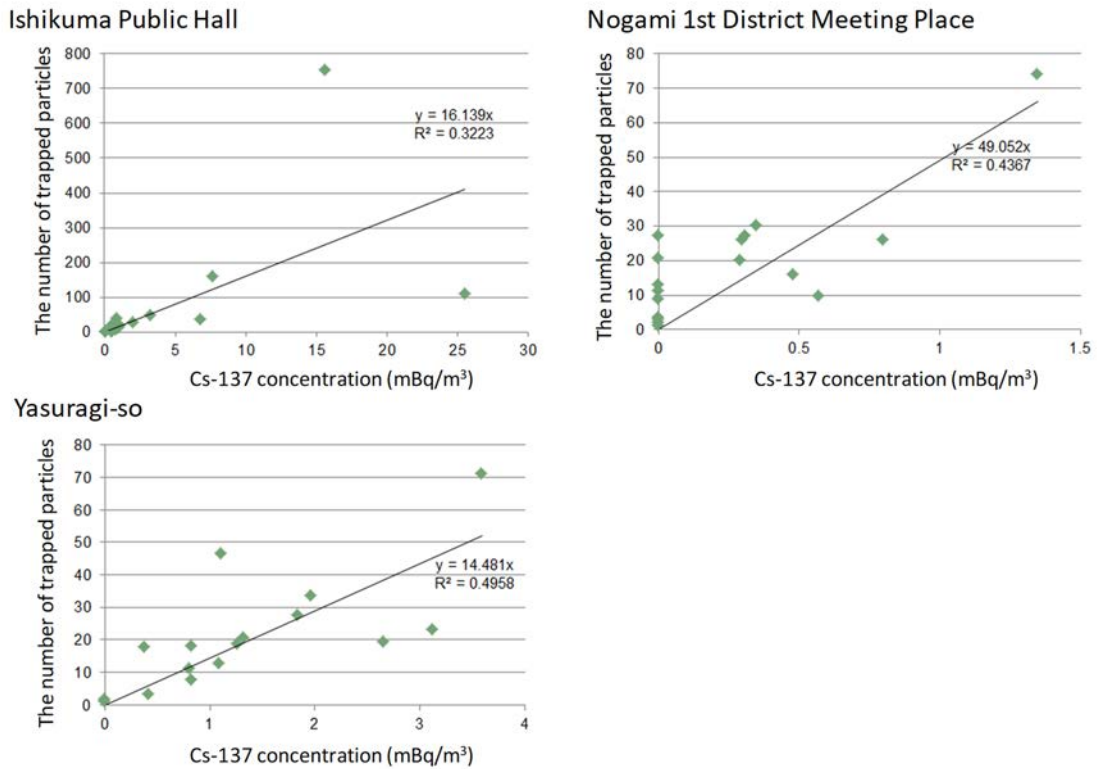


Fig. 6.2-4 Relation between number of trapped particles per field of view of microscope (1740 μm × 1200 μm) and concentration of ¹³⁷Cs (Ishii et al., 2018)¹⁸⁹.



Fig. 6.2-5 Photographs of filters after sampling the atmospheric suspended dust.

- (4) Relationships between wind speed and the number of the trapped airborne particles during fire or normal period

Fig. 6.2-6 shows the relationships between the wind speed and the number of trapped particles in the filter at three spots before and after the fire. From these results, it was observed that the number of the trapped particles was well correlated with the wind speed in the “Yasuragi-So” and the “Nogami 1st District Meeting Place”, while, the correlation was low in the “Ishikuma Public Hall”. At normal period, the wind speed during the sampling of atmospheric dust was less than 2 m/s for three measurement spots (Fig. 6.2-7). During the same period, it was confirmed that many large dump trucks went through around the “Ishikuma Public Hall”. From these results, it was suggested that different phenomena occurred between at “Ishikuma Public Hall” and at the other places. In other words, the factor other than wind increased the amount of trapped particles (radioactive cesium concentration in the filters) at “Ishikuma Public Hall” during fire and normal periods.

Also, from the comparison of the radioactive cesium concentrations in the filters at 3 points both in fire and in normal periods (Table 6.2-1), the concentration was a little high in fire than that in normal time at “Yasuragi-So”. While, no difference was found at other 2 places. The maximum concentration of radioactive cesium was shown in samples collected at “Yasuragi-So” and “Nogami 1st District Meeting Place” on May 8 (Fukushima Prefecture, JAEA and NIES, 2017)¹⁸⁸⁾ during fire and normal periods. On this day, it was recorded as a prominently windy day with the maximum wind speed (9 m

s⁻¹) and the maximum average wind speed (4 m s⁻¹) among this period. Therefore, it is considered that factors other than the fire possible increased the concentration of radioactive cesium.

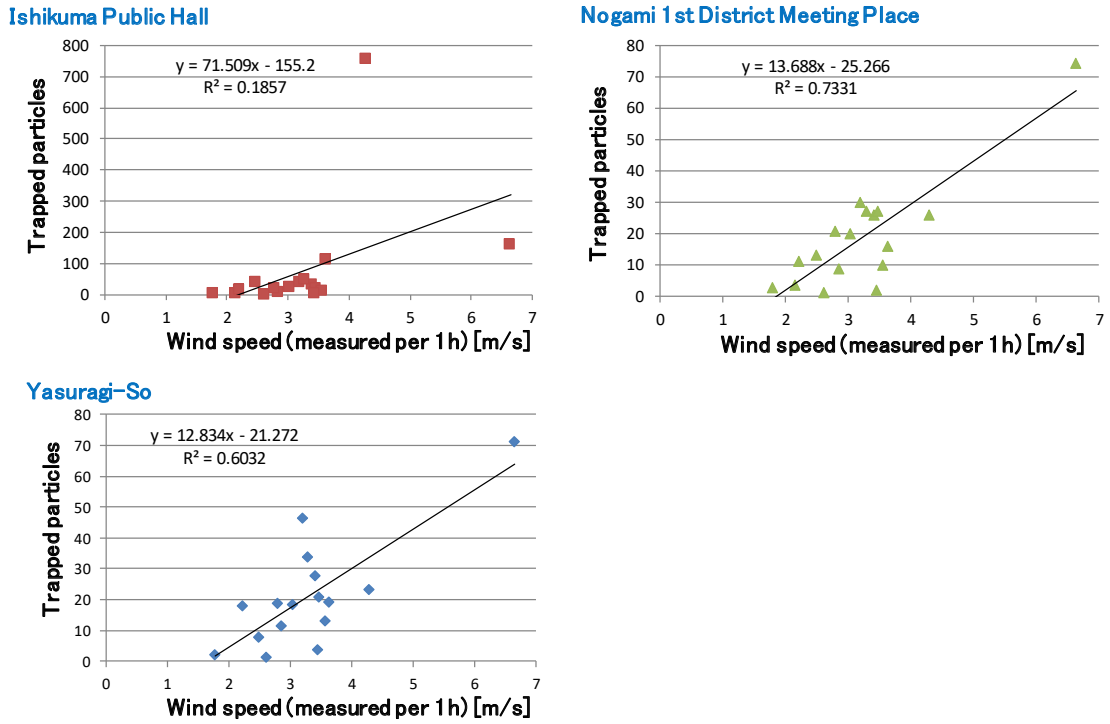


Fig. 6.2-6 Relation between number of trapped particles in a field of view (1740 μm × 1200 μm) of microscope and wind speed (Weather data at Namie Town, Meteorological Agency) (Fukushima Prefecture, JAEA and NIES, 2017)¹⁸⁸).

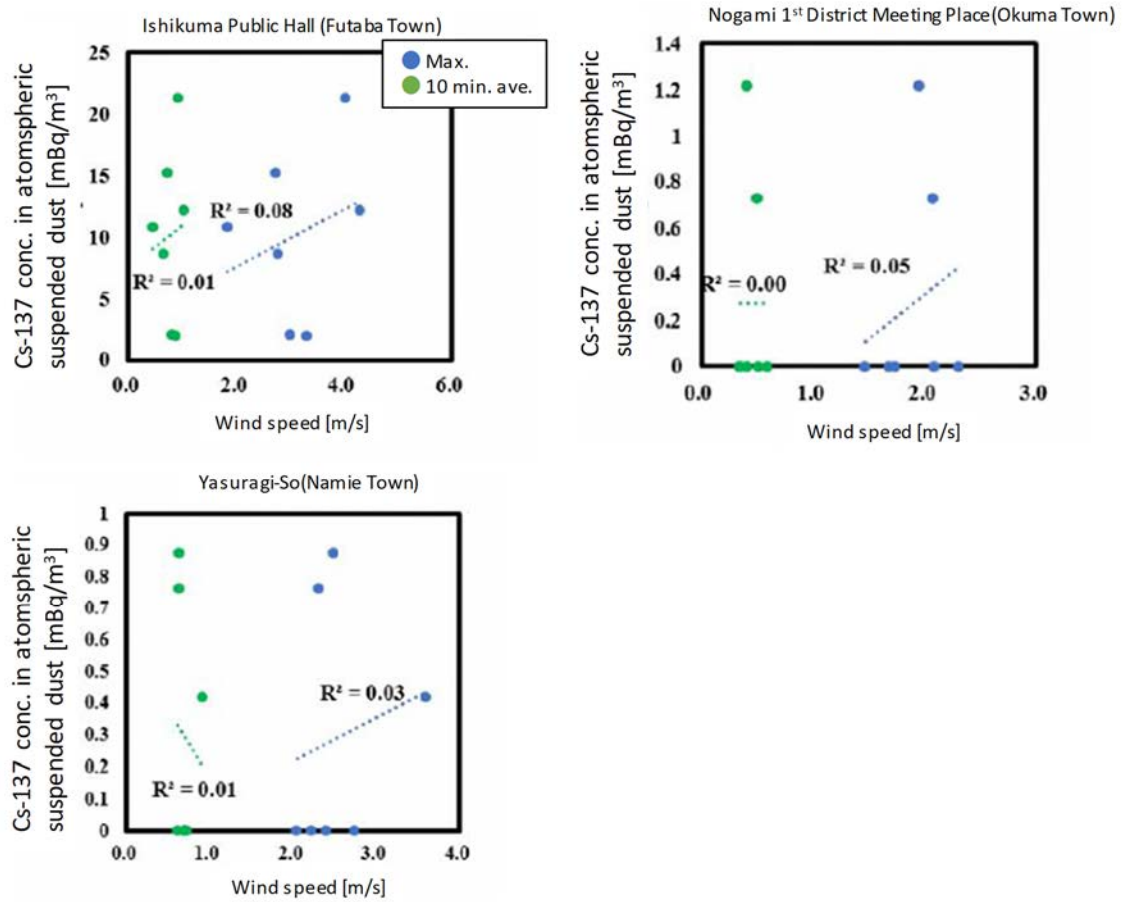


Fig. 6.2-7 Relation between ¹³⁷Cs concentration and wind speed at normal time (Fukushima Prefecture, JAEA and NIES, 2017)¹⁸⁸.

Table 6.2-1 Concentration of ¹³⁷Cs for three places at normal time and at the time of the fire (Fukushima Prefecture, JAEA and NIES, 2017)¹⁸⁸.

Place	Concentration of ¹³⁷ Cs [mBq m ⁻³]	
	Normal time (9/25 – 10/2)	Time of the fire [5/1 – 5/17]
Yasuragi-So	ND – 0.88	ND – 3.59
Ishikuma Public Hall	1.99 – 21.3	ND – 25.5
Nogami 1st District Meeting Place	ND – 1.22	ND – 1.35

(5) Properties of IP-photosensitive particles trapped on the filters

Eight IP-exposing particles were isolated from the filters collected at three places. Specifically, one, two and five particles were isolated from the filters at “Ishikuma Public Hall”, “Nogami 1st District Meeting Place”, and “Yasuragi-So”, respectively. The observation by a digital microscope showed that all particle size were at least 10 μm in diameter, and most of them were larger than 50 μm in diameter (Fig. 6.2-8). Although most of their shapes were aggregates, some individual particle were also found. For “Yasuragi-So”, we compared the isolated particles from the filters during fire and normal periods, any differences in the shapes between them were not found.

Among eight isolated particle, the amount of radioactive cesium (^{137}Cs) was measured for three particles isolated from the filters at “Ishikuma Public Hall” and “Yasuragi-So”. As a result, all radioactivity were less than 0.1 Bq.

Also among eight isolated particle, the elemental composition was investigated by EPMA for two particles isolated from the filters at “Yasuragi-So”. The main components were carbon and oxygen, and their cesium concentrations were lower than the detection limit of energy-dispersive X-ray spectroscopy (EDS).

It is suggested that the properties of these IP-photosensitive particles was differ from the “insoluble radioactive cesium-containing micro particles (CsMP)” that had been reported. The specific radioactivity of isolated IP-photosensitive particles was lower than the CsMP. These elemental compositions were also different. IP-photosensitive particles may be aggregates originating from organic materials or minerals. Based on these results, it was considered that the IP-exposing particles isolated in all places have the same shape and size irrespective of the sampling times, i.e., during the fire or after the fire.

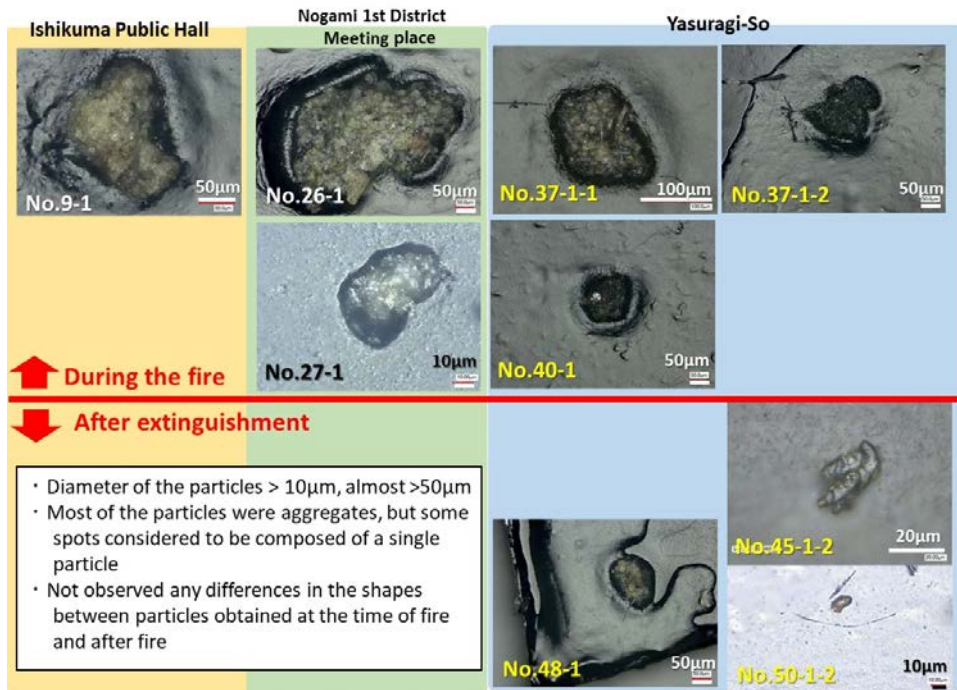


Fig. 6.2-8 Microscope images of particles isolated from the filters at three places.

In summary, the radioactive cesium concentration in atmospheric dust was increased as the number of the trapped particles was increased, as described in (3). Also, as described in (4), the number of trapped particles was correlated with the wind speed (except for “Ishikuma Public Hall”). Therefore, it was considered that one of the causes that change the concentration of radioactive cesium was the wind speed. As mentioned in (2), we confirmed that the fire-indication materials had been dispersed from the fire place to the sampling points of the atmospheric dust during the fire. However, we did not find any difference between the concentration of the fire-indication materials and the concentration of radioactive cesium. Also, as described in (4), there were no difference in the concentration of radioactive cesium between at the fire and at normal periods. From these results, it cannot be denied that radioactive materials were possibly dispersed from the fire site, but it was considered that the effect on radioactive cesium concentration in the atmosphere was small. On the other hand, for “Ishikuma Public Hall”, the number of trapped particles were different by more than one order compared to the other two places, and there were no correlation between the number of the trapped particles and the wind speed. From these results, it was presumed that the particles containing radioactive cesium were trapped from surroundings by some factors other than the wind speed. For the IP-exposing particles, there were no correlation between the existence or number of the particles and the radioactive cesium concentration in the filters. Therefore, it was suggested that the IP-exposing particles did not contribute to the increase the concentration of radioactive cesium in the filters.

6.2.4 Future subjects

Radioactive cesium was detected in atmospheric dust though its amount was too small to affect the radiation exposure. Such radioactive cesium was considered to originate from the resuspension from the surroundings. From now, we will further investigate how to distinguish between the resuspended particles and the particles dispersed from a distance such as the fire site. Specifically, we will develop methods to collect the particles and the methods to evaluate the measurement condition and particle properties.

6.3 Air dose rate at mountainous area

6.3.1 Objectives

JAEA has been measuring the deposition status and migration behavior of radioactive cesium in mountain forests in Fukushima Prefecture since FY2015 (refer to section 2.4). On April 29, 2017, a fire occurred in the area of Mt. Juman. Incidentally, the going-around investigation was carried out in this area in March 2017. Therefore, in order to clarify the changes in the dose rate distribution by the fire, the investigation of the air dose rate was conducted in this area.

6.3.2 Methods

The radiation survey was carried out using “Hotspot finder (HSF)” (detector: CsI(Tl) scintillator) combined GPS. The air dose rate at 1 m and 20 cm height was measured (refer to Section 2.4.2). The measurement area was determined the region including the burnt area, and the investigation was conducted from May to June, 2017.

6.3.3 Results and discussion

Fig. 6.3-1 shows the measurements results of air dose rate. Comparing the air dose rate before and after the fire (March and June, 2017), the changes in the air dose rate were scarcely observed. Even when the air dose rate was compared with that ten months after the fire (March 2018), the changes in the air dose rate were also hardly observed. For the results obtained at three different times, we compared the air dose rate results among the parts measured in the same routes. As a result, it was revealed that the air dose rate decreased just after the fire and further decreased ten months after the fire compared with that before the fire (Fig. 6.3-2). For Mt. Juman and its surroundings, the air dose rate was measured by unmanned helicopter and the existing monitoring posts, but changes in the air dose rate was not observed before and after the fire in both measurements (Fukushima Prefecture, JAEA and NIES, 2017)¹⁸⁸).

From these results of the dose rate measurements, it was considered that the fire did not induce the migration of radioactive materials to the extent to increase the dose rate of the measurement sites.

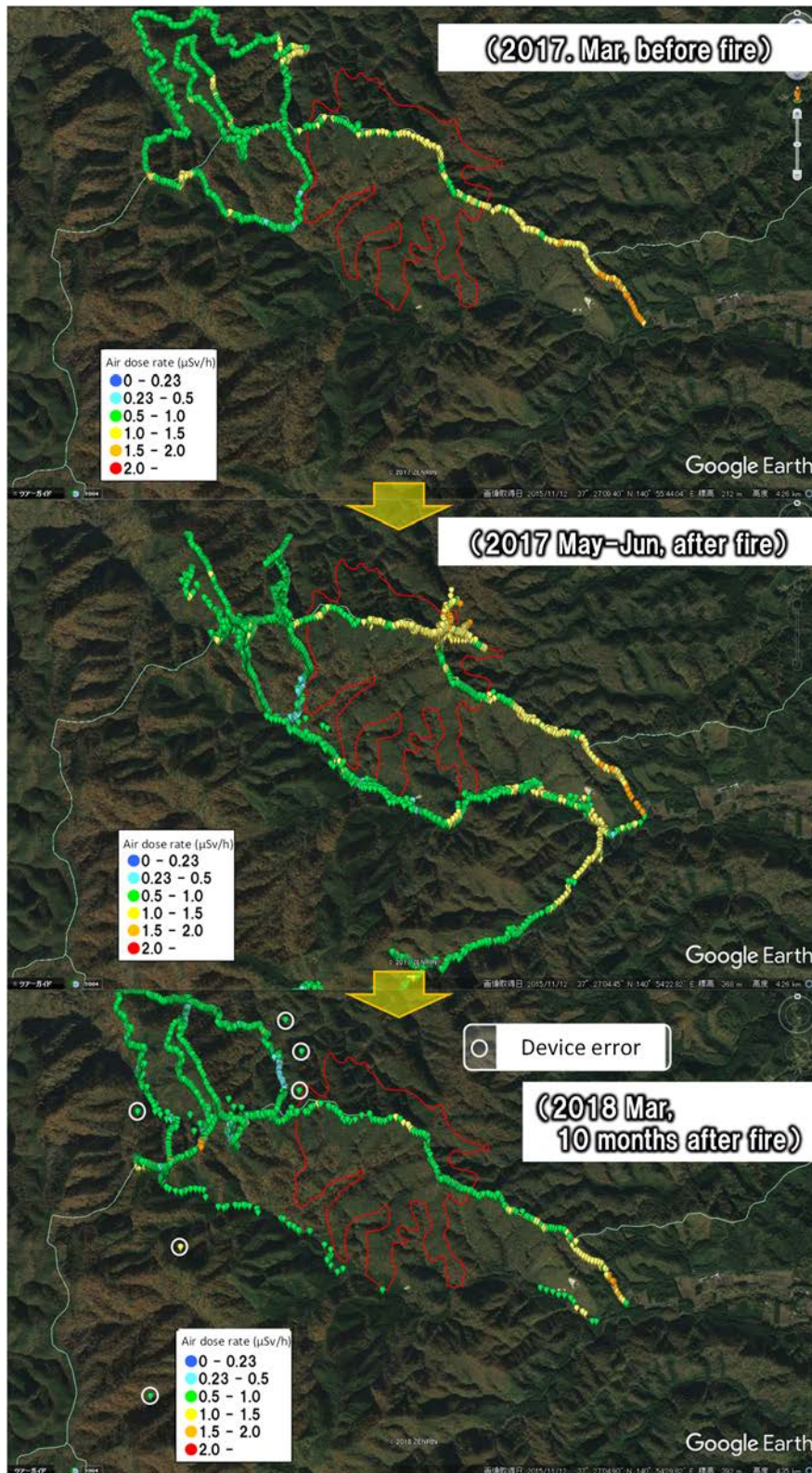


Fig. 6.3-1 Comparison of air dose rate distribution among the time before/after the fire and ten months after the fire (red line: burnt region).

Google Earth, ©2018 ZENRIN

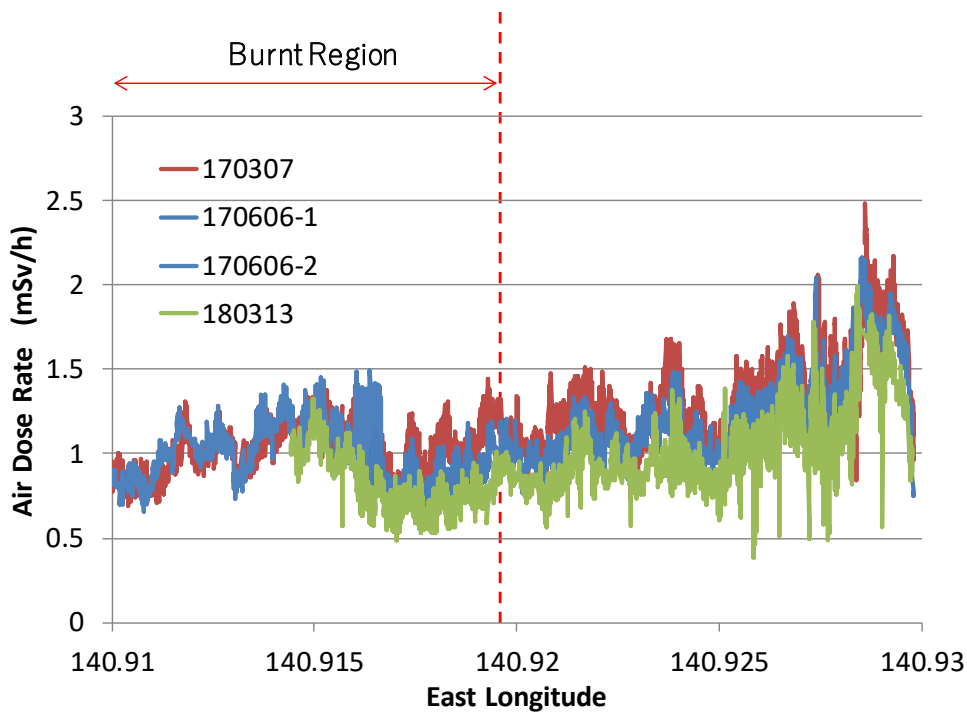


Fig. 6.3-2 Changes in air dose rate.

Air dose rate along the mountain routes before and after fire.

Measured in 7th March, 2017 (red), 6th June, 2017 (blue) and 13th March, 2018 (green).

6.3.4 Future subjects

It is considered that the radiation sources in mountain areas are ground surface and litter layer where radioactive cesium was deposited in forests (Koarashi et al., 2012)³⁴). Therefore, there is a possibility that dose rate will change by the large changes in the ground surface and litter layer at the measurement spots (a large change accompanying the movement of soil). For this reason, we will observe the effluent behavior of radioactive cesium from slopes and investigate the possibility of the dose rate changes.

6.4 Dynamics of forest floor

6.4.1 Objectives

A mountain forest fire occurred in April 2017 in the difficult-to-return zone of Ide District, Namie Town. At that time, it was expected that the amount of soil outflow and accompanying radioactive cesium outflow would increase. Under such circumstance, the distribution and outflow situations of radioactive cesium were investigated at the burnt and unburnt areas. In this section, the results of the radioactive cesium dynamics of forest floor suffered the forest fire are described based on the field investigations.

6.4.2 Methods

The investigations had been conducted at the mountain forests (mountain forests at Mt. Juman) in the difficult-to-return zone located at about 10 km west of the 1F. The air dose rates were mostly in the range from 1.0 to 1.9 $\mu\text{Sv h}^{-1}$. The investigated area is located at the south-west of the 1F that is outside of the relatively high air dose rate region extending to the north-west direction from the 1F (Fig. 6.4-1). The samples related to the distribution status of radioactive cesium were collected at the ridge of the mountain forests at 400 m altitude (around the peak of Mt. Juman) and forest slopes along the mountain stream (Nanoka-sawa) flowing from west to east at the south end of the burnt area (Fig. 6.4-2). At the ridge, deciduous broad-leaved forests (Japanese konara oak (*Quercus serrata*) forest) mainly composed of Japanese red pine (*Pinus densiflora*) forests and konara oaks are distributed, and plantation cedar forests are distributed along the mountain stream. At the burnt and unburnt areas in each forest, the barks and litter in a constant area (10 cm \times 10 cm or 20 cm \times 40 cm) were taken, and the soil up to 20 cm depth was collected using a liner soil sampler with a diameter of 5 cm. The bark samples were taken from standing trees of Japanese red pine, konara oak and cedar. The carbonized and non-carbonized barks were collected from the same tree. For litter and soil samples, the grids of 5 m interval were set in the range of about 20 m square in each forest, and 15-20 samples were collected per a forest. In collecting the litter samples, the litter that had existed at the time of the fire (prefire litter; the whole part or some parts were carbonized) was distinguished from that deposited after the fire (postfire litter; it was not carbonized, and soot was not attached). For soil samples, the whole soil collected by liner soil sampler was fully mixed in the laboratory, and then a required part for radiocesium and chemical analysis was fractionated. The sampling had been conducted from June to November 2017 (Table 6.4-1).

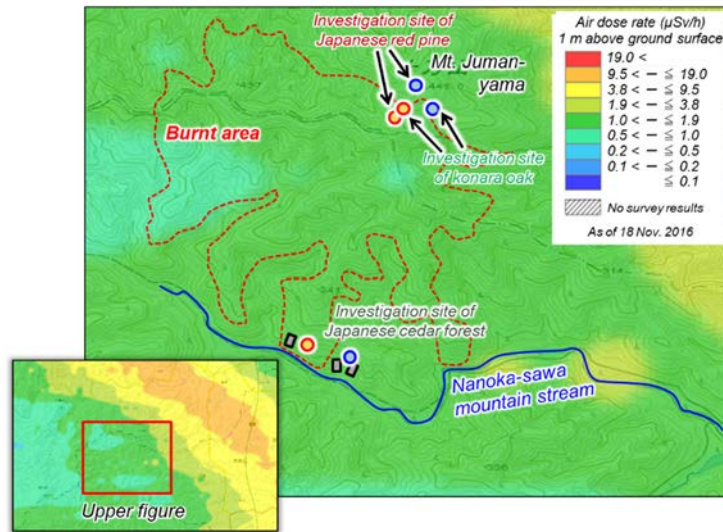


Fig. 6.4-1 Air dose rate around the investigated area (as of November 18, 2016).

Distribution map of air dose rate was cited from the “Extension Site of Distribution Map of Radiation Dose/ Map of the Geospatial Information Authority of Japan”. The burnt area was cited from the Iwaki District Forest Office, Kanto Regional Forest Office, Forestry Agency.

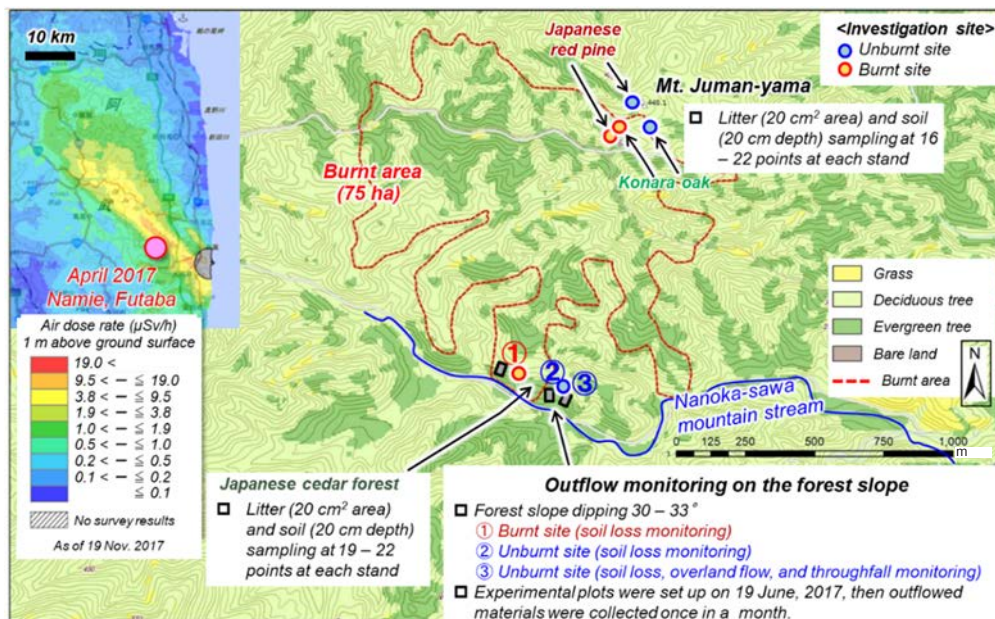


Fig. 6.4-2 Map of investigation sites.

Topographic map is based on the website of the Digital Topographic Map¹⁹⁰⁾, Geospatial Information Authority of Japan. The land-use map is based on the High Resolution Land-Use and Land-Cover Map ver.16.09 (Earth Observation Research Center, Japan Aerospace Exploration Agency (JAXA), 2016)¹⁹¹⁾. Distribution map of air dose rate shown in the upper left is the same as that in Fig. 6.2-1.

The burnt area is the same as that in Fig. 6.4-1.

After the pre-treatment such as drying, the collected samples were homogenized by hand stirring and crushed into fine fragments, then a required amount of the sample was fractionated. The concentration of ^{137}Cs (Bq kg^{-1}) was measured by a Ge semiconductor detector. The data of the ^{137}Cs concentration was corrected to the value on October 1, 2017, considering the physical decay of ^{137}Cs . For the bark samples, the concentration of ^{137}Cs (aggregated transfer factor; $\text{m}^2 \text{kg}^{-1}$) was calculated by normalizing the concentration of ^{137}Cs in the bark with the deposition amount of ^{137}Cs in soil (inventory). The deposition amount of ^{137}Cs in litter and soil (Bq m^{-2}) was calculated from the sampling area, sample weight and the ^{137}Cs concentration.

The monitoring of radioactive cesium outflow was conducted at the experimental plots set on the northern slope along the Nanoka-sawa mountain stream (Fig. 6.4-3). The angle of the slope was about 30 degree. The outflow materials (soil and litter) flowing into the soil trap boxes set at the end of the plot had been collected once in a month from June to the end of December (just before the snowfall) 2017 (Table 6.4-1). Also, the coverage of the forest floor was calculated by analyzing the photograph images of the forest floor. The coverage of the forest floor was calculated by setting 10 cm square grids at the forest floor and identifying the existence of the forest floor covering (litter and understory vegetation such as bamboo grass) at the grid crossing. The amount of ^{137}Cs outflow (Bq m^{-2}) was calculated from dry weight of the outflowed materials, concentration of ^{137}Cs and the area of the experimental plot. The ^{137}Cs outflow rate was defined as the percentage of the ^{137}Cs outflow amount to the ^{137}Cs deposition amount near the plot.

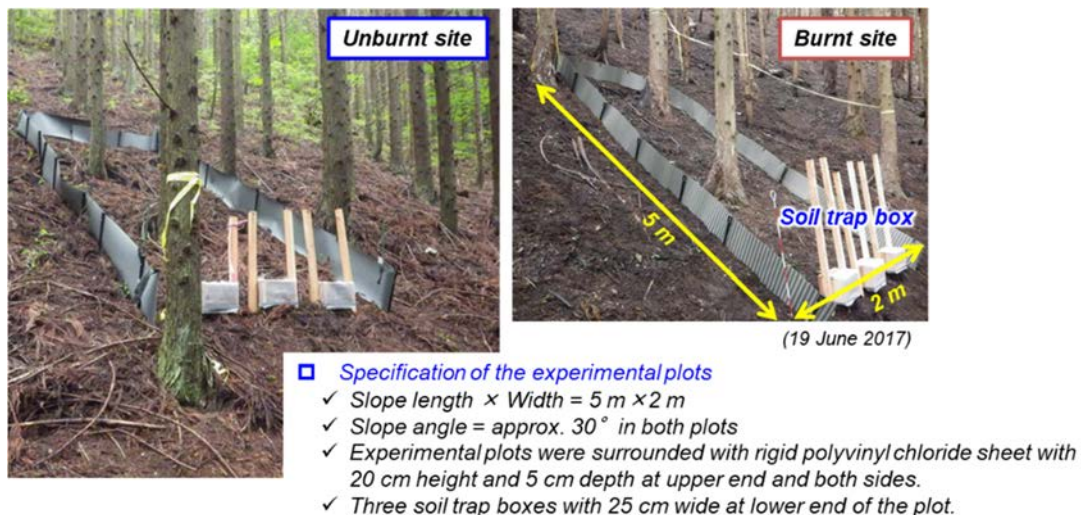


Fig. 6.4-3 Experimental plot set at the cedar forest along the Nanoka-sawa.

Table 6.4-1 Date of sampling.

Sample		Date	
Bark (burnt and unburnt sites)		June 2017 (all stands)	
Litter layer	Burnt stand	Prefire litter	Oct. 2017 (Japanese red pine and konara oak stands), Nov. 2017 (Japanese cedar stand)
		Postfire litter	June 2017 (all stands) Oct. 2017 (Japanese red pine and konara oak stands), Nov. 2017 (Japanese cedar stand)
	Unburnt stand	June 2017 (Japanese cedar stand), Aug. 2017 (Japanese red pine and konara oak stands) Oct. 2017 (all stands), Nov. 2017 (Japanese cedar stand)	
Soil layer (burnt and unburnt stands)		June 2017 (all stands) Oct. 2017 (Japanese red pine and konara oak stands), Nov. 2017 (Japanese cedar stand)	
Outflow monitoring at experimental plots		Monitoring period; June – Dec. 2017, Sampling; once in a month	

Pre- and post-fire litters refer to the litters deposited before and after the forest fire.

6.4.3 Results and discussion

(1) Bark

When compared in each standing tree and forest, no tendency was observed for the aggregated transfer factor (T_{agg}) of ^{137}Cs in bark (upper-left table in Fig. 6.4-4). It is presumed that this result reflected the fact that the degree of the burning was different depending on each tree and the initial ^{137}Cs deposition situation was different between the sampling points of standing tree and the bark. For this reason, the bark samples were divided into unburnt parts and burnt parts irrespective of the tree species. Then, in order to eliminate the difference in the initial deposition amount at the respective sampling spots, the ^{137}Cs concentration in bark was compared by the bark ^{137}Cs concentration (T_{agg}) normalized by the ^{137}Cs deposition amount in soil. As a result, it was found that the T_{agg} tended to be distributed in low range for the unburnt bark, while they were distributed in relatively high range for burnt bark (Fig. 6.4-4). However, it was also found that the distribution ranges of the unburnt and burnt barks were overlapped, and the significant difference between two kinds of bark could not be observed by the statistical analysis. Therefore, it cannot be said that the Cs distribution status in bark changed by the combustion.

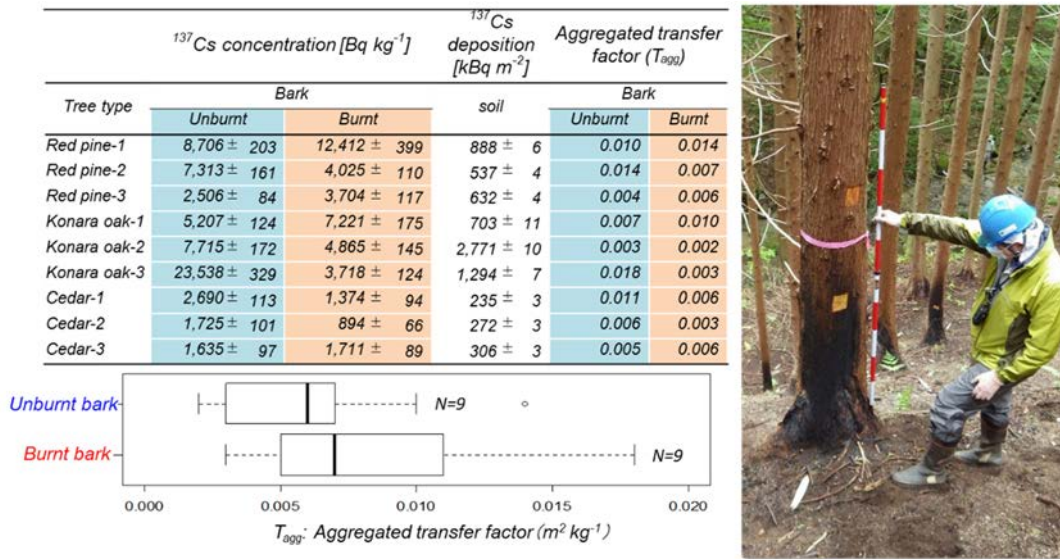


Fig. 6.4-4 Concentration of ¹³⁷Cs in bark and aggregated transfer factor (T_{agg}).

N in the figure represents the total number of the samples. Right photograph: The unburnt and burnt barks at the standing tree in the fire site (the color changed to black by the carbonization.).

(2) Litter and duff layers

For the ¹³⁷Cs concentration in litter and duff layers, it was found that the ¹³⁷Cs concentration was the lowest in the postfire litter deposited after the fire, and then it was middle in the unburnt site. The ¹³⁷Cs concentration was the highest in the prefire litter deposited before the fire (left figure of Fig. 6.4-5). For the prefire litter, it is presumed that the concentration of ¹³⁷Cs became high because ¹³⁷Cs was agglomerated by the spreading of the fire. At the burnt site, most of the litter layer and understory vegetation was lost in all forests after the fire due to the burning. Therefore, it was considered that the lowest ¹³⁷Cs concentration in the postfire litter was the reflection of the tendency that the ¹³⁷Cs concentration in litterfall is decreasing by the year change (Teramage et al., 2014¹⁹²); Kato et al., 2017¹⁶⁹), etc.). Further, the fact that the fluctuation range of the ¹³⁷Cs concentration was large for the prefire litter compared with that for the litter in the unburnt site or postfire litter suggested that the degree of the spreading fire was different among the places. It was revealed that the ¹³⁷Cs deposition amount in litter layer and duff layer tended to be the lowest in the postfire litter in all forests (right figure of Fig. 6.4-5). For Japanese red pine and konara oak forests, the distribution region of the ¹³⁷Cs deposition amount of litter layer in the unburnt site was overlapped with the prefire litter, and the significant difference in the deposition amount could not be observed by the statistical analysis. Therefore, it is hard to say that there was a change in the deposition amount due to the spreading fire. For cedar forests, the fluctuation range of the ¹³⁷Cs deposition amount in the unburnt site was extremely large, and also the amount of litter remaining in the fire site (carbonized litter etc.) was few after the fire. Therefore, it would be difficult to investigate the changes in the ¹³⁷Cs deposition amount

(right figure of Figs. 6.4-5 and 6.4-6). However, for the fire sites of cedar forests, there was no covering of the forest floor by litter layer and understory vegetation that were seen in the unburnt site, so the soil and cedar rootlet were exposed. Thus, the litter layer and understory vegetation were burnt at the time of the fire, so it was considered that they were outflowed by the water for extinguishing fire or rainfall immediately after the fire. Therefore, if the amount of litter and the concentration of ^{137}Cs in the burnt site were the same as those in the unburnt site, it can be presumed that the ^{137}Cs amount corresponding to the amount (3 – 15 kBq m^{-2} , Fig. 6.4-6) deposited in the litter at the unburnt site adjacent to the burnt site decreased at the time of the fire or after the fire.

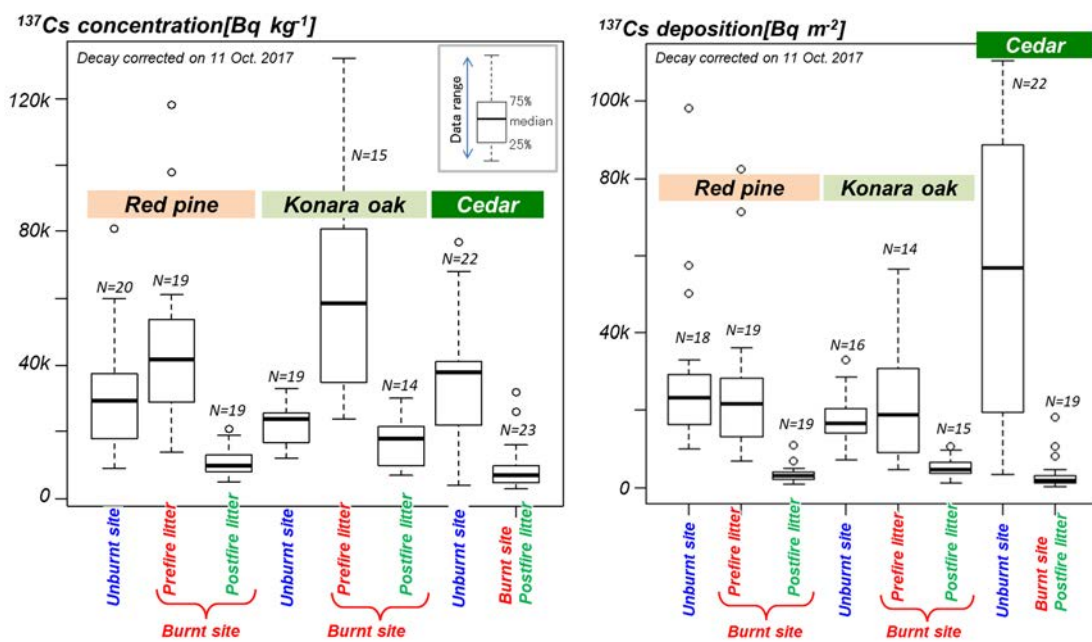


Fig. 6.4-5 Concentration (left) and amount (right) of ^{137}Cs in litter and duff layers.

N in the figure represents the number of the samples. Duff is made up of the Fermentation layer (F) and Humus layer (H) of organic matter underlying litter layer.

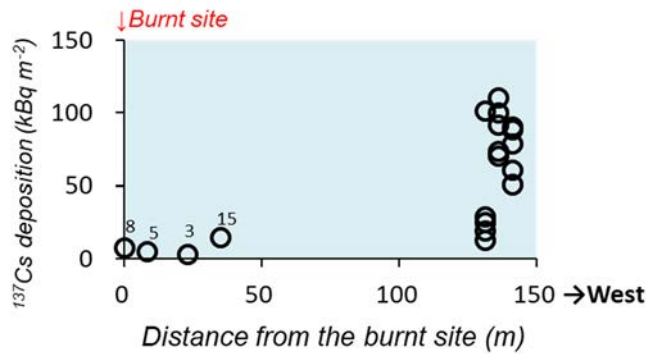


Fig. 6.4-6 Relation between distance from the spreading fire site of cedar forest and ¹³⁷Cs deposition amount in litter layer.

(3) Soil layer

When ¹³⁷Cs concentration and amount in soil layer were compared between burnt sites and unburnt sites, the clear differences were not observed for Japanese pine forest, konara oak forests and cedar forests. Also, the significant difference was not observed even by the statistical analysis (Fig. 6.4-7). For this reason, a change in the ¹³⁷Cs distribution due to forest fires could not be found when soil layer up to about 20 cm or 30 cm below the surface soil was investigated.

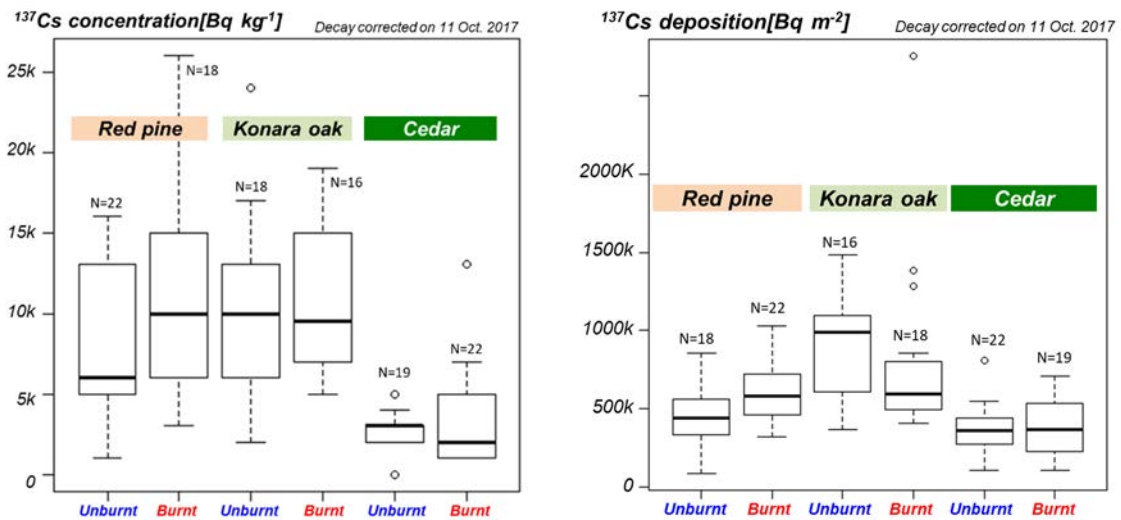


Fig. 6.4-7 Concentration (left) and deposition amount (right) of ¹³⁷Cs in soil layer.

N in the figure represents the number of the samples.

(4) Monitoring of outflow

For the cedar forest floor at the burnt site along the mountain stream, the litter layer had been lost two months after the fire, and granite gravel and carbonized branches/bark were scattered (left figure of Fig. 6.4-8). Herbs and bamboo grass that have grown after the fire were negligible. Although the

terraced (stepwise micro-topography) was developed, linear erosion topography like rill and gully was not confirmed, and soil layer and cedar rootlet were in the exposed situation (left figure of Fig. 6.4-8). The litter layer from 4 to 7 cm thickness existed in the forest floor of the unburnt site at this cedar forest. Although the development of understory vegetation was not observed, the exposure of soil layer could not be confirmed due to the covering of the forest floor by litter layer.

For the coverage situation of the forest floor at the burnt site of cedar forest, the observation had been conducted from the end of June to the end of December 2017 similarly to the observation of the outflow. As a result, it was observed that although the understory vegetation had been recovered from the end of July to the end of September, the understory vegetation had only been withering after the end of October, and it was confirmed that the covering of the forest floor was recovered due to the deposition of cedar litter. For the coverage of the forest floor, it had been 10% range before the end of October, but it recovered to 50% range after the end of November (upper graph of Fig. 6.4-9).

For the amount of outflow material (g m^{-2}) at the forest slope in burnt and unburnt sites, it was found that the amount tended to be relatively high in the burnt site, while it was low in the unburnt site. There was about a 10-fold difference in the amount of outflow material (middle graph of Fig. 6.4-9). The outflow amount of ^{137}Cs (Bq m^{-2}) was changing in accordance with the increase/decrease in the amount of outflow material reflecting the small difference in the ^{137}Cs concentration between the burnt and unburnt sites. There was about a 13-fold difference in the ^{137}Cs outflow amount (lower graph of Fig. 6.4-9). Both the amount of outflow material and ^{137}Cs outflow showed the changes in accordance with the increase/decrease of the intensity of rainfall in the observation period. It was expected that the outflow amount would decrease with the recovery of the forest floor coverage. However, even in the end of November when the coverage at the burnt site recovered to 50% range, the material outflow amount in the burnt site was still considerably different from that in the unburnt site.



Fig. 6.4-8 Situation of forest slope at Japanese cedar forest.

Left photograph: burnt site, Right photograph: unburnt site. The photographs were taken on June 26, 2017.

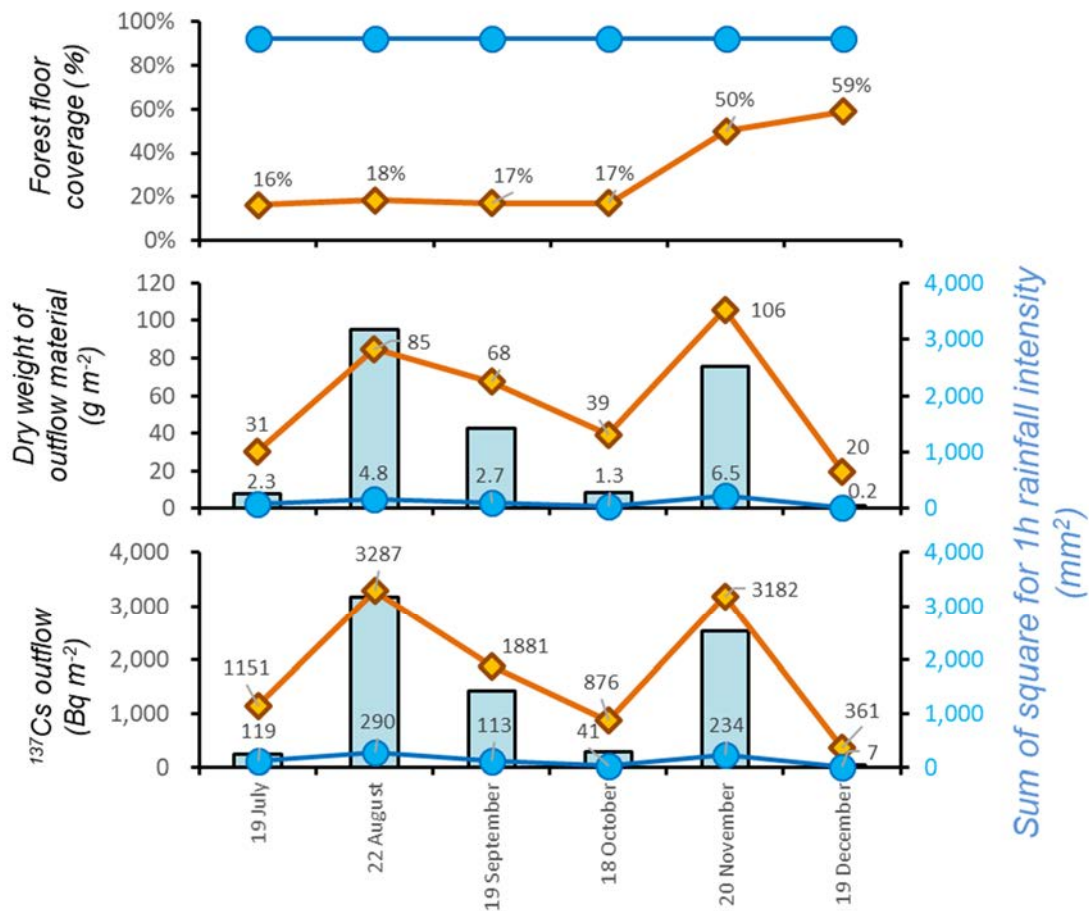


Fig. 6.4-9 Outflow amount of ¹³⁷Cs from forest slope at cedar forest.

Red marks show the burnt site, and blue marks represent the unburnt site. Bar charts indicate the rainfall intensity.

The ¹³⁷Cs outflow rate was calculated from the above monitoring data and the ¹³⁷Cs deposition amount on forest floor near the experimental plots. As a result, the outflow rate was estimated to be about 2.6% during the monitoring period from the end of June to the end of December (Table 6.4-2). From the existing observation of ¹³⁷Cs outflow (Nishikiori et al., 2015²³); Yoshimura et al., 2015⁹⁸); Niizato et al., 2016⁹); Niizato, 2018¹⁹³), the ¹³⁷Cs outflow rate in a year was estimated to be in the range from 0.05% to 3.7%. Compared with these results, the outflow rate at the burnt site was relatively high but within the range of the existing observation results. For this reason, it is hard to say that the outflow amount and the outflow rate of radioactive cesium considerably increased with the changes in the forest floor situation due to the forest fire.

Table 6.4-2 Outflow amount and outflow rate of ¹³⁷Cs in the monitoring period (from June to December, 2017).

Experimental plot	¹³⁷ Cs deposition (around plots) (Bq m ⁻²)	Outflow material (Monitoring period: June 19, 2017 – December 19, 2017)		
		Dry weight (g m ⁻²)	¹³⁷ Cs outflow amount (Bq m ⁻²)	Outflow rate (%)
Burnt site (Coverage: 16 – 58 %)	416k	348	10,738	2.58
Unburnt site (Coverage: 90 – 92 %)	547k	18	805	0.15
Burnt site/Unburnt site	—	19	13	—

6.4.4 Future subjects

We have been investigating the situation of the radioactive cesium distribution and monitoring the outflow of radioactive cesium at the forest slope from about two months after the end of the forest fire, and the following results were obtained.

- It was confirmed that the bark was carbonized by the fire. However, we could not observe any difference in the ¹³⁷Cs concentration in bark normalized by the ¹³⁷Cs deposition amount in soil between burnt and unburnt barks.
- The concentration of ¹³⁷Cs increased in litter and duff layers by the fire, but the deposition amount of ¹³⁷Cs did not change.
- For cedar forests distributed along the mountain stream, the litter layer was lost. It is presumed that the almost all litter layer was lost at the time of the fire or by rainfall immediately after the fire.
- If we suppose that litter layer that is similar to that in the adjacent unburnt area existed in the burnt area, it was calculated that 3 – 15 kBq m⁻² of ¹³⁷Cs (corresponding to 1.5 – 5.8% of the ¹³⁷Cs deposition amount in the burnt area) outflowed at the time of the fire or immediately after the fire.
- The deposition amount of ¹³⁷Cs in soil layer did not change for any investigated forests.
- From the results of the monitoring that had been conducted for about half year from two months after the fire, it was revealed that the amount of outflow material and ¹³⁷Cs at the burnt site was about thirteen times larger than that at the unburnt site.
- The outflow rate of ¹³⁷Cs at the burnt site was calculated to be 2.6%. Although the value was relatively high among the existing observation data, it was within the range of the existing observation data. Therefore, the considerable increase in the outflow rate was not observed.
- The forest floor coverage at the burnt site recovered to 50% range in the end of November 2017, but there was still large difference from the outflow rate at the unburnt site.

- For the forest fire investigated in the present study, the abovementioned results indicated that the main cause of the changes in the ^{137}Cs distribution and outflow situation was the burning of the litter layer and understory vegetation covering the forest floor. Thereby, it is considered that the preparation of the environment that will promote the recovery of the forest floor coverage is important to reduce the outflow of radioactive cesium.

As future subjects, we consider the following research will be important. First, we should estimate the time duration of the effect of the fire by the tracking monitoring of the outflow situation accompanied by the recovery of the forest floor. Secondly, we should estimate the effect of the existing state of radioactive cesium which was considered to be changed by the fire on the migration behavior of cesium in forests.

6.5 Evaluation of effluent effect on the downstream region by the mountain forest fire

6.5.1 Objectives

A mountain fire occurred in April 2017 in Mt. Juman, Namie Town located in the difficult-to-return zone, so it was concerned that radioactive cesium would be scattered to the surrounding areas. Since the evacuation order of the city area in Namie Town had been cancelled just a month before the fire, it was deeply concerned that the radiation would affect the living space of the residents.

Incidentally, JAEA had been investigating the environmental dynamics of radioactive cesium in the Ukedo River and the Maeda River which flow in Namie Town and Futaba Town. Therefore, JAEA started to investigate the effect of the fire just after the fire, and evaluated the effects of the mountain fire on the discharge to the downstream region based on the comparison with the results obtained before the fire. Further, the additional investigation was conducted for two reservoirs at the foot of Mt. Juman (Ishikuma sand-trap dam and Shirasago reservoir). The accumulation situation of radioactive cesium on the bottom of the reservoirs was also investigated.

6.5.2 Methods

The investigated spots are shown in Fig. 6.5-1. The investigation had been conducted for the Ukedo River at the confluence of the branch rivers flowing from Mt. Juman. The investigated places were the TAKR-3 spot of the Takase River and the MAER-6 spot of the Maeda River. The TAKR-3 spot is located in the area where the evacuation order was cancelled in March 2017. On the other hand, the MAER-6 spot was located still in the difficult-to-return zone at that time, but the area was certified as a “Special Reconstruction and Revitalization Zone” in September 2017 and the evacuation order of this area was expected to be cancelled within five years. The investigation of the reservoirs was conducted at the Ishikuma sand-trap dam and Shirasago reservoir which are located in the difficult-to-return zone at the foot of Mt. Juman. The rivers discharging from both reservoirs join the Maeda River

and the Takase River, respectively, at the several km downstream.



Fig. 6.5-1 Investigation spots and the location of Mt. Juman.

For the investigation of rivers, the following three items were investigated; (1) concentration of radioactive cesium in river water, (2) air dose rate at flood plain, and (3) depth distribution of radioactive cesium concentration at flood plain. The contents of each item are as follows.

(1) Concentration of radioactive cesium in river water

At the time of normal water level, river water of 20 L was collected from the bridge using a bucket and rope. The sampling had been conducted once a month before the fire, and twice a month after the fire. Also samples were collected in 2016 and 2017 at the time of flood (three times in each year). The particulate and dissolved components in the sample were separated using a membrane filter (pore size: 0.45 μm). The particulate component on the filter was dried at 90°C for 90 min, and weighed. Cesium in the dissolved component was concentrated using nonwoven fabric impregnated with potassium zinc ferrocyanide (Yasutaka et al., 2015)⁶⁹. The concentration of ^{137}Cs in the samples on the filter and the nonwoven fabric was determined by a Ge semiconductor detector.

(2) Air dose rate at flood plain

At the flood plain, five side lines were set so as to be perpendicular to the flow direction. The interval of the lines was about 10 m. The air dose rate was measured at 1 m height along the line at 1-2 m interval using a gamma plotter H (Mimura et al. 2012)⁷⁵. The measured air dose rate was recorded together with the location information obtained by GPS. The measurements were conducted once in a 1-2 months.

(3) Depth distribution of radioactive cesium concentration at flood plain

Soil in flood plain was collected up to 30 cm depth at the 1 cm interval using a scraper plate. The ^{137}Cs concentration was determined by a Ge semiconductor detector. The sampling had been conducted during November 2016-January 2017 (before the fire) and November

2017-January 2018 (after the fire).

The investigation of reservoirs was carried out in September 2017. Core samples of 7-20 cm were collected at the inflow point and the center of the reservoir using an HR type core sampler (Rigo, Japan). The samples were divided at 1 cm interval, and the concentration of ^{137}Cs was determined by a Ge semiconductor detector. Further, reservoir water of 20 L was collected at the outflowing part, and the ^{137}Cs concentration in particulate and dissolved components was determined similarly to the abovementioned river water.

6.5.3 Results and discussion

Figs. 6.5-2 and 6.5-3 show the temporal changes in the ^{137}Cs concentration in river water at the time of normal water level for the Takase River and the Maeda River, respectively. For both rivers, the ^{137}Cs concentration in particulate and dissolved states had been changing with a certain degree of variation. For the dissolved ^{137}Cs concentration, the seasonal fluctuations were observed (refer to section 3.3). Since a clear increase in the concentration was not observed just after the fire (water sample was taken on May 10, 2017), it is hard to consider that the initial discharge had influenced the concentration of ^{137}Cs in the downstream region. Also, since the significant difference in the ^{137}Cs concentration was not observed between before and after the fire, it was confirmed that the materials with high ^{137}Cs content did not continue to flow out. From the data on the concentration of particulate ^{137}Cs at the time of water discharge (Table 6.5-1), the same conclusion can be derived.

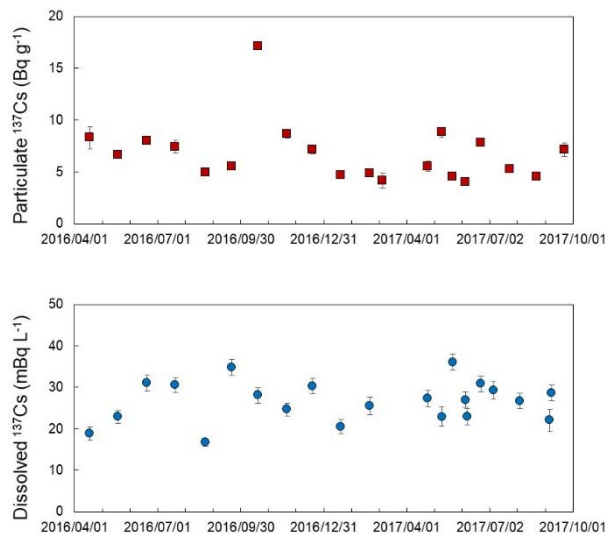


Fig. 6.5-2 Concentration of ^{137}Cs in water of the Takase River at the time of normal water level (upper: particulate state, lower: dissolved state).

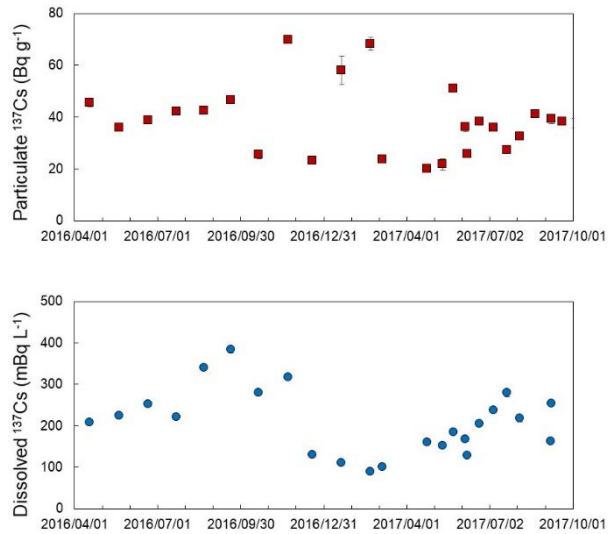


Fig. 6.5-3 Concentration of ¹³⁷Cs in water of the Maeda River at the time of normal water level (upper: particulate state, lower: dissolved state).

Table 6.5-1 Concentration of particulate ¹³⁷Cs (Bq kg⁻¹) in the Takase River and the Maeda River at the time of the water discharge (Bq kg⁻¹).

year	Takase River	Maeda River
2016	3.7 ± 1.2 (n = 3)	50 ± 14 (n = 3)
2017	3.2 ± 1.8 (n = 3)	54 ± 20 (n = 3)

Figs. 6.5-4 and 6.5-5 show the temporal changes in the distribution of air dose rate at the flood plains of the Takase River and the Maeda River, respectively. The difference in the air dose rate distribution was not observed between March 2017 (before the fire) and May 2017 (after the fire). It is understood that the scattering of radioactive cesium by the dust at the time of the fire did not influence the living space. Also, since the increase in the air dose rate was had not been observed until November 2017, it is considered that the water discharge event scarcely influenced the scattering of the radioactive cesium. Figs. 6.5-6 and 6.5-7 show the temporal changes in the depth distribution of ¹³⁷Cs at the investigated flood plains. For both flood plains, the tendency of the ¹³⁷Cs depth distribution hardly changed between before and after the fire. Therefore, it can be regarded that there was no increase in the ¹³⁷Cs concentration in deposited sediment or increase in the amount of the deposited sediment.

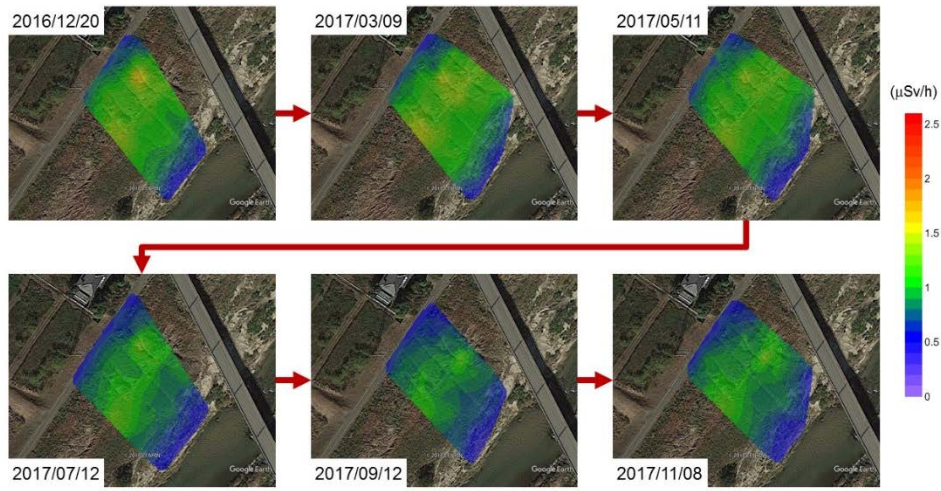


Fig. 6.5-4 Air dose rate at the flood plain of the Takase River.

Google Earth ©2018 ZENRIN.

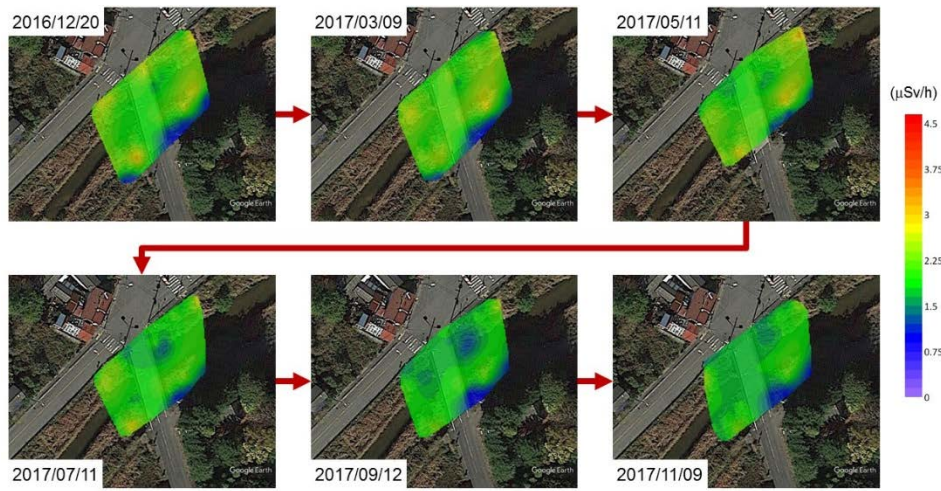


Fig. 6.5-5 Air dose rate at the flood plain of the Maeda River.

Google Earth ©2018 ZENRIN.

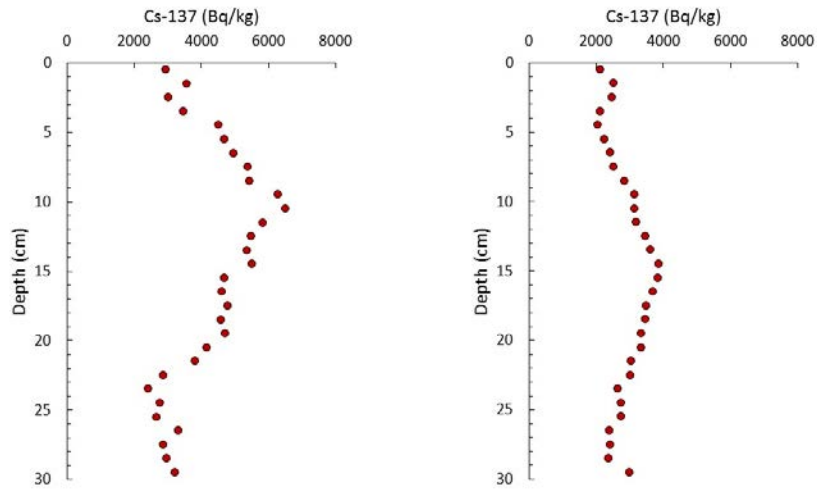


Fig. 6.5-6 Depth distribution of ^{137}Cs concentration at the flood plain of the Takase River.
(left: as of January 13, 2017, right: as of November 16, 2017)

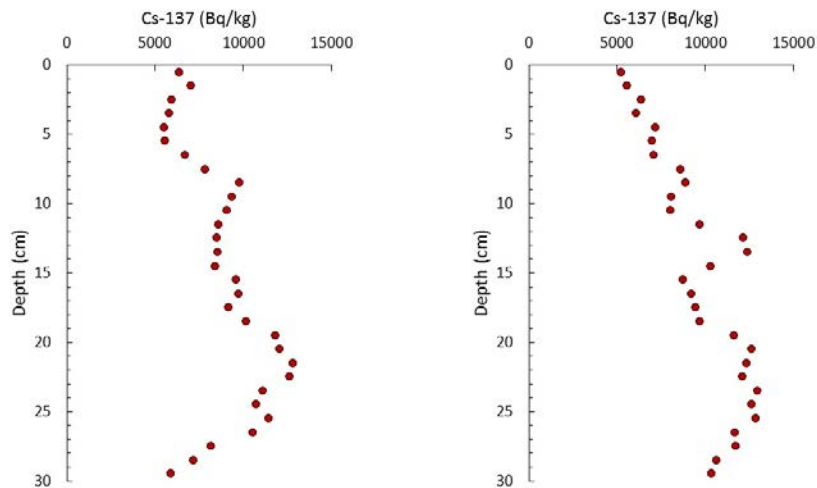


Fig. 6.5-7 Depth distribution of ^{137}Cs concentration at the flood plain of the Maeda River.
(left: as of November 17, 2016, right: as of January 9, 2018)

From the above results, it was confirmed that the discharge of radioactive cesium due to the mountain fire did not influence the living space in the downstream. Then, we investigated the possibility that the radioactive cesium accumulated in the reservoirs located at the middle of the downstream. The observation results at the Ishikuma sand-trap dam and Shirasago reservoir are presented in Figs. 6.5-8 and 6.5-9. For the Ishikuma sand-trap dam, sediment tends to be deposited at the center of the lake, so the ^{137}Cs deposition after the earthquake was observed up to 20 cm depth. Since the burnt areas of the fire at Mt. Juman are mostly located in the river basis of the Ishikuma sand-trap dam, it is considered that the influence of the mountain fire on the discharge of radioactive

cesium can be easily observed. However, the concentration peak was not observed in the ^{137}Cs depth distribution at the center of the lake. Therefore, it is considered that there was scarcely any effect of the fire on the discharge of radioactive cesium. In Shirasago reservoir, there were two kinds of bottom ^{137}Cs distribution. One is sandy bottom at the inflow part where deposition of thick sediment with low ^{137}Cs concentration was observed, and the other is muddy bottom at the center of the reservoir where deposition of thin sediment with high ^{137}Cs concentration was observed. However, we could not specify the part where the fire influenced the discharge of radioactive cesium.

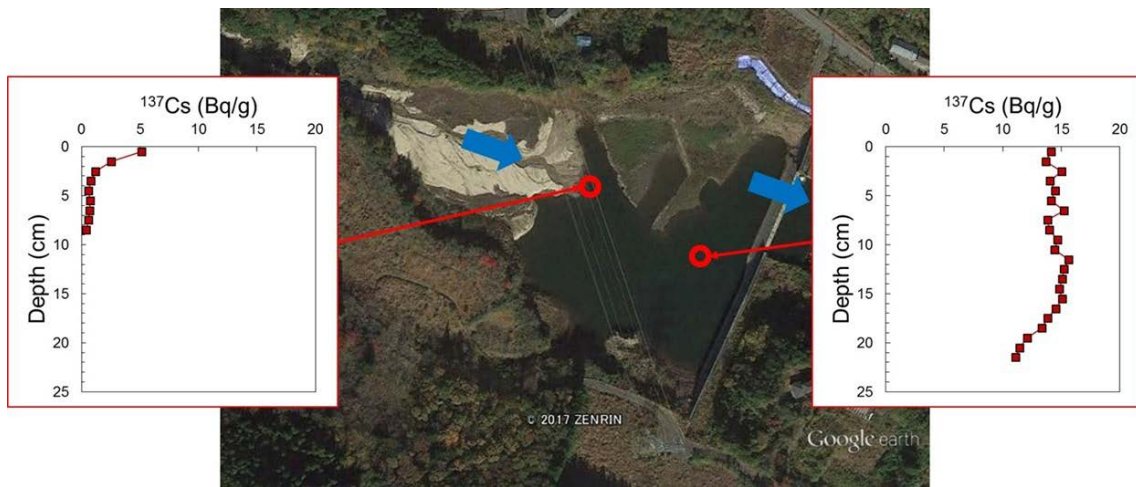


Fig. 6.5-8 Depth distribution of ^{137}Cs concentration at the bottom sediment of Ishikuma sand-trap dam (left: inflow part, right: center of the lake).

Google Earth ©2017 ZENRIN.



Fig. 6.5-9 Depth distribution of ^{137}Cs concentration at the bottom sediment of Shirasago reservoir (left: inflow part, right: center of the lake).

Google Earth ©2017 ZENRIN.

6.5.4 Future subjects

From the present investigation results, two possible reasonings are considered; (1) the discharge amount of radioactive cesium increased due to the forest fire, and (2) the ^{137}Cs concentration in the effluent was not so high. However, from the results shown in section 7.2, it was confirmed that the discharge rate of ^{137}Cs at the burnt area was about thirteen times larger than that at the non-burnt area, and the concentration of ^{137}Cs in the effluent at the burnt area became high. The result denies the above reasonings (1) and (2), and lead to the other conclusion, that is, (3) the ratio of the burnt area against the river basin was considerably low (10%). Namely, the present fire incidentally did not influence the discharge of radioactive cesium into the downstream region, which means that the future fire will not necessarily lead to the same results. Therefore, it is an urgent subject to construct a system that can evaluate the effect of the future fire on the downstream region.

7 Comprehensive evaluation system

7.1 Outline

Radioactive materials have been widely distributed in the environment after the accident. Among various radioactive materials released in the environment, JAEA has extensively investigated the distribution of radioactive cesium and associated air dose rates from the accident to present (investigation on distribution status of radioactive materials)¹⁹⁴⁾.

On the other hand, it has been clarified that most of radioactive cesium deposited on ground remains in forests that have not been decontaminated. Hence, we have been conducting environmental dynamics research to investigate and evaluate the effects of radioactive cesium focusing on; 1) the effects on air dose rate due to the migration of radioactive cesium by rain erosion of forest floors and its deposition on flood plains (from the viewpoint of external exposure), and 2) the effects on agricultural, forest, and fishery products due to the outflow of dissolved cesium from forests (from the viewpoint of external exposure). The objectives of these studies are to understand the phenomena that have occurred up to present, clarify its mechanism, construct a phenomenological model based on the results, and confirm the reproducibility of the model by simulation, thereby, to complement the region without data by estimation, or estimate the temporal changes. Such phenomenological model has advantages; 1) we can analyze sudden events (e.g. typhoon) which cannot be dealt with by statistical models, and 2) the model is possibly applied to the estimation of main factors influencing the phenomena and the confirmation of effectiveness for countermeasures such as decontamination because the virtual case study can be conducted.

JAEA has been developed "comprehensive evaluation system", which provides information based on scientific evidences (Saito et al., 2018)¹⁹⁵⁾. This system is consisted of three components below; "environmental monitoring database", "environmental restoration knowledge base" and "integrated analysis supporting environment" (Saito et al., 2018)¹⁹⁵⁾.

JAEA has been compiling and releasing information on the distribution of deposited radioactive cesium in the environment and air dose rates, which have been obtained by the government, municipalities, and the Tokyo Electric Power Company Holdings Inc. as the "environmental monitoring database", focusing on the information obtained in the investigation on the status of radioactive-material distribution. From May 2016, the information on the results obtained by the environmental dynamics research has been registered in this database. Also, JAEA has been releasing easy-to-understand information on the answers to the questions which the residents want to know including the information on grounds for answers, as the "environmental restoration knowledge base" (open: March 2016, renewal: March 2018).

The above information is the summary of knowledge that has been obtained from the accident to present. However, the evacuation order in most of the municipalities except for the difficult-to-return zones had been cancelled before April 2017. Therefore, it will become needed from now to present information that is helpful to promote the residents' return.

Under such circumstances, it is essential to develop a method for the future estimation based on the accumulated data and consider the countermeasures through various case studies. Therefore, we plan to prepare the "integrated analysis supporting environment", where users view the results of the analytical studies and perform the future estimation using analytical models. We published the "database for analysis examples" in March 2019, where the results of the analytical studies are aggregated (<https://simu.jaea.go.jp/simulations/>).

Three sites above, the environmental monitoring database, the environmental restoration knowledge base, and the database for analysis examples, systemically arranged past, present and future information about the radioactive concentrations and air dose rate. These sites are named “Fukushima Comprehensive Environmental Information Site”, FaCEIS (Fig. 7.1-1).

Using the present system, we present and frequently update the results obtained from real data on monitoring/investigation and future prediction by the analytical simulation as information based on scientific ground. Thereby, we will use the system for planning of evacuation-order cancellation and residents’ return by the local governments, and making reasonable safety measures for radiation dose reduction.

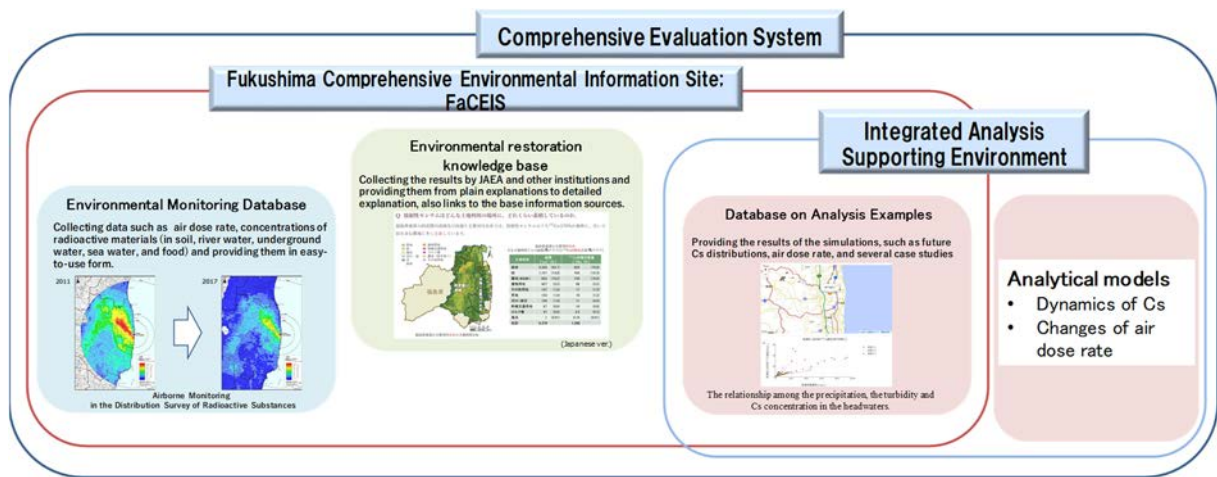


Fig. 7.1-1 Conceptual diagram of comprehensive evaluation system.

7.2 Environmental monitoring database

After the accident, many organizations such as the government, Fukushima Prefecture, universities, and the other institutes have been investigating the distribution of radioactive materials and air dose rates, and concentration of radioactivity in living thing. Although a large amount of data has been obtained by these institutes, the problem is that the objects of these studies are too versatile. For this reason, the users of the data (researchers) cannot understand where the data they need are. In addition, the data format has not been unified, resulting in the low availability. Under these circumstances, in the environmental monitoring database (<https://emdb.jaea.go.jp/emdb/>), JAEA has been collecting, compiling and releasing the information on the results of air dose rates and concentration of radioactivity in soil, topsoil, sea water, river water, low-land soil, underground water, and foods, which have been obtained by JAEA and the other institutes, with a unified format (CSV format in UTF-8 and Shift-JIS). Also, the released data have been visualized so that the users can instinctively understand the situation. Fig. 7.2-1 shows the example where the investigation results of aerial monitoring are displayed on the environmental monitoring database. As shown in the figure, we can see the visualized images in time series as well as expand the images.

As described above, the information that has been obtained in the environmental dynamics research by JAEA (investigation of dams, estuaries, rivers and forests) is also being registered and released.

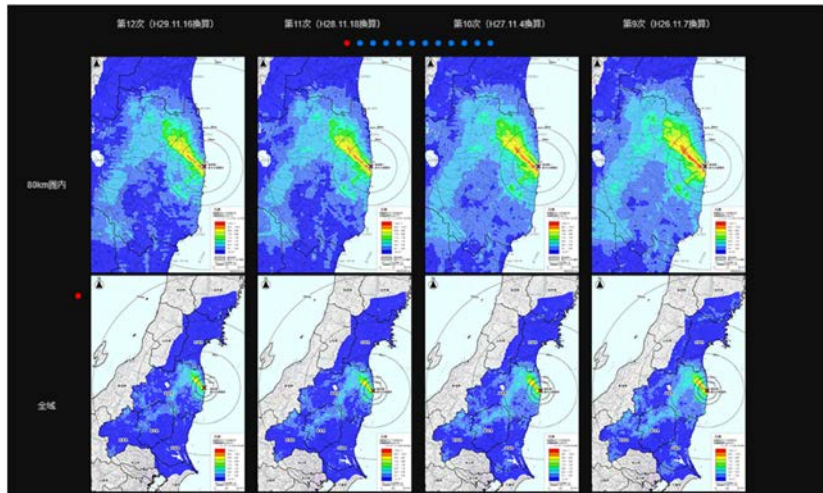


Fig. 7.2-1 Displayed example of environmental radiation monitoring database (measurement results of air dose rates by aerial monitoring).

7.3 Integrated analysis supporting environment

7.3.1 Outline

As shown in chapter 5, JAEA is developing tools to evaluate the behavior of cesium in environment and air dose rate based on various analytical research. In such analysis based on the model calculation, there are uncertainty and errors accompanied by the model and input data. Therefore, it is necessary to present the analytical results in a set with such information. Accordingly, we compiled the results obtained by the tool and present as “database on analysis examples”, while being separate from the environmental monitoring database based on the measured values, and presented. In the analysis example base, the analytical results are presented for each result.

River basin

- How much soil and accompanying radioactive cesium outflowed after the accident?
- What characteristics of the river basin influence the amount of radioactive cesium outflow?
- How will the turbidity (degree of muddiness) and radioactive cesium concentration of water change depending on the intensity of rainfall?
- From where and how much radioactive cesium flows out from the river?

Dam lake

- What are the characteristics of the behavior of radioactive cesium in dam lake?

Flood plain • Estuary

- Where is radioactive cesium easy to accumulate in rivers?
- How does radioactive cesium carried in the river move in the ocean?

Depth profile of radioactive cesium in soil

- What is the mechanism of radioactive cesium migration to underground?

Evaluation of air dose rate

- Based on the current knowledge, how is the air dose rate assumed to change?
- What is the range of radioactive cesium affecting the air dose rate in flat land?

- What will be the air dose rate in consideration of topography and ground structures?
- How will the air dose rate be reduced by the decontamination? (difference depending on decontamination method)
- How much air dose rate can be reduced by the decontamination in the specific restoration base?
- How will the air dose rate change due to the distribution of radioactive cesium in forests?

Evaluation of agricultural, forest and fishery produces

- How will be the temporal change in the distribution of radioactive cesium in forests?
- Where did radioactive cesium in freshwater fish come from?

Migration of radioactive cesium in environment

- To what extent does radioactive cesium move in the environment?

Then, we constructed a framework where we can inspect the “situation for model development and uncertainty” so that we can understand how much uncertainty and errors are in the respective results (see the chapter 5 for details).

On the other hand, for local governments etc. who need to estimate the circumstances of several years later even if there remains uncertainty, we constructed an environment where several tools can be used so that the case studies can be implemented. The contents to be implemented in this environment will be described below.

7.3.2 Analytical models

As information requested by the returning residents, it is necessary to present not only wide-area maps of future air dose rates presented by the analysts but also individual and specific future information such as the air dose rate at a specific place and concentration of radioactive cesium in freshwater fish. For this purpose, it is essential to estimate the future situation using the models developed on the basis of the abovementioned environmental dynamics research. As to the air dose rate at a specific place, we have developed a model that can estimate the amount of deposited radioactive cesium and air dose rate at each place with resolution of several 10 m × several 10 m. Concerning the agricultural, forest, and fishery products, we are developing a model that can estimate the concentration of radioactivity in these products per each river although the data represent the averaged amount in the area of several km × several km resolution.

For air dose rate at a specific place, we focused on the fact that the redistribution of radioactive cesium is mainly dominated by the migration of cesium adsorbed on sediment. Therefore, we evaluated the air dose rate by the program that can calculate such migration process. Two programs that can estimate from different sides were prepared for this calculation. One is the program that can conduct the long-term estimation of annual mean data, and the other is the program that can estimate the changes depending on the strength of short-term rain. The former program is called SACT (Soil And Cesium Transfer), which analyzes the changes in the distribution of radioactive cesium migrating with soil. Based on the analysis, the program shows maps of changes in radioactive-cesium deposition and associated air dose rate changes on display (resolution of the map: 100 m×100 m) in order to correspond to the residents’ needs that they want to know the long-term radiation exposure in future after returning home (Yamaguchi et al., 2013)¹²⁹). Further, the program can estimate the accumulated radiation by giving the decontamination coefficients at a specific place, in order to

correspond to the needs to know the future changes of accumulated radiation after the decontamination (Fig. 7.3-1).

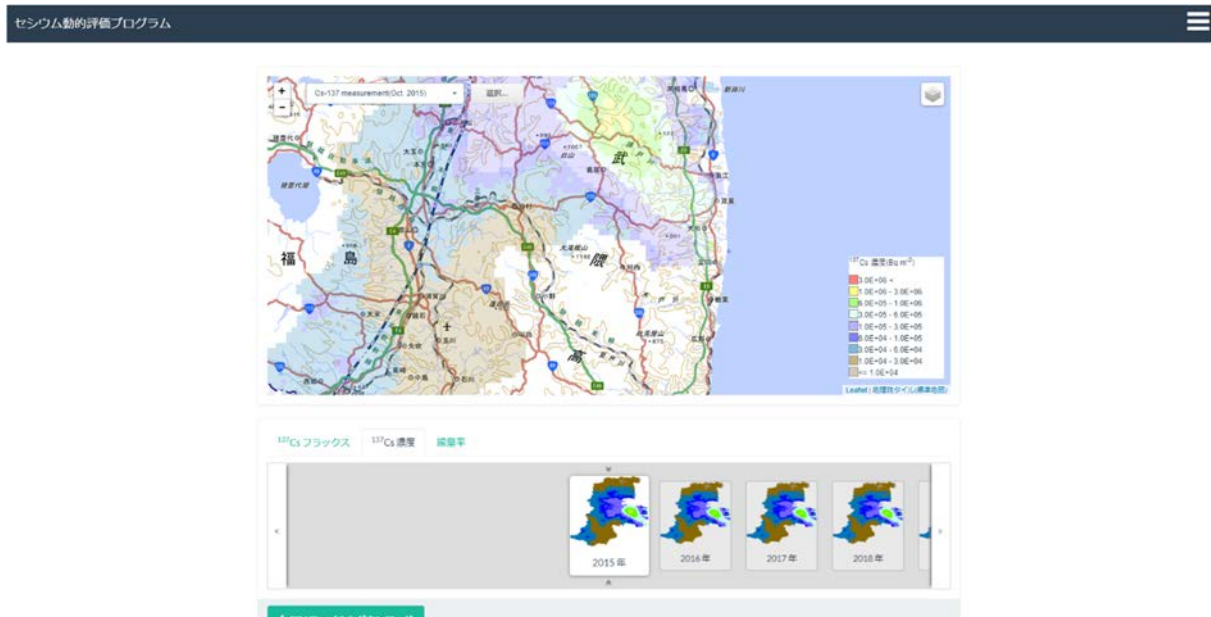


Fig. 7.3-1 Example of the analytical results (concentration of radioactive cesium) by SACT displayed on a web browser.

On the other hand, concerning the effects of short-term changes in rainfall by typhoon etc., there remains residents' anxiety as to whether or not large amount of soil with radioactive cesium flows out from forest floors, rivers, and bottom of dam lakes at the time of heavy rain. As a simulation tool that can analyze such short-term events, we are conducting investigation using the GETFLOWS (GENERAL purpose Terrestrial fluid-FLOW Simulator; Geosphere Environmental Technology Corp.) (e.g., Sakuma et al., 2018¹⁴⁹). Using the GETFLOWS, we can analyze the short-term migration of radioactive cesium at the events such as heavy rain. Herewith, the radiation map can be displayed (resolution of the map: 30 m×30 m around river, and about 100 m×100 m in deep mountain) in order to correspond to the needs such as to estimate where radioactive cesium remains depending on the strength of rainfall. Further, we can show the graphs of time-dependence of concentration in order to correspond to the needs such as to estimate how concentration of radioactive cesium in river water used for agriculture change depending on the strength of rainfall.

As to the latter question, it is needed to consider wide-range phenomena with different scale and mechanism such as the circulation in forests (tree crown, litter layer, and soil layer), the migration into forest products, the deposition of radioactive cesium flowing out from forests on river beds, flood plains and lake bottoms, and the cesium migration into fish and shellfish. To conduct such analysis, the simple compartment model is suitable. In this model, various parts in the environment are first divided into elements (here, the element is called “compartment”), then the migration of radioactive cesium among the compartments are calculated by multiplying the coefficients such as migration rate, migration coefficient, and concentration factor. Accordingly, JAEA developed the compartment model (CMFW: Compartment Model for Forests and Water) that is the combination of the forest model with the river system model. Using this model, it has

become possible to analyze the concentration of radioactive cesium in various things (trees, forest products, fishery products, etc.) in the environment (Kurikami et al., 2016)¹⁴⁴). This model presents approximate order-level evaluation (resolution of the evaluation: 1 km×1 km - 10 km×10 km for river basin) in order to correspond to the needs such as to evaluate the status of radioactive cesium in various parts in the environment including agricultural, forest, and fishery products for every river (Fig.7.3-2).

In order to clearly present the analytical results based on these needs, the results are displayed on the map, then we can see the results focusing on the condition of the place where we want to know (for example, concentration of radioactive cesium and associated air dose rate in the residential area and long stay place of the user, concentration of radioactive cesium in a river after heavy rain, etc.). In the CMFW, we can refer to the future estimation values by showing the graphs for calculated results of concentration per each upstream and downstream of a main river (for example, concentration in mushroom at a certain place, sweetfish “Ayu” in the upstream of a river, etc.). However, it should be noted that there remain subjects to be solved, such as the effect of dynamics of dissolved cesium, the reproducibility of measured data, etc. Therefore, we plan to upgrade the models according to the progress in the research including the scope of the presented results.

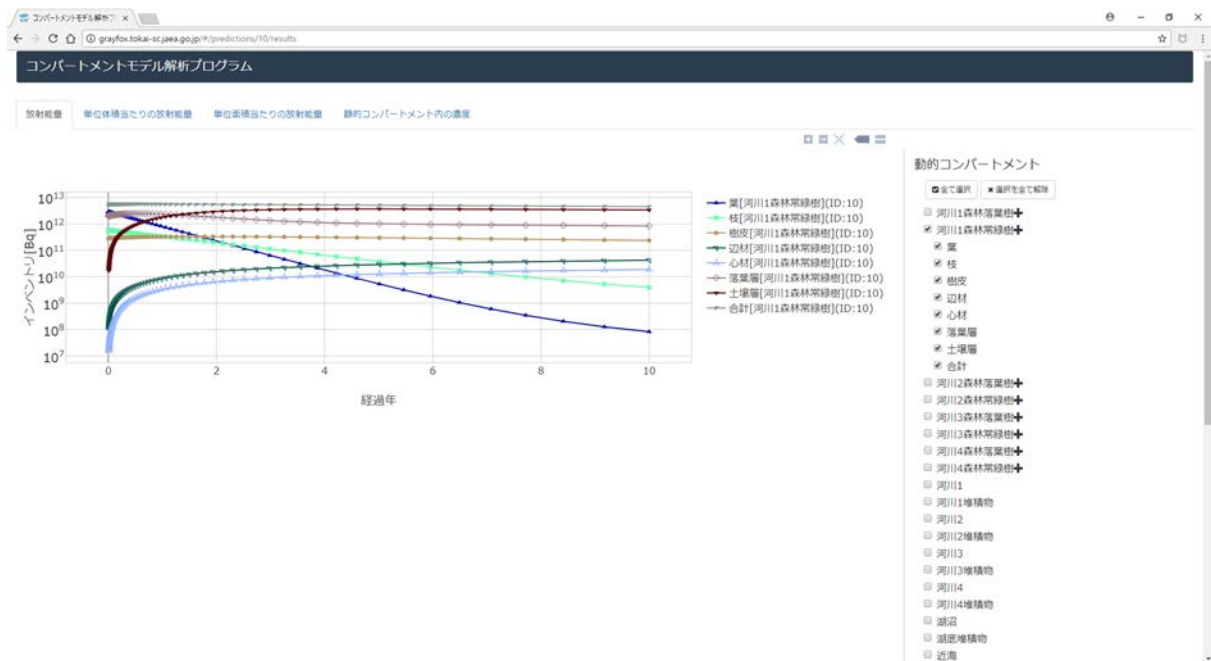


Fig. 7.3-2 Example of the displayed analytical results (amount of radioactivity in forest) by CMFW on a web browser.

In order to ensure the accuracy and validity of the analytical results, the accuracy and validity of the input values and the boundary conditions are also important factors. Therefore, in the preparation towards the release of the support environment for comprehensive analysis, we are constructing the abovementioned framework to use data taken from the environmental radiation monitoring database as input values in the tools. Also it should be noted that the information that a user wants to obtain is versatile depending on the interest of the user. For example, some users do not intend to analyze the result by themselves, but simply

want to know the situation including the interpretation of the results. For these users, it is necessary not only to present the analytical results on the support environment for comprehensive analysis but also to properly reflect the associate knowledge on the environmental restoration knowledge base. For this purpose, we plan to add the question-and-answer (Q&A) based on the analytical results at the time of renewal in the end of FY2018. Also, it is needed to consider the framework where the results observed by the user can be linked to the original analytical results.

7.4 Environmental restoration knowledge base

In order to reflect the measured data and associated knowledge by the analysis on the residents' return and the countermeasures by the local governments, it is not enough to simply publish the results in reports and scientific papers. The important point is rather to construct an environment where the obtained results are released and explained with easy-to-understand words. For this purpose, JAEA opens a "Base Information Q&A Site" (<https://fukushima.jaea.go.jp/QA/>) as the environmental restoration knowledge base. In this website, the knowledge obtained in the Fukushima Environmental Dynamics Research is arranged and released in the question-to-answer form. It has passed seven years after the accident, so some of the residents have already obtained detailed knowledge. Therefore, the level of knowledge that should be released has widely expanded compared with the past. In order to correspond to the wide range of the users, the multiple stages are presented in the environmental restoration knowledge base depending on the knowledge and interests of the users. These stages are; answering to the question with easy-to-understand words (the first stage), explaining by one page or more slides with a little detailed figures, tables and photographs (the second stage), explaining the specific and detailed information by text (the third stage), and presenting the links to the base information source (scientific papers, reports, website of government offices, etc.) (the fourth stage) (Fig. 7.4-1). Using these four stages, the users can obtain the information they want by accessing one of the stages which they can understand. Further, if necessary, the users can obtain the route to access the basic information source.

8. Future Subjects

This report contains the results of the researches and studies about the radioactive cesium dynamics in the forests, river system, the urban area, modeling researches based on the results of researches, unexpected event of the mountain fire and the framework for information disclosure. Knowledge gained from our researches is summarized in 1.3 and Table 1.1.

We are continuing the researches and studies focusing below.

- Forest dynamics
 - Estimation of the contribution of sap on the Cs concentration in the trees
 - Tendency of the change of the radioactive cesium inventory and the concentrations in each part of the trees
- Dynamics in river system
 - Research of the dissolved Cs concerning not only watershed inventory but also the effect of vegetation
 - Continuing the observation of the rivers where the Cs concentration in fresh water fish exceeds the reference value
 - Estimation of the amount of the mineral species in river basin and their potential of sorption of Cs
 - Quantitative analysis of the deposition and remobilization behavior in the river mouth and estuary
- Urban area
 - Relationships between the characteristic of air dose rate decreasing and Cs behavior in the urban area
 - Quantitative evaluation of the urban area specific weathering effect
- Modeling research
 - Incorporating the phenomena that is now insufficiently concerned, e.g., migration in vertical direction, origin of the dissolved Cs, thermocline, leaching from deposits, flocculation and improvement of the reproducibility of the measured values
 - High resolution of the dose rate analysis
- Forest fire
 - Estimation of the duration of effect of the forest fire by monitoring the run-off and recovery of the coverage on forest bed
 - Estimation of the effect on migration behavior of the Cs in forest by the Cs form which might change by forest fire.
- Comprehensive evaluation system
 - Continuing addition of the new data and knowledge in the system
 - Improvement of the assessment models corresponding to progress of the modeling research
 - Improvement of the usability of the system reflecting needs of users

Acknowledgement

We would thank the local governments of Fukushima prefecture, cities, towns, and villages in Fukushima prefecture and relevant organizations in and out of the prefecture for their supports on our researches and studies in this report.

In modelling research, we would thank Dr. Yasuo Onishi, Director of Fukushima Reconstruction Creation Laboratory, Higashi Nippon International University, for providing us TODAM, FLESCOT and technical support. We would also thank Dr. Yasuyuki Shimizu, Professor of Hokkaido University, providing us Nays2D.

In chapter 6, “6.4 Dynamics of forest floor” is a part of the result of the joint investigation of three institutes in Fukushima Prefectural Centre for Environmental Creation (CEC), Fukushima Branch of National Institute for Environmental Studies (NIES), Research Department of CEC and Fukushima Environmental Safety Center of JAEA. The researchers of Fukushima Branch of NIES and Research Department of CEC made great effort on this work. We would thank them all.

References

- 1) Kitamura, A., Yamaguchi, M., Kurikami, H., Yui, M. and Onishi, Y., Predicting Sediment and Cesium-137 Discharge from Catchments in Eastern Fukushima, *Anthropocene*, vol.5, 2014, pp.22-31.
- 2) Nuclear Regulation Authority, Japan, Results of the twelfth airborne monitoring and airborne monitoring out of the 80 km zone of Fukushima Dai-ichi NPP (20th February 2018), 2018.
http://radioactivity.nsr.go.jp/ja/contents/14000/13500/24/180220_12th_air.pdf <access date 7th Aug. 2018> (in Japanese).
- 3) Nuclear Regulation Authority, Extension Site of Distribution Map of Radiation Dose, etc.
<https://ramap.jmc.or.jp/map/> <access date 20th Sept. 2018>.
- 4) Ministry of Agriculture, Forestry and Fisheries, Japan, The 88th Statistical yearbook of Ministry of Agriculture, Forestry and Fisheries Japan, 2014.
http://www.library-archive.maff.go.jp/index/200418770_0001 <access date 10th Jul. 2019> (in Japanese).
- 5) Japan Aerospace Exploration Agency Earth Observation Research Center, Homepage of high-resolution land use and land cover map products (whole Japan, ver.12.08),
http://www.eorc.jaxa.jp/ALOS/lulc/lulc_jindex_v1208.htm <access date 20th Sept. 2018> (in Japanese).
- 6) Japan Meteorological Agency, Past weather data retrieve,
<https://www.data.jma.go.jp/obd/stats/etrn/index.php> <access date 10th Jul. 2019> (in Japanese).
- 7) National Astronomical Observatory of Japan (ed.), Chronological Scientific Tables 2017 (Rika Nenpyo 2017), Maruzen Publishing Co.,Ltd., Tokyo, 2016. (in Japanese).
- 8) Chino, M., Nakayama, H., Nagai, H., Terada, H., Katata, G. and Yamazawa, H., Preliminary Estimation of Release Amounts of ¹³¹I and ¹³⁷Cs Accidentally Discharged from the Fukushima Daiichi Nuclear Power Plant into the Atmosphere, *Journal of Nuclear Science and Technology*, vol. 48, 2011, pp.1129-1134.
- 9) Niizato, T., Abe, H., Mitachi, K. Sasaki, Y. Ishii, Y. Watanabe, T., Input and output budgets of radiocesium concerning the forest floor in the mountain forest of Fukushima released from the TEPCO's Fukushima Dai-ichi nuclear power plant accident, *Journal of Environmental Radioactivity*, vol.161, 2016, pp. 11-21.
- 10) Mahara, Y., Ohta, T., Ogawa, H. and Kumata, A., Atmospheric direct uptake and long-term fate of radiocesium in trees after the Fukushima nuclear accident, *Scientific Reports*, vol.20, no.4, 2014, DOI: 10.1038/srep07121.
- 11) Wang, W., Hanai, Y. and Ozawa, H., Cesium absorption through bark of Japanese cedar (*Cryptomeria japonica*), *Journal of Forest Research*, vol. 21, no.5, 2016, pp.251-258.
- 12) Kuroda, K., Kagawa, A. and Tonosaki, M., Radiocesium concentrations in the bark, sapwood and heartwood of three tree species collected at Fukushima forests half a year after the Fukushima Dai-ichi nuclear accident, *Journal of Environmental Radioactivity*, vol.122, 2013, pp.37-42
- 13) Kanasashi, T. et al., Radiocesium distribution in sugi (*Cryptomeria japonica*) in eastern Japan: translocation from needles to pollen, *Journal of Environmental Radioactivity*, vol.139, 2015, pp.398-

- 406.
- 14) Kuroda, K., Tree composition/structure and moisture conductance, *Green Age*, no.417, 2008, pp. 36-39 (in Japanese).
 - 15) Sasaki, Y., Abe, H., Mitachi, K., Watanabe, T., Ishii, Y. and Niizato, T., The transfer of radiocesium from the bark to the stemflow of chestnut trees (*Castanea crenata*) contaminated by radionuclides from the Fukushima Dai-ichi nuclear power plant accident, *Journal of Environmental Radioactivity*, vol.161, 2016, pp.58-65.
 - 16) Ito, S., Sasaki, Y., Niizato, T., Watanabe, T. and Mitachi, K., Radiocesium distribution of above- and under-ground parts of wild vegetable (*Eleutherococcus sciadophylloides*), *Proceedings of the 20th Workshop on Environmental Radioactivity*, 2019.
 - 17) Ishikawa, N., Uchida, S., Tagami, K., Effects of clay minerals on radiocesium sorption behavior onto paddy field soils, *Radioisotopes*, vol.56, 2007, pp. 519-528 (in Japanese with English abstract).
 - 18) Wakamatsu, T., Ikeda, H., Nakaya, K., Abe, S. and Saeki, A., Forest Floor Coverage Effects on Surface Runoff Generated on a Forested Slope, *Journal of Japan society of hydrology and water resources*, vol.29, no.2, 2016, pp.116-129.
 - 19) Watanabe, T., Oyama, T., Ishii, Y., Niizato, T., Abe, H., Mitachi, K., Sasaki, Y., Amount of radioactive cesium sedimentation in a soil saving dam with 3D laser scanner, *KEK Proceedings 2017-6 (Proceedings of the 18th Workshop on Environmental Radioactivity, KEK, Tsukuba, Japan, March 14 - 16, 2017)*, 2017, pp. 122-126.
 - 20) Ministry of Agriculture, Forestry and Fisheries, Japan, Press Release: FY2015 Investigation results for the distributional situation of radioactive materials in forest, 2016,
<http://warp.da.ndl.go.jp/info:ndljp/pid/11252077/www.rinya.maff.go.jp/j/kaihatu/jittaihaaku/zentai.html> <access date 10th Jul. 2019> (in Japanese).
 - 21) Kajimoto, T., Takano, T., Saito, S., Kuroda, K., Fujiwara, T., Komatsu, M., Kawasaki, T., Ohashi, S. and Kiyono, Y., 2014, Methods for assessing the spatial distribution and dynamics of radiocesium in tree components in forest ecosystems, *Bulletin of FFPRI*, vol. 13, no.3(no.432), 2014, pp. 113-136. (in Japanese with English abstract).
 - 22) Ministry of Land, Infrastructure, Transport and Tourism, Water Management and Land Conservation Bureau, Hydrological and water chemistry database.
<http://www1.river.go.jp/> <access date 17th Aug. 2018> (in Japanese).
 - 23) Nishikiori, T., Ito, S., Tsuji, H., Yasutaka, T., Hayashi, S., Influence of forest floor covering on radiocesium wash-off associated with forest soil erosion, *Journal of the Japanese Forest Society*, vol. 97, no.1, 2015, pp. 63-69.
 - 24) Wischmeier, W. H., and Smith, D. D., Predicting rainfall erosion losses – a guide to conservation planning, *Agriculture Handbook No.537.*, USDA, Washington D.C., 1978, 58p.
 - 25) Hillel, D., *Introduction to Environmental Soil Physics*, Elsevier (USA), 2003, 494p.
 - 26) Japan Meteorological Agency, 2015, Weather report at the time disaster: September 2015 heavy rainfall in the Kanto and Tohoku regions and heavy rainfall caused by Typhoon no.18 in 2015 (4th Dec. 2015)
http://www.jma.go.jp/jma/kishou/books/saigaiji/saigaiji_2015/saigaiji_201501.pdf <access date 12th Feb. 2020> (in Japanese).

- 27) Fukushima Prefecture, Fukushima Mori map, 2017,
<http://www2.wagmap.jp/fukushima-shinrin/Portal> <access date 14th Sept. 2018> (in Japanese).
- 28) Imamura, N., Komatsu, M., Ohashi, S., Hashimoto, S., Kajimoto, T., Kaneko, S., Takano, T., 2017,
 Temporal changes in the radiocesium distribution in forests over the five years after the Fukushima Daiichi Nuclear Power Plant accident, *Scientific Reports* vol. 7, 8179, 2017, DOI:10.1038/s41598-017-08261-x.
- 29) Forestry Agency, Ministry of Agriculture, Forestry and Fisheries, 2017,
http://www.rinya.maff.go.jp/j/kaihatu/jyosen/H29_jittaihaaku.html <access date 12th Sept. 2018> (in Japanese).
- 30) Shaw, G., Avila, R., Fesenko, S., Dvornik, A., Zhuchenko, T., Modelling the behavior of radiocaesium in forest ecosystems, In: Scott, E.M.(ed.) *Modelling Radioactivity in the Environment*. Elsevier Science Publishers, Amsterdam, Chapter 11., 2003, pp. 315-351.
- 31) Nuclear Regulation Authority, Investigation for radiocesium transfer situation in forested environment, Report for the FY2014 contracted investigation and measurement of radioactive materials: integration of distribution data and development of transfer model for radioactive materials associated with TEPCO's Fukushima Dai-ichi Nuclear power plant accident, part 2, 2015, pp. 108-143.
https://radioactivity.nsr.go.jp/ja/contents/11000/10921/36/2-1_H26forest.pdf <access date 7th Nov. 2018> (in Japanese).
- 32) Seaward, M. R. D., Lichens as monitors of radioelements, *Monitoring with Lichens: Monitoring Lichens*, Kluwer Academic Publishers, Dordrecht, 2002, pp. 85-96.
- 33) Nash III, T. H., Nutrients, elemental accumulation, and mineral cycling, In: *Lichen Biology*, 2008, pp. 236-253.
- 34) Koarashi, J., Atarashi-Andoh, M., Matsunaga, T., Sato, T., Nagao, S., Nagai, H., Factors affecting vertical distribution of Fukushima accident-derived radiocesium in soil under different land-use conditions, *Science of the total environment*, 2012, vol. 431, pp. 392-401.
- 35) Adachi, K., Kajino, M., Zaizen, Y., Igarashi, Y., Emission of spherical caesium-bearing particles from an early stage of the Fukushima nuclear accident, *Scientific Reports*, vol. 3, 2554, 2013.
- 36) Abe, Y., Iizawa, Y., Terada, Y., Adachi, K., Igarashi, Y., Nakai, I., Detection of uranium and chemical state analysis of individual radioactive microparticles emitted from the Fukushima nuclear accident using multiple synchrotron radiation X-ray analyses, *Analytical Chemistry*, 2014, vol. 86, no.17, pp. 8521-8525.
- 37) Yamaguchi, N., Mitome, M., Akiyama-Hasegawa, K., Asano, M., Adachi, K., Kogure, T., Internal structure of cesium-bearing radioactive microparticles released from Fukushima nuclear power plant, *Scientific Reports*., vol. 6, 20548, 2016.
- 38) Satou, Y., Sueki, K., Sasa, K., Adachi, K., Igarashi, Y., First successful isolation of radioactive particles from soil near the Fukushima Daiichi Nuclear Power Plant, *Anthropocene*, vol. 14, 2016, pp. 71-76.
- 39) Ono, T., Iizawa, Y., Abe, Y., Nakai, I., Terada, Y., Satou, Y., Sueki, K., Adachi, K., Igarashi, Y., Investigation of the chemical characteristics of individual radioactive microparticles emitted from reactor 1 by the Fukushima Daiichi Nuclear Power Plant accident by using multiple synchrotron radiation X-ray analyses, *BUNSEKI KAGAKU*, vol. 66, no. 4, 2017, pp. 251-261. (in Japanese).

- 40) Dohi, T., Ohmura, Y., Kashiwadani, H., Fujiwara, K., Sakamoto, Y., Iijima, K., Radiocaesium activity concentrations in parmelioid lichens within a 60 km radius of the Fukushima Dai-ichi Nuclear Power Plant, *Journal of Environmental Radioactivity*, vol.146, 2015, pp.125-133.
- 41) Dohi, T., Application of lichens for the record of Fukushima fallout, *JAEA R&D Review* 2015, 2016, p.15. ISSN(PRINT)2423-9992.
- 42) Ministry of Education, Culture, Sports, Science and Technology, 2011, Concentration map of radiocesium in soils in Fukushima Prefecture, <https://radioactivity.nsr.go.jp/ja/contents/6000/5043/view.html>. <access date 16th Jun. 2019> (in Japanese).
- 43) Ministry of Education, Culture, Sports, Science and Technology, 2011, Results of radionuclides (¹³⁴Cs and ¹³⁷Cs) in soils, http://www.mext.go.jp/b_menu/shingi/chousa/gijyutu/017/shiryo/_icsFiles/afiedfile/2011/09/02/1310688_1.pdf <access date 16th Apr. 2019> (in Japanese).
- 44) IAEA (International Atomic Energy Agency), Quantification of Radionuclide Transfer in Terrestrial and Freshwater Environments for Radiological Assessments, IAEA-TECDOC-1616, 2009, 624p.
- 45) Dohi, T., Fujiwara, K., Kikuchi, N., Hagiwara, H., Iijima, K., Radiation dose distribution of mountainous area around the Fukushima Daiichi Nuclear Power Plant (1) Field investigation, Abstract of annual meeting of Atomic Energy Society of Japan (AESJ). 2016, 2J22. (in Japanese).
- 46) Geospatial Information Authority of Japan, Basic map information, <http://www.gsi.go.jp/kiban/> <access date 16th Apr, 2019>.
- 47) Japan Aerospace Exploration Agency, AVNIR-2 High-Resolution Land use and Land Cover Map ver.16.02, http://www.eorc.jaxa.jp/ALOS/lulc/lulc_jindex.htm <access date 4th Apr. 2019>.
- 48) Oda, Y., Dohi, T., Kanaizuka, S., Iijima, K., Radiation dose distribution of mountainous area around the Fukushima Daiichi Nuclear Power Plant (2) Data analysis, Abstract of annual meeting of Atomic Energy Society of Japan. 2016, 2J23, (in Japanese).
- 49) Satou, Y., Sueki, K., Sasa, K., Yoshikawa, H., Nakama, S., Minowa, H., Abe, Y., Nakai, I., Ono, T., Adachi, K., Igarashi, Y., Analysis of two forms of radioactive particles emitted during the early stages of the Fukushima Dai-ichi Nuclear Power Station accident, *Geochemical Journal*, vol. 52, no. 2, 2018, pp.137-143.
- 50) Okumura, T., Yamaguchi, N., Dohi, T., Iijima, K., Kogure, T., Loss of radioactivity in radiocesium-bearing microparticles emitted from the Fukushima Dai-ichi nuclear power plant by heating. *Scientific Reports.*, 2018, vol. 8, 9707.
- 51) Tagomori, H., Ishii, Y., Kanaizuka, S., Dohi, T., Iijima, K., Examination of the isolation method of the radioactive microparticles in the environmental sample, Abstract of The Japan Society of Nuclear and Radiochemical Sciences 2017 Meeting, 2017, p.152.
- 52) Dohi, T., Tagomori, H., Ohmura, Y., Fujiwara, K., Kanaizuka, S., Iijima, K., Electron microscopic analysis of the radiocaesium micro particles in lichens collected around the Fukushima Dai-ichi NPP, Abstract of 13th International symposium on nuclear and environmental radiochemical analysis (ERA13), 2018, pp. 103-104.
- 53) Hanson W. C., Fallout radionuclide distribution in lichen communities near Thule, Arctic, 1971, Vol. 24, No.4, pp. 269-276.

- 54) Sawidis, T., Heinrich, G., Chettri, M. K., Cesium-137 monitoring using lichens from Macedonia, northern Greece, *Canadian Journal of Botany.*, vol. 75, no. 12, 1997, pp. 2216-2223.
- 55) Kogure T., Yamaguchi, N., Segawa, H., Mukai, H., Motai, S., Akiyama-Hasegawa, K., Mitome, M., Hara, T., Yaita, T., Constituent elements and their distribution in the radioactive Cs-bearing silicate glass microparticles released from Fukushima nuclear plant, *Microscopy*, vol.65, no.5, 2016, pp. 451-459.
- 56) Furuki, G., Imoto, J., Ochiai, A., Yamasaki, S., Nanba, K., Ohnuki, T., Grambow, B., Ewing, R. C., Utsunomiya, S., Caesium-rich micro-particles: A window into the meltdown events at the Fukushima Daiichi Nuclear Power Plant, *Scientific Reports.*, vol. 7, 42731, 2017.
- 57) Imoto, J., Ochiai, A., Furuki, G., Suetake, M., Ikehara, R., Horie, K., Takehara, M., Yamasaki, S., Nanba, K., Ohnuki, T., Law, G. T. W., Grambow, B., Ewing, R. C., Utsunomiya, S., Isotopic signature and nano-texture of cesium-rich micro-particles: Release of uranium and fission products from the Fukushima Daiichi Nuclear Power Plant, *Scientific Reports*, vol. 7, 5409, 2017.
- 58) Ochiai, A., Imoto, J., Suetake, M., Komiya, T., Furuki, G., Ikehara, R., Yamasaki, S., Law, G. T. W., Ohnuki, T., Grambow, B., Ewing, R. C., Utsunomiya, Uranium dioxides and debris fragments released to the environment with cesium-rich microparticles from the Fukushima Daiichi Nuclear Power Plant, S., *Environmental Science & Technology*, vol. 52, no.52, 2018, pp. 2586-2594.
- 59) Tsuji, H., Yasutaka, T., Kawabe, Y., Onishi, T., Komai, T., Distribution of dissolved and particulate radiocesium concentrations along rivers and the relations between radiocesium concentration and deposition after the nuclear power plant accident in Fukushima, *Water Research*, vol. 60, 2014, pp. 15-27.
- 60) Shinomiya, Y., Tamai, K., Kobayashi, M., Ohnuki, Y., Shimizu, T., Iida, S., Nobuhiro, T., Sawano, S., Tsuboyama, Y., Hiruta, T., Radioactive cesium discharge in stream water from a small watershed in forested headwaters during a typhoon flood event, *Soil Science and Plant Nutrition*, vol. 60, no. 6, 2014, pp. 765-771.
- 61) Tsuji, H., Nishikiori, T., Yasutaka, T., Watanabe, M., Ito, S., Hayashi, S., Behavior of dissolved radiocesium in river water in a forested watershed in Fukushima Prefecture, *Journal of Geophysical Research: Biogeosciences*, vol. 121, no. 10, 2016, pp. 2588-2599.
- 62) Murakami, M., Ohte, N., Suzuki, T., Ishii, N., Igarashi, Y., Tanoi, K., Biological proliferation of cesium-137 through the detrital food chain in a forest ecosystem in Japan, *Scientific Reports*, vol. 4, 2014, 3599, DOI: 10.1038/srep03599.
- 63) Sakai, M., Gomi, T., Negishi, J.N., Fallout volume and litter type affect ¹³⁷Cs concentration difference in litter between forest and stream environments, *Journal of Environmental Radioactivity*, vol. 164, 2016, pp. 169-173.
- 64) Nuclear Regulation Authority, Monitoring information of environmental radioactivity level, <http://radioactivity.nsr.go.jp/ja/list/362/list-1.html> <access date 25th Jun. 2018> (in Japanese).
- 65) Japan Aerospace Exploration Agency, Advanced land observing satellite, <http://www.eorc.jaxa.jp/ALOS/en/index.htm> <access date 25th Jun. 2018>.

- 66) Yoshimura, K., Onda, Y., Sakaguchi, A., Yamamoto, M., Matsuura, Y., An extensive study of the concentrations of particulate/dissolved radiocaesium derived from the Fukushima Dai-ichi Nuclear Power Plant accident in various river systems and their relationship with catchment inventory, *Journal of Environmental Radioactivity*, vol. 139, 2015, pp. 370-378.
- 67) Iwagami, S., Tsujimura, M., Onda, Y., Nishino, M., Konuma, R., Abe, Y., Hada, M., Pun, I., Sakaguchi, A., Kondo, H., Yamamoto, M., Miyata, Y., Igarashi, Y., Temporal changes in dissolved ^{137}Cs concentrations in groundwater and stream water in Fukushima after the Fukushima Dai-ichi Nuclear Power Plant accident, *Journal of Environmental Radioactivity*, vol.166, no. 3, 2017, pp. 458-465.
- 68) Smith, J.T., Belova, N.V., Bulgakov, A.A., Comans, R.N.J., Konoplev, A.V., Kudelsky, A.V., Madruga, M.J., Voitsekhovitch, O.V., Zibold, G., The "AQUASCOPE" simplified model for predicting $^{89,90}\text{Sr}$, ^{131}I , $^{134,137}\text{Cs}$ in surface water after a large-scale radioactive fallout, *Health Physics*, vol.89, no. 6 2005, pp. 628-644.
- 69) Yasutaka, T., Tsuji, H., Kondo, Y., Suzuki, Y., Takahashi, A., Kawamoto, T., Rapid quantification of radiocesium dissolved in water by using nonwoven fabric cartridge filters impregnated with potassium zinc ferrocyanide, *Journal of Nuclear Science and Technology*, vol. 52, no. 6, 2015, pp. 792-800.
- 70) Ochiai, S., Ueda, S., Hasegawa, H., Kakiuchi, H., Akata, N., Ohtsuka, Y., Hisamatsu, S., Effects of radiocesium inventory on ^{137}Cs concentrations in river waters of Fukushima, Japan, under base-flow conditions, *Journal of Environmental Radioactivity*, vol.144, 2015, pp. 86-95.
- 71) Muto, K., Atarashi-Andoh, M., Koarashi, J., Takeuchi, E., Nishimura, S., Tsuduki, K., Matsunaga, T., Sources of ^{137}Cs fluvial export from a forest catchment evaluated by stable carbon and nitrogen isotopic characterization of organic matter, *Journal of Radioanalytical and Nuclear Chemistry*, vol. 314, 2017, pp. 403-411.
- 72) Koarashi, J., Nishimura, S., Nakanishi, T., Atarashi-Andoh, M., Takeuchi, E., Muto, K., Post-deposition early-phase migration and retention behavior of radiocesium in a litter–mineral soil system in a Japanese deciduous forest affected by the Fukushima nuclear accident, *Chemosphere*, vol. 165, 2016, pp. 335-341.
- 73) Ministry of the Environment, Results of the radioactive material monitoring in the water environment/Digital Japan, http://www.env.go.jp/jishin/monitoring/results_r-pw.html <access date 22nd Jul. 2019> (in Japanese).
- 74) Iwagami, S., Onda, Y., Tsujimura, M., Abe, Y., Contribution of radioactive ^{137}Cs discharge by suspended sediment, coarse organic matter, and dissolved fraction from a headwater catchment in Fukushima after the Fukushima Dai-ichi Nuclear Power Plant accident, *Journal of Environmental Radioactivity*, Vol.166, no.3, 2017, pp. 466-474.
- 75) Mimura, R., Okada, T., Kawatsuma, S., Fukushima, M., Development of dose mapping system for environment, 2012 Fall Meeting of the Atomic Energy Society of Japan, 2012, p. 643.
- 76) Ochiai, S., Ueda, S., Hasegawa, H., Kakiuchi, H., Akata, N., Ohtsuka, Y., Hisamatsu, S., Spatial and temporal changes of ^{137}Cs concentrations derived from nuclear power plant accident in river waters in eastern Fukushima, Japan during 2012–2014, *Journal of Radioanalytical and Nuclear Chemistry*, vol. 307, no.3, 2016, pp. 2167-2172.

- 77) Eyrolle-Boyer, F., Boyer, P., Garcia-Sanchez, L., Metivier, J.-M., Onda, Y., De Vismes, A., Cagnat, X., Boulet, B., Cossonnet, C., Behaviour of radiocaesium in coastal rivers of the Fukushima Prefecture (Japan) during conditions of low flow and low turbidity – Insight on the possible role of small particles and detrital organic compounds, *Journal of Environmental Radioactivity*, vol. 151, 2016, pp. 328-340.
- 78) Naulier, M., Eyrolle-Boyer, F., Boyer, P., Métivier, J.-M., Onda, Y., Particulate organic matter in rivers of Fukushima: An unexpected carrier phase for radiocesiums, *Science of The Total Environment*, vol. 579, 2017, pp. 1560-1571.
- 79) Mishra, S., Sahoo, S.K., Bossew, P., Sorimachi, A., Tokonami, S., Vertical migration of radio-caesium derived from the Fukushima Dai-ichi Nuclear Power Plant accident in undisturbed soils of grassland and forest, *Journal of Geochemical Exploration*, vol. 169, 2016, pp. 163-186.
- 80) Imamura, N., Komatsu, M., Ohashi, S., Hashimoto, S., Kajimoto, T., Kaneko, S., Takano, T., Temporal changes in the radiocesium distribution in forests over the five years after the Fukushima Daiichi Nuclear Power Plant accident. *Scientific Reports*, vol. 7, 8179, 2017, DOI:10.1038/s41598-017-08261-x.
- 81) He, Q., Walling, D.E., Interpreting particle size effects in the adsorption of ^{137}Cs and unsupported ^{210}Pb by mineral soils and sediments, *Journal of Environmental Radioactivity*, vol. 30, no. 2, 1996, pp. 117-137.
- 82) Facchinelli, A., Gallini, L., Barberis, E., Magnoni, M., Hursthouse, A.S., The influence of clay mineralogy on the mobility of radiocaesium in upland soils of NW Italy, *Journal of Environmental Radioactivity*, vol. 56, no. 3, 2001, pp. 299-307.
- 83) Korobova, E.M., Chizhikova, N.P., Distribution and mobility of radiocesium in relation to the clay fraction mineralogy and soil properties in the Iput River floodplain, *Eurasian Soil Science*, vol. 40, no. 10, 2007, pp. 1062-1075.
- 84) Sawhney, B.L., Potassium and Cesium Ion Selectivity in Relation to Clay Mineral Structure, *Clays and Clay Minerals*, vol. 18, 1970, pp. 47-52.
- 85) Mukai, H., Hatta, T., Kitazawa, H., Yamada, H., Yaita, T., Kogure, T., Speciation of Radioactive Soil Particles in the Fukushima Contaminated Area by IP Autoradiography and Microanalyses, *Environmental Science & Technology*, vol. 48, no. 22, 2014, pp. 13053-13059.
- 86) Editorial committee of TOHOKU, part 2 of regional geology of Japan, 1989, *Regional Geology of Japan part 2 TOHOKU*. (in Japanese).
- 87) Tanaka, K., Iwatani, H., Sakaguchi, A., Fan, Q., Takahashi, Y., Size-dependent distribution of radiocesium in riverbed sediments and its relevance to the migration of radiocesium in river systems after the Fukushima Daiichi Nuclear Power Plant accident, *Journal of Environmental Radioactivity*, vol. 139, 2015, pp. 390-397.
- 88) Mukai, H., Hirose, A., Motai, S., Kikuchi, R., Tanoi, K., Nakanishi, T.M., Yaita, T., Kogure, T., Cesium adsorption/desorption behavior of clay minerals considering actual contamination conditions in Fukushima, *Scientific Reports*, vol. 6, 21543, 2016.
- 89) Allard, B., Ittner, T., Torstenfelt, B., Migration of Trace-Elements into Water-Exposed Natural Fissure Surfaces of Granitic Rock, *Chemical Geology*, vol. 49, no.1-3, 1985, pp. 31-42.

- 90) Granizo, N., Missana, T., Mechanisms of cesium sorption onto magnetite, *Radiochimica Acta*, vol. 94, no. 9, 2006, pp. 671-677.
- 91) Akiba, K., Hashimoto, H., Kanno, T., Distribution Coefficient of Cesium and Cation-Exchange Capacity of Minerals and Rocks, *Journal of Nuclear Science and Technology*, vol. 26, no. 12, 1989, pp. 1130-1135.
- 92) Ohnuki, T., Kozai, N., Adsorption behavior of radioactive cesium by non-mica mineral, *Journal of Nuclear Science and Technology*, vol. 50, no. 4, 2013, pp. 369-375.
- 93) Wentworth, C.K., A Scale of Grade and Class Terms for Clastic Sediments, *The Journal of Geology*, vol. 30, no. 5, 1922, pp. 377-392.
- 94) Konoplev, A., Golosov, V., Laptev, G., Nanba, K., Onda, Y., Takase, T., Wakiyama, Y., Yoshimura, K., Behavior of accidentally released radiocesium in soil-water environment: looking at Fukushima from a Chernobyl perspective, *Journal of Environmental Radioactivity*, vol.151, 2016, pp. 568-578.
- 95) Ministry of Education, Culture, Sports, Science and Technology, Results of the fourth airborne monitoring survey by MEXT, 2011,
http://radioactivity.nsr.go.jp/ja/contents/5000/4901/24/1910_1216.pdf <access date 10th Jul. 2019> (in Japanese).
- 96) MAFF, Actual state and countermeasure of radioactive cesium in Ogaki dam -for the agriculture revival in Ukedogawa Area-, 2016, 16p. (in Japanese).
- 97) Funaki, H., Yoshimura, K., Sakuma, K., Iri, S., Oda, Y., Evaluation of particulate ¹³⁷Cs discharge from a mountainous forested catchment using reservoir sediments and sinking particles, *Journal of Environmental Radioactivity*, vol. 189, 2018, pp.48-56.
- 98) Yoshimura, K., Onda, Y., Kato, H., Evaluation of radiocaesium wash-off by soil erosion from various land uses using USLE plots, *Journal of Environmental Radioactivity*, vol. 139, 2015, pp. 362-369.
- 99) Hayashi, H., Tsuji, H., Ito, S., Nisikiori, T., Yasutaka, T. Export of radioactive cesium in an extreme flooding event by typhoon Etau, *Journal of Japan Society of Civil Engineers, Ser.G (Environmental Research)*, vol. 72, no.7, 2016, pp.III_37-III_43. (in Japanese).
- 100) Otsuka, S., Kobayashi, T., Sedimentation and remobilization of radiocesium in the coastal area of Ibaraki, 70 km south of the Fukushima Dai-ichi Nuclear Power Plant, *Environmental Monitoring and Assessment*, vol. 185, no.7, 2013, pp. 5419-5433.
- 101) Kusakabe, M., Oikawa, S., Takata H., Misonoo, J., Spatiotemporal distributions of Fukushima-derived radionuclides in nearby marine surface sediments. *Biogeosciences*, vol. 10, 2013, pp. 5019-5030.
- 102) Black, E E., Buesseler, K. O., Spatial variability and the fate of cesium in coastal sediments near Fukushima, Japan. *Biogeosciences*, vol. 11, 2014, pp. 5123-5137.
- 103) Ono, T., Ambe, D., Kaeriyama, H., Shigenobu, Y., Fujimoto, K., Sogame, K., Nishimura, N., Fujikawa, T., Morita, T., Watanabe, T., Concentration of ¹³⁴Cs + ¹³⁷Cs bonded to the organic fraction of sediments offshore Fukushima, Japan, *Geochemical Journal*, vol. 49, 2015, pp. 219-227.
- 104) Tsumune, D., Tsubono, T., Aoyama, M., Hirose, K., Distribution of oceanic ¹³⁷Cs from the Fukushima Dai-ichi Nuclear Power Plant simulated numerically by a regional ocean model, *Journal of Environmental Radioactivity*, vol. 111, 2012, pp. 100-108.

- 105) Misumi, K., Tsumune, D., Tsubono, T., Tateda, Y., Aoyama, M., Kobayashi, T., Hirose, K., Factors controlling the spatiotemporal variation of ^{137}Cs in seabed sediment off the Fukushima coast: implications from numerical simulations, *Journal of Environmental Radioactivity*, vol. 136, 2014, pp. 218-228.
- 106) Ambe, D., Kaeriyama, H., Shigenobu, Y., Fujimoto, K., Ono, T., Sawada, H., Saito, H., Miki, S., Setou, T., Morita, T., Watanabe, T., Five-minute resolved spatial distribution of radiocesium in sea sediment derived from the Fukushima Dai-ichi Nuclear Power Plant, *Journal of Environmental Radioactivity*, vol. 138, 2014, pp. 264-275.
- 107) Kubo, K., Yanagisawa, Y., Yoshioka, T., Takahashi, Y., Geology of the Namie and Iwaki-Tomioka district, Geological Survey of Japan., Niigata (7), No. 46 and 47, 1994. (in Japanese with English Abstract). https://www.gsj.jp/Map/JP/docs/5man_doc/07/07_046-047.htm <access date 10th Jul. 2019>.
- 108) Mii, H., Coastal geology of Tanabe Bay, Tohoku University Scientific Reports (Geology), vol. 34, 1962, pp. 1-93.
- 109) Hoshino, M., Tairikudana (Continental shelf), Kaiyo kagaku kiso koza 7 Senkai chishitsugaku (Basic course for marine science 7; Shallow sea geology), Tokai University Press, 1971, pp. 254-439 (in Japanese).
- 110) Uda, T., Serizawa, M., Kumada, T., Karube, R., Mimura, M., Relations among wave climate, longshore sand transport rate and closure depth, *Proceedings of civil engineering in the ocean*, vol. 18, 2002, pp. 803-808. (in Japanese with English abstract).
- 111) Tsuruta, T., Harada, H., Misonou, T., Matsuoka, T., Hodotsuka, Y., Horizontal and vertical distributions of ^{137}Cs in seabed sediments around the river mouth near Fukushima Daiichi Nuclear Power Plant, *Journal of Oceanography*, vol. 73, no. 5, 2017, pp. 547-558.
- 112) Otsuka, S., Kato, Y., Radiocesium derived from the Fukushima Daiichi Nuclear Power Plant accident in seabed sediments: initial deposition and inventories, *Environ Science: Processes & Impacts*, vol. 16, 2014, pp. 978-990.
- 113) Nakanishi, T., River study in “JAEA’s Activities for Decommissioning and Environmental Restoration related to Fukushima Daiichi Nuclear Power Station accident in 2014”, 2014, pp. 76-77 (in Japanese), <https://fukushima.jaea.go.jp/initiatives/cat05/pdf/fukushimaR&D2014.pdf> <access date 12th Nov. 2018>.
- 114) Otsuka, S., Processes affecting long-term change in ^{137}Cs concentration in surface sediments off Fukushima, *Journal of Oceanography*, vol. 73, no. 5, 2017, pp. 559-570.
- 115) Sanada, Y. and Torii, T., Aerial radiation monitoring around the Fukushima Dai-ichi nuclear power plant using an unmanned helicopter. *Journal of Environmental Radioactivity*, vol.139, 2015, pp.294-299.
- 116) Andoh, M., Nakahara, Y., Tsuda, S., Yoshida, T., Matsuda, N., Takahashi, F., Mikami, S., Kinouchi, N., Sato, T., Tanigaki, M., Takamiya, K., Sato, N., Okumura, R., Uchihori, Y., Saito, K., Measurement of air dose rates over a wide area around the Fukushima Dai-ichi Nuclear Power Plant through a series of car-borne surveys, *Journal of Environmental Radioactivity*, vol. 139, 2015, pp. 266-280.
- 117) Yoshimura, K., Fujiwata, K., Nakama, S., Applicability of an autonomous unmanned helicopter survey of air dose rate in sub-urban area. *Radiation Protection Dosimetry*, vol. 184, 2019, pp. 315-318.

- 118) Malins, A., Okumura, M., Machida, M., Takemiya, H., Saito, K., Fields of View for Environmental Radioactivity. Proceedings of the International Symposium on 437 Radiological Issues for Fukushima's Revitalized Future, Kyoto University Research Reactor Institute, 2015, pp. 28-34, 2015, <https://www.rri.kyoto-u.ac.jp/en> <access date 23th Jul. 2019>.
- 119) JAEA, Report for the project entrusted from the Nuclear Regulation Authority in 2017, 2018, <https://radioactivity.nsr.go.jp/ja/contents/14000/13159/view.html> <access date 16th Jul. 2019>, (in Japanese).
- 120) Japan Atomic Energy Agency, report for Decontamination pilot projects for the environmental remediation of evacuation areas contaminated with radioactive materials discharged from the Fukushima Daiichi Nuclear Power Plant accident, 2013, <https://fukushima.jaea.go.jp/fukushima/result/entry02.html> <access date 16th Jul. 2018>.
- 121) Nakama, S., Yoshimura, K., Fujiwara, K., Ishikawa, H., Iijima, K., Decrease in air dose rate after decontamination relating to difference in the ground surface properties, Proceedings of 19th Workshop on Environmental Radioactivity, pp. 154-158, (in Japanese with English abstract).
- 122) Kakamu, T., Kanda, H., Tsuji, M., Kobayashi, D., Miyake, M., Hayakawa, T., Katsuda, S., Mori, Y., Okouchi, T., Hazama, A., Fukushima, T., Differences in rates of decrease of environmental radiation dose rates by ground surface property in Fukushima city after the Fukushima Daiichi nuclear power plant accident. Health Physics, vol. 104, no. 1, 2013, pp.102-107.
- 123) IAEA, Environmental Consequences of the Chernobyl Accident and Their Remediation: Twenty Years of Experience. Reports of the Chernobyl Forum Experts Group “Environment”, IAEA, STI/PUB/1239, 2006, 166p.
- 124) Yoshimura, K., Saito, K., Fujiwara, K., Distribution of ¹³⁷Cs on components in urban area four years after the Fukushima Dai-ichi Nuclear Power Plant accident, Journal of Environmental Radioactivity, vol. 178-179, 2017, pp.48-54.
- 125) Mikami, S., Maeyama, T., Hoshide, Y., Sakamoto, R., Sato, S., Okuda, N., Demongeot, S., Gurriaran, R., Uwamino, Y., Kato, H., Fujiwara, M., Sato, T., Takemiya, H., Saito, K., Spatial distributions of radionuclides deposited onto ground soil around the Fukushima Dai-ichi Nuclear Power Plant and their temporal change until December 2012, Journal of Environmental Radioactivity, vol. 139, 2015, pp. 320-343.
- 126) Yoshimura, K., Estimation of discharge rate of Cs-137 from urbanized catchment based on the decrease in deposition amount on urban components, Proceedings of the 19th Workshop on Environmental Radioactivity, KEK, 2018, pp. 36-40. (In Japanese with English abstract).
- 127) Morino, Y., Ohara, T., Nishizawa, M., Atmospheric behavior, deposition, and budget of radioactive materials from the Fukushima Daiichi nuclear power plant in March 2011. Geophys. Res. Lett. vol.38, 2011, L00G11.
- 128) Kurikami, H., Kitamura, A., Yamada, S., Machida, M., Modeling approach to various time and spatial scale environmental issues in Fukushima - Related to radioactive cesium migration in aquatic systems-, Proceedings of ICONE-23, 2015, ICONE23-2125.
- 129) Yamaguchi, M., Maekawa, K., Takeuchi, S., Kitamura, A., Onishi, Y., Development of a model to predict a radionuclide distribution based on soil migration after Fukushima Dai-ichi Nuclear Power

- Plant accident, *Journal of Nuclear Fuel Cycle and Environment*, vol.20, no.2, 2013, pp. 53-69 (in Japanese with English Abstract).
- 130) Yamaguchi, M., Kitamura, A., Oda, Y., Onishi, Y., Predicting the long-term ¹³⁷Cs distribution in Fukushima after the Fukushima Dai-ichi nuclear power plant accident: a parameter sensitivity analysis, *Journal of Environmental Radioactivity*, vol.135, 2014, pp. 135-146.
- 131) Tosaka, H., Itoh, K., Furuno, T., Fully coupled formulation of surface flow with 2-phase subsurface flow for hydrological simulation, *Hydrological Processes*, vol. 14, 2000, pp. 449-464.
- 132) Mori, K., Tada, K., Tawara, Y., Ohno, K., Asami, M., Kosaka, K., Tosaka, H., Integrated watershed modeling for simulation of spatiotemporal redistribution of post-fallout radionuclides: application in radiocesium fate and transport processes derived from the Fukushima accidents, *Environmental Modelling and Software*, vol. 72, 2015, pp. 126-146.
- 133) Onishi, Y., Kivva, S.L., Zheleznyak, M.J., Voitsekhovich, O.V., Aquatic assessment of the Chernobyl nuclear accident and its remediation, *Journal of Environmental Engineering*, vol. 133, no. 11, 2007, pp. 1015-1023.
- 134) Onishi, Y., Kurikami, H., Yokuda, S.T., Simulation of sediment and cesium transport in the Ukedo River and the Ogi Dam reservoir during a rainfall event using the TODAM code, PNNL-23255, 2014.
- 135) Shimizu, Y., Mutual relation between riverbed and bank variation characteristics in river channel landform formation, *Proceedings of Hydraulic Engineering*, vol. 47, 2003, pp. 643-648.
- 136) Shimizu Y., Inoue, T., Hamaki, M., Iwasaki, T. (ed), *iRIC Software Nays2D Solver Manual iRIC Project*, 2012,
http://people.eri.ucsb.edu/~lharrison/MeanderModelLit/NAYS/Nays2D_SolverManual.pdf
 <access date 8th Nov. 2018>.
- 137) Onishi, Y., Graber, H.C., Trent, D.S., Preliminary modeling of wave-enhanced sediment and contaminant transport in New Bedford harbor, coastal and estuarine studies, Vol. 42, *Nearshore and Estuarine Cohesive Sediment Transport*, A. J. Mehta ed., American Geophysical Union, 1993.
- 138) Onishi, Y., Kurikami, H., Yokuda, S.T., Preliminary three-dimensional simulation of sediment and cesium transport in the Ogi Dam reservoir using FLESCOT – Task 6, subtask 2, PNNL-23257, 2014.
- 139) Haidvogel, D.B., Arango, H.G., Hedstrom, K., Beckmann, A., Malanotte-Rizzoli, P., Shchepetkin, A.F., Model evaluation experiments in the North Atlantic Basin: simulations in nonlinear terrain-following, *Dynamics of Atmospheres and Oceans*, vol.32, no. 3-4, 2000, pp. 239-281.
- 140) Kurikami, H., Malins, A., Takeishi, M., Saito, K., Iijima, K., Coupling the advection-dispersion equation with fully kinetic reversible/irreversible sorption terms to model radiocesium soil profiles in Fukushima Prefecture, *Journal of Environmental Radioactivity*, vol. 171, 2017, pp. 99-109.
- 141) Sato, T., Iwanoto, Y., Hashimoto, S., Ogawa, T., Furuta, T., Abe, S., Kai, T., Tsai, P.E., Matsuda, N., Iwase, H., Shigyo, N., Sihver, L., Niita, K., Features of Particle and Heavy Ion Transport Code System PHITS Version 3.02, *Journal of Nuclear Science and Technology*, vol. 55, no. 6, 2018, pp. 684-690.
- 142) Malins, A., Kurikami, H., Nakama, S., Saito, T., Okumura, M., Machida, M., Kitamura, A., Evaluation of ambient dose equivalent rates influenced by vertical and horizontal distribution of radioactive cesium in soil in Fukushima Prefecture, *Journal of Environmental Radioactivity*, vol. 151, 2016, pp. 38-49.

- 143) Kim, M., Malins, A., Yoshimura, K., Sakuma, K., Kurikami, K., Kitamura, A., Machida, M., Hasegawa, Y., Yanagi, H., Simulation study of the effects of buildings, trees and paved surfaces on ambient dose equivalent rates outdoors at three suburban sites near Fukushima Dai-ichi, *Journal of Environmental Radioactivity*, vol. 210, 105803, 2019, DOI: 10.1016/j.jenvrad.2018.09.001.
- 144) Kurikami, H., Niizato, T., Tsuruta, T., Kato, T., Kitamura, A., Kanno, M. and Kurosawa, N., A Compartment model of radionuclide migration in environment based on exposure pathways, *JAEA-Research 2016-020*, 2017, 50p. (in Japanese).
- 145) Vanoni, V.A. (ed.), *Sedimentation Engineering*, ASCE Manuals and Report on Engineering Practice, American Society of Civil Engineers, 1975, New York.
- 146) Liu, X., Machida, M., Kitamura, A., Kurikami, H., Simulations of radiocesium discharge from Abukuma River with improved cesium wash-off model, 2018 Fall Meeting of Atomic Energy Society of Japan, 2018, 2K14.
- 147) Kitamura, A., Kurikami, H., Sakuma, K., Malins, A., Okumura, M., Machida, M., Mori, K., Tada, K., Tawara, Y., Kobayashi, T., Yoshida, T., Tosaka, H., Redistribution and export of contaminated sediment within eastern Fukushima Prefecture due to typhoon flooding, *Earth Surface Processes and Landforms*, vol.41, no.12, 2016, pp. 1708-1726.
- 148) Sakuma, K., Kitamura, A., Malins, A., Kurikami, H., Machida, M., Mori, K., Tada, K., Kobayashi, T., Tawara, Y., Tosaka, H., Characteristics of radio-caesium transport and discharge between different basins near to the Fukushima Dai-ichi Nuclear Power Plant after heavy rainfall events, *Journal of Environmental Radioactivity*, vol. 169-170, 2017, pp. 137-150.
- 149) Sakuma, K., Malins, A., Funaki, H., Kurikami, H., Niizato, T., Nakanishi, T., Mori, K., Tada, K., Kobayashi, T., Kitamura, A., Hosomi, M., Evaluation of sediment and ¹³⁷Cs redistribution in the Oginosawa River catchment near the Fukushima Dai-ichi Nuclear Power Plant using integrated watershed modeling, *Journal of Environmental Radioactivity*, vol. 182, 2018, pp. 44-51.
- 150) Sakuma, K., Tsuji, H., Hayashi, S., Funaki, H., Malins, A., Yoshimura, K., Kurikami, H., Kitamura, A., Iijima, K., Hosomi, M., Applicability of K_d for modelling dissolved ¹³⁷Cs concentrations in Fukushima river water: Case study of the upstream the Ohta River, *Journal of Environmental Radioactivity*, vol. 185, 2018, pp. 53-62.
- 151) Kurikami, H., Kitamura, A., Yokuda, S.T., Onishi, Y., Sediment and ¹³⁷Cs behaviors in the Ogaki Dam Reservoir during a heavy rainfall event, *Journal of Environmental Radioactivity*, vol.137, 2014, pp. 10-17.
- 152) Yamada, S., Kitamura, A., Kurikami, H., Yamaguchi, M., Malins, A., Machida, M., Sediment and ¹³⁷Cs transport and accumulation in the Ogaki Dam of eastern Fukushima, *Environmental Research Letters*, vol.10, 2015, 014013.
- 153) Kurikami, H., Funaki, H., Malins, A., Kitamura, A., Onishi, Y., Numerical study of sediment and ¹³⁷Cs discharge out of reservoirs during various scale rainfall events, *Journal of Environmental Radioactivity*, vol. 164, 2016, pp. 73-83.
- 154) Yamada, S., Kitamura, A., Kurikami, H., Machida, M., High performance simulation for sediment transport on rivers on Fukushima area: Parallelization of 2D river simulation code Nays2D, *Proceedings of M&C+SNA+MC 2015*, 2015.

- 155) Sanada, Y., Kondo, A., Sugita, T., Nishizawa, Y., Yuuki, Y., Ikeda, K., Shoji, Y., Torii, T., Radiation monitoring using an unmanned helicopter in the evacuation zone around the Fukushima Daiichi nuclear power plant, *Exploration Geophysics*, vol. 45, no. 1, 2013, pp. 3-7.
- 156) He, Q., Walling, D., The distribution of fallout ^{137}Cs and ^{210}Pb in undisturbed and cultivated soils, *Applied Radiation and Isotopes*, vol.48, no. 5, 1997, pp. 677-690.
- 157) Antonopoulos-Domis, M., Clouvas, A., Hiladakis, A., Kadi, S., Radiocesium distribution in undisturbed soil: Measurements and diffusion-advection model, *Health Physics*, vol. 69, no. 6, 1995, pp. 949-953.
- 158) Matsuda, N., Mikami, S., Shimoura, S., Takahashi, J., Nakano, M., Shimada, K., Uno, K., Hagiwara, S., Saito, K., Depth profiles of radioactive cesium in soil using a scraper plate over a wide area surrounding the Fukushima Dai-ichi Nuclear Power Plant, Japan, *Journal of Environmental Radioactivity*, vol.139, 2015, pp. 427-434.
- 159) Takahashi, J., Tamura, K., Suda, T., Matsumura, R., Onda, Y., Vertical distribution and temporal changes of ^{137}Cs in soil profiles under various land uses after the Fukushima Dai-ichi Nuclear Power Plant accident, *Journal of Environmental Radioactivity*, vol. 139, 2015, pp. 351-361.
- 160) Toso, J.P., Velasco, R.H., Describing the observed vertical transport of radiocesium in specific soils with three time-dependent models, *Journal of Environmental Radioactivity*, vol.53, no. 2, 2001, pp. 133-144.
- 161) Miyahara, K., McKinley, I., Saito, K., Hardie, S., Iijima, K., Use of Knowledge and Experience Gained from the Fukushima Daiichi Nuclear Power Station Accident to Establish the Technical Basis for Strategic Off-site Response, *JAEA-Review 2015-001*, 2015, 90p.
- 162) Malins, A., Okumura, M., Machida, M., Saito, K., Topographic effects on ambient dose equivalent rates from radiocesium fallout, *Proceedings of ANS MC2015*, 2015, in CD-ROM.
- 163) Sakuma, K., Niizato, T., Kim, M., Malins, A., Machida, M., Yoshimura, K., Kurikami, H., Kitamura, A., Development of the evaluation tool for air dose rate in forest using a Monte Carlo radiation transport code (PHITS). *Journal of the Society for Remediation of Radioactive Contamination in the Environment*, vol. 6, no. 3, 2018, pp. 145-152 (in Japanese with English abstract).
- 164) Furuta, T., Takahashi, F., Study of radiation dose reduction of buildings of different sizes and materials, *Journal of Nuclear Science and Technology*, vol. 52, no. 6, 2015, pp. 897-904.
- 165) Imamura, N., Komatsu, M., Ohashi, S., Hashimoto, S., Kajimoto, T., Kaneko S., Takano, T., Temporal changes in the radiocesium distribution in forests over the five years after the Fukushima Daiichi Nuclear Power Plant accident. *Scientific Reports*, vol.7, 8179, 2017, DOI:10.1038/s41598-017-08261-x.
- 166) Ohashi, S., Kuroda, K., Takano, T., Suzuki, Y., Fujiwara, T., Abe, H., Kagawa, A., Sugiyama, M., Kubojima, Y., Zhang, C., Yamamoto K., Temporal trends in ^{137}Cs concentrations in the bark, sapwood, heartwood, and whole wood of four tree species in Japanese forests from 2011 to 2016, *Journal of Environmental Radioactivity*, vol. 178-179, 2017, pp. 335-342.
- 167) Malins, A., Kurikami, H., Kitamura, A., Machida, M., Effect of remediation parameters on in-air ambient dose equivalent rates when remediating open sites with radiocesium-contaminated soil, *Health Physics*, vol. 111, no. 4, 2016, pp. 357-366.

- 168) Ministry of Agriculture, Forestry and Fisheries, Report by Forestry Agency, 2015 (in Japanese), <http://www.rinya.maff.go.jp/j/press/kaihatu/pdf/150327-01.pdf> <access date 8th Nov. 2018>.
- 169) Kato, H., Onda, Y., Hisadome, K., Loffredo, N., Kawamori, A., Temporal changes in radiocesium deposition in various forest stands following the Fukushima Dai-ichi Nuclear Power Plant accident, *Journal of Environmental Radioactivity*, vol. 166, no. 3, 2017, pp. 449-457.
- 170) Japan Fisheries Research and Education Agency, Report on the Monitoring of Radionuclides in Fishery Products, 2017 (in Japanese), <http://www.jfa.maff.go.jp/j/housyanou/attach/pdf/kekka-114.pdf> <access date 12th Nov. 2018>.
- 171) Kurikami, H., Sakuma, K., Numerical study of transport pathways of radiocesium from forests to freshwater fish, JpGU2018, 2018, MAG33-P05 (in Japanese).
- 172) Onishi, Y., Kurikami, H., Yokuda, S.T., Simulation of sediment and cesium transport in the Ukedo River and the Ogi Dam reservoir during a rainfall event using the TODAM code, PNNL-23255, 2014.
- 173) Saito, K., Onda, Y., Outline of the national mapping projects implemented after the Fukushima accident, *Journal of Environmental Radioactivity*, vol. 139, 2015, pp. 240-249.
- 174) Mikami, S. et al., Spatial distributions of radionuclides deposited onto ground soil around the Fukushima Dai-ichi Nuclear Power Plant and their temporal change until December 2012, *Journal of Environmental Radioactivity*, vol. 139, 2015, pp. 250-259.
- 175) Kurikami, H. Malins, A., Numerical study on sorption kinetics affecting vertical profile of radiocesium in soil and air dose rates, JpGU2017, 2017, MAG34-09 (in Japanese).
- 176) Malins, A., Sakuma, K., Nakanishi, T., Yamada, S., Kurikami, H., Machida, M., Kitamura, A., Modelling evolution of air dose rates in river basins in Fukushima Prefecture affected by sediment-sorbed radiocesium redistribution, AGU Fall Meeting 2015, 2015.
- 177) Sanada, Y., Nishizawa, Y., Yamada, T., Ikeda, K., Matsui, M., Tsuchida, K., Sato, Y., Hirayama, H., Takamura, Y., Nishihara, K., Imura, M., Ishida, M., Urabe, Y., Shikaze, Y., Sugita, T., Kondo, A., Torii, T., Radiation monitoring using the unmanned helicopter after the accident of the nuclear power plant, JAEA-Research 2013-049, 2014 129p. (in Japanese with English abstract).
- 178) Saegusa, H., Ohyama, T., Iijima, K., Onoe, H., Takeuchi, R., Hagiwara, H., Deposition of radiocesium on the river flood plains around Fukushima, *Journal of Environmental Radioactivity*, vol. 164, 2016, pp. 36-46.
- 179) Nakanishi, T., River study in “JAEA’s Activities for Decommissioning and Environmental Restoration related to Fukushima Daiichi Nuclear Power Station accident in 2015”, 2016, pp. 68-69 (in Japanese), <https://fukushima.jaea.go.jp/initiatives/cat05/pdf/fukushimaR&D2015.pdf> <access date 12th Nov. 2018>.
- 180) Fukushima Prefecture, 2018, Transition of evacuation designated zones, Fukushima Revitalization Station, <http://www.pref.fukushima.lg.jp/site/portal-english/en03-08.html> <access date 12th Feb. 2020>.
- 181) Goto, Y., Forest fire, Forestry and Forest Products Research Institute eds., *An encyclopedia of Forest*, Asakura Publishing Co., Ltd., Tokyo, 2009, pp. 149-152, (in Japanese).
- 182) Nogami, K., Tending before crown closure, Kawana, A., et al., (eds.), *Forestry* 3rd ed., Asakura Publishing Co., Ltd., Tokyo, 1992, pp. 127-137, (in Japanese).
- 183) Ando, T., Tending after crown closure, Kawana, A., et al., eds., *Forestry* 3rd ed., Asakura Publishing Co., Ltd., Tokyo, 1992, pp. 137-159, (in Japanese).

- 184) Fukushima Prefectural Government and Fukushima Prefectural Centre for Environmental Creation (FPCEC), Survey results for an understanding of environmental impacts of radioactive materials due to the forest fire in Namie Town (interim report), 2017.
<https://www.pref.fukushima.lg.jp/uploaded/attachment/245261.pdf> <access date 31st Jul. 2018> (in Japanese).
- 185) Forestry Agency, Ministry of Agriculture, Forestry and Fisheries, Japan, The results of the field survey in fire site of the national forest land in Namie and Futaba Towns, Fukushima Prefecture, Forestry Agency, 2018, <http://www.rinya.maff.go.jp/j/press/gyoumu/170623.html> <access date 31st Jul. 2018> (in Japanese).
- 186) Fukushima Prefectural Government, Current situation and future prospects of radioactive materials in the Fukushima forest. Forestry Planning Division, Agriculture, Forestry and Fishery Department, Fukushima Prefectural Government, 2018,
<http://www.pref.fukushima.lg.jp/uploaded/attachment/281737.pdf> <access date 31st, Jul. 2018> (in Japanese).
- 187) Fukushima Prefecture, Results of radiation monitoring around the site of forest fire in Ide district, Namie Town, 2018, <http://www.pref.fukushima.lg.jp/site/namie-rinyakasai-201704-05/> <access date 31st Jul. 2018> (in Japanese).
- 188) Fukushima Prefectural Government and Fukushima Prefectural Centre for Environmental Creation (FPCEC), Survey results for an understanding of environmental impacts of radioactive materials due to the forest fire in Namie Town (interim report), 2017.
<https://www.pref.fukushima.lg.jp/uploaded/attachment/241494.pdf> <access date 31st Jul. 2018> (in Japanese).
- 189) Ishii, Y., Muto, K., Hagiwara, H., Ito, S., Takahashi, M., Tagomori, H., Dohi, T., Kitamura, A., Origin of atmospheric particle matter captured near at the location where Namie-city forest fire has occurred, 19th Workshop on Environmental Radioactivity, KEK, 2018. (in Japanese with English abstract).
- 190) Geospatial Information Authority of Japan, GSI web map (Denshi Kokudo Web)
<http://maps.gsi.go.jp/#5/36.104611/140.084556/&base=std&ls=std&disp=1&vs=c1j0h0k0l0u0t0z0r0s0f1> <access date 31st Jul. 2018> (in Japanese).
- 191) Japan Aerospace Exploration Agency (JAXA) Earth Observation Research Center (EORC), 2016, Homepage of high-resolution land use and land cover map products (released on September 2016, ver.16.09) http://www.eorc.jaxa.jp/ALOS/lulc/jlulc_jpn.htm <access date 31st Jul. 2018>.
- 192) Teramage, M., T., Onda, Y., Kato, H., Gomi, T., The role of litterfall in transferring Fukushima-derived radiocesium to a coniferous forest floor, Science of the Total Environment, vol. 490, no.15, 2014, pp. 435-439.
- 193) Niizato, T., F-TRACE (1) Forest investigation, JAEA's activities for the decommissioning related to the accident of the Fukushima Daiichi Nuclear Power Station, Tokyo Electric Power Company Holdings Inc. and environmental restoration (2017 edition), Japan Atomic Energy Agency, 2017, pp. 82-83.
- 194) Nuclear Regulation Authority, <http://radioactivity.nsr.go.jp/ja/list/338/list-1.html> (in Japanese). <access date 10th Oct. 2018>.

- 195) Saito, H., Nozawa, T., Takemiya, H., Seki, A., Matsubara, T., Saito, K., Kitamura, A., Comprehensive evaluation system for environmental remediation of Fukushima; Toward integration of three components as a whole system, JAEA-Research 2017-040, 2018, 34p.

This is a blank page.

国際単位系 (SI)

表1. SI 基本単位

基本量	SI 基本単位	
	名称	記号
長さ	メートル	m
質量	キログラム	kg
時間	秒	s
電流	アンペア	A
熱力学温度	ケルビン	K
物質량	モル	mol
光度	カンデラ	cd

表2. 基本単位を用いて表されるSI組立単位の例

組立量	SI 組立単位	
	名称	記号
面積	平方メートル	m ²
体積	立方メートル	m ³
速度	メートル毎秒	m/s
加速度	メートル毎秒毎秒	m/s ²
波数	毎メートル	m ⁻¹
密度, 質量密度	キログラム毎立方メートル	kg/m ³
面積密度	キログラム毎平方メートル	kg/m ²
比体積	立方メートル毎キログラム	m ³ /kg
電流密度	アンペア毎平方メートル	A/m ²
磁界の強さ	アンペア毎メートル	A/m
量濃度 ^(a) , 濃度	モル毎立方メートル	mol/m ³
質量濃度	キログラム毎立方メートル	kg/m ³
輝度	カンデラ毎平方メートル	cd/m ²
屈折率 ^(b)	(数字の)	1
比透磁率 ^(b)	(数字の)	1

(a) 量濃度 (amount concentration) は臨床化学の分野では物質濃度 (substance concentration) ともよばれる。
 (b) これらは無次元量あるいは次元1をもつ量であるが、そのことを表す単位記号である数字の1は通常は表記しない。

表3. 固有の名称と記号で表されるSI組立単位

組立量	SI 組立単位			
	名称	記号	他のSI単位による表し方	SI基本単位による表し方
平面角	ラジアン ^(b)	rad	1 ^(b)	m/m
立体角	ステラジアン ^(b)	sr ^(e)	1 ^(b)	m ² /m ²
周波数	ヘルツ ^(d)	Hz		s ⁻¹
力	ニュートン	N		m kg s ⁻²
圧力, 応力	パスカル	Pa	N/m ²	m ⁻¹ kg s ⁻²
エネルギー, 仕事, 熱量	ジュール	J	N m	m ² kg s ⁻²
仕事率, 工率, 放射束	ワット	W	J/s	m ² kg s ⁻³
電荷, 電気量	クーロン	C		s A
電位差 (電圧), 起電力	ボルト	V	W/A	m ² kg s ⁻³ A ⁻¹
静電容量	ファラド	F	C/V	m ² kg ⁻¹ s ⁴ A ²
電気抵抗	オーム	Ω	V/A	m ² kg s ⁻³ A ⁻²
コンダクタンス	ジーメン	S	A/V	m ² kg ⁻¹ s ³ A ²
磁束	ウェーバ	Wb	Vs	m ² kg s ⁻² A ⁻¹
磁束密度	テスラ	T	Wb/m ²	kg s ⁻² A ⁻¹
インダクタンス	ヘンリー	H	Wb/A	m ² kg s ⁻² A ⁻²
セルシウス温度	セルシウス度 ^(e)	°C		K
光照射量	ルーメン	lm	cd sr ^(e)	cd
放射線量	グレイ	Gy	J/kg	m ² s ⁻²
放射性核種の放射能 ^(f)	ベクレル ^(d)	Bq		s ⁻¹
吸収線量, 比エネルギー分与, カーマ	グレイ	Gy	J/kg	m ² s ⁻²
線量当量, 周辺線量当量, 方向性線量当量, 個人線量当量	シーベルト ^(g)	Sv	J/kg	m ² s ⁻²
酸素活性化	カタール	kat		s ⁻¹ mol

(a) SI接頭語は固有の名称と記号を持つ組立単位と組み合わせても使用できる。しかし接頭語を付した単位はもはやコヒーレントではない。
 (b) ラジアンとステラジアンは数字の1に対する単位の特別な名称で、量についての情報をつたえるために使われる。実際には、使用する時には記号rad及びsrが用いられるが、習慣として組立単位としての記号である数字の1は明示されない。
 (c) 測光学ではステラジアンという名称と記号srを単位の表し方の中に、そのまま維持している。
 (d) ヘルツは周期現象についてのみ、ベクレルは放射性核種の統計的過程についてのみ使用される。
 (e) セルシウス度はケルビンの特別な名称で、セルシウス温度を表すために使用される。セルシウス度とケルビンの単位の大きさは同一である。したがって、温度差や温度間隔を表す数値はどちらの単位で表しても同じである。
 (f) 放射性核種の放射能 (activity referred to a radionuclide) は、しばしば誤った用語で"radioactivity"と記される。
 (g) 単位シーベルト (PV, 2002, 70, 205) についてはCIPM勧告2 (CI-2002) を参照。

表4. 単位の中に固有の名称と記号を含むSI組立単位の例

組立量	SI 組立単位		
	名称	記号	SI 基本単位による表し方
粘力のモーメント	パスカル秒	Pa s	m ⁻¹ kg s ⁻¹
表面張力	ニュートンメートル	N m	m ² kg s ⁻²
角速度	ニュートン毎メートル	N/m	kg s ⁻²
角加速度	ラジアン毎秒	rad/s	m m ⁻¹ s ⁻¹ = s ⁻¹
熱流密度, 放射照度	ラジアン毎秒毎秒	rad/s ²	m m ⁻¹ s ⁻² = s ⁻²
熱容量, エントロピー	ワット毎平方メートル	W/m ²	kg s ⁻³
比熱容量, 比エントロピー	ジュール毎ケルビン	J/K	m ² kg s ⁻² K ⁻¹
比エネルギー	ジュール毎キログラム毎ケルビン	J/(kg K)	m ² s ⁻² K ⁻¹
熱伝導率	ジュール毎キログラム	J/kg	m ² s ⁻²
体積エネルギー	ワット毎メートル毎ケルビン	W/(m K)	m kg s ⁻³ K ⁻¹
電界の強さ	ジュール毎立方メートル	J/m ³	m ⁻¹ kg s ⁻²
電荷密度	ジュール毎立方メートル	J/m ³	m kg s ⁻³ A ⁻¹
電表面積	クーロン毎立方メートル	C/m ³	m ⁻³ s A
電束密度, 電気変位	クーロン毎平方メートル	C/m ²	m ⁻² s A
誘電率	クーロン毎平方メートル	C/m ²	m ⁻² s A
透磁率	ファラド毎メートル	F/m	m ³ kg ⁻¹ s ⁴ A ²
モルエネルギー	ヘンリー毎メートル	H/m	m kg s ⁻² A ⁻²
モルエントロピー, モル熱容量	ジュール毎モル	J/mol	m ² kg s ⁻² mol ⁻¹
照射線量 (X線及びγ線)	ジュール毎モル毎ケルビン	J/(mol K)	m ² kg s ⁻² K ⁻¹ mol ⁻¹
吸収線量率	クーロン毎キログラム	C/kg	kg ⁻¹ s A
放射線強度	グレイ毎秒	Gy/s	m ² s ⁻³
放射輝度	ワット毎ステラジアン	W/sr	m ⁴ m ⁻² kg s ⁻³ = m ² kg s ⁻³
酵素活性濃度	ワット毎平方メートル毎ステラジアン	W/(m ² sr)	m ² m ⁻² kg s ⁻³ = kg s ⁻³
	カタール毎立方メートル	kat/m ³	m ³ s ⁻¹ mol

表5. SI 接頭語

乗数	名称	記号	乗数	名称	記号
10 ²⁴	ヨタ	Y	10 ¹	デシ	d
10 ²¹	ゼタ	Z	10 ²	センチ	c
10 ¹⁸	エクサ	E	10 ³	ミリ	m
10 ¹⁵	ペタ	P	10 ⁶	マイクロ	μ
10 ¹²	テラ	T	10 ⁹	ナノ	n
10 ⁹	ギガ	G	10 ¹²	ピコ	p
10 ⁶	メガ	M	10 ⁻¹⁵	フェムト	f
10 ³	キロ	k	10 ⁻¹⁸	アト	a
10 ²	ヘクト	h	10 ⁻²¹	ゼプト	z
10 ¹	デカ	da	10 ⁻²⁴	ヨクト	y

表6. SIに属さないが、SIと併用される単位

名称	記号	SI単位による値
分	min	1 min=60 s
時	h	1 h=60 min=3600 s
日	d	1 d=24 h=86 400 s
度	°	1°=(π/180) rad
分	'	1'=(1/60)°=(π/10 800) rad
秒	"	1"=(1/60)'=(π/648 000) rad
ヘクタール	ha	1 ha=1 hm ² =10 ⁴ m ²
リットル	L, l	1 L=1 l=1 dm ³ =10 ³ cm ³ =10 ⁻³ m ³
トン	t	1 t=10 ³ kg

表7. SIに属さないが、SIと併用される単位で、SI単位で表される数値が実験的に得られるもの

名称	記号	SI単位で表される数値
電子ボルト	eV	1 eV=1.602 176 53(14)×10 ⁻¹⁹ J
ダルトン	Da	1 Da=1.660 538 86(28)×10 ⁻²⁷ kg
統一原子質量単位	u	1 u=1 Da
天文単位	ua	1 ua=1.495 978 706 91(6)×10 ¹¹ m

表8. SIに属さないが、SIと併用されるその他の単位

名称	記号	SI単位で表される数値
バール	bar	1 bar=0.1MPa=100 kPa=10 ⁵ Pa
水銀柱ミリメートル	mmHg	1 mmHg=133.322Pa
オングストローム	Å	1 Å=0.1nm=100pm=10 ⁻¹⁰ m
海里	M	1 M=1852m
バイン	b	1 b=100fm ² =(10 ¹² cm ²) ² =10 ⁻²⁸ m ²
ノット	kn	1 kn=(1852/3600)m/s
ネーパ	Np	SI単位との数値的関係は、 対数量の定義に依存。
ベレル	B	
デシベル	dB	

表9. 固有の名称をもつCGS組立単位

名称	記号	SI単位で表される数値
エルグ	erg	1 erg=10 ⁻⁷ J
ダイン	dyn	1 dyn=10 ⁻⁵ N
ポアズ	P	1 P=1 dyn s cm ⁻² =0.1Pa s
ストークス	St	1 St=1cm ² s ⁻¹ =10 ⁻⁴ m ² s ⁻¹
スチルブ	sb	1 sb=1cd cm ⁻² =10 ⁴ cd m ⁻²
フオト	ph	1 ph=1cd sr cm ⁻² =10 ⁴ lx
ガリ	Gal	1 Gal=1cm s ⁻² =10 ⁻² ms ⁻²
マクスウェル	Mx	1 Mx=1 G cm ² =10 ⁻⁸ Wb
ガウス	G	1 G=1Mx cm ⁻² =10 ⁻⁴ T
エルステッド ^(a)	Oe	1 Oe _e =(10 ³ /4π)A m ⁻¹

(a) 3元系のCGS単位系とSIでは直接比較できないため、等号「△」は対応関係を示すものである。

表10. SIに属さないその他の単位の例

名称	記号	SI単位で表される数値
キュリー	Ci	1 Ci=3.7×10 ¹⁰ Bq
レントゲン	R	1 R=2.58×10 ⁻⁴ C/kg
ラド	rad	1 rad=1cGy=10 ⁻² Gy
レム	rem	1 rem=1 cSv=10 ⁻² Sv
ガンマ	γ	1 γ=1 nT=10 ⁻⁹ T
フェルミ	f	1 フェルミ=1 fm=10 ⁻¹⁵ m
メートル系カラット		1 メートル系カラット=0.2 g=2×10 ⁻⁴ kg
トル	Torr	1 Torr=(101 325/760) Pa
標準大気圧	atm	1 atm=101 325 Pa
カロリ	cal	1 cal=4.1858J (「15°C」カロリ), 4.1868J (「IT」カロリ), 4.184J (「熱化学」カロリ)
マイクロ	μ	1 μ=1μm=10 ⁻⁶ m

